



DITHIOCARBAMATES: NEW ORGANIC CATALYSTS FOR THE PHOTOCHEMICAL GENERATION OF RADICALS

Daide Spinnato

ADVERTIMENT. L'accés als continguts d'aquesta tesi doctoral i la seva utilització ha de respectar els drets de la persona autora. Pot ser utilitzada per a consulta o estudi personal, així com en activitats o materials d'investigació i docència en els termes establerts a l'art. 32 del Text Refós de la Llei de Propietat Intel·lectual (RDL 1/1996). Per altres utilitzacions es requereix l'autorització prèvia i expressa de la persona autora. En qualsevol cas, en la utilització dels seus continguts caldrà indicar de forma clara el nom i cognoms de la persona autora i el títol de la tesi doctoral. No s'autoritza la seva reproducció o altres formes d'explotació efectuades amb finalitats de lucre ni la seva comunicació pública des d'un lloc aliè al servei TDX. Tampoc s'autoritza la presentació del seu contingut en una finestra o marc aliè a TDX (framing). Aquesta reserva de drets afecta tant als continguts de la tesi com als seus resums i índexs.

ADVERTENCIA. El acceso a los contenidos de esta tesis doctoral y su utilización debe respetar los derechos de la persona autora. Puede ser utilizada para consulta o estudio personal, así como en actividades o materiales de investigación y docencia en los términos establecidos en el art. 32 del Texto Refundido de la Ley de Propiedad Intelectual (RDL 1/1996). Para otros usos se requiere la autorización previa y expresa de la persona autora. En cualquier caso, en la utilización de sus contenidos se deberá indicar de forma clara el nombre y apellidos de la persona autora y el título de la tesis doctoral. No se autoriza su reproducción u otras formas de explotación efectuadas con fines lucrativos ni su comunicación pública desde un sitio ajeno al servicio TDR. Tampoco se autoriza la presentación de su contenido en una ventana o marco ajeno a TDR (framing). Esta reserva de derechos afecta tanto al contenido de la tesis como a sus resúmenes e índices.

WARNING. Access to the contents of this doctoral thesis and its use must respect the rights of the author. It can be used for reference or private study, as well as research and learning activities or materials in the terms established by the 32nd article of the Spanish Consolidated Copyright Act (RDL 1/1996). Express and previous authorization of the author is required for any other uses. In any case, when using its content, full name of the author and title of the thesis must be clearly indicated. Reproduction or other forms of for profit use or public communication from outside TDX service is not allowed. Presentation of its content in a window or frame external to TDX (framing) is not authorized either. These rights affect both the content of the thesis and its abstracts and indexes.



UNIVERSITAT
ROVIRA i VIRGILI



Dithiocarbamates: new organic catalysts for the photochemical generation of radicals

Davide Spinnato



Doctoral Thesis

2022

UNIVERSITAT ROVIRA I VIRGILI
DITHIOCARBAMATES: NEW ORGANIC CATALYSTS FOR THE PHOTOCHEMICAL GENERATION OF RADICALS
Davide Spinnato

UNIVERSITAT ROVIRA I VIRGILI
DITHIOCARBAMATES: NEW ORGANIC CATALYSTS FOR THE PHOTOCHEMICAL GENERATION OF RADICALS
Davide Spinnato

Davide Spinnato

**Dithiocarbamates: new organic catalysts for the
photochemical generation of radicals**

Doctoral Thesis

Supervised by Prof. Paolo Melchiorre

ICIQ – Institut Català d'Investigació Química



UNIVERSITAT
ROVIRA i VIRGILI

Tarragona

2022



UNIVERSITAT
ROVIRA i VIRGILI



Prof. Paolo Melchiorre, ICREA Research Professor & ICIQ Group Leader

I STATE that the present study, entitled “Dithiocarbamates: new organic catalysts for the photochemical generation of radicals”, presented by Davide Spinnato for the award of the degree of Doctor, has been carried out under my supervision at the Institut Català d’Investigació Química (ICIQ).

Tarragona, June 23rd, 2022

Doctoral Thesis Supervisor

Prof. Paolo Melchiorre

UNIVERSITAT ROVIRA I VIRGILI
DITHIOCARBAMATES: NEW ORGANIC CATALYSTS FOR THE PHOTOCHEMICAL GENERATION OF RADICALS
Davide Spinnato

Acknowledgements

First of all, I want to thank my PhD supervisor, Professor Paolo Melchiorre, for allowing me to work in his incredible research group and for all the support I received during this long journey. Without his mentorship I could not have matured as a chemist and, most importantly, as a person.

I am grateful for having met so many nice people and amazing scientist which have been part of the Melchiorre group in the last four years. The international environment that has distinguished the group has been an exceptional element to look at the world and at science with a different perspective. Specifically, I want to thank *Bertrand* for introducing me to the dithiocarbamate world, *Luca* for being the most humble and well-prepared chemist I have ever met, *Giulio* for the ability to calm me down with his way to face life, *Daniele* and *Giandomenico* for their guidance during the first months of my PhD and for the nice evenings we spent together, *Eduardo* for the interesting discussion about my stupid chemistry ideas, *Adriana* for being always smiling, *Emilien* for its way of approaching chemistry, *Enrico* for the incredible enthusiasm that he showed while being a visiting student in the group, *Igor* (also known as the Russian Shark) for the nice discussion on chemistry and for the time we spent together in Tarragona. I also want to thank *Will* for being an amazing human being, for all the funny moments we had in the lab and outside, and for helping me every time I needed. Last but not least, I want to thank my dear friend and lab mate *Matteo Balletti* for this three years we spent together; his arrival in Tarragona and in the group made me feel at home once again.

I am grateful to *Nuria* for being so helpful for all the administrative support I received and for sharing with all the group what Catalan traditions are.

I also want to thank all the people I met during my short stay in the Cornella Group at the Max Planck Institute. In particular, a special thanks goes to *Pep* for giving me the opportunity to spend four months in his lab, *Yue* for introducing me to the world of Bimsuth(I) and for the interesting talks about life, and *Marc* for being a great cigarette and office mate.

Un grande ringraziamento va ai miei genitori i quali, nonostante tutti i guai che gli ho fatto passare in questi trent'anni, sono stati sempre al mio fianco. Senza il loro amore e l'educazione che mi hanno insegnato non sarei mai potuto arrivare fin qui.

Finally, my gratitude goes also to the ICIQ community and to the URV for the organization of an incredible PhD adventure. I also want to share my appreciation towards the European Research Council for the ERC consolidator grant (681840-CATA-LUX). Additionally, I am personally grateful to:

- ICIQ-Severo Ochoa International Mobility grant.



UNIVERSITAT ROVIRA I VIRGILI
DITHIOCARBAMATES: NEW ORGANIC CATALYSTS FOR THE PHOTOCHEMICAL GENERATION OF RADICALS
Davide Spinnato

List of Publications

Some of the results presented in this thesis have been published, accepted, or deposited:

- Spinnato, D.;⁺ Schweitzer-Chaput, B.;⁺ Goti, G.; Ošek, M.; Melchiorre, P.* “A Photochemical Organocatalytic Strategy for the α -Alkylation of Ketones by using Radicals” *Angew. Chem. Int. Ed.* **2020**, *59*, 9485–9490.
- de Pedro Beato, E.; Spinnato, D.; Zhou, W.; Melchiorre, P.* “A General Organocatalytic System for Electron Donor–Acceptor Complex Photoactivation and Its Use in Radical Processes” *J. Am. Chem. Soc.* **2021**, *143*, 31, 12304–12314.
- Georgiou, E.;⁺ Spinnato, D.;⁺ Chen, K.; Melchiorre, P.;* Muñiz, K. “Switchable Photocatalysis for the Chemodivergent Benzoylation of 4-Cyanopyridines” *Chem. Sci.* DOI: 10.1039/D2SC02698H.

UNIVERSITAT ROVIRA I VIRGILI
DITHIOCARBAMATES: NEW ORGANIC CATALYSTS FOR THE PHOTOCHEMICAL GENERATION OF RADICALS
Davide Spinnato

List of Abbreviations

The abbreviations and acronyms used in my doctoral thesis are based on the recommendations of the ACS “Guidelines for authors” and they can be found at <https://www.cas.org/support/documentation/references/cas-standard-abbreviations#listinga>.

UNIVERSITAT ROVIRA I VIRGILI
DITHIOCARBAMATES: NEW ORGANIC CATALYSTS FOR THE PHOTOCHEMICAL GENERATION OF RADICALS
Davide Spinnato

To my grandmas Margherita and Maria

UNIVERSITAT ROVIRA I VIRGILI
DITHIOCARBAMATES: NEW ORGANIC CATALYSTS FOR THE PHOTOCHEMICAL GENERATION OF RADICALS
Davide Spinnato

Table of Contents

Chapter I: General Overview	1
1.1 Photochemistry	1
1.2 Direct Excitation of Organocatalytic Intermediates	6
1.3 General Objectives and Summary	9
1.3.1 A Photochemical Organocatalytic Strategy for the Radical α -Alkylation of Ketones	10
1.3.2 A General Organocatalytic System for Electron Donor–Acceptor Complex Photoactivation and Its Use in Radical Processes	12
Chapter II: A Photochemical Organocatalytic Strategy for the α-Alkylation of Ketones by Using Radicals	13
2.1 Introduction	13
2.2 Radical Generation Strategies: an Overview	15
2.2.1 Methods Relying on Redox Properties	15
2.2.2 Methods Relying on Bond Dissociation Energy	16
2.3 Thiocarbonyl-based Compounds	18
2.3.1 Barton Esters.....	18
2.3.2 Xanthate Derivatives	19
2.4 A New Photo-Organocatalytic Strategy for Radical Generation	22
2.5 Target of the Project	23
2.5.1 Radical-based α -Functionalization of Ketones	23
2.5.2 Design Plan.....	26
2.6 Result and Discussion.....	26
2.6.1 Reaction Optimization	26
2.6.2 Scope evaluation	28
2.6.3 Reaction Limitations.....	31
2.6.4 A Dual Organocatalytic System for the Stereoselective α -Alkylation of Ketones	32
2.6.5 Proposed Mechanism.....	33
2.6.6 Alternative Mechanisms	35
2.7 Conclusions	37
2.8 Experimental Section.....	37
2.8.1 Experimental Set-up	40
2.8.2 Substrate Synthesis	42
2.8.3 General Procedure	46
2.8.4 Characterization Data	46
2.8.5 Gram Scale Reaction	63
2.8.6 Screening of Hydrolysis Conditions	64
2.8.7 Mechanistic Investigations	64
2.8.7.1 Synthesis and Characterization of Dithiocarbamate Intermediate 30a	65
2.8.7.2 Synthesis and Characterization of Dimer 56	66
2.8.7.3 Involvement of 30a in the Catalytic Cycle.....	69
2.8.7.4 Involvement of dimer 56 in the catalytic cycle	69
2.8.7.5 Detection of dimer 56 in the reaction mixture.....	69
2.8.7.6 Involvement of 30a as radical precursor	71
2.8.7.7 Quantum Yield Measurement	72
2.8.7.8 Mechanistic Alternatives.....	75
2.8.8 α -Alkylation of Acetophenone by Enolate Chemistry	78

2.8.9 Enantioselective Radical α -Alkylation of Cyclic Ketones	80
2.8.9.1 General Procedure.....	80
2.8.9.2 Characterization Data.....	81
2.8.9.3 Optimization Studies.....	86
Chapter III: A General Organocatalytic System for Electron Donor–Acceptor Complex Photoactivation and its Use in Radical Processes	89
3.1 Introduction	89
3.2 Electron Donor-Acceptor Complexes.....	91
3.2.1 Synthetic Applications of Stoichiometric EDA Complexes	92
3.2.2 EDA Complex with Substoichiometric Amount of Donors.....	94
3.2.3 EDA Complex Chemistry Using Sacrificial Donors and Redox Auxiliaries	95
3.2.4 Catalytic EDA complexes.....	98
3.3 Target of the Project	102
3.3.1 Design Plan.....	102
3.4 Results and Discussion	103
3.4.1 Developing Redox-Neutral Transformations	104
3.4.2 Redox-Neutral Processes	110
3.4.3 Minisci Reaction.....	114
3.4.4 Further Application of the EDA Catalytic System.....	117
3.5 Conclusion.....	117
3.6 Experimental Session	118
3.6.1 General Informations	118
3.6.2 Substrate Synthesis	119
3.6.3 Experimental set-ups	120
3.6.3.1 Set-up 1 - 3D printed reactor with LED strip	120
3.6.3.2 Set-up 2 - Kessil lamp.....	120
3.6.3.3 Set-up 3 - Temperature-controlled 4-position reactor with LED strip.....	120
3.6.3.4 Set-up 4 - Temperature controlled one-position reactor with LED strip	122
3.6.4 Giese Addition.....	120
3.6.4.1 General Procedure A.....	123
3.6.4.2 Characterization of Products with General Procedure A.....	123
3.6.4.3 General Procedure B (One-Pot Telescoped from Carboxylic Acids).....	124
3.6.4.4 Characterization of Products with General Procedure B	125
3.6.4.5 General procedure C (One-Pot Domino from Carboxylic Acids)	126
3.6.4.6 Characterization of Products with General Procedure C	126
3.6.4.7 General procedure D (Using Pyridinium Salts).....	128
3.6.4.8 Characterization of Products with General Procedure D.....	128
3.6.4.9 General Procedure E (Telescoped Reaction from Amine)	129
3.6.4.10 Characterization of Products with General Procedure E	129
3.6.5 Reduction.....	120
3.6.5.1 General Procedure F (Barton Decarboxylation).....	130
3.6.5.2 Characterization of Products with General Procedure F	130
3.6.5.3 General procedure G (Deaminative Reduction)	132
3.6.5.4 Characterization of Products with General Procedure G.....	132
3.6.6 α -Alkylation of Silyl Enol Ethers	133
3.6.6.1 General Procedure H.....	133
3.6.6.2 Characterization of Products with General Procedure H.....	133

3.6.6.3 General Procedure I (Three-Component Reaction).....	138
3.6.6.4 Characterization of Products with General Procedure I	138
3.6.7 Minisci Reaction.....	141
3.6.7.1 General Procedure J	141
3.6.7.2 Characterization of Products with General Procedure J	141
3.6.7.3 General Procedure K (Enantioselective Variant)	146
3.6.7.4 Characterization of Products General Procedure K (Enantioselective Variant).....	146
3.6.8 Trifluoromethylation.....	147
3.6.9 Amydil Radical.....	147
3.6.10 Large Scale Reactions	148
3.6.10.1 Barton Decarboxylation	148
3.6.10.2 Minisci Reaction	149
3.6.11 Unsuccessful substrates	149
3.7 Mechanistic Studies	150
3.7.1 Control Experiments.....	150
3.7.1.1 Experiments with green Light	150
3.7.1.2 Optimization Studies.....	150
3.7.1.3 TEMPO Trapping Experiment	152
3.7.2 Catalysts' stability experiments	153
3.7.3 UV-Vis Spectroscopy	154
3.7.4 Transient Absorption Spectroscopy (TAS).....	155
3.7.5 Cyclic Voltammetry Measurements.....	156
3.7.6 Quantum Yield Determination.....	160
3.7.6.1 Giese Addition	160
3.7.6.2 Barton Decarboxylation	162
3.7.6.3 Alkylation Enol Ethers.....	164
3.7.6.4 Minisci Reaction	166
Chapter IV: General Conclusions	168

UNIVERSITAT ROVIRA I VIRGILI
DITHIOCARBAMATES: NEW ORGANIC CATALYSTS FOR THE PHOTOCHEMICAL GENERATION OF RADICALS
Davide Spinnato

UNIVERSITAT ROVIRA I VIRGILI
DITHIOCARBAMATES: NEW ORGANIC CATALYSTS FOR THE PHOTOCHEMICAL GENERATION OF RADICALS
Davide Spinnato

Chapter I

General Overview

1.1 Photochemistry

Photochemistry is the branch of chemistry focusing on the understanding of the chemical interactions between photons and matter.¹ The first observation of light-induced chemical transformations dates back to 1777, when C. W. Scheele realized that silver chloride degrades under violet-light irradiation.¹ Two basic principles formulated at the beginning of the 19th and 20th centuries defined the theoretical grounds of the photochemistry field:²

- *Grotthuss-Draper law*: “only the light absorbed by a substance or substances is effective in bringing about chemical change”.
- *Stark-Einstein law*: “in a photochemical process for each quantum of radiation (or photon) absorbed, one molecule of the substance reacts”.

The two laws offer an incomplete and simplistic version of today’s knowledge, however both were important in the development of photochemistry. A fundamental theoretical advancement came about when Einstein, following Planck’s theory,³ proposed that bundles of energy constitutes the electromagnetic waves and each bundle, by being discrete and localized, is called “light quantum”.⁴ The quantum theory opened up the possibility to correlate quantitatively the interaction between light and matter as we know it today.¹

The interaction between a molecule in its *ground state* (the initial state, *i*) and a photon possessing suitable energy promotes an electronic transition from the highest occupied molecular orbital (HOMO, Figure 1.1a) to the lowest unoccupied molecular orbital (LUMO, Figure 1.1a) of the absorbing compound.¹ This light-promoted transition brings the molecule in an electronically *excited state* (the final state, *f*). The electronic distribution of the ground and excited states are described by wave functions Ψ (Ψ_i and Ψ_f), while E_i and E_f correspond to their relative energies (Figure 1.1b).

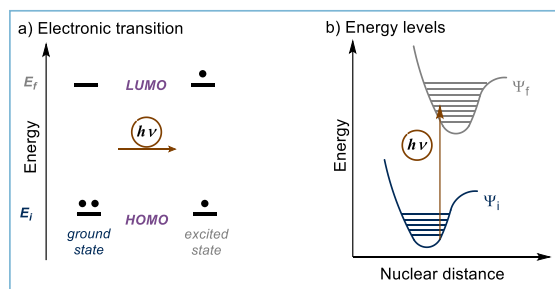


Figure 1.1. a) Schematic representation of a photo-stimulated electronic transition. b) Energy difference between the ground-state wavefunction (Ψ_i) and the excited-state wavefunction (Ψ_f).

¹ Balzani, V.; Ceroni, P.; Juris, A. "Photochemistry and Photophysics: Concepts, Research, Applications" **2014**, John Wiley & Sons.

² Rennie, R.; Law J. "A Dictionary of Chemistry" **2016**, Oxford University Press.

³ Haar, D. "The old quantum theory" **1967**, Oxford, New York, Pergamon Press.

⁴ Einstein, A. "Über einen die Erzeugung und Verwandlung des Lichtes betreffenden heuristischen Gesichtspunkt" **1905**, Annalen der Physik.

In order to have a productive transition, the photon must possess an energy equal to the energy difference between the ground and the excited state (Eq. 1.1):¹

$$h\nu = E_f - E_i \quad (1.1)$$

The different electronic distribution of a molecule in the excited state greatly influences its chemical behavior. Excitation may therefore allow access to chemical reactivity that thermal activation cannot achieve.⁵

At the very beginning of the 20th century, the Italian chemist Giacomo Ciamician laid the foundations of synthetic photochemistry demonstrating the potential of solar energy for the pursuit of a more energetically sustainable chemical synthesis.⁶ For a long time, the *direct excitation* of organic molecules represented the most straightforward approach in synthetic photochemistry. The Paternò-Büchi reaction, a [2+2] photocycloaddition between a carbonyl compound (e.g. an aldehyde, **1**) and an alkene **2**, was one of the first applications of the aforementioned approach (Figure 1.2).⁷ In particular, ultraviolet (UV) irradiation promotes the electronic transition ($\Psi_i \rightarrow \Psi_f$) of **1**, leading to the aldehyde's excited state (**1***). This photon-based activation grants access to a thermally-disallowed [2+2] cycloaddition with olefin **2** to produce the oxetane product **3**.

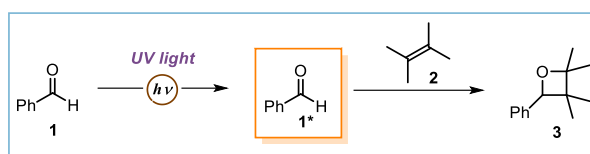


Figure 1.2. The Paternò-Büchi reaction.

One of the main issues related to unimolecular *direct-excitation* processes is that most organic substrates only absorb photons in the UV region, due to their large HOMO-LUMO gap. Furthermore, organic substances usually possess a low molar attenuation coefficient and a short excited-state lifetime. In order to overcome these limitations and so widen the applicability of light-promoted chemical reactions, a bimolecular approach was developed, which served to obviate the intrinsic requirement of the substrate to absorb light. Specifically, photocatalysis, by using a substoichiometric *photomediator* or *photocatalyst* (**PC**), can activate substrates through non-thermal mechanistic pathways, while relying on the absorption properties of the photocatalyst alone. These compounds are usually metal-based complexes or organic dyes with exceptionally convenient photophysical properties, such as high molar attenuation coefficients or long excited-state lifetimes.⁸ Importantly, photomediators possess an absorption profile which falls in the visible region. This means that low-energy light can be used in place of high-energy UV-light. Recently, photocatalysis has developed to become a whole new field of organic synthetic chemistry. In general, when a photocatalyst absorbs light to reach an excited state, substrate *S* can be perturbed by two mechanistically

⁵ (a) Turro N. J.; Ramamurthy V.; Scaiano J. C. "Modern Molecular Photochemistry of Organic Molecules" **2010**, University Science Books. (b) Hoffmann. "Photochemical Reactions as Key Steps in Organic Synthesis" *Chem. Rev.* **2008**, *108*, 1052–1103.

⁶ (a) Ciamician, G.; Silber, P. "Chemische Lichtwirkungen" *Berichte der deutschen chemischen Gesellschaft* **1900**, *33*, 2911. (b) Ciamician, G. "The photochemistry of the future" *Science* **1912**, *36*, 385.

⁷ (a) Paternò, E.; Cheffi, G. "Sintesi in chimica organica per mezzo della luce. Nota II. Composti degli idrocarburi non saturi con aldeidi e chetoni" *Gazz. Chim. Ital.* **1909**, *39*, 341–361. (b) Büchi, G.; Inman, C. G.; Lipinsky, E. S. "Light-catalyzed Organic Reactions. I. The Reaction of Carbonyl Compounds with 2-Methyl-2-butene in the Presence of Ultraviolet Light" *J. Am. Chem. Soc.* **1954**, *76*, 4327–4331.

⁸ Yoon, T. P.; Ischay, M. A.; Du, J. "Visible Light Photocatalysis as a Greener Approach to Photochemical Synthesis" *Nat. Chem.* **2010**, *2*, 527–532.

different processes: *energy transfer*⁹ (EnT) or *electron transfer* (ET).¹⁰ In energy transfer manifolds, the excited-state photocatalyst (**PC***) decays to the corresponding ground state by delivering the absorbed photonic energy to *S*, leading to the excited-state substrate (**S***, Figure 1.3a). The energy can be transferred to the target substrate following two possible mechanisms, which are a direct consequence of the two underlying electron-electron interactions described by quantum mechanics, coulombic and exchange interactions.¹¹ In the first mechanism, called Forster Resonance Energy Transfer (FRET),¹² electronic oscillation from **PC*** induces a dipole in *S*, which perturbs the electronic oscillation within the substrate. Finally, the induced electronic oscillation within *S* promotes the desired electronic transition towards **S***.¹² The second mechanism, firstly described by Dexter (Dexter Energy Transfer, Dexter EnT),¹³ proceeds through an intermolecular exchange between the electrons of the excited-state photocatalyst and the ground state of the substrate. In this case, the two partners need to form a “solvent-shared encounter complex” since adequate orbital overlap is required for an effective electron exchange.¹¹ Regardless the mechanism involved, once in its excited state, the substrate can undergo the desired transformation. For example, one of the seminal studies on energy transfer, reported by Wrighton in 1973,¹⁴ demonstrated the ability of a ruthenium complex to act as a photocatalyst to achieve *E*→*Z* isomerization of alkenes (Figure 1.3b). The chosen photocatalyst, tris(2,2'-bipyridine)ruthenium(II) chloride (often referred to as Ru(bpy)₃Cl₂), would later become one of the most commonly used photocatalysts of the 21st century.¹

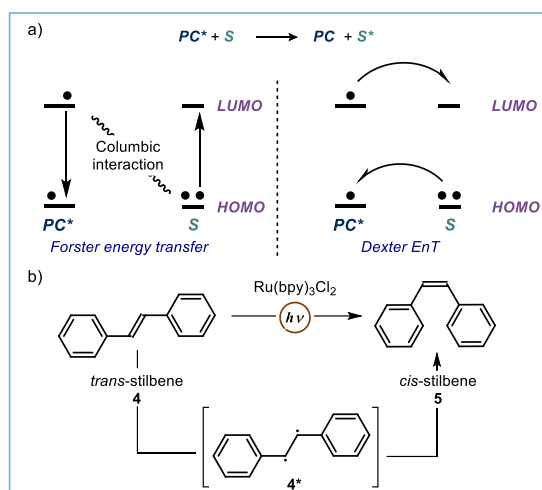


Figure 1.3. a) Energy-transfer: Forster and Dexter mechanisms. b) Pioneering work on energy transfer.

The other mode of photocatalytic activation is through single-electron-transfer (SET), in which the enhanced redox behavior of **PC*** is exploited (Figure 1.4a). When an electron belonging to the photocatalyst is promoted from the HOMO to the LUMO, the **PC**'s ionization potential (IP) is lowered, while the electron affinity (EA) increases.¹ From a thermodynamic point of view, the removal of one electron from the half-filled LUMO of the **PC**'s excited state is more favorable than from the HOMO of the ground state. On the

⁹ Strieth-Kalthoff, F.; James, M. J.; Teders, M.; Pitzer, L.; Glorius, F. "Energy transfer catalysis mediated by visible light: principles, applications, directions" *Chem. Soc. Rev.* **2018**, *47*, 7190-7202.

¹⁰ Kavarnos, G. J. "Fundamentals of Photoinduced Electron Transfer" **1993**, VCH.

¹¹ Turro, N. J. *Modern Molecular Photochemistry*, **1991**, University Science Books, Sausalito.

¹² Forster, T. "Zwischenmolekulare Energiewanderung und Fluoreszenz" *Ann. Phys.*, **1948**, *437*, 55-75.

¹³ Dexter, D. L. "A Theory of Sensitized Luminescence in Solids" *J. Chem. Phys.*, **1953**, *21*, 836-850

¹⁴ Wrighton M.; Markham J. "Quenching of the Luminescent State of Tris(2,2'-bipyridine)ruthenium(II) by Electronic Energy Transfer" *J. Phys. Chem.* **1973**, *77*, 3042-3044.

other hand, the addition of one electron to the half-filled HOMO of the excited state is energetically more favorable than addition to the LUMO of the ground state.¹ It follows that light-promoted excitation results in the simultaneous increase of *both* oxidative and reductive power of the photocatalyst. One of the first reports showcasing the potential of SET-based photoredox catalysis was developed by Cano-Yelo and Deronzier in 1984 (Figure 1.4b).¹⁵ In their work, the ruthenium-based photocatalyst $\text{Ru}(\text{bpy})_3\text{Cl}_2$ was proposed to transfer one electron from its excited state (PC^*) to substrate **6**, affording radical **7** after liberation of nitrogen gas. The open-shell intermediate **7** underwent a radical cyclization followed by an SET to deliver product **8**. This second SET regenerated the ground-state photocatalyst to close the catalytic cycle. Interestingly, the quantum efficiency of the process was much higher under photoredox conditions than when the transformation was promoted by the direct excitation of substrate **6**, highlighting the potential of photoredox catalysis.

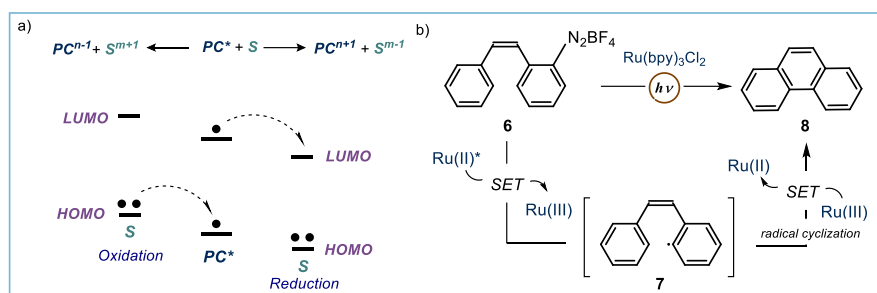


Figure 1.4. a) Electron transfer from the excited-state photocatalyst (PC^*) to a substrate **S** promotes the formation of a radical. b) Pioneering work on SET.

Even if the first applications of photocatalysis in synthetic chemistry were developed in the 1980's, the field remained underdeveloped until the MacMillan group reported the visible-light-promoted enantioselective α -alkylation of aldehydes in 2008 (Figure 1.5).¹⁶ The proposed mechanism involves initial condensation of aldehyde **9** with chiral aminocatalyst **11** to generate enamine **I**. Visible-light irradiation promotes the excitation of $[\text{Ru}(\text{bpy})_3]^{2+}$, which can drive a sacrificial SET oxidation of enamine **I**, delivering the reduced state $[\text{Ru}(\text{bpy})_3]^+$. A favorable SET between the reduced photocatalyst and alkyl bromide **10** generates radical **II**. The electrophilic nature of **II** makes the stereoselective trap by the nucleophilic enamine **11** kinetically favored.¹⁷ The ensuing α -amino radical **III** is oxidized by the photo-excited Ru(II) complex to form iminium ion **IV**, which undergoes hydrolysis to afford aminocatalyst **11** and the chiral product **12** in high enantiomeric excess. A detailed mechanistic investigation by the Yoon group proved that a chain propagation mechanism was operative and its efficient propagation was sustained by an SET event between intermediate **III** and the radical precursor **10**.¹⁸

¹⁵ Cano-Yelo, H.; Deronzier, A. "Photocatalysis of the Pschorr reaction by tris-(2,2'-bipyridyl)ruthenium(II) in the phenanthrene series" *J. Chem. Soc. Perkin Trans. 2*, **1984**, 1093-1098.

¹⁶ Nicewicz, D. A.; MacMillan, D. W. C. "Merging photoredox catalysis with organocatalysis: the direct asymmetric alkylation of aldehydes" *Science* **2008**, *322*, 77-80.

¹⁷ Parsaee, F.; Senarathna, M. C.; Kannangara, P. B.; Alexander S. N.; Arche P. D. E.; Welin E.R. "Radical philicity and its role in selective organic transformations" *Nat. Rev. Chem.* **2021**, *5*, 486-499.

¹⁸ Cismesia, M. A.; Yoon, T. P. Characterizing Chain Processes in Visible Light Photoredox Catalysis. *Chem. Sci.* **2015**, *6*, 5426-5434

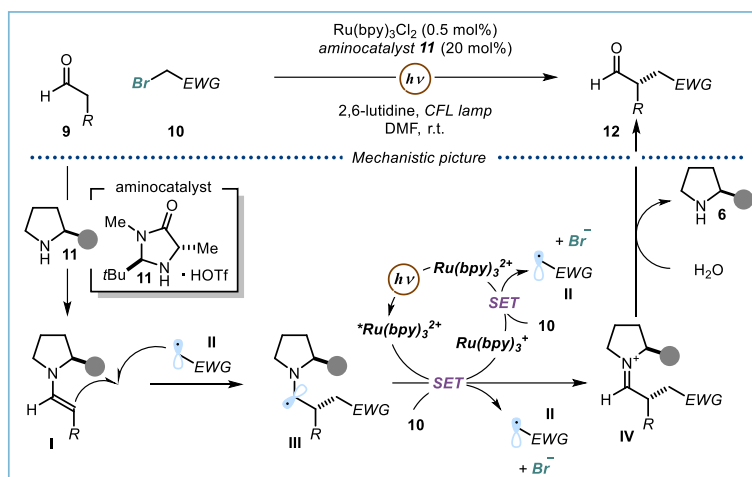


Figure 1.5. Tandem organo-photoredox catalysis for the α -alkylation of aldehydes with electron-poor alkyl bromides.

In the very same year, the Yoon group exploited the photoredox properties of $\text{Ru}(\text{bpy})_3\text{Cl}_2$ to develop a [2+2] photocycloaddition of enones **13** (Figure 1.6).¹⁹ Mechanistically, light-mediated excitation of $[\text{Ru}(\text{bpy})_3]^{2+}$ promotes an SET oxidation event of *N,N*-diisopropylethylamine (DIPEA), delivering the reduced $[\text{Ru}(\text{bpy})_3]^+$. Thermodynamically favored SET reduction of **13** delivers **V** and the ground-state photocatalyst. Radical-induced diastereoselective cyclization delivers highly reducing ketyl radical **VI**,²⁰ which can promote an efficient radical chain propagation upon reduction of a second molecule of **13**.

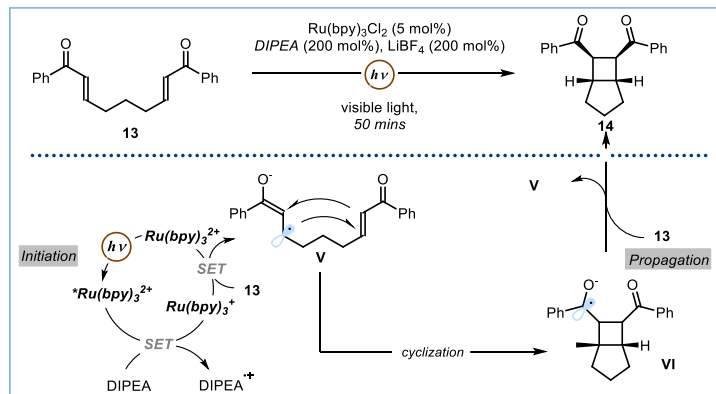


Figure 1.6. [2+2] photocycloaddition of enones.

Shortly after, in 2009, Stephenson and co-workers demonstrated how photoredox catalysis could offer a catalytic alternative to drive organic reactions traditionally performed using stoichiometric amounts of hazardous and highly toxic reagents (Figure 1.7).²¹ Specifically, $\text{Ru}(\text{bpy})_3\text{Cl}_2$ was used for the development of a tin-free reductive dehalogenation.

¹⁹ Ischay, M. A.; Anzovino, M. E.; Du, J.; Yoon, T. P. "Efficient visible light photocatalysis of [2+ 2] enonecycloadditions" *J. Am. Chem. Soc.* **2008**, *130*, 12886-12887.

²⁰ Peter, A.; Agasti, S.; Knowles, O.; Pye, E.; Procter, D. J. "Recent advances in the chemistry of ketyl radicals" *Chem. Soc. Rev.* **2021**, *50*, 5349-5365.

²¹ Narayanam, J. M. R.; Tucker, J. W.; Stephenson, C. R. J. "Electron-Transfer Photoredox Catalysis: Development of a Tin-Free Reductive Dehalogenation Reaction" *J. Am. Chem. Soc.* **2009**, *131*, 8756-8757.

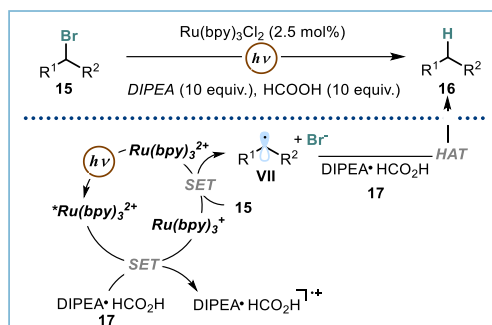


Figure 1.7. Photoredox-mediated dehalogenation.

From a mechanistic point of view, it was proposed that upon, reductive quenching of the excited-state photocatalyst by ammonium formate **17**, the highly reducing Ru(I) could reduce the carbon-halogen bond within the substrate's core **15**. This SET delivered the carbon-centered radical **VII** while returning the photocatalyst in its original oxidation state. Subsequent hydrogen abstraction from **17** delivered the desired product **16** in high yields.

The seminal works by MacMillan,¹⁶ Yoon,¹⁹ and Stephenson²¹ pinpointed the renaissance of synthetic photochemistry, highlighting the potential of *photoredox catalysis* as a mild and effective way to generate high-in-energy radical intermediates under mild conditions.²²

1.2 Direct excitation of organocatalytic intermediates

In the last two decades, the combination of two or more catalytic systems has allowed chemists to develop useful chemical transformations.²³ For example, the mild conditions of photoredox catalysis facilitated the merger with well-established organocatalytic platforms, as testified by the pioneering study by MacMillan discussed above in Figure 1.5.²⁴ Later, it was found that an external photocatalyst was not always required to enable such radical-based manifolds when using specific organocatalytic intermediates. For example, the Melchiorre group have shown that some established organocatalytic intermediates (e.g. chiral enamines), with a proven reactivity in polar pathways, can engage in photoinduced SET processes upon light excitation. In fact, upon reaching their excited state, these organocatalytic intermediates can promote the formation of radicals that are subsequently trapped in a stereoselective fashion. Combining the photo-activity and the ground-state activity of organocatalytic intermediates allowed the development of transformations unachievable in the thermal domain.²⁵ For instance, our group found that, when an electron-poor benzylic bromide (**19**) was mixed with the chiral enamine **VIII**, the colorless reaction mixture changed color to become bright yellow (Figure 1.8a).²⁶ This empirical observation was rationalized on the basis of the *electron donor-acceptor* (EDA) theory. According to Mulliken quantum mechanical rationalization,²⁷ the association of an electron-rich species, the *donor*, and an electron-poor species, the *acceptor*, can promote

²² McAtee, R. C.; McClain, E. J.; Stephenson, C. R. J. "Illuminating Photoredox Catalysis" *Trends Chem.* **2019**, *1*, 111-125.

²³ Wasilke J.-C.; Obrey S. J.; Baker R. T.; Bazan G. C. "Concurrent Tandem Catalysis" *Chem. Rev.* **2005**, *105*, 1001-1020.

²⁴ (a) Shaw, M. H.; Twilton, J.; MacMillan, D. W. C., Photoredox Catalysis in Organic Chemistry. *J. Org. Chem.* **2016**, *81*, 6898-6926. (b) DiRocco, D. A.; Rovis, T. "Catalytic asymmetric α -acylation of tertiary amines mediated by a dual catalysis mode: N-heterocyclic carbene and photoredox catalysis" *J. Am. Chem. Soc.* **2012**, *134*, 8094-8097. (c) Uraguchi, D.; Kinoshita, N.; Kizu, T.; Ooi, T. "Synergistic catalysis of ionic Brønsted acid and photosensitizer for a redox neutral asymmetric α -coupling of N-arylaminoethanes with aldimines" *J. Am. Chem. Soc.* **2015**, *137*, 13768-13771.

²⁵ Silvi, M.; Melchiorre, P. "Enhancing the potential of enantioselective organocatalysis with light" *Nature*, **2018**, *554*, 41-49.

²⁶ Arceo, E.; Jurberg, I. D.; Álvarez-Fernández, A.; Melchiorre, P. "Photochemical Activity of a Key Donor-Acceptor Complex Can Drive Stereoselective Catalytic α -alkylation of Aldehydes" *Nat. Chem.* **2013**, *5*, 750-756.

²⁷ (a) Mulliken, R. S. "Molecular Compounds and their Spectra. III. The Interaction of Electron Donors and Acceptors" *J. Phys. Chem.* **1952**, *56*, 801-822. (b) Crisenza, G. E. M.; Mazzarella, D.; Melchiorre, P. "Synthetic Methods Driven by the Photoactivity of Electron Donor-Acceptor Complexes" *J. Am. Chem. Soc.* **2020**, *142*, 5461-5476.

the formation of a new ground-state complex. This new chemical entity, called an *EDA complex*, possesses singular physical properties derived from new molecular orbitals generated through the hybridization of the frontier orbitals of the two partners (the HOMO of the donor and the LUMO of the acceptor). The energy associated to the $\Psi_i \rightarrow \Psi_f$ often lies within the visible region, meaning that the transient ground-state EDA complex can be excited by visible light. Irradiation of the EDA complex promotes an SET from the donor to the acceptor, which eventually leads to radical generation.²⁷ For the α -alkylation of aldehydes, the electron-rich enamine **VIII** acted as the donor, whereas the electron-poor bromide **19** was the acceptor partner (Figure 1.8, orange box). Light-mediated intra-complex SET reduced the benzyl bromide which, after mesolysis of the C-Br bond, delivered the reactive benzyl radical **IX**. Stereoselective trapping of the carbon-centered radical by enamine **VIII** afforded product **22a**.

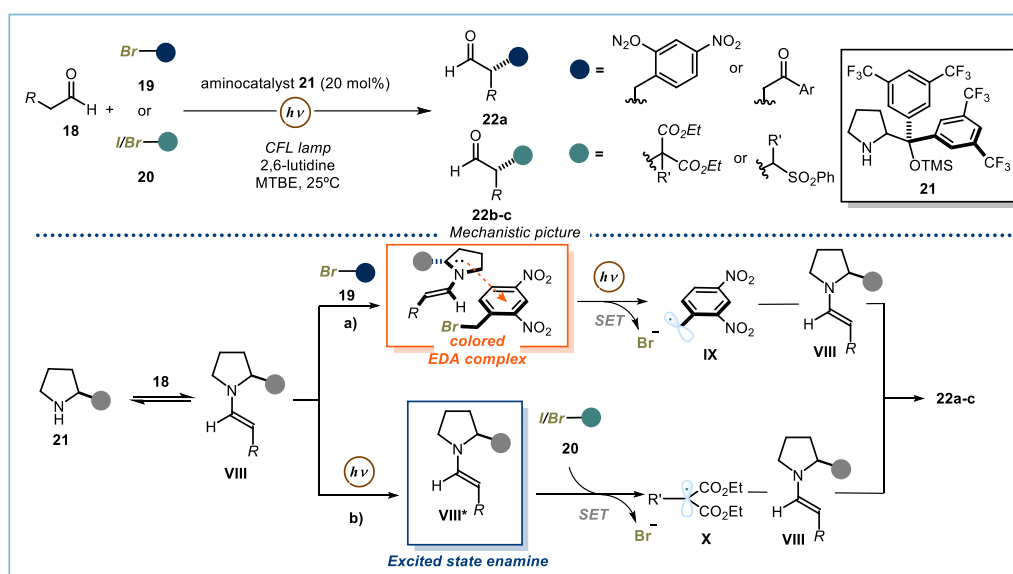


Figure 1.8. Photochemical asymmetric α -alkylation of aldehydes: a) Enamine-based EDA complex approach. b) Enamine direct excitation approach.

The photochemical ability of chiral enamines **VIII** to generate open-shell species is not restricted to the formation of EDA complexes. Indeed, enamine **VIII** can be directly excited under near-visible light irradiation ($\lambda_{\text{max}} = 390 \text{ nm}$) to achieve an excited-state intermediate that can act as a strong SET reductant (estimated $E_{\text{red}}^*(\text{VIII}^+/\text{VIII}^*) \sim -2.50 \text{ V vs. Ag/AgCl}$, Figure 1.8b, blue box). The excited organocatalytic enamine **VIII*** can activate bromomalonate²⁸ or α -iodo-sulphone derivatives²⁹ **20** via SET reduction. The SET delivered the electrophilic alkyl radicals **X**, which were trapped by the ground-state chiral enamine **VIII** to give the enantioenriched products **22b-c**. Mechanistically, kinetic and photophysical studies³⁰ demonstrated that this transformation is governed by an effective self-propagating radical chain.

The demonstration of enamines as competent photo-organocatalytic intermediates motivated our group to study the excited-state behavior of other well-known organocatalytic species. It was reasoned that if nucleophilic enamines **VIII** can act as strong photo-reductants upon excitation, it seems feasible that

²⁸ Silvi, M.; Arceo, E.; Jurberg, I. D.; Cassani, C.; Melchiorre, P. "Enantioselective Organocatalytic Alkylation of Aldehydes and Enals Driven by the Direct Photoexcitation of Enamines" *J. Am. Chem. Soc.* **2015**, *137*, 6120-6123.

²⁹ Filippini, G.; Silvi, M.; Melchiorre, P. "Enantioselective Formal α -Methylation and α -Benzylation of Aldehydes by Means of Photo-organocatalysis" *Angew. Chem. Int. Ed.* **2017**, *56*, 4447-4451.

³⁰ Bahamonde, A.; Melchiorre, P. "Mechanism of the Stereoselective α -Alkylation of Aldehydes Driven by the Photochemical Activity of Enamines" *J. Am. Chem. Soc.* **2016**, *138*, 8019-8030.

electrophilic intermediates, such as iminium ion **XI**, might act as oxidants in their excited state (**XI***, Figure 1.9a, blue box).³¹ Indeed, upon condensation of cinnamaldehyde derivatives **23** and aminocatalyst **26**, a colored iminium ion **XI** is generated. When irradiated at 420 nm, the chiral iminium ion **XI** reaches its excited state **XI*** and can perform SET oxidation of benzyl silanes **24**. Upon desilylation, benzylic radical **XII** is formed, which undergoes stereoselective radical coupling with the chiral β -enaminy radical **XIII**. Ultimately, hydrolysis delivers the enantioenriched β -alkylation product **28** while regenerating the chiral aminocatalyst **26**. Similarly to the enamine case, the photochemical ability of iminium ions to generate radicals is not limited to the direct excitation approach. In 2019, the Gilmour group developed an intermolecular radical-based Stetter reaction between α -keto acids **25** and enals **23**, which is proposed to operate via the photoactivation of an intermediate EDA complex (Figure 1.9b, orange box). In this work, the keto acid **25** possesses a double function: *i*) it facilitates the formation of iminium ion **XIV** through acid-catalyzed condensation; and *ii*) it ensures the formation of a photoactive EDA complex with **XV** due to its electron-rich carboxy anion moiety. Light excitation of the EDA complex promotes an SET that, after decarboxylation, generates the acyl radical **XVI** and the β -enaminy radical **XVII**.³² Radical-radical coupling between **XVI** and **XVII**, followed by hydrolysis, delivers the final product **29** and regenerates the aminocatalyst **27**. Contrarily to the excited-state iminium ion approach developed in the Melchiorre group, the formal Stetter reaction could not be developed in a stereoselective fashion.

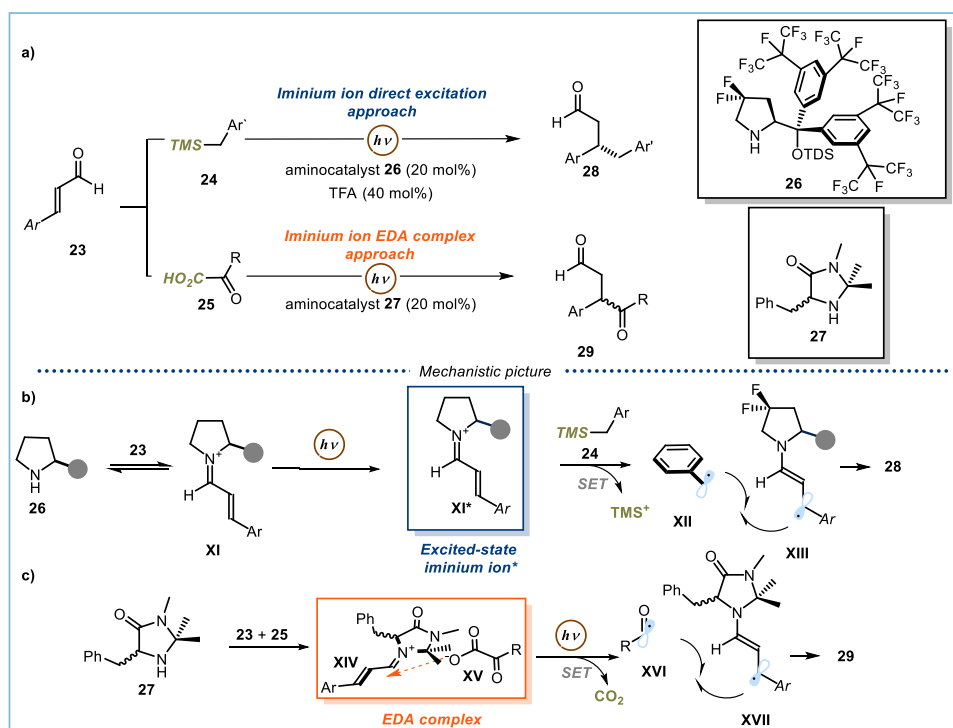


Figure 1.9. a) Photochemical organocatalytic stereoselective β -alkylations of enals. b) Direct excitation of iminium ions. c) Iminium ion-based EDA complex approach.

A vast part of radical generation strategies relies on SET pathways using strongly reducing or oxidizing catalysts. Our laboratories have recently disclosed a photochemical organocatalytic strategy for radical

³¹ Silvi, M.; Verrier, C.; Rey, Y. P.; Buzzetti, L.; Melchiorre, P., "Visible-Light Excitation of Iminium Ions Enables the Enantioselective Catalytic β -Alkylation of Enals" *Nat. Chem.* **2017**, *9*, 868-873.

³² Morack, T.; Muck-Lichtenfeld, C.; Gilmour R. "Bioinspired Radical Stetter Reaction: Radical Umpolung Enabled by Ion-Pair Photocatalysis" *Angew. Chem. Int. Ed.* **2019**, *58*, 1208–1212.

generation that does not rely on the redox properties of the substrate.³³ This was possible by translating the stoichiometric xanthate-based chemistry, developed by Barton³⁴ and Zard 40 years ago,³⁵ into a catalytic regime.³⁶ This catalytic radical generation strategy required the design of a nucleophilic organic catalyst **32**, adorned with an indole-based light absorbing unit (Figure 1.10a). The *dithiocarbamate catalyst* **32** could readily activate a wide range of alkyl electrophiles **30** via an S_N2 path.

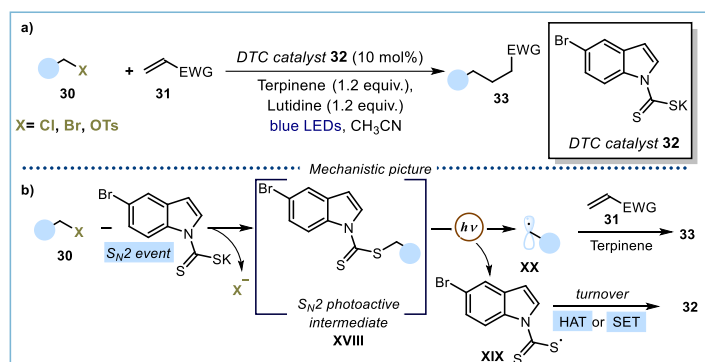


Figure 1.10. (a) Radical formation from alkyl (pseudo)halides using the nucleophilic organocatalyst **32**. (b) Mechanistic proposal.

After S_N2 reaction, the resulting photoactive S_N2 adduct **XVIII** (Figure 1.10b, blue box) is excited upon irradiation and undergoes homolytic cleavage of the labile C-S bond to deliver carbon-centered radical **XX** and thiyl radical **XIX**. The resulting nucleophilic radical **XX** is then trapped by an electron-poor olefin **31** to deliver the desired Giese-type product **33**. This catalytic S_N2-based approach differs from other radical generation strategies since it relies on the electrophilic properties of the radical precursor and on the bond dissociation energy of the ensuing intermediate **XVIII**.

1.3 General objectives and summary

The renaissance of photocatalysis demonstrated that one-electron logic strategies can offer effective and sustainable solutions to important synthetic problems. The use of organocatalytic intermediates in their excited state actively contributed to this field. The main target of my doctoral thesis was to further develop this research line by designing new organocatalytic strategies for generating radicals, and use them in synthetically useful transformation. Specifically, I further explored the reactivity of dithiocarbamate-based organocatalytic intermediates in their excited states.

In Chapter II, I will show how the newly designed dithiocarbamate catalyst of type **32**³³ could be useful to develop an effective method for the α -alkylation of silyl enolates. The possibility to combine the photocatalytic radical generation strategy with a cinchona-based primary amine catalyst served to develop a rare example of enantioselective organocatalytic radical α -alkylation of ketones.

In Chapter III, I will illustrate how the mechanistic knowledge gathered on our dithiocarbamate catalysts served to design a new photocatalytic strategy that goes beyond the S_N2 manifold. As previously shown in

³³ Schweitzer-Chaput, B.; Horwitz, M. A.; de Pedro Beato, E.; Melchiorre, P. "Photochemical generation of radicals from alkyl electrophiles using a nucleophilic organic catalyst" *Nat. Chem.* **2019**, *11*, 129–135.

³⁴ Barton, D. H. R.; McCombie, S. W. "A New Method for the Deoxygenation of Secondary Alcohols" *J. Chem. Soc. Perkin Trans. 1*, **1975**, 1574–1585.

³⁵ Zard, S. Z. "On the Trail of Xanthates: Some New Chemistry From an Old Functional Group" *Angew. Chem. Int. Ed.* **1997**, *36*, 672–685.

³⁶ A detailed picture on how xanthate chemistry has been used for radical generation will be discussed in Chapter 2.

section 1.2, some organocatalytic intermediates can unlock distinct excited-state reactivity under irradiation. For instance, the direct excitation of enamines has promoted the radical α -alkylation of aldehydes starting from bromomalonates or iodo-sulphones (Figure 1.8b, blue box). When electron-poor benzyl bromides were employed as radical precursors, enamines intermediates triggered the formation of photo-absorbing EDA complexes, which upon light excitation promoted the formation of radicals (Figure 1.8a, orange box). Chapter III will detail our efforts to exploit dithiocarbamate anion catalysts as catalytic donors for EDA complex formation upon activation of electron-poor redox active radical precursors. Light excitation promoted to the formation of radicals under mild conditions. I will show how this alternative catalytic approach allowed us to generate radicals inaccessible by our previous S_N2 -based methodology, and to use them in mechanistically different processes.

1.3.1 A Photochemical Organocatalytic Strategy for the Radical α -Alkylation of Ketones³⁷

Chapter II details a new photochemical approach for the α -alkylation of aromatic and aliphatic ketones (Figure 1.11). The method exploits the nucleophilicity of the nucleophilic organocatalyst **32** to activate alkyl halide, mesylates, and nosylates **30** via S_N2 activation.³³ The resulting photo-absorbing intermediate **XVIII** (Figure 1.11, orange box) undergoes homolytic cleavage of the weak C-S bond upon blue light irradiation. The photogenerated radical **XX** are intercepted by weakly nucleophilic silyl enolates **33**, which are not able to undergo nucleophilic substitution on the electrophile **30** via a traditional two-electron pathway.

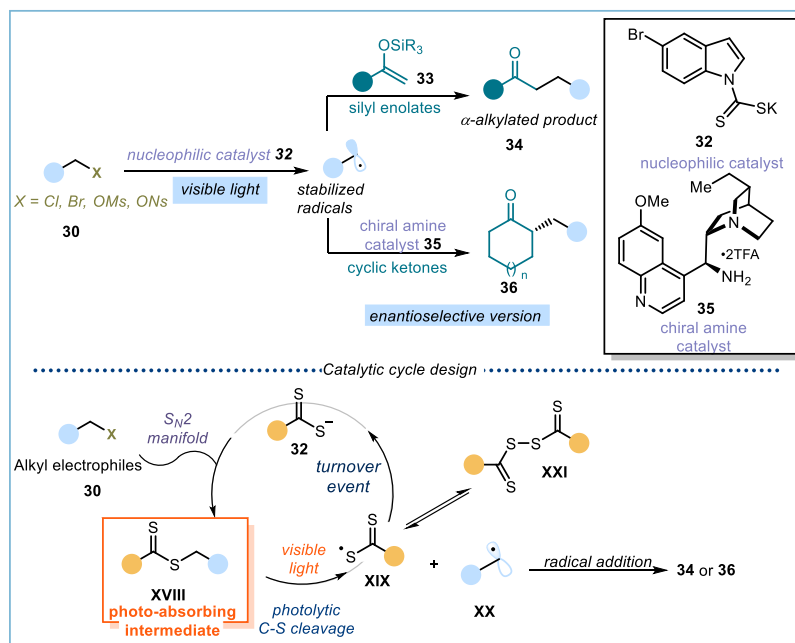


Figure 1.11. Photochemical organocatalytic α -alkylation of ketones by using radicals

Key to success was the ability of catalyst **32** to activate substrates that are inert towards SET or hydrogen atom transfer activation. The mild conditions and the redox-neutral nature of the radical generation strategy allowed us to functionalize complex structures. In addition, we further applied our platform for the stereoselective radical alkylation of cyclic ketones by combining the photocatalytic process with a chiral

³⁷ Spinnato, D.; Schweitzer-Chaput, B.; Goti, G.; Ošeka, M.; Melchiorre, P. "A Photochemical Organocatalytic Strategy for the α -Alkylation of Ketones by using Radicals" *Angew. Chem. Int. Ed.* **2020**, *59*, 9485–9490.

cinchona-based primary amine catalyst **35**. Furthermore, by studying the mechanism of the reaction, we discovered a photon-controlled dimerization process that effectively confers a longer lifetime to the thiyl radical **XIX**, a crucial mechanism which facilitates catalyst turnover.

1.3.2 A General Organocatalytic System for Electron Donor–Acceptor Complex Photoactivation and Its Use in Radical Processes³⁸

Chapter III details the development of a different catalytic strategy for radical generation based on dithiocarbamate-based anions **32** or **38** (Figure 1.12). In particular, we took advantage of the electron donicity of dithiocarbamate catalysts to design a catalytic EDA strategy where the organocatalyst acts as the donor partner. A wide range of radical precursors **37**, derived from abundant feedstock, delivered photoactive EDA complexes upon aggregation with the catalytic donor (Figure 1.12, orange box). Excitation with blue light granted access to stabilized and non-stabilized alkyl radicals, trifluoromethyl radicals, and nitrogen-centered radicals (**XXII**). The modular nature of the commercially available dithiocarbamate and xanthate catalysts (including the ability to be turned over *via* two possible manifolds, hydrogen atom transfer (HAT) or SET), allowed us to develop mechanistically distinct net-reductive and redox-neutral processes. This aspect highlights the novelty of our methodology since catalytic EDA strategy for the development of net-reductive transformations was yet to be realized.

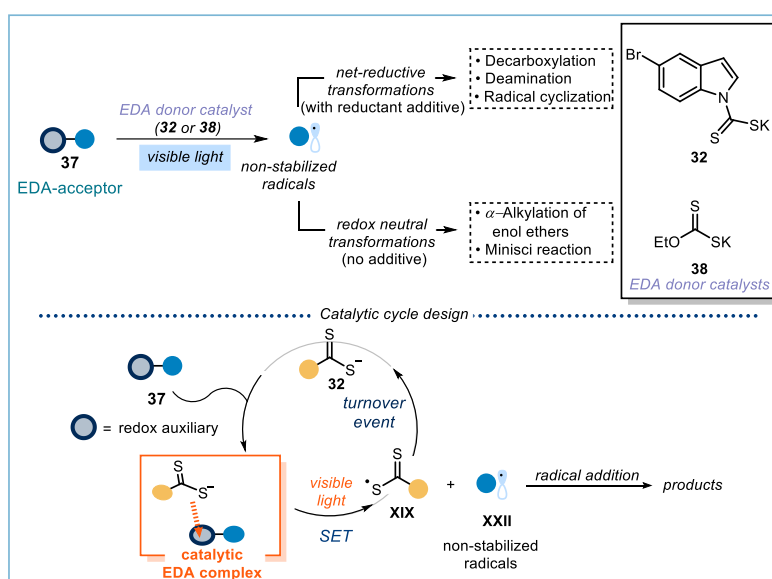


Figure 1.12 Catalytic EDA strategy exploiting dithiocarbamate-based scaffold as catalytic donor.

Mechanistic investigations by means of quantum yield determinations suggested that a closed catalytic cycle was operative in all the developed transformations, showcasing the propensity of the catalyst to drive each catalytic cycle. Finally, the functionalization of pharmaceutically relevant compounds and the combination of our radical generation strategy with asymmetric Brønsted-acid catalysis highlighted the generality of our approach.

³⁸ de Pedro Beato, E.; Spinnato, D.; Zhou, W.; Melchiorre, P. "A General Organocatalytic System for Electron Donor–Acceptor Complex Photoactivation and Its Use in Radical Processes" *J. Am. Chem. Soc.* **2021**, *143*, 12304–12314.

Chapter II

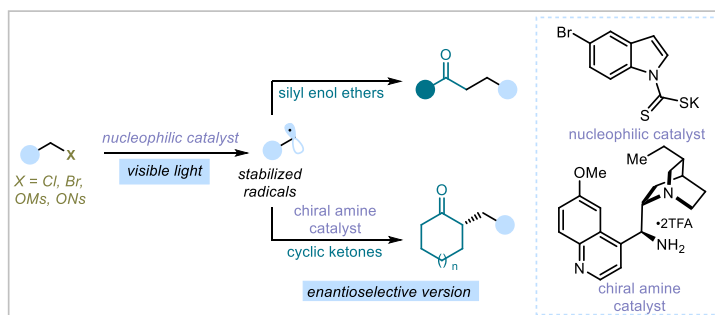
A Photochemical Organocatalytic Strategy for the α -Alkylation of Ketones by using Radicals

Target

Study and development of a new radical-based strategy for the α -alkylation of ketones and its implementation in asymmetric organocatalysis.

Tool

Using the nucleophilic character of a dithiocarbamate catalyst to activate alkyl halides and then generate radicals, which are intercepted by nucleophilic silyl enol ethers. The use of a cinchona-based chiral amine catalyst allowed the development of a stereoselective version of the designed transformation.¹



2.1 Introduction

The α -alkylation of ketones is a fundamental C-C bond forming process.² Usually, the reaction of highly nucleophilic alkali metal enolates **I** with alkyl halides delivers the desired α -functionalized ketone **3** (Figure 2.1) through bimolecular nucleophilic substitution (S_N2) pathway.³ This ionic strategy has been widely used in organic synthesis, however it does not come without limitations. Indeed, the strong basicity and high nucleophilicity of enolates of type **I** usually causes poor selectivity and incompatibilities with many polar functional groups. For example, double alkylation can be a significant side reaction if the product could undergo a second deprotonation event (product **1**, Figure 2.1).

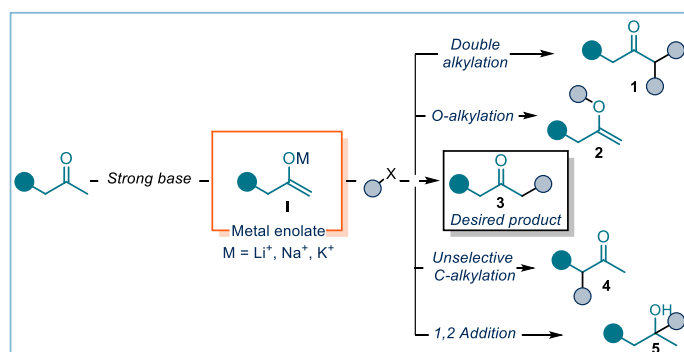


Figure 2.1. Challenges in the two electron-based alkylation of enol ethers.

¹ The project discussed in this chapter was conducted in collaboration with Dr. Bertrand Schweitzer-Chaput, Dr. Giulio Goti, and Dr. Maksim Ošeka. I was involved in the optimization studies, scope evaluation, and in the mechanistic studies. This work has been published, see: Spinnato, D.; Schweitzer-Chaput, B.; Goti, G.; Ošeka, M.; Melchiorre, P. "A Photochemical Organocatalytic Strategy for the α -Alkylation of Ketones by using Radicals" *Angew. Chem. Int. Ed.* **2020**, 59, 9485–9490.

² (a) R. E. Ireland. "Organic Synthesis" **1969**, Prentice-Hall, Englewood Cliffs. (b) Carreira, E. M.; Kvaerno, L. "Classics in Stereoselective Synthesis" **2007**, Wiley-VCH, Weinheim.

³ (a) Carey, F. A.; Sundberg, R. J. "Advanced Organic Chemistry Part B: Reactions and Synthesis" **2007**, 5th Ed., Springer, New York. (b) Kuwajima, I.; Nakamura, E. "Quaternary ammonium enolates as synthetic intermediates. Regiospecific alkylation reaction of ketones" *J. Am. Chem. Soc.* **1975**, 97, 3257–3258.

Additionally, other by-products can be formed under these conditions, including the *O*-alkylation product **2**, the adduct arising from alkylation at the more substituted position (product **4**), or the 1,2 addition product **5**.⁴ Therefore, the development of new methodologies that avoid the use of metal enolates is of synthetic importance.

Silyl enol ethers **6** (Figure 2.2), which are commonly employed as stable enolate surrogates, are easy to synthesize and can be stored for months without the need of special precautions.⁵ Their reactivity has been used extensively in nucleophilic addition chemistry (Michael additions, aldol additions/condensations, and Mannich-type transformations).⁶ Nevertheless, their relatively low nucleophilicity⁷, if compared to the corresponding alkali metal enolate **I**, hampers the alkylation with alkyl halides via an S_N2 path. To overcome this limitation, strong Lewis acids, such as TiCl₄, FeCl₃, or InBr₃, were used to activate alkyl halides **7** towards the formation of carbocations, thus facilitating S_N1 substitution processes (Figure 2.2).⁸ Needless to say, this approach can be operational only when stabilized carbocations of type **II** can be formed.

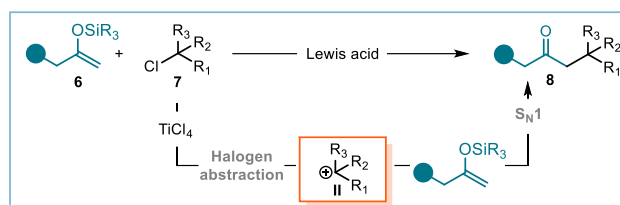


Figure 2.2. S_N1-based alkylation of silyl enolates.

On the other hand, open-shell intermediates have offered new opportunities in C-C bond formation processes⁹ and their high reactivity might be advantageous in engaging the weakly nucleophilic silyl enol ethers. In principle, moving from an ionic logic to a radical reactivity scheme could avoid issues related with chemoselectivity and functional group tolerance. In order to obtain the desired reactivity and selectivity, a mild and efficient radical generation strategy is required. The most common radical generation strategies are discussed in the next section.

⁴ Caine, D. "Alkylations of Enols and Enolates. In Carbon-Carbon σ -Bond Formation" **1991**, Pergamon Press: Oxford, U.K.
⁵ (a) Stork, G.; Hudrlik, P. F. "Isolation of ketone enolates as trialkylsilyl ethers" *J. Am. Chem. Soc.* **1968**, *90*, 4462-4464; (b) J. K. Rasmussen, "O-Silylated Enolates-Versatile Intermediates for Organic Synthesis" *Synthesis* **1977**, 91-110.
⁶ (a) Narasaka, K.; Soai, K.; Mukaiyama, T. "The new Micheal reaction" *Chem. Lett.* **1974**, *3*, 1223-1224. (b) Evans, D. A.; Rovis, T.; Kozłowski, M. C.; Downey, C. W.; Tedrow, J. S. "Enantioselective Lewis Acid Catalyzed Michael Reactions of Alkylidene Malonates. Catalysis by C₂-Symmetric Bis(oxazoline) Copper(II) Complexes in the Synthesis of Chiral, Differentiated Glutarate Esters" *J. Am. Chem. Soc.* **2000**, *122*, 9134-9142. (c) Mukaiyama, T.; Narasaka, K.; Banno, K. "New aldol reaction" *Chem. Lett.* **1973**, *2*, 1011-1014. (d) Mukaiyama, T.; Banno, K.; Narasaka, K. "New cross-aldol reactions. Reactions of silyl enol ethers with carbonyl compounds activated by titanium tetrachloride" *J. Am. Chem. Soc.* **1974**, *96*, 7503-7509; (e) Kobayashi, S.; Ishitani, H. "Catalytic Enantioselective Addition to Imines" *Chem. Rev.* **1999**, *99*, 1069-1094.
⁷ Leonov, A. I.; Timofeeva, D. S.; Ofial, A. R.; Mayr, H. "Metal Enolates - Enamines - Enol Ethers: How Do Enolate Equivalents Differ in Nucleophilic Reactivity?" *Synthesis* **2019**, *51*, 1157-1170.
⁸ (a) Reetz, M. T.; Maier, W. F. "tert-Alkylation of Ketones and Aldehydes" *Angew. Chem. Int. Ed.* **1978**, *17*, 48-49. (b) Nishimoto, Y.; Yasuda, M.; Baba, A. "Coupling Reaction of Alkyl Chlorides with Silyl Enolates Catalyzed by Indium Trihalide" *Org. Lett.* **2007**, *9*, 4931-4934; (c) Nishimoto, Y.; Saito, T.; Yasuda, M.; Baba, A. "Indium-catalyzed coupling reaction between silyl enolates and alkyl chlorides or alkyl ethers" *Tetrahedron* **2009**, *65*, 5462-5471.
⁹ (a) Renaud, P.; Sibi, M. P. "Radicals in Organic Synthesis" **2001** Wiley-VCH: Weinheim, Germany. (b) Chatgililoglu, C.; Studer, A. "Encyclopedia of Radicals in Chemistry, Biology and Materials" **2012** John Wiley & Sons. (c) Yan, M.; Lo, J. C.; Edwards, J. T.; Baran, P. S. "Radicals: Reactive Intermediates with Translational Potential" *J. Am. Chem. Soc.* **2016**, *138*, 12692-12714.

2.2 Radical Generation Strategies: an Overview

Over the years, the synthetic chemistry community has witnessed the development of many ingenious radical generation strategies. These methodologies can be categorized depending on which chemical property they rely on: (i) those taking advantage of the redox behavior of the radical precursor; and (ii) those focusing on the low bond-dissociation energy (BDE) within a specific substrate.¹⁰

2.2.1 Methods relying on redox properties

The redox behavior of an organic molecule is governed mostly by the electronic nature of the functional groups it possesses. Traditionally, stoichiometric amounts of metal-based reductants or oxidants were used to access open-shell intermediates **III** through single-electron transfer (SET), followed by fragmentation (Figure 2.3a).^{9a} However, regardless of the chemical efficiency in such radical generation processes, there are significant environmental concerns due to the need for harsh reaction conditions and the unavoidable production of toxic metal waste. This is why researchers have focused on the development of more sustainable alternatives where the metal salt is used in catalytic amount, while an organic compound is used as the final oxidant or reductant.^{9a} Electrochemistry is an environmental friendly alternative in which electrical energy is used to break chemical bonds and promote the generation of the desired radical (Figure 2.3b).¹¹ In this case, SET takes place at the interface between the electrodes (cathode or anode) and the solution. Judicious selection of the appropriate applied potential enables the selective reduction or oxidation of specific functional groups within the substrates. However, electrochemical approaches suffer from mass transport issues due to the biphasic nature of the reaction lowering the reaction kinetics. In addition, passivation, *i.e.* the accumulation of material on the electrodes' surface, can hamper the desired reactivity.¹¹

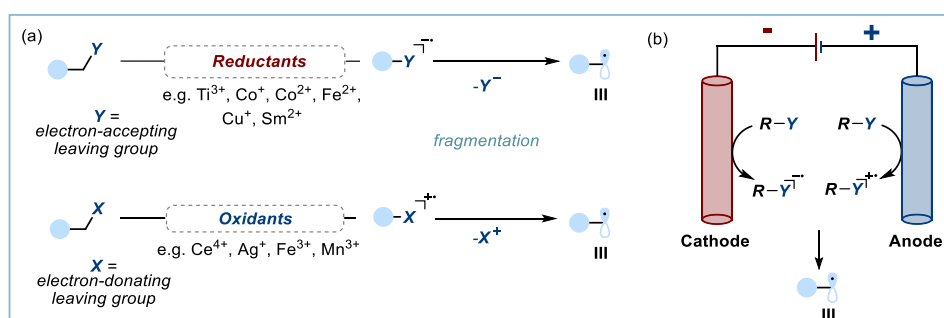


Figure 2.3. Radical generation strategies capitalizing on the redox potential of the starting material.

The increasing demand for mild and catalytic approaches to access the single-electron reactivity of organic compounds has found in photoredox catalysis a valid alternative to more traditional approaches based on stoichiometric oxidant or reductant (Figure 2.4). The ability of photocatalysts to reach their electronically excited state (**PC***) upon excitation of low-energy visible light, and then activate redox-active compounds towards radical formation has allowed the development of radical processes that were previously unattainable.¹² Chemists can tailor the redox properties of the photocatalysts' excited state to match the redox potentials of the substrates, enabling wide diversity in substrates susceptible to SET activation.¹³

¹⁰ Lalevée, J.; Fouassier, J. P. "Encyclopedia of Radicals in Chemistry, Biology and Materials, Vol 1." 2012, John Wiley & Sons.

¹¹ (a) Yan, M.; Kawamata, Y.; Baran, P. S., "Synthetic Organic Electrochemical Methods Since 2000: On the Verge of a Renaissance" *Chem. Rev.* 2017, 117, 13230-13319. (b) Kingston, C.; Palkowitz, M. D.; Takahira, Y.; Vantourout, J. C.; Peters, B. K.; Kawamata, Y.; Phil S. Baran "A Survival Guide for the "Electro-curious" *Acc. Chem. Res.* 2020, 53, 72-83.

¹² (a) Shaw, M. H.; Twilton, J.; MacMillan, D. W. C. "Photoredox Catalysis in Organic Chemistry" *J. Org. Chem.* 2016, 81, 6898-6926. (b) Matsui, J. K.; Lang, S. B.; Heitz, D. R.; Molander, G. A. "Photoredox-mediated Routes to Radicals: the Value of Catalytic Radical Generation in Synthetic Methods Development" *ACS Catal.* 2017, 7, 2563-2575.

¹³ Buzzetti, L.; Crisenza, G. E. M.; Melchiorre, P. "Mechanistic Studies in Photocatalysis" *Angew. Chem. Int. Ed.* 2019, 58, 3730-3747.

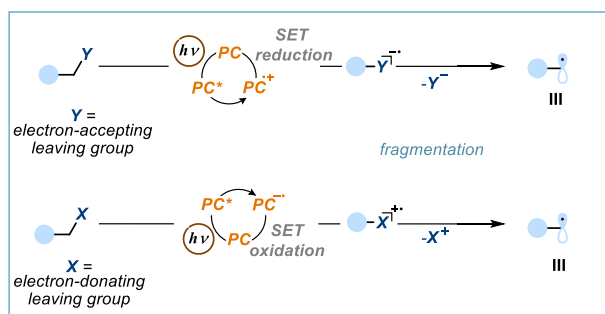


Figure 2.4. Photocatalysis for the generation of radicals. PC: photocatalyst; SET: single-electron transfer.

2.2.2 Methods relying on bond dissociation energy

When a target substrate possesses in its scaffold a bond with a low bond dissociation energy (BDE), radicals can be usually generated through hydrogen atom abstraction (HAT) or halogen atom abstraction (XAT). Historically, this approach relied on the use of stoichiometric radical initiators (In-In, Figure 2.5), which are hazardous and highly unstable compounds possessing one or more weak bonds (e.g. oxygen-oxygen).¹⁴

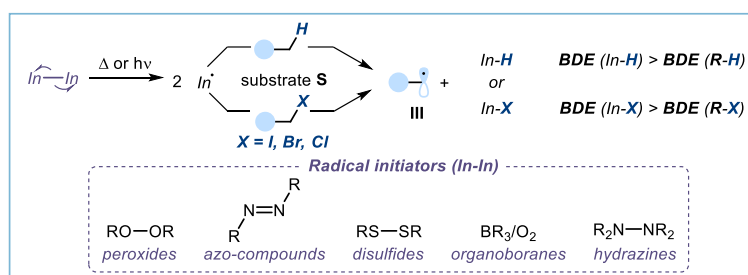


Figure 2.5. The use of radical initiators (In-In) for radical generation.

Thermal (Δ) or high-energy photochemical (UV-light) activation can homolyze weak σ -bonds, delivering free radicals. The resulting fleeting open-shell species ($\text{In}\cdot$) can react with the substrate through hydrogen or halogen abstraction, delivering the target radical **III** (Figure 2.5). As a rule of thumb, radical-initiated reactions proceed efficiently when strong bonds are formed at the expense of much weaker bonds (e.g. $\text{BDE}(\text{In-H}) > \text{BDE}(\text{R-H})$).¹⁵

The advent of photoredox catalysis has also influenced BDE-based strategies, offering initiator-free access to open-shell species. Specific photocatalysts,¹⁶ such as tetrakis(tetrabutylammonium) decatungstate

¹⁴ Denisov, E. T.; Denisova, T. G.; Pokidova, T. S. "Handbook of Free Radical Initiators" **2005**, John Wiley & Sons.

¹⁵ Gilbert, B. C.; Parsons, A. F. "The use of free radical initiators bearing metal-metal, metal-hydrogen and non-metal-hydrogen bonds in synthesis" *J. Chem. Soc., Perkin Trans.* **2002**, 2, 367–387.

¹⁶ For catalytic HAT processes involving the use of TBADT see: (a) Tzirakis, M. D.; Lykakis, I. N.; Orfanopoulos, M. "Decatungstate as an efficient photocatalyst in organic chemistry" *Chem. Soc. Rev.* **2009**, 38, 2609–2621. (b) Murugesan, V.; Ganguly, A.; Karthika, A.; Rasappan, R. "C–H Alkylation of Aldehydes by Merging TBADT Hydrogen Atom Transfer with Nickel Catalysis" *Org. Lett.* **2021**, 23, 5389–5393. (c) Quattrini, M. C.; Fujii, S.; Yamada, K.; Fukuyama, T.; Ravelli, D.; Fagnoni, M.; Ryu, I. "Versatile cross-dehydrogenative coupling of heteroaromatics and hydrogen donors via decatungstate photocatalysis" *Chem. Commun.* **2017**, 53, 2335–2338. (d) Laudadio, G.; Deng, Y.; van der Wal, K.; Ravelli, D.; Nuño, M.; Fagnoni, M.; Guthrie, D.; Sun, Y.; Noël, T. "C(sp³)-H functionalizations of Light Hydrocarbons Using Decatungstate Photocatalysis in Flow" *Science*, **2020**, 369, 92–96. For the use of benzophenone-based catalyst for HAT-mediated radical generation see: (e) Tripathi, C. B.; Ohtani, T.; Corbetta, M. T.; Ooi, T. "Photoredox ketone catalysis for the direct C–H imidation and acyloxylation of arenes" *Chem. Sci.* **2017**, 8, 5622–5627. (f) Shen, Y.; Gu, Y.; Martin, R. "sp³ C–H Arylation and Alkylation Enabled by the Synergy of Triplet Excited Ketones and Nickel Catalysts" *J. Am. Chem. Soc.* **2018**, 140, 12200–12209.

(TBADT), upon near-ultraviolet (UV) light irradiation reach an excited state that can *directly* abstract hydrogen atoms from weak to strong C(sp³)-H fragments (Figure 2.6).¹⁷ However, due to the abundance of C-H bonds in organic molecules, achieving selectivity in the HAT step can be difficult.

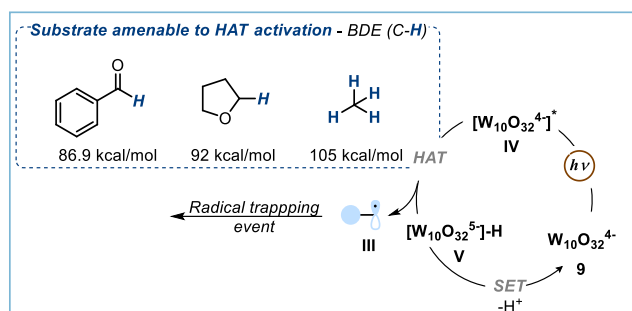


Figure 2.6. Direct HAT from photocatalyst's excited state.

Photocatalysis has also been used for the generation of alkyl radicals from readily available alkyl or aryl halides (iodides or bromides) via halogen atom abstraction manifold (Figure 2.7). Leonori and co-workers demonstrated that tertiary amines, such as triethylamine, could undergo photoredox-mediated oxidation-deprotonation by an excited-state photocatalyst (PC*), to generate an α -amino radical VI capable of promoting cleavage of carbon-halogen bonds. This sequence affords open-shell intermediates III through radical abstraction of the halogen (X) atom within the substrate scaffold 10.¹⁸ This manifold has been used to develop a wide number of transformations, however it could not be extended to the activation of more stable and inexpensive alkyl/aryl chlorides. Furthermore, the chemistry was limited to the formation of *nucleophilic* carbon-centered radicals.

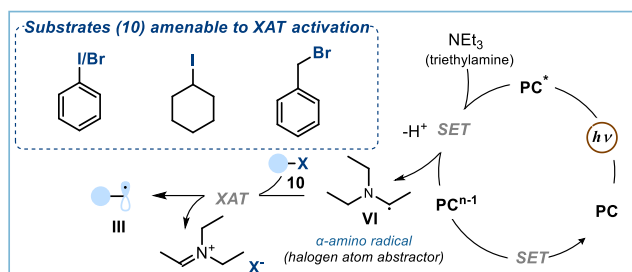


Figure 2.7. Photoredox catalysis for the generation of alkyl radical through indirect XAT.

For the use of Eosin Y in HAT-mediated radical generation see: (g) Fan, X.; Rong, J.; Wu, H.; Zhou, Q.; Deng, H.; Tan, J. Da; Xue, C.; Wu, L.; Tao, H.; Wu, J. "Eosin Y as a Direct Hydrogen-Atom Transfer Photocatalyst for the Functionalization of C-H Bonds" *Angew. Chem. Int. Ed.* **2018**, *57*, 8514–8518. For a review on photocatalyzed HAT processes see: (h) Capaldo, L.; Ravelli, D.; Fagnoni, M. "Direct Photocatalyzed Hydrogen Atom Transfer (HAT) for Aliphatic C-H Bonds Elaboration" *Chem. Rev.* **2022**, *122*, 1875–1924.

¹⁷ Luo, Y. R. "Handbook of Bond Dissociation Energies in Organic Compounds" **2002**, CRC press.

¹⁸ Constantin, T.; Zanini, M.; Regni, A.; Sheikh, N. S.; Juliá, F.; Leonori, D. "Aminoalkyl radicals as halogen-atom transfer agents for activation of alkyl and aryl halides" *Science*, **2020**, *367*, 1021–1026.

2.3 Thiocarbonyl-based compounds

The use of thiocarbonyl-containing substrates offers a useful alternative for the generation of open-shell intermediates within the context of BDE-based methodologies. The thiocarbonyl bond is inherently weak due to the poor π -orbital overlap between carbon and sulphur, which offers a rich and diverse chemistry.¹⁹ In particular, these compounds can deliver carbon-centered radical under mild conditions. The use of thiocarbonyl-containing compounds for radical generation will be discussed in the next sections.

2.3.1 Barton esters

In the early 1980's, Nobel Laureate D. H. R. Barton introduced the thiocarbonyl-based reagents **13** (Figure 2.8a) as efficient radical precursors.²⁰

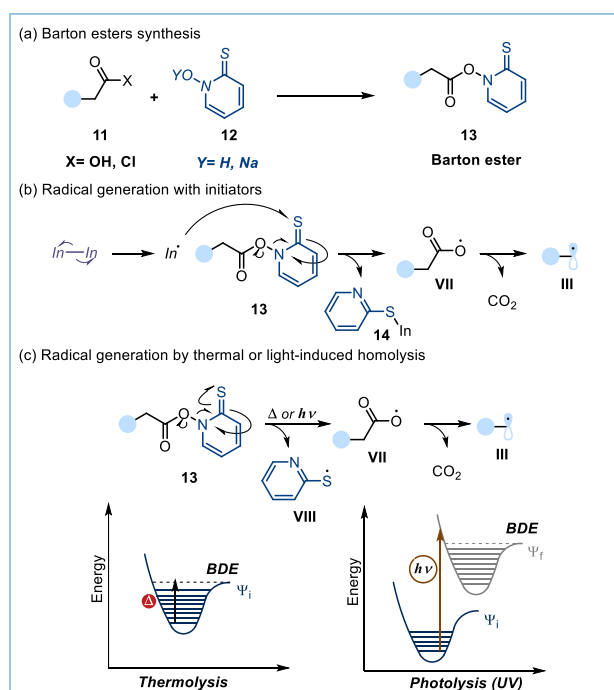


Figure 2.8. a) Barton esters synthesis. b) Generation of radicals by using initiators. c) Heat or light-promoted radical generation from Barton esters.

These compounds, known as Barton esters, can be easily synthesized from *N*-hydroxy-2-thiopyridone **12** and the desired carboxylic acid **11** or its acyl chloride derivative. Radical generation from Barton esters **13** relies on the extremely weak N-O bond; the BDE of the N-O bond in **13** has been calculated to be approximately 28 kcal/mol.²¹ Cleavage of N-O bonds can be achieved by use of radical initiators, thermal energy, or light irradiation. In the first case, the fragmented initiator *In*• reacts at sulphur within **13**, promoting the formation of the carboxylic acid radical **VII** and aromatic byproduct **14** (Figure 2.8b). Finally, **VII** undergoes fast and irreversible BDE decarboxylation to deliver the desired carbon-centered radical **III**.

¹⁹ Crich, D.; Quintero, L. "Radical chemistry associated with the thiocarbonyl group" *Chem. Rev.* **1989**, *89*, 1413–1432.

²⁰ (a) Barton, D. H. R.; Crich, D.; Motherwell, W. B. "New and improved methods for the radical decarboxylation of acids" *J. Chem. Soc., Chem. Commun.* **1983**, 939–941. (b) Barton, D. H. R.; Hervé, Y.; Potier, P.; Thierry, J. "Reductive Radical Decarboxylation of Amino-Acids and Peptides" *J. Chem. Soc., Chem. Commun.* **1984**, 1298–1299. (c) Barton, D. H. R.; Crich, D.; Motherwell, W. B. "The Invention of New Radical Chain Reactions. Part VII. Radical Chemistry of Thiohydroxamic Esters: A New Method for the Generation of Carbon Radicals from Carboxylic Acids" *Tetrahedron* **1985**, *41*, 3901–3924.

²¹ For computational details, see: Allonas, X.; Dietlin, C.; Fouassier, J.-P.; Casiraghi, A.; Visconti, M.; Norcini, G.; Bassi, G. "Barton Esters as New Radical Photoinitiators for Flat Panel Display Applications" *J. Photopolym. Sci. Technol.* **2008**, *21*, 505–509.

Due to the weak nature of the N-O bond, spontaneous homolysis occurs at temperatures higher than 62 °C. Therefore, upon applied thermal energy, ester **13** undergoes N-O homolytic cleavage, delivering the 2-pyridylthiyl radical **VIII** and the oxygen-centered radical **VII**, which furnishes the desired carbon-centered radical **III** after extrusion of carbon dioxide (Figure 2.8c). In addition, compounds of type **13** possess an absorption maxima in the near UV region ($\lambda_{\max} \approx 365$ nm), ascribed to the chromophoric thiopyridone moiety.²² Upon irradiation with UV light, the $\Psi_i \rightarrow \Psi_f$ (HOMO to LUMO) electronic transition is promoted, ultimately delivering the open-shell species **III** (Figure 2.7c).

2.3.2 Xanthate derivatives

The use of thiocarbonyl compounds to generate carbon-centered radicals is not restricted to Barton esters. Zard and co-workers introduced xanthates or dithiocarbonates **17** as versatile reagents that can engage in efficient radical chain processes (Figure 2.9).²³ These compounds can be easily synthesized by nucleophilic substitution from dithiocarbamate or xanthate anions **16** with a suitable alkyl electrophile **15** (Figure 2.8a). Like Barton esters, xanthates or dithiocarbonates are characterized by a weak C-S bond that undergoes homolytic cleavage when thermal or photonic energy is applied. However, the use of initiators represents the most common approach to drive radical processes involving dithiocarbonates. When using initiators, the resulting radical In^\bullet adds to the thiocarbonyl sulphur atom within **17** promoting C-S bond breaking, ultimately leading to the thermodynamically favored formation of **18** and the target radical **III** (Figure 2.9b).

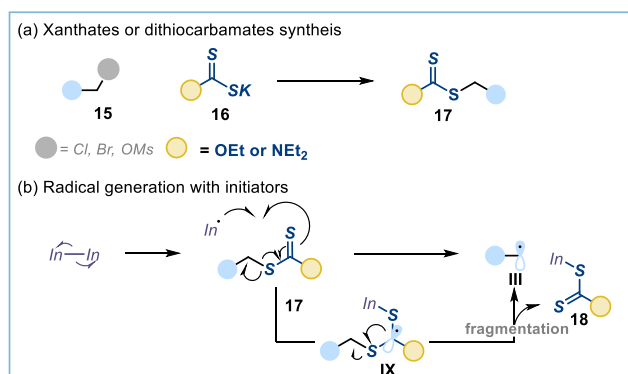


Figure 2.9. a) Xanthates and dithiocarbonates synthesis. b) Radical generation from xanthates by means of initiators.
In: Initiator.

When dithiocarbamate or xanthate derivatives are adorned with a chromophoric unit that enables efficient light absorption, irradiation can directly trigger the radical generation process (Figure 2.10). For example, the weak C-S bond within the carbazole-based dithiocarbamate **19** could be homolytically cleaved when irradiated with UV-light ($\lambda_{\max} \approx 365$ nm, Figure 2.10a).²⁴ Another class of dithiocarbamate-based compounds where light irradiation triggers radical generation is acyl xanthates **20**.²³ Due to the additional

²² (a) Barton, D. H. R.; Blundell, P.; Jaszberenyi, J. C. "Quantum Yields in the Photochemically Induced Radical Chemistry of Acyl Derivatives of Thiohydroxamic Acids" *J. Am. Chem. Soc.* **1991**, *113*, 6937–6942. (b) Bohne, C.; Boch, R.; Scaiano, J. C. "Exploratory Studies of the Photochemistry of N-hydroxypyridine-2-thione Esters. Generation of Excited Radicals by Laser Flash Photolysis and in a Conventional Fluorescence Spectrometer" *J. Org. Chem.* **1990**, *55*, 5414–5418.

²³ (a) Barton, D. H. R.; Zard, S. Z. "Invention of new reactions useful in the chemistry of natural products" *Pure Appl. Chem.* **1986**, *58*, 675–684. (b) Zard, S. Z. "On the Trail of Xanthates: Some New Chemistry from an Old Functional Group" *Angew. Chem. Int. Ed.* **1997**, *36*, 672–685. (c) Quiclet-Sire, B.; Zard, S. Z. "Powerful Carbon-Carbon Bond Forming Reactions Based on a Novel Radical Exchange Process" *Chem. Eur. J.* **2006**, *12*, 6002–6016.

²⁴ Lalevée, J.; Blanchard, N.; El-Roz, M.; Allonas, X.; Fouassier, J. P. "New Photoinitiators: Respective Role of the Initiating and Persistent Radicals" *Macromolecules* **2008**, *41*, 2347–2352.

carbonylic moiety within their core, these compounds have a yellow color and can deliver acyl radicals **X** upon excitation with visible light (Figure 2.10b).

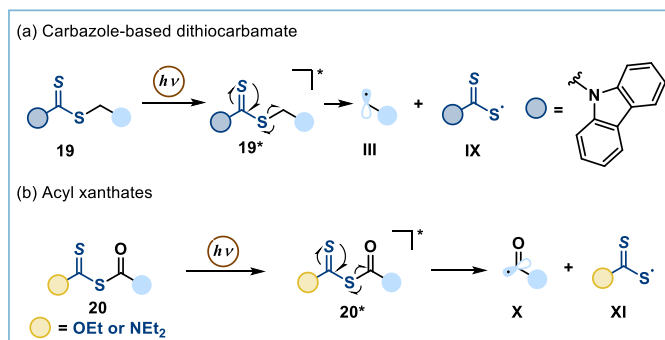


Figure 2.10. Photolytic cleavage of carbazole-based dithiocarbamates and acyl xanthates.

Radical reactions involving xanthate intermediates are usually governed by the so-called *degenerative xanthate transfer* process, which is characterized by specific thermodynamic features.²⁵ A general picture representing this transfer manifold is shown in Figure 2.11b. The first stage consists of an initiation step, driven by an external agent or by light/heat-promoted homolysis of xanthate **17a**, which affords radical **III**. The fate of this open-shell intermediate can follow two different avenues: *i*) in the first scenario, olefin **21** intercepts **III** forging the desired C-C bond within **XIII** (right side in Figure 2.11b), which can further react with a second molecule of **17a** (*group transfer step*). Fragmentation of **XIV** provides a second equivalent of **III** ensuring an efficient chain propagation and the formation of the desired group transfer product **24**; *ii*) alternatively, upon capture of radical **III** by the starting xanthate **17a**, the highly stabilized open-shell intermediate **XV** is formed. Importantly, the release of a high-in-energy ethyl radical from the ethoxy group does not represent an available pathway due to the unfavorable energetic requirements to break the strong C-O bond over the labile C-S bond within **XV** (left side in Figure 2.11b).²³

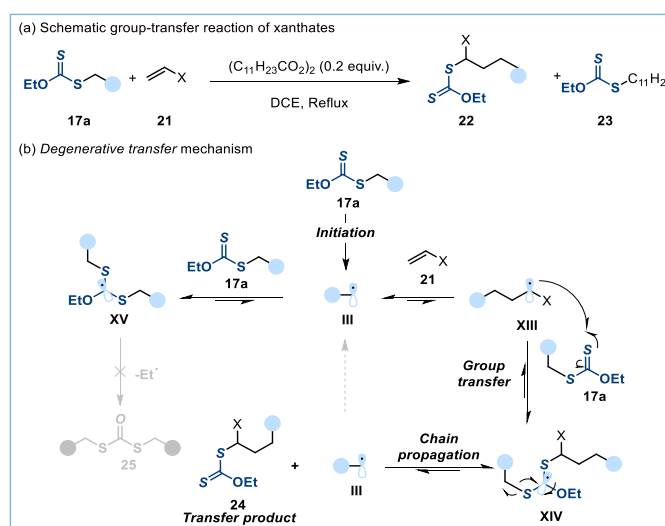


Figure 2.11. Group transfer reaction of xanthate.

²⁵ (a) Delduc, P.; Tailhan, C.; Zard, S. Z. "A convenient source of alkyl and acyl radicals" *J. Chem. Soc., Chem. Commun.* **1988**, 308-310. (b) Quiclet-Sire, B.; Zard, S. Z. "Fun with radicals: Some new perspectives for organic synthesis" *Pure Appl. Chem.* **2011**, *83*, 519-551. (c) Quiclet-Sire, B.; Zard, S. Z. "Radical Instability in Aid of Efficiency: A Powerful Route to Highly Functional MIDA Boronates" *J. Am. Chem. Soc.* **2015**, *137*, 6762-6765.

As depicted in Figure 2.11, every step involved in this *degenerative group transfer* manifold is reversible and this brings about thermodynamic considerations. Studies from Zard demonstrated that efficient group transfer propagation in xanthate chemistry requires certain thermodynamic features to be met. Specifically, dragging the equilibrium towards the formation of the key intermediate **XIV** requires the progenitor radical **XIII** to be less stable (higher BDE) than radical **III**, which ultimately leads to a successful radical addition to non-activated alkenes **21**.^{23,25, 26} This addition-fragmentation scenario effectively regulates the concentration of reactive radicals in solution and avoids their over-accumulation, suppressing the formation of side products (e.g. arising from radical-radical coupling). Unfortunately, the thermodynamic requirements that ensure degenerative xanthate transfer processes forbid access to non-stabilized radicals of type **III**. Indeed, in this scenario, **XIII** would be more stable than **III** and its further reactivity in a group transfer manifold would be thermodynamically unfavored preventing the reaction from proceeding. In other words, the process would lack of a sufficient driving force to go from **XIII** to **24**. An interesting example which highlights the importance of the relative stability between radicals **XIII** and **III** (Figure 2.11) in degenerative group transfer reactions was developed by Zard and co-worker in 2015.^{25c} The authors compared the radical addition of xanthate **17a** to allyl boronate **24** and vinyl boronate **26** (Figure 2.12a-b). The reaction efficiently proceeded when **24** was used as the radical trap; however, when the vinyl congener **26** was employed as trap, the desired product was not obtained. The authors claimed that, when radical **III** is trapped by **24**, the ensuing open-shell intermediate **XVI** had comparable stability to typical secondary carbon-centered radical, with minimal influence of adjacent boronate group (Figure 2.12a), so fulfilling the thermodynamic rule described before. Contrarily, radical **XVII** is thermodynamically more stable than **III** due to delocalization onto the vicinal p-orbital of the boron atom, hence hampering the desired reactivity (Figure 2.12b). In contrast, a vinyl *N*-methyl imidodiacetic acid (MIDA) boronate **28** was a suitable olefin partner (Figure 2.12c). This was because the boron atom could not delocalize the adjacent radical since its vacant p-orbital was occupied due to a strong Lewis pair interaction between the boron and nitrogen atom of the MIDA group. The non-stabilized nature of **XVIII** could permit the degenerative group transfer manifold to occur. Therefore, the reaction between **17a** and **28** proceeded smoothly delivering the desired product in high yield, proving the necessity of radical of type **XIII** to be more stable than their progenitor **III**.

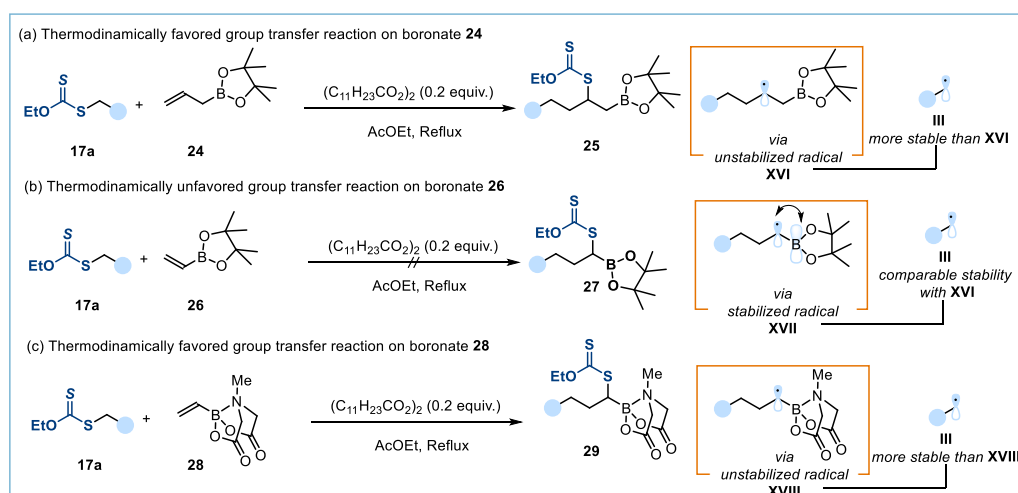


Figure 2.12. Radical stability influence on the xanthate addition on allyl and vinyl boronate.

²⁶ Reversible addition-fragmentation chain-transfer polymerization (RAFT) are based on these principles. For a perspective in RAFT polymerization see: Perrier, S. "50th Anniversary Perspective: RAFT Polymerization—A User Guide" *Macromolecules* **2017**, *50*, 7433-7447.

2.4 A new photo-organocatalytic strategy for radical generation

The strategies for radical generation reported so far rely on low BDEs of specific compounds or exploit the intrinsic redox properties of the radical precursors. Recently, our group has developed a new catalytic strategy for radical generation that relies only on the ability of the substrate to act as a polar electrophile.²⁷ This new strategy was inspired by the rich radical chemistry of dithiocarbamates developed by Zard and discussed in Section 2.3.2.^{23,25} To move the Zard's chemistry from a stoichiometric into a catalytic scheme, it was necessary to design a nucleophilic dithiocarbonyl catalyst²⁸ (DTC catalyst **A**, Figure 2.13) that could activate alkyl (pseudo)halides **15** through a bimolecular nucleophilic substitution (S_N2) pathway. The new catalyst was adorned with a chromophoric unit so to allow intermediate **30**, generated upon the S_N2 path, to absorb low energy photons (blue light). This photochemical step promoted a C-S bond cleavage, producing the desired radical **III** and the sulphur-centered radical **XIX**. In this strategy, the ability to reduce the sulphur-centered radical **XIX** was fundamental to enable catalyst turnover, thus realizing a catalytic process.

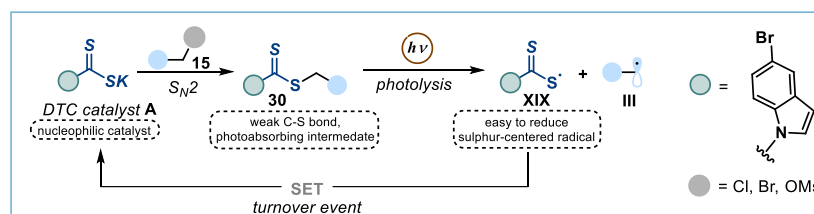


Figure 2.13. Dithiocarbonyl catalyst to promote the formation of radicals via an S_N2 pathway.

In order to be successful, the new catalytic system had to fulfill specific requirements: *i*) the DTC catalyst had to be a good nucleophile to effectively deliver intermediate **30** via S_N2 reaction with alkyl (pseudo)halides; *ii*) intermediate **30** had to absorb visible light; *iii*) the BDE of the C-S bond in **30** needed to be low enough to undergo homolytic cleavage upon excitation; *iv*) finally, the sulphur-centered radical **XIX**, produced after C-S bond cleavage, should have sufficient kinetic stability²⁹ and be easy to reduce in order to secure effective catalyst turnover. These requirements were met by the dithiocarbamate salt **A**. This catalyst was used to deliver Giese-type addition products by using alkyl electrophile **15** as radical precursors (Figure 2.14).²⁷ These electrophilic precursors (e.g. benzyl chloride) were unreactive under previously reported radical generation strategies due a difficult SET reduction ($E_{\text{red}}(\text{BnCl}/\text{BnCl}^-) = -2.13$ V vs SCE)³⁰. Indeed, most of the commonly used photoredox catalysts do not possess such strong reducing excited states.³¹ Consequently, formation of benzyl radical would necessitate the use of stoichiometric amounts of highly reactive SET reductants, which would not be compatible with the majority of the functional groups found in organic compounds limiting the practicality of the methodology.²⁷ Contrarily, benzyl chloride is an archetypical substrate for S_N2 reactions and this makes it a well-suited substrate for activation by the nucleophilic catalyst **A**. Overall, activation of the substrates via nucleophilic substitution delivers the photo-absorbing intermediate **30**. Upon blue light irradiation (465 nm), homolytic cleavage of

²⁷ Schweitzer-Chaput, B.; Horwitz, M. A.; de Pedro Beato, E.; Melchiorre, P. "Photochemical generation of radicals from alkyl electrophiles using a nucleophilic organic catalyst" *Nat. Chem.* **2019**, *11*, 129-135.

²⁸ Duan, X.-H.; Maji, B.; Mayr, H. "Characterization of the nucleophilic reactivities of thiocarboxylate, dithiocarbonate and dithiocarbamate anions" *Org. Biomol. Chem.* **2011**, *9*, 8046-8050.

²⁹ The sulphur-centered radical **XIX** has to be persistent in order to be turned over. This aspect will be discussed in Section 2.6.5.

³⁰ Isse, A. A.; Falciola, L.; Mussinib, P. R.; Gennaro, A. "Relevance of electron transfer mechanism in electrocatalysis: the reduction of organic halides at silver electrodes" *Chem. Commun.* **2006**, 344-346.

³¹ Brasholz, M. "Super-reducing" photocatalysis: consecutive energy and electron transfers with polycyclic aromatic hydrocarbons" *Angew. Chem. Int. Ed.* **2017**, *56*, 10280-10281.

the weak C-S bond occurs, producing the carbon-centered radical **III** and dithiocarbonyl radical **XIX**. Radical **III** reacts with electron-poor olefins **31** to form a new C-C-bond. The resulting electrophilic radical **XX** abstracts a hydrogen atom from a stoichiometric organic reductant, such as γ -terpinene (shown in Figure 2.14), forming the desired product **33** and the bis-allylic radical **XXI**. At this stage, the turnover of catalyst **A** ($E(\mathbf{A}/\mathbf{XIX}) = +0.44$ V versus Ag/Ag^+ in CH_3CN)³² occurs through a thermodynamically favored SET reduction from the cyclohexadienyl radical **XXI** ($E_{\text{red}} = -0.05$ V versus Ag/Ag^+ in CH_3CN).³³

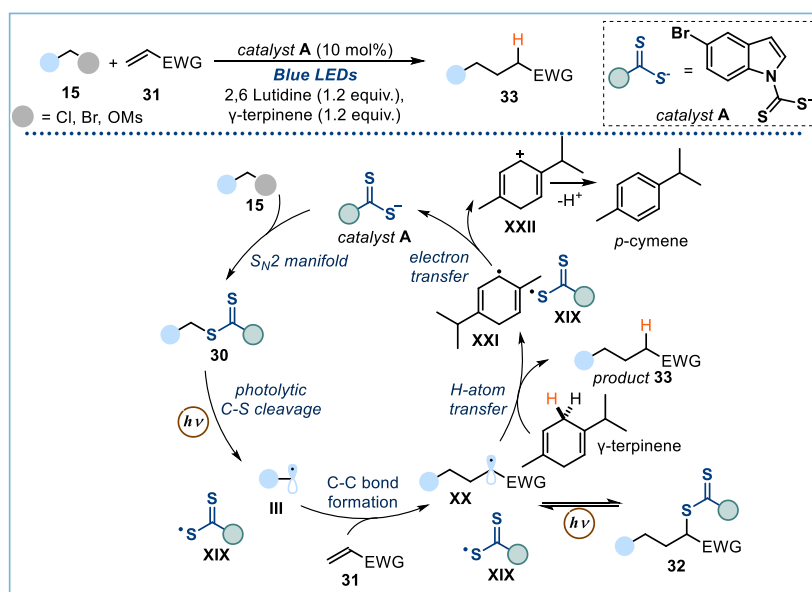


Figure 2.14. Giese-type addition reaction starting from alkyl (pseudo) halides. EWG: Electron-withdrawing group. DTC: Dithiocarbamate. LEDs: Light emitting diodes.

2.5 Target of the Project

The project discussed in this chapter aims at expanding the synthetic utility of the new photochemical catalytic radical generation strategy based on the dithiocarbonyl anion catalyst **A**.²⁷ In particular, we targeted the development of a protocol for the α -alkylation of ketones using non-activated alkyl halides as radical precursors. So far, only a limited number of reports have been disclosed for the radical functionalization of silyl enol ethers, which are discussed in the following section.

2.5.1 Radical-based α -functionalization of ketones

One of the most widely used approaches for the α -alkylation of ketones relies on the use of reactive alkali metal enolates as nucleophiles in $\text{S}_{\text{N}}2$ reactions with alkyl halides.³ However, this ionic approach was usually characterized by insufficient selectivity and poor functional group tolerance.⁴ Instead, radical-based chemistry had proven to be complementary to two-electron logic while offering new opportunities in C-C bond formation processes *under mild conditions*. So far, only a limited number of examples exploiting open-shell species had been developed for the α -alkylation of ketones. In 1990, Oshima and Utimoto developed a radical-based strategy for the α -perfluoroalkylation of trialkylsilyl enol ethers **34** (Figure

³² Dag, Ö.; Yaman, S. Ö.; Önal, A. M.; İsci, H. "Spectroelectrochemistry of Potassium Ethylxanthate, Bis(ethylxanthato)nickel(II) and Tetraethylammonium Tris(ethylxanthato)nickelate(II)" *J. Chem. Soc., Dalton Trans.* **2001**, 2819-2824.

³³ Bahtia, K.; Schuler, R. H. "Oxidation of Hydroxycyclohexadienyl Radical by Metal Ions" *J. Phys. Chem.* **1974**, *78*, 2335-2338.

2.15).³⁴ In this seminal report, perfluoro α -alkylation of ketones was possible by using perfluoro-iodides **35** as radical precursors in combination with $\text{Et}_3\text{B}/\text{O}_2$ as an initiating system. Mechanistically, the process proceeds as follows: *i*) in the initiation step, the $\text{Et}_3\text{B}/\text{O}_2$ mixture delivered highly reactive ethyl radical **XXIII** that, upon XAT, promoted the formation of perfluoro radical **XXIV** from **35**; *ii*) the electrophilic radical **XXIV** underwent a radical addition³⁵ into the silyl enol ether **34**, generating the radical intermediate **XXV**; *iii*) finally, a SET from **XXV** to a second molecule of perfluoroalkyl iodide **35** delivered the desired product **36** while generating a second equivalent of radical **XXIV**, which can efficiently propagate a radical chain.

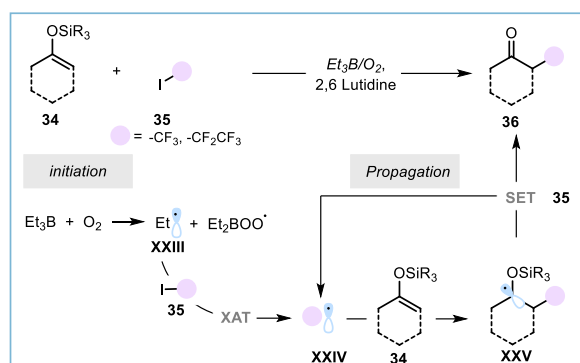


Figure 2.15. Radical α -perfluoroalkylation of enol ethers using $\text{Et}_3\text{B}/\text{O}_2$ as initiator. Et: ethyl

In 1994, Baciocchi and Muraglia showed that silyl enol ethers derived from aliphatic ketones (**37** and **40**, Figure 2.16) can undergo α -alkylation when an α -iodo ester **38** is employed as radical precursor in combination with Et_3B , leading to products **39** or **41**.³⁶ The approach was limited in terms of radical precursors and enolate traps, and it required hazardous radical initiator to drive the desired transformation.

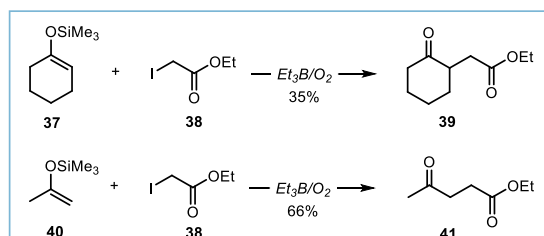


Figure 2.16. a) α -alkylation of enol ethers by means of $\text{Et}_3\text{B}/\text{O}_2$. Et: Ethyl

Since the renaissance of photoredox catalysis, many strategies have been developed to overcome the limitations linked to the use of radical initiators, also in the context of ketone alkylation. Twenty years after the seminal report by Oshima and Utimoto, the MacMillan group exploited the potential of photoredox catalysis to drive the α -perfluoroalkylation of ketones (Figure 2.17a).³⁷

³⁴ Miura, K.; Taniguchi, M.; Nozaki, K.; Oshima, K.; Utimoto, K. "Triethylborane induced perfluoroalkylation of silyl enol ethers or germyl enol ethers with perfluoroalkyl iodides" *Tetrahedron Lett.* **1990**, *31*, 6391–6394.

³⁵ Parsaee, F.; Senarathna, M. C.; Kannangara, P. B.; Alexander S. N.; Arche P. D. E.; Welin E.R. "Radical philicity and its role in selective organic transformations" *Nat. Rev. Chem.* **2021**, *5*, 486–499.

³⁶ Baciocchi, E.; Muraglia, E. "Synthesis of γ -haloesters and γ -ketoesters by homolytic addition of carbon radicals generated by α -haloesters and triethylborane to alkenes and silyl enol ethers" *Tetrahedron Lett.* **1994**, *35*, 2763 – 2766.

³⁷ Pham, P. V.; Nagib, D. A.; MacMillan, D. W. C. "Photoredox Catalysis: A Mild, Operationally Simple Approach to the Synthesis of α -Trifluoromethyl Carbonyl Compounds" *Angew. Chem. Int. Ed.* **2011**, *50*, 6119–6122.

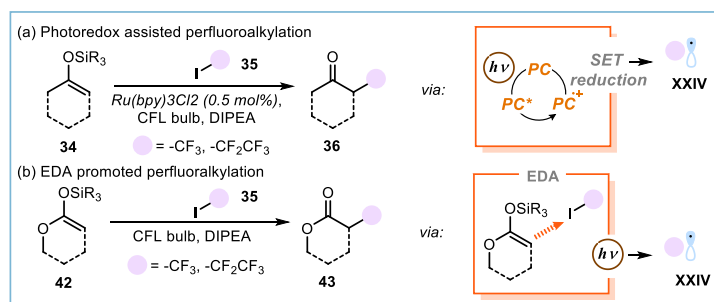


Figure 2.17. α -Perfluoroalkylation of enol ethers and silylketene acetals.

A ruthenium-based photocatalyst served to generate radical **XXIV** from **35** via an SET reduction. **XXIV** initiated a radical chain process similar to the one depicted in Figure 2.15a. Interestingly, if silylketene acetals **42** were used in place of silyl enol ethers, the photocatalyst was not required. In this case, the authors suggested that a photon-induced electron donor-acceptor (EDA) complex mechanism was likely to be operative (Figure 2.17b), in which the electron-rich acetal **42** acted as the donor, whereas the perfluoroalkyl iodide was electron-poor enough to accommodate electron density in its LUMO orbital.³⁸ While the methodology represented a step towards a general and mild procedure for the α -functionalization of ketone and ester surrogates, it was limited by the few radical precursors that could be employed. In 2019, Shang and Fu discovered that the combination of triphenylphosphine (PPh_3) and sodium iodide (NaI) catalyzed the radical alkylation of silyl enol ethers **44** with redox-active esters **45** via EDA complex-mediated decarboxylation (Figure 2.18). Additionally, the Togni's reagent **47** effectively delivered the α -trifluoromethylated ketone **48**.³⁹

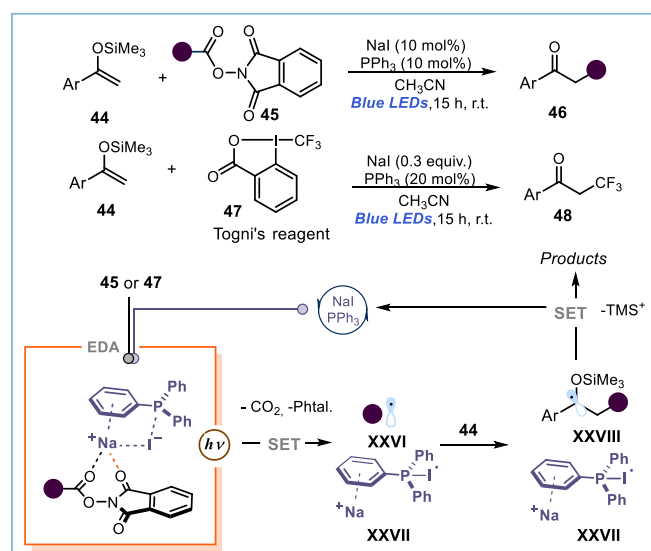


Figure 2.18. α -Functionalization of ketones by means of excitation of catalytic EDA complexes.

Mechanistically, the combination of PPh_3 , NaI, and electron-poor redox active substrates, such as **45** or **47**, was proposed to form a photoactive three-component EDA³⁸ complex (Figure 2.18, orange box). Upon light-induced intra-complex SET from the iodide anion to the phthalimide moiety within **44**, CO_2 extrusion

³⁸ Crisenza, G. E. M.; Mazzarella, D.; Melchiorre, P. "Synthetic Methods Driven by the Photoactivity of Electron Donor-Acceptor Complexes" *J. Am. Chem. Soc.* **2020**, *142*, 12, 5461–5476.

³⁹ Fu, M.-C.; Shang, R.; Zhao, B.; Wang, B.; Fu, Y. "Photocatalytic decarboxylative alkylations mediated by triphenylphosphine and sodium iodide" *Science* **2019**, *363*, 1429–1434.

resulted in the formation of the open-shell intermediate **XXVI**. Radical **XXVI** was then intercepted by silyl enol ether **44** delivering intermediate **XXVIII**, which, after SET oxidation from **XXVII**, produced the desired α -alkylated ketone **46** and regenerated the NaI and PPh₃ catalytic system. Even though the protocol was effective for a wide variety of alkyl electrophiles (also leading to non-stabilized primary radicals, as well as secondary, tertiary and trifluoromethyl radicals), the process was limited to acetophenone-derived silyl enol ethers.

2.5.2 Design plan

We wondered whether the photochemical S_N2-based radical generation strategy for the activation of alkyl electrophiles, previously developed in our laboratories,²⁷ could provide a general platform for the α -alkylation of ketones using silyl enol ethers as radical traps (Figure 2.19). This approach should complement traditional two-electron strategies and enrich the plethora of protocols based on open-shell intermediates.

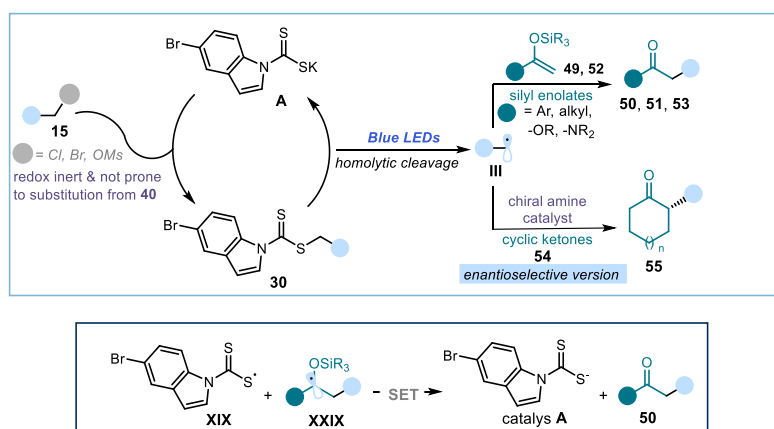


Figure 2.19. α -Alkylation of enol ethers using dithiocarbamate catalysis.

As illustrated in Figure 2.19, we envisioned that an S_N2 reaction of the nucleophilic organic catalyst **A** with substrate **15** would form a light-absorbing adduct **30** (Figure 2.19, light blue box). Photolysis of the latter would produce the alkyl radical **III**, which could be rapidly intercepted by the nucleophilic double bond of silyl enol ethers **49** to afford the α -alkylated product **50**. The proposed turnover of catalyst **A** would depend on the transfer of one electron from the α -oxo radical **XXIX**, generated upon radical trap of **III** by **49**, to the sulphur-centered radical **XIX**. This step (Figure 2.19, dark blue box) would regenerate catalyst **A** while delivering the desired product **50** upon acidic work-up. We also surmised that the use of chiral amines as organocatalysts for the catalytic formation of chiral enamines (which exhibit similar reactivity to silyl enol ethers) could be synergistically combined with the action of catalyst **A** to accomplish the enantioselective radical α -alkylation of ketones.

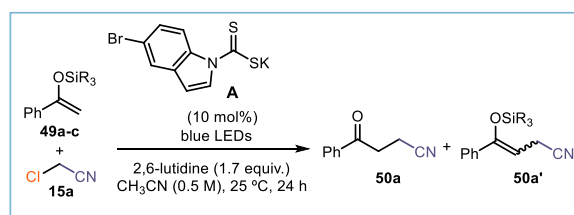
2.6 Results and Discussion

2.6.1 Reaction optimization

Our exploration started by studying the α -alkylation of acetophenone-derived silyl enol ether **49**, using the commercially available chloroacetonitrile **15a** as the radical precursor (Table 2.1). The experiments were performed at room temperature in acetonitrile, using a blue LED strip emitting at 465 nm, 10 mol% of the dithiocarbonyl anion catalyst **A**, and a slight excess of radical trap **49** (1.5 equiv.). When using the

trimethylsilyl derivative **49a**, these conditions furnished the desired ketone product **50a** in good yield along with traces of the silyl derivative **50a'** (entry 1). The use of alternative silyl protecting groups with more sterically demanding substituents, such as *tert*-butyldimethylsilyl (TBS) and triisopropylsilyl (TIPS), provided better chemical yields while selectively favoring the formation of the *O*-silylated adduct **50a'** (entries 2 and 3, respectively). Based on these initial screening, we continued our investigations with the TBS derivative **49b**. Adding water to the reaction mixture as silicon scavenger allowed us to directly achieve ketone **50a** as the major product (entry 4). However, due to partial inconsistencies in the hydrolysis step for all the silyl enol ethers evaluated, we decided to perform a different work-up, treating the crude mixture with trifluoroacetic acid or tetrabutylammonium fluoride (TBAF). This work-up quantitatively and consistently led to complete conversion of **50a'** into the target product **50a** (entry 5). Quantitative hydrolysis could be also achieved in the presence of other acids, since methanesulfonic acid or HCl in H₂O (4 equiv., entry 6) afforded the desired product **50a** in high yields. Control experiments confirmed that the alkylation reaction could not proceed in the absence of light or catalyst **A** (entries 7 and 8). The presence of a radical scavenger (TEMPO, 1 equiv.) completely suppressed the reaction (entry 9), and the cyanomethyl-TEMPO adduct could be detected in 10% NMR yield in the crude mixture. Finally, we demonstrated that the strongly reducing *fac*-Ir(ppy)₃ photoredox catalyst, when used in place of catalyst **A**, provided vastly inferior results (entry 10), presumably because of a difficult generation of the reactive radical from **15a**

Table 2.1. Optimization studies and control experiments.^[a]

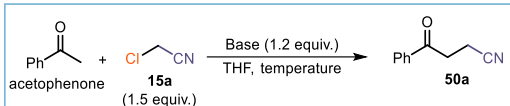


entry	deviation	SiR ₃	49	[%] yield 50a/50a' ^[b]
1	none	TMS	a	71 / 5
2	none	TBS	b	7 / 93
3	none	TIPS	c	<5 / >95
4	H ₂ O (20 equiv.)	TBS	b	90 / 8
5	Work up: TFA or TBAF	TBS	b	91 ^[c] / 0
6	Work up: CH ₃ SO ₃ H or HCl _(aq)	TBS	b	>95 / 0
7	no light	TBS	b	0
8	no catalyst A	TBS	b	0
9	TEMPO (1 equiv.)	TBS	b	0
10	<i>fac</i> -Ir(ppy) ₃ (1 mol%); no catalyst A	TBS	b	5 / 40

^[a] Reactions performed on a 0.2 mmol scale at 25 °C for 24 h using 0.4 mL of CH₃CN under illumination by blue LED strip (λ_{max} = 465 nm, 14 W) and using catalyst **A** (10 mol%), 1.5 equiv. of **49b**, and 1.7 equiv. of 2,6-lutidine. ^[b] Yield and distribution of products **50a** and **50a'** were determined by ¹H NMR analysis of the crude mixture using trichloroethylene as the internal standard. ^[c] Yield of isolated **50a**. ^[d] After work up with TFA. TMS: trimethylsilyl, TBS: *tert*-butyldimethylsilyl, TIPS: triisopropylsilyl, TFA: trifluoroacetic acid, TBAF: tetrabutyl ammonium fluoride.

Importantly, our attempts to perform the model reaction using classical metal enolate chemistry met with failure (Table 2.2). Subjection of the electrophile **15a** to a range of metal enolates, generated from acetophenone and non-nucleophilic alkali bases such as LDA or LiHMDS, led to either the formation of various side-products (when the reaction was allowed to warm to room temperature), or no conversion was observed. Even when more reactive electrophiles (e.g., bromo- or iodoacetonitrile) were used as electrophiles, only traces of product were obtained. These experiments confirmed the necessity of milder approaches to achieve a general method for the α -alkylation of ketones using primary alkyl electrophiles not prone to S_N1 manifolds.

Table 2.2 Screening of lithium enolates for the alkylation of acetophenone with chloroacetonitrile.



acetophenone + **15a** (1.5 equiv.) $\xrightarrow[\text{THF, temperature}]{\text{Base (1.2 equiv.)}}$ **50a**

entry	base	Temperature	[%] yield 50a
1	LDA (commercial)	-78 °C to rt	Complex mixture
2	LDA (freshly prepared)	-78 °C to rt	Complex mixture
3	LDA (freshly prepared)	-78 °C	Unreacted 14a
4	LiHMDS	-78 °C to rt	Complex mixture
5	NaHMDS	-78 °C to rt	Complex mixture
6	KHMDS	-78 °C to rt	14a
7 ^[a]	LDA	-78 °C to rt	9
8 ^[b]	LDA	-78 °C to rt	5

^[a] Reaction performed using bromoacetonitrile as electrophile. ^[b] Reaction performed using iodoacetonitrile as electrophile.

2.6.2 Scope Evaluation

With optimized conditions in hand (Table 2.1, entry 5), we tested the generality of the photochemical organocatalytic radical α -alkylation process (Figure 2.20). We first evaluated the scope of carbon-centered radicals that could be trapped by silyl enol ether **49b**. A large variety of electrophilic primary radicals afforded the corresponding α -alkylated ketones in good yields (products **50a**, **50e**, **50h**). Secondary radicals could also be generated and efficiently intercepted by **49b** to afford adducts **50b-d**, **50f-g**. However, in these cases, heating the reaction mixture at 60 °C was necessary to drive the formation of the photoactive intermediate **30**, due to a slow S_N2 step. Benzylic radical precursors, bearing electron-donating or electron-withdrawing groups on the aryl moiety, were also suitable substrates (products **50i-n**). The strategy could be used to implement a radical α -aminomethylation process, allowing the introduction of a protected primary amine (product **50o**) along with a trifluoromethyl moiety (product **50p**). The reaction can be scaled-up to one gram without any loss in chemical efficiency (7.0 mmol scale, **50a** obtained in 91% yield, 1.0 g). We then tested the compatibility with unprotected functional groups, which is an important factor when evaluating the method's applicability for the synthesis of biorelevant complex molecules.⁴⁰ Our catalytic platform displayed a good level of tolerance towards electrophiles containing nitrogen, sulphur, and oxygen heterocycles (products **50q-s**). Functional groups that would be incompatible with classical anionic

⁴⁰ (a) Blakemore, D. C.; Castro, L.; Churcher, I.; Rees, D. C.; Thomas, A. W.; Wilson, D. M.; Wood, A. "Organic synthesis provides opportunities to transform drug discovery" *Nat. Chem.* **2018**, *10*, 383–394; (b) Pitt, W. R.; Parry, D. M.; Perry, B. G.; Groom, C. R. "Heteroaromatic rings of the future" *J. Med. Chem.* **2009**, *52*, 2952–2963.

alkylation strategies or Lewis acid activation, such as unprotected alcohols (product **50t**), amide N-H bonds (product **50p**), esters (products **50e** and **50r**), ketones (products **50g** and **50h**), enones (product **50t**), and aldehydes (product **50i**), were tolerated well. Finally, drug-like compounds, including *cortisone* and *chloramphenicol* derivatives, could be used as radical precursors leading to adducts **50t** and **50u**, respectively. A benefit of this protocol is that it can rely on radical precursors bearing different leaving groups, including halides (Cl or Br) and sulfonates (OMs or ONs). The choice of the leaving group can therefore be dictated by its ease of access or compatibility with other functional groups in a complex synthetic plan.²⁷

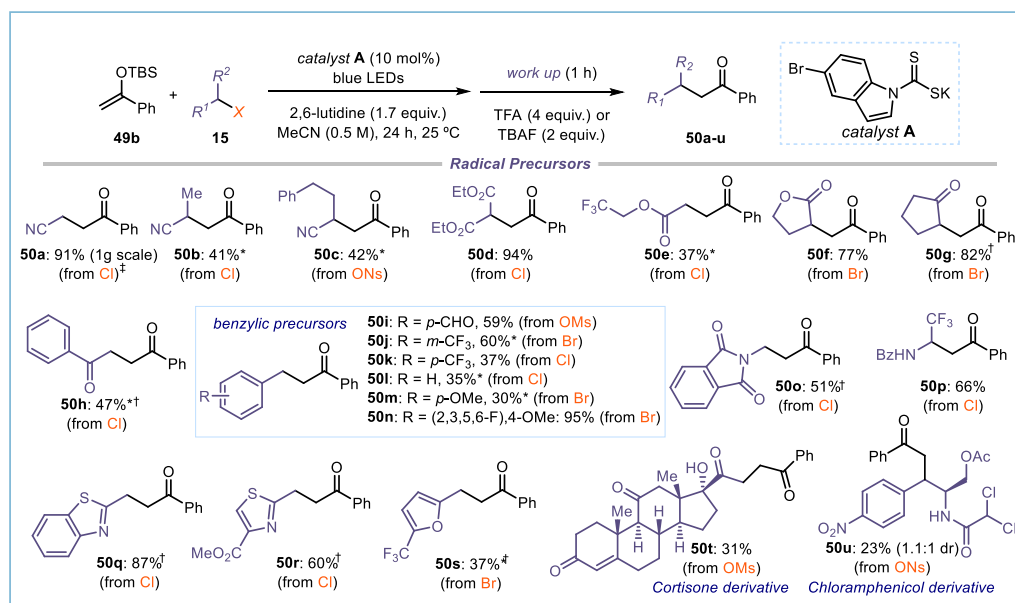


Figure 2.20. Survey of the radical precursors that can participate in the process. Reactions performed on 0.5 mmol scale using 1.5 equiv. of **49b** and 1.0 mL of acetonitrile. Yields of products **50a–u** refer to isolated material after purification. *Performed at 60 °C. [†]Using dichloroethane as the solvent. TFA: trifluoroacetic acid, TBAF: tetrabutylammonium fluoride, Ms: mesyl, Ns: nosyl.

We then examined the scope of silyl enol ethers, derived from aromatic ketones, that could participate in the alkylation with the electrophilic radicals generated from chloroacetonitrile **15a** (Figure 2.21). A variety of substitution patterns on the aryl ring, with different electronic (products **51a–e**) or steric profiles (products **51e** and **51f**), could be easily accommodated. Importantly, easily oxidizable heterocyclic substrates (products **51l–m**) or nitrogen-containing heterocycles (adducts **51n–p**) were readily tolerated. An *azaperone*'s derivative, containing an aminopyridine and a piperazine moiety, could be alkylated in moderate yield (product **51q**). Cyclic and acyclic silyl enol ethers derived from aliphatic ketones could also be used in this radical alkylation process, delivering the desired α -alkylated ketones from moderate to excellent yields (adducts **51r–51x**). Interestingly, selective alkylation at the terminal position of a β -ketoester was achieved (product **51v**). This was possible due to the modularity of silyl enolate synthesis compared to classical alkali metal enolates. The effectiveness of our methodology was highlighted by the possibility to forge quaternary carbon centers starting from different silyl enol ethers (products **51k** and **51x**).

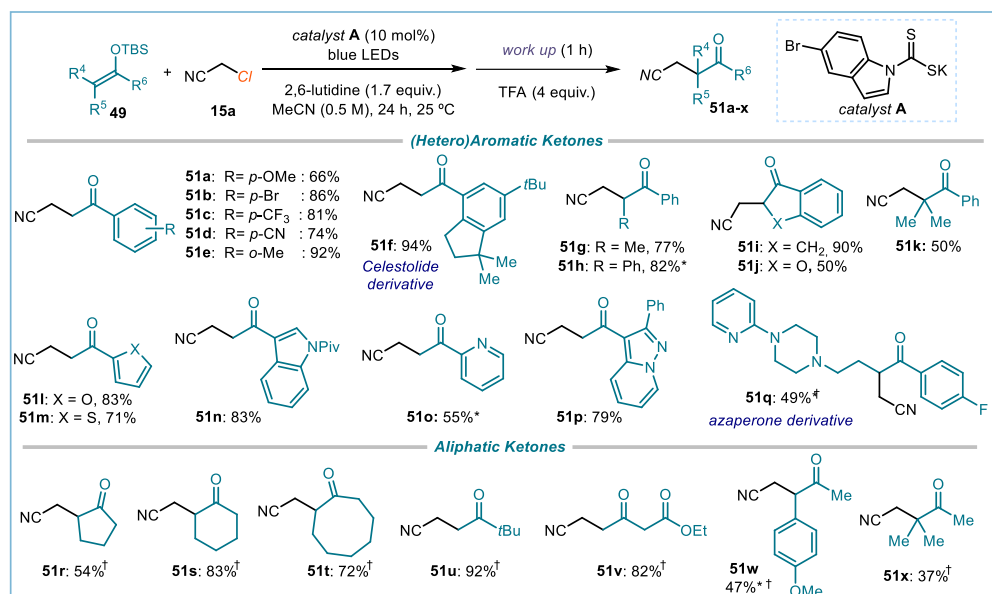


Figure 2.21. Scope evaluation for aromatic and aliphatic ketones: reactions performed on 0.5 mmol scale using 1.5 equiv. of **49** in 1.0 mL of acetonitrile; yields of products **51** refer to isolated material after purification. *Performed at 60 °C. †Using dichloroethane as the solvent. TFA: trifluoroacetic acid, TBAF: tetrabutylammonium fluoride.

Finally, *O-O* and *N-O* silyl ketene acetals were also suitable substrates affording the corresponding α -alkylated esters and amides in high yields (**53a-g**, Figure 2.22). Sterically crowded tertiary alcohol derivatives (product **53e**) could be synthesized through addition of electrophilic radicals to cyclic extended silyl ketene acetals. Moreover, the difficult α -alkylation of esters to achieve quaternary centers was accomplished with the synthesis of adduct **53f**. Unfortunately, our attempts to develop a diastereoselective process by including a classic chiral auxiliary (*Evans' oxazolidinone*) within the substrate did not yield significant results, as product **53g** could be obtained only with low diastereoselectivity (2.8:1 dr).

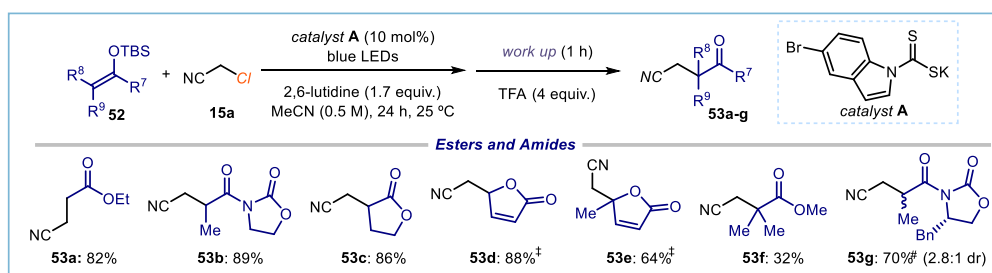


Figure 2.22. Further scope evaluation: reactions performed on 0.5 mmol scale using 1.5 equiv. of **52** and 1.0 mL of acetonitrile; yields of products **53** refer to isolated material after purification. ‡ Reaction time: 48 hours, # 3.0 equiv. of silyl enolate. TFA: trifluoroacetic acid, TBAF: tetrabutylammonium fluoride.

2.6.3 Reaction limitations

Along with the successful examples highlighted in the previous section, we also defined the limitations of this alkylation protocol (Figure 2.23).

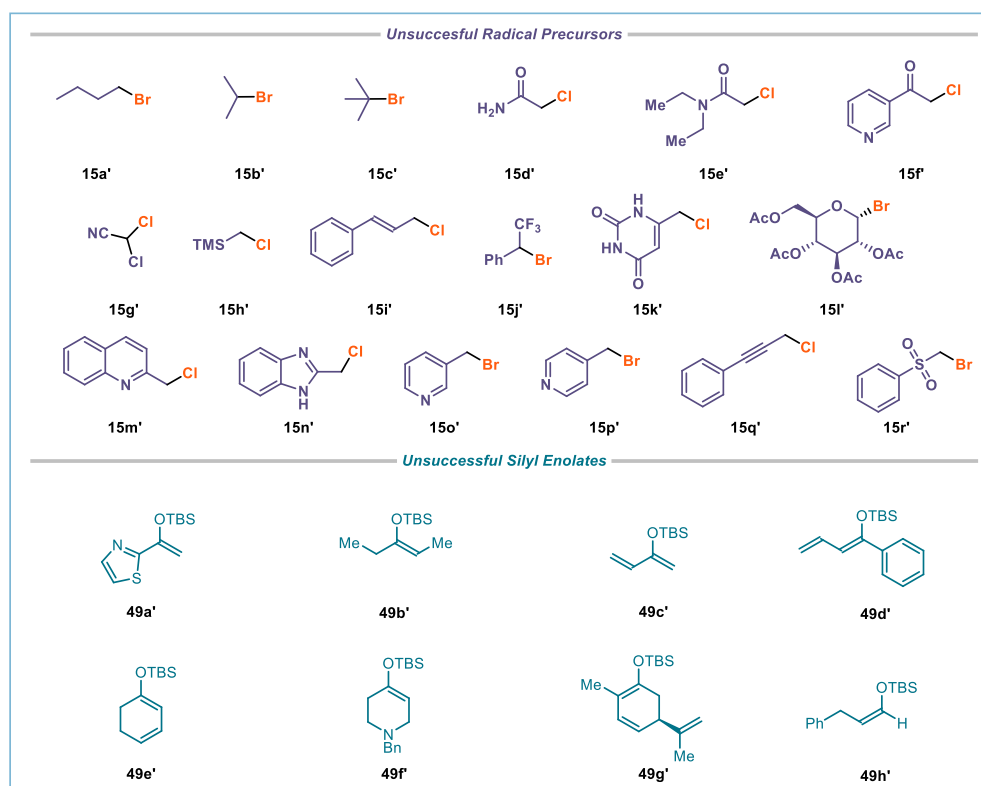


Figure 2.23. Substrates that failed to provide synthetically useful yields of the alkylation products.

In the case of radical precursors, three main reasons could account for the lack of reactivity: *i*) difficult S_N2 path leading to the formation of the photo-active intermediate of type **XV** due to the steric hindrance around the electrophilic carbon. This is usually the case for secondary and tertiary alkyl halides such as **15b'**, **15c'**, **15g'**, **15j'**, **15l'** (Figure 2.23, upper part). In some cases, increasing the temperature of the reaction had a positive effect on the reaction outcome allowing us to obtain products **50b** and **50c** (Figure 2.20) in moderate yields; *ii*) solubility issues of the photoactive intermediate greatly hampered the reactivity (e.g. **15m-p**, Figure 2.23). This issue could be partially solved in some cases by switching the solvent system from CH_3CN to DCE and/or by running the reaction at 60 °C (e.g. products **50q-s**, Figure 2.20); *iii*) for primary unbiased alkyl halides such as **15a'**, the photoactive intermediate is readily formed, but the cleavage of the C-S bond did not occur because of the high energy required to break that bond and to form a non-stabilized carbon-centered radical. The inability of our catalytic system to generate non-stabilized radicals was already observed in our previously developed methodologies.⁴¹ The next chapter will detail how we successfully solved this issue, therefore addressing the limitation. For the silyl enolates, we observed the formation of the over-oxidized starting material when this possessed C-H bonds delivering the corresponding unsaturated derivative (e.g. **49e'-g'**, Figure 2.23), whereas in the other cases, the turnover event is hampered by specific properties of the ensuing α -oxo radical.

⁴¹ Mazzarella, D.; Magagnano, G.; Schweitzer-Chaput, B.; Melchiorre, P. "Photochemical Organocatalytic Borylation of Alkyl Chlorides, Bromides, and Sulfonates" *ACS Catal.* **2019**, *9*, 5876–5880.

2.6.4 A dual organocatalytic system for the stereoselective α -alkylation of ketones

To showcase the synthetic utility of our system, we wondered whether a catalytic asymmetric α -alkylation of ketones could be developed by combining the dithiocarbamate-based radical generation strategy with chiral enamine organocatalysis (Figure 2.24).⁴² While few procedures have been developed for the stereoselective α -alkylation of ketones, they are mostly restricted to ionic chemistry.⁴³ Unlike the radical functionalization of aldehydes, where the merger of enamine-based catalysis and photoredox catalysis has been successfully studied and implemented,⁴⁴ the corresponding radical-based stereoselective α -alkylation of ketones remains underdeveloped.⁴⁵ The lack of enamine-mediated radical functionalization of ketones can be ascribed to the structure of the cinchona-based primary amine **B** (Figure 2.24).⁴⁶ This chiral amine **B** is often the catalyst of choice for the enamine-based functionalization of ketones in ionic chemistry. This is because **B** effectively generates reactive enamine intermediates from ketones while controlling the stereoselective approach of various electrophiles with consistently high enantiocontrol. However, the easily oxidizable tertiary amine moiety within the catalyst's bicyclic scaffold in **B** significantly hampers its compatibility with common photoredox catalysts. Quenching of the photocatalysts' excited state through SET from the cinchona alkaloids tertiary nitrogen may promote the degradation of the organocatalyst. In principle, the redox-neutral nature of our radical generation strategy means that effective coexistence of catalysts **A** and **B** may be possible. As depicted in Figure 2.24, this possibility was translated into experimental reality to develop an enantioselective radical α -alkylation of cyclic ketones **54**.

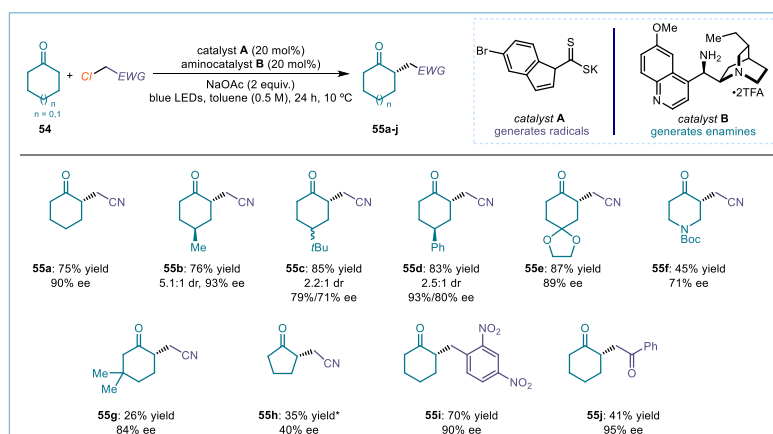


Figure 2.24. Aminocatalytic enantioselective photochemical α -alkylation of cyclic ketones with radicals derived from alkyl chlorides. Reactions performed on a 0.2 mmol scale; yields of products **55** refer to isolated material after purification. The reactivity was completely inhibited in the absence of light. *Reaction performed at 25 °C.

⁴² For a review on chiral enamine in organocatalysis see: Mukherjee, S.; Yang, J. W.; Hoffmann, S.; List, B. "Asymmetric Enamine Catalysis" *Chem. Rev.* **2007**, *107*, 5471–5569.

⁴³ (a) Job, A.; Janeck, C. F.; Bettray, W.; Peters, R.; Enders, D. "The SAMP-/RAMP-hydrazone methodology in asymmetric synthesis" *Tetrahedron* **2002**, *58*, 2253–2329; (b) Cano, R.; Zakarian, A.; McGlacken, G. P.; "Direct Asymmetric Alkylation of Ketones: Still Unconquered" *Angew. Chem. Int. Ed.* **2017**, *56*, 9278–9290.

⁴⁴ (a) D. A. Nicewicz, D. W. C. MacMillan, "Merging Photoredox Catalysis with Organocatalysis: The Direct Asymmetric Alkylation of Aldehydes" *Science* **2008**, *322*, 77–80. For a review: (b) Silvi, M.; Melchiorre, P. "Enhancing the potential of enantioselective organocatalysis with light" *Nature* **2018**, *554*, 41–49.

⁴⁵ (a) Mastracchio, A.; Warkentin, A. A.; Walji, A. M.; MacMillan, D. W. C. "Direct and enantioselective α -allylation of ketones via singly occupied molecular orbital (SOMO) catalysis" *Proc. Natl. Acad. Sci. U.S.A.*, **2010**, *107*, 20648–20651; (b) Arceo, E.; Bahamonde, A.; Bergonzini, G.; Melchiorre, P. "Enantioselective direct α -alkylation of cyclic ketones by means of photo-organocatalysis" *Chem. Sci.* **2014**, *5*, 2438–2442; (c) Zhu, Y.; Zhang, L.; Luo, S. "Asymmetric α -Photoalkylation of β -Ketocarbonyls by Primary Amine Catalysis: Facile Access to Acyclic All-Carbon Quaternary Stereocenters" *J. Am. Chem. Soc.* **2014**, *136*, 14642–14645.

⁴⁶ Melchiorre, P. "Cinchona-based Primary Amine Catalysis in the Asymmetric Functionalization of Carbonyl Compounds" *Angew. Chem. Int. Ed.* **2012**, *51*, 9748–9770.

The dithiocarbamate anion catalyst **A** effectively activated chloride **15a** toward radical formation, while the hydroquinidine-derived primary amine **B** secured the formation of a chiral enamine upon condensation. The bond-forming event between the electrophilic α -cyano radical, generated by catalyst **A**, and the electron-rich enamine, generated by catalyst **B**, can be rationalized through a favorable polarity-match of the two species.³⁵ This photochemical strategy successfully afforded the corresponding chiral α -cyanoalkylation products **55a-h** with good to high level of stereocontrol.⁴⁷ Cyclohexanone derivatives provided the highest levels of enantio-induction (products **55a-g**), while the more challenging five-membered cyclopentanone gave product **55h** in diminished yield and enantioselectivity. Interestingly, acid-sensitive functionalities, including an acetal or a Boc group, were well tolerated (products **55e** and **55f**). This asymmetric alkylation could be extended to other alkyl chlorides as radical precursors, since 2,4-dinitrobenzyl chloride and phenacyl chloride afforded the corresponding alkylated ketones **55i** and **55j**, respectively, with good results.

2.6.5 Proposed Mechanism

Our proposed catalytic cycle of the photochemical radical alkylation of silyl enol ethers is outlined in Figure 2.25. The nucleophilic catalyst **A** undergoes S_N2 reaction with the alkyl halide **15** to form the photon-absorbing intermediate **30**.²⁷ Blue light irradiation triggers the cleavage of the weak C-S bond to generate the pair of radicals **III** and **XIX**.

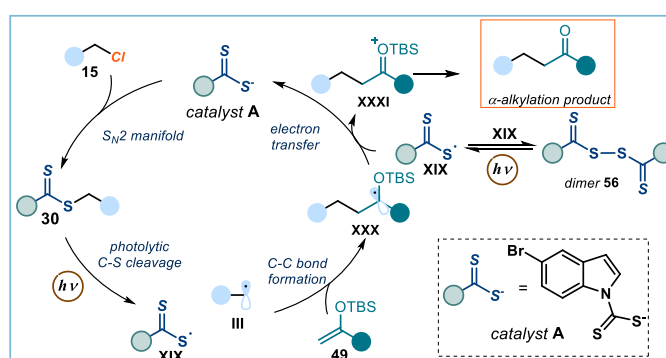


Figure 2.25. Proposed mechanism for the photochemical organocatalytic α -alkylation of ketones.

The silyl enol ether **49** is reactive enough to intercept the carbon-centered radical **III**, leading to the α -oxo stabilized radical **XXX**. SET between **XXX** and the sulphur-centered radical **XIX** regenerates catalyst **A** and forms the oxocarbenium ion **XXXI**, which can be hydrolyzed to afford the final α -alkylated product. To glean insights into the mechanism, a series of experiments were performed to investigate each elementary steps of our proposed catalytic cycle. Firstly, with the aim to evaluate its direct implication within the mechanistic path, we synthesized adduct **30a** by reacting equimolar amounts of the dithiocarbonyl anion **A** and chloroacetonitrile **15a**. When 10 mol% of **30a** was used as catalyst of the model reaction, the desired product **50a** was obtained in quantitative yield, proving the intermediacy of adduct **30a** in the catalytic cycle (Figure 2.26a).

⁴⁷ For an example of asymmetric catalytic α -cyanoalkylation of aldehydes using easily reducible bromoacetonitrile as the radical precursor, see: Welin, E. R.; Warkentin, A. A.; Conrad, J. C.; MacMillan, D. W. C. "Enantioselective α -Alkylation of Aldehydes by Photoredox Organocatalysis: Rapid Access to Pharmacophore Fragments from β -Cyanoaldehydes" *Angew. Chem. Int. Ed.* **2015**, *54*, 9668–9672.

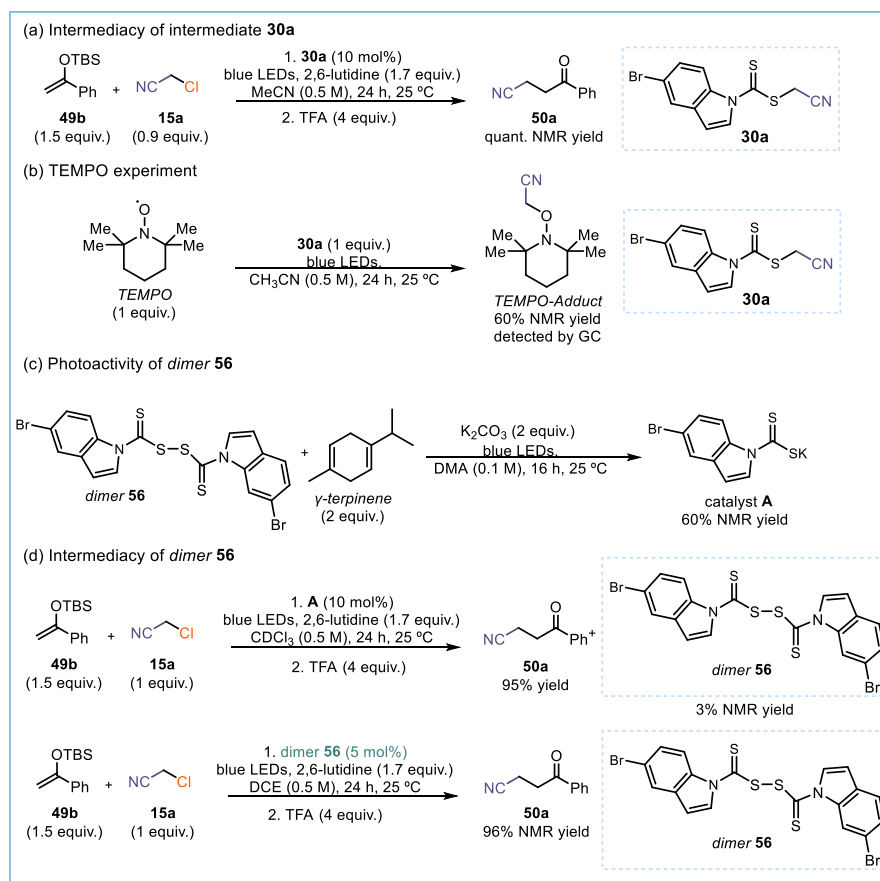


Figure 2.26. Mechanistic experiments.

In addition, light irradiation of adduct **30a** in the presence of TEMPO led to the formation of the cyanomethyl-TEMPO adduct in 60%, confirming the α -cyanomethyl radical as an intermediate in the reaction (Figure 2.26b). Our mechanistic proposal requires that the photoactivity of intermediate **30** regulates the formation of each molecule of the product. This scenario stands in contrast to an alternative radical chain propagation manifold, which would require the photoactivity of intermediate **30** to serve only as an initiator. A tool to discriminate between these two mechanistic possibilities is to measure the quantum yield (Φ) of the overall reaction. This experiment measures how many moles of product are formed per mole of photons absorbed by the system. When the absorption of one mole of photons results in the formation of *more than one* mole of product, a radical chain mechanism is operative and the measured quantum yield will be > 1 .^{48,13} We performed this measurement on the model reaction between **49b** and **15a** employing 10% of **30a**,⁴⁹ and the quantum yield was found to be as low as 0.055 ($\lambda = 460$ nm, using potassium ferrioxalate as the actinometer). The measurement was repeated under different conditions, using a stoichiometric amount of intermediate **30a**, which afforded a comparably low quantum yield ($\Phi = 0.06$). This low quantum yield is congruent with the closed-photocatalytic cycle depicted in Figure 2.25. This result suggests that a radical chain process, based on a dithiocarbamate group transfer manifold or a SET from **XXX** to **30** is highly unlikely (see section 2.6.6 for alternative mechanistic pathways).

Furthermore, while performing standard NMR spectroscopic analysis of the crude reaction mixtures, I observed the formation of a new diamagnetic compound which appeared to be similar in structure to catalyst

⁴⁸ Cismesia, M. A.; Yoon, T. P. "Characterizing chain processes in visible light photoredox catalysis" *Chem. Sci.* **2015**, *6*, 5426-5434.

⁴⁹ The use of **30a** as pre-catalyst was chosen in order to avoid the formation of insoluble KCl which would hamper an accurate quantum yield measurement.

A, based on its ^1H NMR signals. Therefore, I purified the unknown compound using column chromatography, hoping to uncover a product that might suggest how catalyst **A** was degrading under the reaction conditions. Interestingly, I isolated dimer **56** (Figure 2.26c), which can be formed by dimerization of the sulphur-centered radical **XIX**,⁵⁰ an intermediate we initially assumed to be detrimental to our catalytic system. Further investigations suggested that dimer **56** was a photo-absorbing compound. Under photoactivation with blue light, it may be expected that excitation may promote homolytic cleavage of the weak S-S bond. Indeed, when dimer **56** was exposed to visible light irradiation in the presence of an H-donor such as γ -terpinene, catalyst **A** was obtained in 60% yield (Figure 2.26c). This experiment also proved that the thiyl radical **XIX** could be reduced back to its anion form, not only via SET from an intermediate of the catalytic cycle, but via hydrogen atom transfer (HAT) too.⁵¹ The ability of thiyl radical **XIX** to be in a light-controlled equilibrium with its dimer **56** was key to ensure catalyst turnover. In our catalytic cycle, the turnover event is a SET between two radical intermediates, which usually possess short lifetimes. Generally, this is not a likely scenario since unproductive SET events and radical-radical couplings could hamper the desired reactivity. On the other hand, some radicals possess high kinetic stability and they are defined as *persistent radicals*.⁵² When one of the two fleeting species involved in a SET event is persistent, the process becomes kinetically permitted. The observation that dimer **56** is a photoactive species in equilibrium with the progenitor radical **XIX** and its dimerization manifold effectively confers a longer lifetime to **XIX**, overall facilitating the turnover of catalyst **A**. The persistent character of **XIX**, which is gained through a light-controlled dimerization equilibrium, will be essential for the development of net-reductive and redox-neutral transformations that will be discussed in details in Chapter III.

Finally, when an authentic sample of **56** was prepared and applied in the reaction as a catalyst (5 mol%), product **50a** was formed in quantitative yield (Figure 2.26d), confirming **56** as an effective pre-catalyst.

2.6.6 Alternative mechanisms

Ethyl-xanthates and dithiocarbamates are classical reagents used in group transfer processes, as extensively demonstrated by Zard.^{23,25} Accordingly, we considered an alternative mechanistic scenario where the photoactive intermediate **30** would merely act as an initiating system in a group transfer process, according to Figure 2.27.

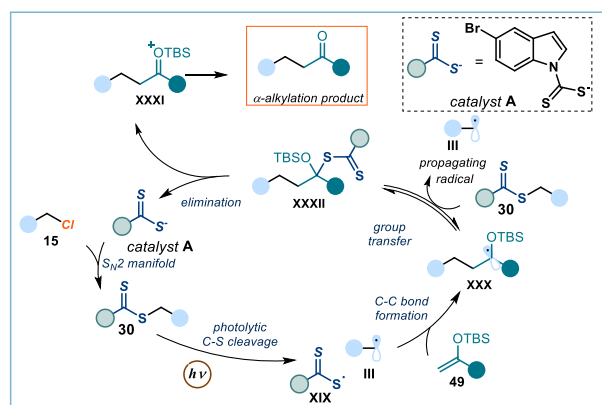


Figure 2.27. Alternative mechanistic scenario based on group transfer.

⁵⁰ Thang, S.; Chong, Y. K.; Mayadunne, R. T. A.; Moad, G.; Rizzardo, E. "A Novel Synthesis of Functional Dithioesters, Dithiocarbamates, Xanthates and Trithiocarbonates" *Tetrahedron Lett.* **1999**, *40*, 2435-2438.

⁵¹ For further details about the ability of dimer of type **56** to be reduced to the corresponding anion see: de Pedro Beato, E.; Mazzarella, D.; Balletti, M.; Melchiorre, P. "Photochemical generation of acyl and carbamoyl radicals using a nucleophilic organic catalyst: applications and mechanism thereof" *Chem. Sci.* **2020**, *11*, 6312-6324.

⁵² (a) Leifert, D.; Studer, A. "The Persistent Radical Effect in Organic Synthesis" *Angew. Chem. Int. Ed.* **2020**, *59*, 74-108; (b) Focsaneanu, K. S.; Scaiano, J. C. "The Persistent Radical Effect: From Mechanistic Curiosity to Synthetic Tool" *Helv. Chim. Acta.* **2006**, *89*, 2473-2482.

However, the very low quantum yield measured for the model reaction is incongruent with a group transfer–based mechanism, which would require a radical chain propagation to be operative. Furthermore, in extensive studies from Zard, it was demonstrated that, to have an efficient group transfer propagation in xanthate chemistry, the adduct radical **XXX** must be less stable than the radical **III** (see Section 2.3.2.). This requirement is not met for the radicals involved in our model reaction. For example, the primary α -cyano radical derived from chloroacetonitrile **15a** is less stable than the tertiary benzylic α -oxo radical **XXX**, based on their relative stabilities from the BDE of the corresponding C-H bonds.¹⁷ Bond dissociation energy values for benzylic C-H bonds are inversely proportional to substitution. Based on the reported values and considering the stabilization effect of the α -oxy moiety, the tertiary benzylic radical **XXX** may possess a significantly higher stability than the primary radical derived from **15a** (BDE = 97.0 kcal/mol).⁵³ This would go against the thermodynamic requirement governing classical xanthate chemistry, therefore preventing an efficient group transfer chain propagation. Nevertheless, we surmised that, if a group transfer-based mechanism was operative, the xanthate intermediate **57** (which does not absorb at 465 nm) would outcompete, or be comparably reactive to intermediate **30a** in a group transfer manifold. Therefore, we would expect an efficient propagation after the photolysis of the weak C-S bond within the photoactive intermediate **30a**. In such scenario, we should obtain similar yield to that obtained under catalytic conditions.

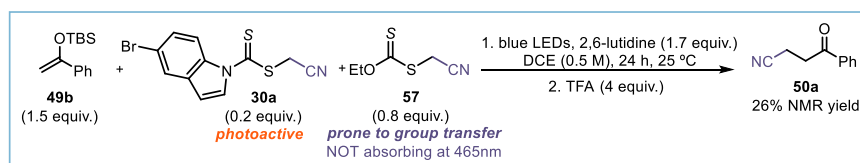


Figure 2.28. Mechanistic experiment that proves the inefficiency of group transfer mechanism.

Nonetheless, the yield in the experiment depicted in Figure 2.28 is comparable to the amount of **30a** present in solution, suggesting that a group transfer mechanism from intermediate **57** is not an efficient pathway.

We also considered the possibility of a second alternative pathway based on an SET event between radical **XXX** and the intermediate **30**, leading to intermediate **XXXI** while generating catalyst **A** and the propagating radical **III** (Figure 2.29).

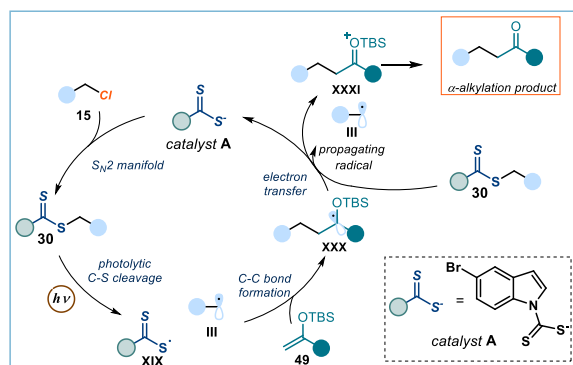


Figure 2.29. Alternative mechanistic scenario based on SET from **XXX** to **30**.

⁵³ (a) Coote, M. L.; Lin, C. Y.; Beckwith, A. L. J.; Zavitsas, A. A. "A comparison of methods for measuring relative radical stabilities of carbon-centred radicals" *Phys. Chem. Chem. Phys.* **2010**, *12*, 9597–9610; For BDE of benzylmethylether see: (b) K. R. Przybylak, M. T. D. Cronin Correlation between bond dissociation energies and spin distribution for the radicals of ethers: A DFT study" *J. Mol. Struct.: THEOCHEM* **2010**, *955*, 165–170; for the BDE of the remaining compounds see: (c) Luo, Y. R. "Comprehensive Handbook of Chemical Bond Energies", **2007**, CRC Press, Boca Raton, FL.

This mechanism, which would require a radical chain propagation, is not consonant with the very low quantum yield measured for the model reaction. In order to further disprove the possibility of an SET between **XXX** and **30**, we performed an additional experiment using a mixture of triethylborane/O₂ as initiation system in the presence of stoichiometric amount of **30a** (Figure 2.30). The mixture triethylborane/oxygen is an efficient radical initiator in xanthate/dithiocarbamate chemistry and, if an efficient radical chain propagation mechanism were operative, high yields of **50a** would be expected when employing stoichiometric amount of **30a** as radical precursor.⁵⁴

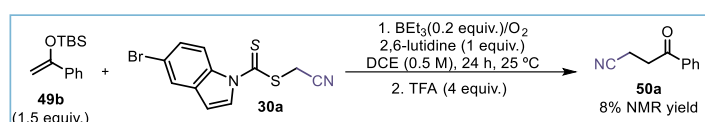


Figure 2.30. Mechanistic experiment for the SET from **XXX** to **30a**.

However, the initiation system was ineffective when applied to our system, affording product **50a** in 8% yield only. These results indicate that a radical initiation system is not sufficient to trigger the model reaction, further suggesting that a radical chain propagation (either via an SET mechanism or a group transfer manifold) is not operative in this process. We therefore consider the mechanism proposed in Figure 2.25, where catalyst **A** is involved in every radical generation cycle, as the more probable one.

2.7 Conclusion

In summary, we have developed a visible-light-mediated organocatalytic strategy for the radical α -alkylation of ketones using silyl enol ethers as stable nucleophiles, which synthetically complements traditional two-electron strategies. The method's mild reaction conditions and functional group tolerance allowed us to install, at the ketones' α position, moieties not compatible with classical anionic processes. In addition, the redox neutral conditions of this process make it tolerant of a cinchona-based amine catalyst, which was used to develop an enantioselective variant. These findings, along with the experimental simplicity and the low cost of the catalysts, suggest that this method can find further synthetic applications in asymmetric radical processes.

2.8 Experimental Section⁵⁵

The NMR spectra were recorded at 300, 400 MHz and 500 MHz for ¹H and 75, 100 or 125 MHz for ¹³C. The chemical shift (δ) for ¹H and ¹³C are given in ppm relative to residual signals of the solvents (CHCl₃ @ 7.26 ppm ¹H NMR and 77.16 ppm ¹³C NMR and tetramethylsilane @ 0 ppm. Coupling constants are given in Hertz. The following abbreviations are used to indicate the multiplicity: s, singlet; d, doublet; q, quartet; m, multiplet; bs, broad signal; app, apparent. 1D ¹H NOESY were performed at 25 °C on a Bruker Avance 500 spectrometer equipped with a BBFO using a 1D selective NOESY pulse sequence (selnpgp, Bruker).

High resolution mass spectra (HRMS) were obtained from the ICIQ HRMS unit on MicroTOF Focus and Maxis Impact (Bruker Daltonics) with electrospray ionization. (ESI) or Atmospheric Pressure Chemical Ionization (APCI). HPLC analysis on chiral stationary phase was performed on an Agilent 1200-series

⁵⁴ Boivin, J.; Nguyen, V. T. "Triethylborane-air: a suitable initiator for intermolecular radical additions of S-2-oxoalkylthionocarbonates (S-xanthates) to olefins" *Beilstein Journal of Organic Chemistry*, 2007, 3, 47.

⁵⁵ The ¹H NMR, ¹⁹F NMR, ¹³C NMR spectra and UPC² traces are available in literature¹ and are not reported in the present dissertation.

instrument, employing Daicel Chiralpak IA, IB, ID, IC and IC-3 columns, or a Waters ACQUITY® UPC² instrument, using Trefoil AMY1, CEL1, and CEL2 and Daicel Chiralpak IC chiral columns.

General Procedures. All reactions were set up under an argon atmosphere in oven-dried glassware using standard Schlenk techniques, unless otherwise stated. Synthesis grade solvents were used as purchased; anhydrous solvents were taken from a commercial SPS solvent dispenser. Chromatographic purification of products was accomplished using forced-flow chromatography (FC) on silica gel (35-70 mesh). For thin layer chromatography (TLC) analysis throughout this work, Merck pre-coated TLC plates (silica gel 60 GF₂₅₄, 0.25 mm) were employed, using UV light as the visualizing agent and an acidic mixture of vanillin or basic aqueous potassium permanganate (KMnO₄) stain solutions, and heat as developing agents. Organic solutions were concentrated under reduced pressure on a Büchi rotatory evaporator (in vacuo at 40 °C). Yields refer to isolated materials of >95% purity, as determined by ¹H NMR analysis.

Materials. The majority of substrates used in this study are commercially available and were purchased at the highest purity available from Sigma-Aldrich, Fluka, Alfa Aesar, Fluorochem, and used as received, without further purifications. The synthesis of the nucleophilic organic catalyst **A** is described in the literature.²³ The substrates displayed in Figure 2.28 were synthesized according to procedures reported in the literature.

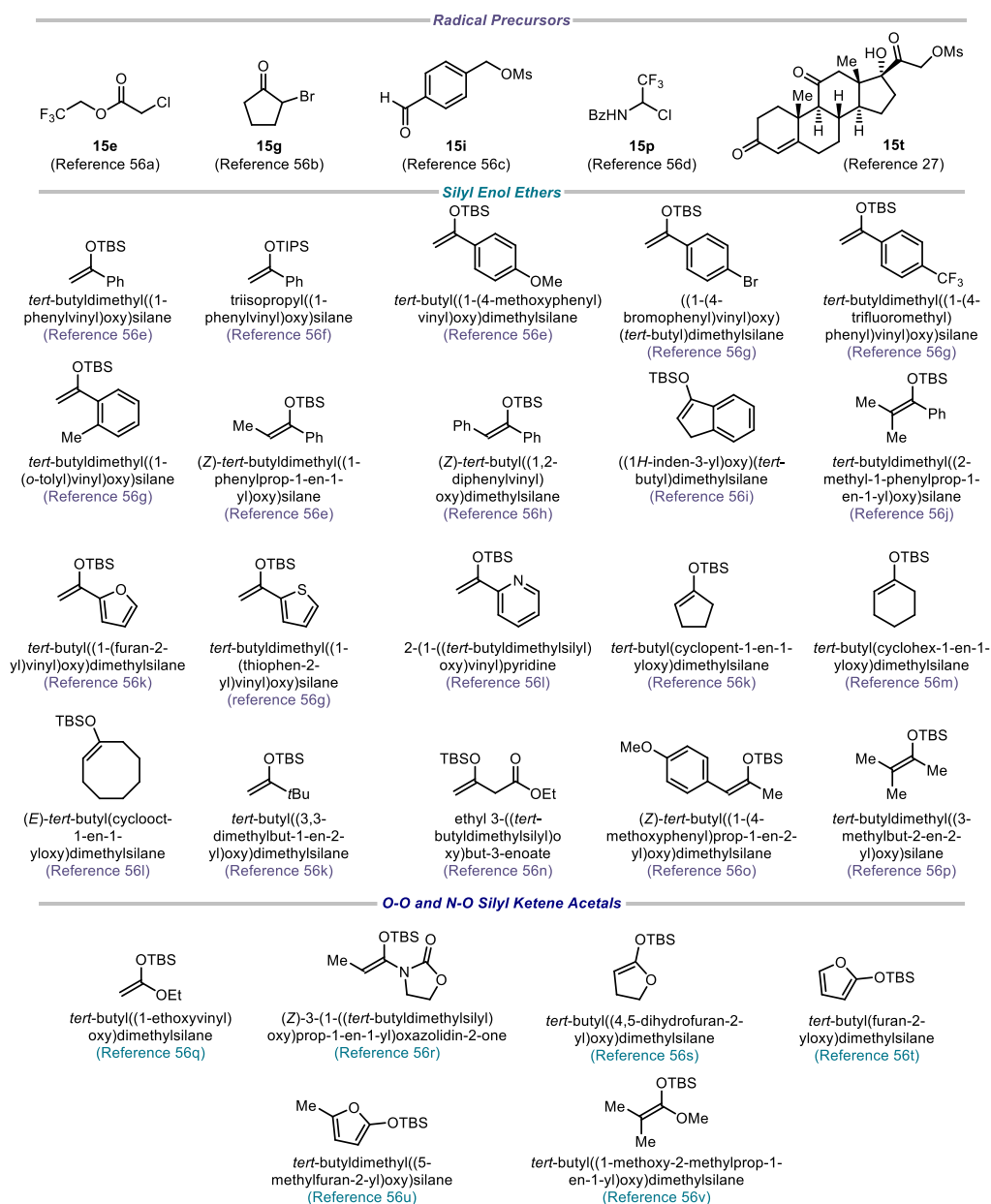


Figure 2.31. Starting materials synthesized according to literature precedents and corresponding references.⁵⁶

⁵⁶ a) Song, J.; H. Yamataka, H.; Rappoport, Z. "Dialkoxyphosphinyl-Substituted Enols of Carboxamides" *J. Org. Chem.* **2007**, *72*, 7605-7624. b) Tanemura, K.; Suzuki, T.; Nishida, Y.; Satsumabayashi, K.; Horaguchi, T. "A mild and efficient procedure for α -bromination of ketones using N-bromosuccinimide catalysed by ammonium acetate" *Chem. Comm.* **2004**, 470-471. c) Rosowsky, A.; Papoulis, A. T.; Forsch, R. A.; Queener, S. F. "Synthesis and antiparasitic and antitumor activity of 2, 4-diamino-6-(arylmethyl)-5,6,7,8-tetrahydroquinazoline analogues of piritrexim" *J. Med. Chem.* **1999**, *42*, 1007-1017. d) Tanaka, K.; Ishiguro, Y.; Mitsuhashi, K. "N-Acyl-1-chloro-2,2,2-trifluoroethylamine as a 2,2,2-Trifluoroethylamine-Building Block" *Bull. Chem. Soc. Jpn.* **1993**, *66*, 661-663. e) D. Perrotta, D.; Racine, S.; Vuilleumier, J.; de Nanteuil, F.; Waser, J. "[4+2]-Annulations of Aminocyclobutanes" *Org. Lett.* **2015**, *17*, 1030-1033. f) de Nanteuil, F.; Serrano, E.; Perrotta, D.; Waser, J. "Dynamic Kinetic Asymmetric [3 + 2] Annulation Reactions of Aminocyclopropanes" *J. Am. Chem. Soc.* **2014**, *136*, 6239-6242. g) Khan, I.; B. G. Reed-Berendt, B. G.; Melen, R. L.; Morrill, L. C. "FLP-Catalyzed Transfer Hydrogenation of Silyl Enol Ethers" *Angew. Chem., Int. Ed.* **2018**, *57*, 12356-12359. h) Hayashi, M.; Shibuya, M.; Iwabuchi, Y. "Catalytic Oxidation of Silyl Enol Ethers to 1,2-Diketones Employing Nitroxyl Radicals" *Synlett* **2012**, *23*, 1025-1030. i) Kang, T.; Cao, W.; Hou, L.; Tang, Q.; Zou, S.; Liu, X.; Feng, X. "Chiral Zinc(II)-Catalyzed Enantioselective Tandem α -Alkenyl Addition/Proton Shift Reaction of Silyl Enol Ethers with Ketimines" *Angew. Chem., Int. Ed.* **2019**, *58*, 2464-2468. j) Ishikawa, T.; Okano, M.; Aikawa, T.; Saito, S. "Novel Carbon-Carbon Bond-Forming Reactions Using Carbocations Produced from Substituted Propargyl Silyl Ethers by the Action of TMSOTf" *J. Org. Chem.* **2001**, *66*, 4635-4642. k) Li, Y.; Liu, J.; Zhao, S.; Du, X.; Guo, M.; Zhao, W.; Tang, X.; Wang, G. "Copper-Catalyzed Fluoroolefination of Silyl Enol Ethers and Ketones toward the Synthesis of β -Fluoroenones" *Org. Lett.* **2018**, *20*, 917-920. l) Clark, R. D.; Untch, K. G. "[2 + 2] Cycloaddition of ethyl propiolate and silyl enol ethers" *J. Org. Chem.* **1979**, *44*, 248-253. m) Zhang, J.; Wang, L.; Liu, Q.; Yang, Z.; Huang, Y. "Synthesis of α,β -unsaturated carbonyl

2.8.1. Experimental Setup

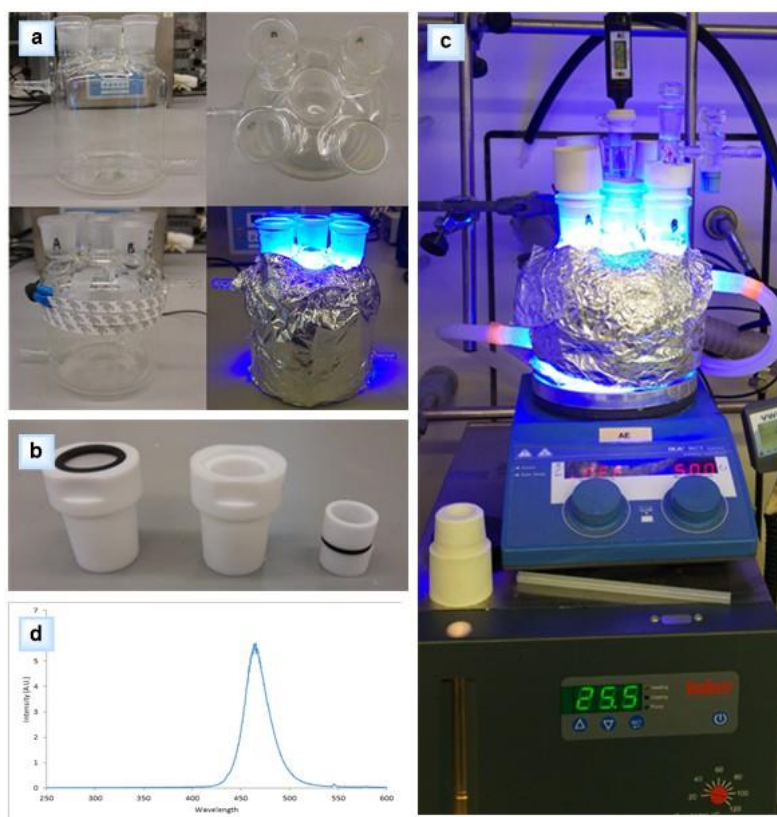


Figure 2.32. (a) Photoreactor used in this study. (b) Teflon adaptors used to accommodate Schlenk tubes in the photoreactor. (c) Fully assembled photoreactor in operation. (d) Emission spectrum of the 465 nm blue LED strip used in this study.

The photoreactor consisted of a 12.5 cm diameter jar, fitted with 4 standard 29 sized ground glass joints arranged in a square and a central 29 sized joint. A commercial 1-meter LED strip was wrapped around the jar, followed by a layer of aluminium foil and cotton for insulation (Figure 2.30a). Each of the joints could be used to fit a standard 16 mm or 25 mm diameter Schlenk tube with a Teflon adaptor (Figure 2.30b). An inlet and an outlet allow the circulation of liquid from a Huber Minichiller 300 inside the jar. This setup allows to perform reactions at temperatures ranging from $-20\text{ }^{\circ}\text{C}$ to $80\text{ }^{\circ}\text{C}$ with accurate control of the reaction temperature ($\pm 1^{\circ}\text{C}$, Figure 2.30c). To maintain a consistent illumination during different

compounds via a visible-light-promoted organocatalytic aerobic oxidation" *Chem. Comm.* **2013**, *49*, 11662-11664. n) M. Rathke, W.; Sullivan, D. F. "Condensation of O-silyl ketene acetals with acid chlorides. A synthesis of β -keto esters" *Tetrahedron Lett.* **1973**, *14*, 1297-1300. o) Saito, I.; Nagata, R.; Kotsuki, H.; Matsuura, T. "Regiospecific ortho oxyfunctionalization of substituted benzenes with singlet oxygen" *Tetrahedron Lett.* **1982**, *23*, 1717-1720. p) Woźniak, L.; Magagnano, G.; P. Melchiorre, P. "Enantioselective Photochemical Organocascade Catalysis" *Angew. Chem., Int. Ed.* **2018**, *57*, 1068-1072. q) Pommerening, P.; Mohr, J.; Friebe, J.; Oestreich, M. "Synthesis of a Chiral Borate Counteranion, Its Trityl Salt, and Application Thereof in Lewis-Acid Catalysis" *Eur. J. Org. Chem.* **2017**, *16*, 2312-2316. r) Bigot, A.; Williamson, A. E.; Gaunt, M. J. "Enantioselective α -Arylation of N-Acyloxazolidinones with Copper(II)-bisoxazoline Catalysts and Diaryliodonium Salts" *J. Am. Chem. Soc.* **2011**, *133*, 13778-13781. s) Heathcock, C. H.; Davidsen, S. K.; Hug, K. T.; Flippin, L. A. "Acyclic stereoselection. 36. Simple diastereoselection in the Lewis acid mediated reactions of enol silanes with aldehydes" *J. Org. Chem.* **1986**, *51*, 3027-3037. t) Kemppainen, E. K.; Sahoo, G.; Valkonen, A.; Pihko, P. M. "Mukaiyama-Michael Reactions with Acrolein and Methacrolein: A Catalytic Enantioselective Synthesis of the C₁₇-C₂₈ Fragment of Pectenotoxins" *Org. Lett.* **2012**, *14*, 1086-1089. u) Jefford, C. W.; Sledeski, A. W.; Rossier, J.-C.; Boukouvalas, J. "A short route to furanosesquiterpenes using a new siloxyfuran building block. The synthesis of freelingite and dehydrolasiosperman" *Tetrahedron Lett.* **1990**, *31*, 5741-5744. v) Nicolaou, K. C.; Bellavance, G.; Buchman, M.; Pulukuri, K. K. "Total Syntheses of Disorazoles A₁ and B₁ and Full Structural Elucidation of Disorazole B₁" *J. Am. Chem. Soc.* **2017**, *139*, 15636-15639.

experiments, only the four external positions were used to perform reactions while the central one was used to monitor the temperature inside a Schlenk tube identical to those used to perform reactions.

The light source used in this study consisted of a 1 m strip, 14.4W 'LEDXON MODULAR 9009083 LED, SINGLE 5050' purchased from Farnell, catalog number 9009083. The emission spectrum of these LEDs was recorded (Figure 2.30d).

For the scope reactions of the asymmetric α -alkylation of cyclic ketones, a variation of this setup was used (Figure 2.31). It consisted of a 4 cm diameter jar fitted with a standard 29 sized ground glass joint. A commercial 1 meter LED strip was wrapped around the jar, followed by a layer of aluminium foil and cotton for insulation. An inlet and an outlet allow the circulation of liquid from a Huber Minichiller 300 inside the jar. This setup allows to perform reactions at temperatures ranging from -20 °C to 80 °C with accurate control of the reaction temperature (± 1 °C).

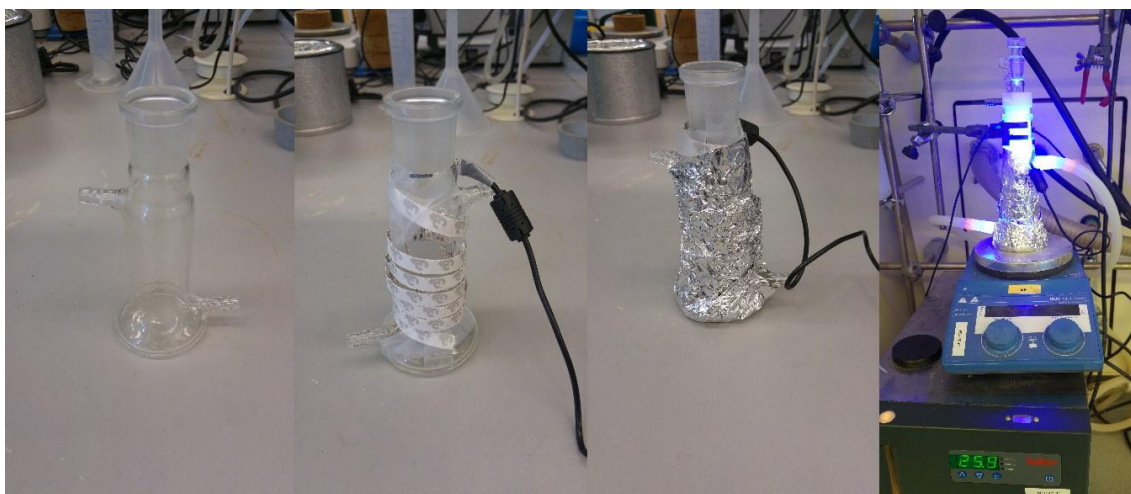
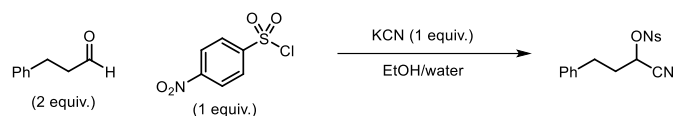


Figure 2.33. Fully assembled photoreactor in operation for the asymmetric catalytic α -alkylation of cyclic ketones.

2.8.2 Substrate Synthesis

Synthesis of 1-cyano-3-phenylpropyl 4-nitrobenzenesulfonate .



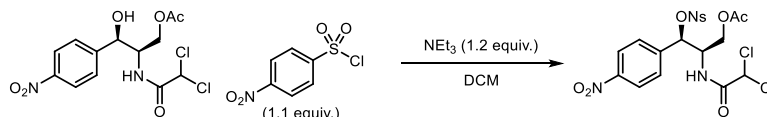
In a round bottom flask under argon, 4-nitrobenzenesulfonyl chloride (4 mmol, 886 mg), hydrocinnamaldehyde (8 mmol, 1053 μ L) and ethanol (2 mL) were combined and the resulting solution cooled in an ice bath. Under strong stirring, a solution of KCN (4 mmol, 260 mg) in distilled water (1 mL) was added and the mixture left to react overnight, allowing a slow warm up to room temperature. The mixture was transferred to an extraction funnel and AcOEt (25 mL), water (10 mL), and a saturated solution of NaHCO_3 (10 mL) were added. The phases were separated and the aqueous layer extracted twice with AcOEt. The organic fractions were combined, washed with brine, dried (MgSO_4) and concentrated to a yellow oil. The residue was then suspended in a 1:1 mixture of ethanol and water, heated to boiling, and then cooled in a freezer. The crystals formed were filtered and washed with a small amount of cold ethanol to afford product **2c** as slightly yellow crystals (665 mg, 47% yield, purity of 90% estimated by H NMR analysis, used without further purification).

$^1\text{H NMR}$ (400 MHz, CDCl_3) δ 8.50-8.43 (m, 2H); 8.21-8.12 (m, 2H); 7.38-7.31 (m, 2H); 7.31-7.26 (m, 1H); 7.22-7.16 (m, 2H); 5.11 (dd, $J = 7.0, 6.4$ Hz, 1H); 2.42-2.28 (m, 2H); 1.36-1.21 (m, 2H).

$^{13}\text{C NMR}$ (101 MHz, CDCl_3) δ 151.6 (C); 141.1 (C); 138.3 (C); 129.9 (CH); 129.3 (CH); 128.7 (CH); 127.4 (CH); 125.1 (CH); 114.9 (C); 66.9 (CH); 35.2 (CH_2); 30.5 (CH_2).

HRMS: calculated for $\text{C}_{16}\text{H}_{14}\text{N}_2\text{NaO}_5\text{S}$ ($\text{M}+\text{Na}^+$): 369.0516, found 369.0506.

Synthesis of (2*R*,3*R*)-2-(2,2-dichloroacetamido)-3-(4-nitrophenyl)-3-(((4-nitrophenyl)sulfonyl)oxy)propyl acetate



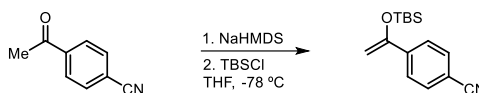
In a round bottom flask, chloramphenicol acetate (3.75 mmol, 1.369 g) was dissolved in dry DCM (15 mL) then cooled to 0°C in an ice bath. Triethylamine (4.5 mmol, 627 μ L) was added, followed by 4-nitrobenzenesulfonyl chloride (4.13 mmol, 914 mg). The cold bath was removed and the mixture allowed to react at room temperature overnight. The mixture was transferred to an extraction funnel, then DCM (25 mL) and water (30 mL) were added. The phases were separated and the aqueous layer extracted twice with DCM. The organic fractions were combined, washed with brine, dried (MgSO_4), and concentrated to a yellow glassy oil. The crude residue was purified by flash column chromatography (DCM/hexanes/acetone 72:25:5 as eluent) to afford the product as a white foam (1.203 g, 58% yield).

$^1\text{H NMR}$ (400 MHz, CDCl_3) δ 8.36-8.29 (m, 2H); 8.21-8.15 (m, 2H); 8.06-7.98 (m, 2H); 7.50-7.42 (m, 2H); 6.87 (br d, $J = 9.1$ Hz, 1H); 5.93 (d, $J = 5.2$ Hz, 1H); 5.87 (s, 1H); 4.66-4.56 (m, 1H); 4.19 (dd, $J = 11.8, 5.3$ Hz, 1H); 4.09 (dd, $J = 11.8, 6.2$ Hz, 1H); 2.11 (s, 3H).

$^{13}\text{C NMR}$ (101 MHz, CDCl_3) δ 170.4 (C); 164.3 (C); 151.0 (C); 148.5 (C); 141.3 (C); 140.7 (C); 129.2 (CH); 127.6 (CH); 124.5 (CH); 124.1 (CH); 80.3 (CH); 65.8 (CH); 61.6 (CH_2); 53.0 (CH); 20.6 (CH_3).

HRMS: calculated for $\text{C}_{19}\text{H}_{17}\text{Cl}_2\text{N}_3\text{NaO}_{10}\text{S}$ ($\text{M}+\text{Na}^+$): 571.9904, found 571.9914.

Synthesis of 4-(1-((*tert*-butyldimethylsilyloxy)viny)benzonitrile.



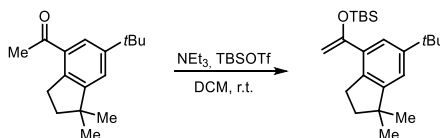
In an oven dried round bottom Schlenk flask kept under nitrogen, 4-acetylbenzonitrile (3.58 mmol, 520 mg) was dissolved in anhydrous THF. The solution was cooled down to $-78\text{ }^{\circ}\text{C}$ and a 1 M solution of NaHMDS (4.4 mL) was added dropwise. The cold bath was removed and the pale yellow solution was stirred for 1 hour at ambient temperature. Then the reaction was cooled again at $-78\text{ }^{\circ}\text{C}$, *tert*-butylchlorodimethylsilane (4.3 mmol, 650 mg) was added and the reaction mixture stirred at ambient temperature overnight. The reaction was quenched by adding a cold NH_4Cl saturated solution (20 mL) and the product was extracted in diethylether (3x 20 mL). The combined organic fractions were dried over anhydrous Na_2SO_4 , filtered and evaporated under reduced pressure. The crude residue was purified by flash column chromatography with deactivated silica (treated with hexanes + 2% triethylamine) eluting with hexanes to yield the product as a white solid (685 mg, 74% yield).

$^1\text{H NMR}$ (500 MHz, CDCl_3) δ 7.71-7.67 (m, 2H); 7.63-7.59 (m, 2H); 5.00 (d, $J=2.2$ Hz, 1H); 4.57 (d, $J=2.2$ Hz, 1H); 1.00 (s, 9H), 0.22 (s, 6H).

$^{13}\text{C NMR}$ (75 MHz, CDCl_3) δ 154.3 (C); 142.2 (C); 132.1 (CH); 125.8 (CH); 119.0 (C); 111.6 (C); 93.8 (CH₂); 25.9 (CH₃); 18.4 (C), -4.6 (CH₃).

HRMS: calculated for $\text{C}_{15}\text{H}_{22}\text{NOSi}$ ($\text{M}+\text{H}^+$): 260.1465, found 260.1476.

Synthesis of *tert*-butyl((1-(6-(*tert*-butyl)-1,1-dimethyl-2,3-dihydro-1*H*-inden-4-yl)vinyloxy)dimethylsilane.



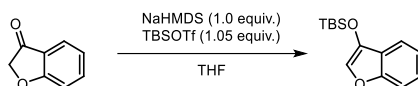
In an oven dried round bottom flask kept under nitrogen, 1-(6-(*tert*-butyl)-1,1-dimethyl-2,3-dihydro-1*H*-inden-4-yl)ethan-1-one (4.5 mmol, 1.1 g) was dissolved in dry DCM (9 mL). Triethylamine (5.4 mmol, 750 μL) was added and the reaction mixture stirred for 1 hour at ambient temperature. Then TBSOTf (4.95 mmol, 1.14 mL) was added dropwise and the reaction mixture was stirred for 3 hours. The reaction was quenched with cold saturated NH_4Cl (50 mL) and extracted with diethyl ether (2x30 mL). The combined organic fractions were dried over anhydrous MgSO_4 , filtered and evaporated under reduced pressure. The crude residue was purified by flash column chromatography over deactivated silica eluting with hexanes + 2% of triethylamine to yield the product as a colorless oil (1.13 g, 70% yield).

$^1\text{H NMR}$ (300 MHz, CDCl_3) δ 7.42 (d, $J=1.9$ Hz, 1H); 7.10 (d, $J=1.9$ Hz, 1H); 4.58-4.56 (m, 2H); 2.95 (t, $J=7.1$ Hz, 2H); 1.90 (t, $J=7.1$ Hz, 2H); 1.32 (s, 9H); 1.26 (s, 6H); 0.98 (s, 9H); 0.17 (s, 6H).

$^{13}\text{C NMR}$ (101 MHz, CDCl_3) δ 156.6 (C); 153.1 (C); 149.5 (C); 137.2 (C); 134.4 (C); 122.4 (CH); 118.7 (CH); 94.6 (CH₂); 43.9 (C); 41.8 (CH₂); 34.9 (C); 31.8 (CH₃); 30.8 (CH₂); 28.8 (CH₃); 26.0 (CH₃); 18.4 (C); -4.5 (CH₃).

HRMS: calculated for $\text{C}_{23}\text{H}_{39}\text{OSi}$ ($\text{M}+\text{H}^+$): 359.2765, found 359.2759.

Synthesis of (benzofuran-3-yloxy)(*tert*-butyl)dimethylsilane.



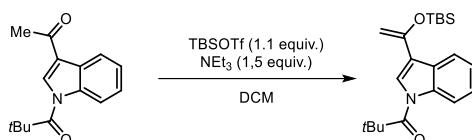
To an oven dried round bottom flask kept under nitrogen was added benzofuranone (3 mmol, 402 mg) and dry THF (6 mL). The solution was cooled to $-78\text{ }^{\circ}\text{C}$ in a dry ice/acetone bath and NaHMDS (3 mmol, 1 M solution in THF, 3mL) was added dropwise. The mixture was stirred for 20 minutes. TBSOTf (3.15 mmol, 723 μL) was then added dropwise, the cold bath was removed and the mixture allowed to warm up to room temperature. The reaction mixture was then filtered over Celite (washed with hexanes) and the filtrate concentrated under reduced pressure. The residue was purified by flash column chromatography (hexanes containing 1% NEt_3) to afford the product as a yellowish oil (684 mg, 92% yield).

$^1\text{H NMR}$ (400 MHz, CDCl_3) δ 7.54-7.50 (m, 1H); 7.39-7.35 (m, 1H); 7.28-7.23 (m, 2H); 7.22-7.17 (m, 1H); 1.02 (s, 9H); 0.21 (s, 6H).

$^{13}\text{C NMR}$ (101 MHz, CDCl_3) δ 153.9 (C); 139.5 (C); 130.2 (CH); 124.8 (CH); 124.4 (C); 122.4 (CH); 119.0 (CH); 112.0 (CH); 26.0 (CH_3); 18.6 (C); -4.4 (CH_3).

HRMS: calculated for $\text{C}_{14}\text{H}_{21}\text{O}_2\text{Si}$ ($\text{M}+\text{H}^+$): 149.1305, found 249.1295.

Synthesis of 1-(3-(1-((*tert*-butyldimethylsilyl)oxy)vinyl)-2,2-dimethylpropan-1-onyl)-1H-indol-1-yl)-2,2-dimethylpropan-1-one.



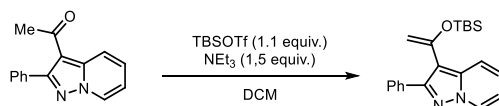
In an oven dried round bottom flask kept under nitrogen, *N*-pivaloyl indole (2.466 mmol, 600 mg) was dissolved in dry DCM (5 mL) and the resulting solution was cooled in an ice bath. Triethylamine (3.7 mmol, 516 μL) was added followed by TBSOTf (2.71 mmol, 623 μL). The mixture was stirred for two hours at this temperature and poured into water/DCM in an extraction funnel. The phases were separated and the water phase was extracted twice with DCM, the combined organic fractions dried (MgSO_4) and concentrated to dryness. The residue was purified by flash column chromatography (hexanes/ EtOAc 95/5 containing 1% NEt_3) to afford the product as a clear oil (420 mg, 47% yield).

$^1\text{H NMR}$ (400 MHz, CDCl_3) δ 8.60-8.51 (m, 1H); 7.96 (s, 1H); 7.87-7.82 (m, 1H); 7.43-7.29 (m, 2H); 4.98 (d, $J = 1.6$ Hz, 1H); 4.63 (d, $J = 1.6$ Hz, 1H); 1.53 (s, 9H); 1.04 (s, 9H); 0.27 (s, 6H).

$^{13}\text{C NMR}$ (101 MHz, CDCl_3) δ 177.0 (C); 150.7 (C); 137.8 (C); 126.4 (C); 125.2 (CH); 124.6 (CH); 123.8 (CH); 120.0 (CH); 117.5 (CH); 93.4 (CH_2); 41.3 (C); 28.6 (CH_3); 25.8 (CH_3); 18.2 (C); 1.0 (C); -4.5 (CH_3).

HRMS: calculated for $\text{C}_{21}\text{H}_{32}\text{NO}_2\text{Si}$ ($\text{M}+\text{H}^+$): 358.2197, found 258.2193.

Synthesis of 3-(1-((*tert*-butyldimethylsilyl)oxy)vinyl)-2-phenylpyrazolo[1,5-*a*]pyridine.



In an oven dried round bottom flask kept under nitrogen, 1-(2-phenylpyrazolo[1,5-*a*]pyridin-3-yl)ethan-1-one (3.17 mmol, 750 mg) was dissolved in dry DCM (6.5 mL) and the resulting solution was cooled in an ice bath. Triethylamine (4.76 mmol, 664 μL) was added followed by TBSOTf (3.49 mmol, 802 μL). The mixture was stirred for two hours at this temperature and then poured into water/DCM in an extraction funnel. The water phase was extracted twice with DCM, the combined organic fractions dried (MgSO_4)

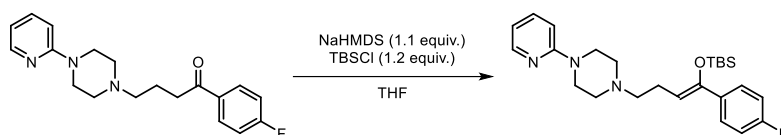
and concentrated to dryness. The residue was purified by flash column chromatography (hexanes/EtOAc 95/5 containing 1% NEt₃) to afford the product as a yellow oil (632 mg, 57% yield).

¹H NMR (400 MHz, CDCl₃) δ 8.49-8.42 (m, 1H); 7.91-7.85 (m, 2H); 7.76-7.70 (m, 1H); 7.47-7.40 (m, 2H); 7.40-7.34 (m, 1H); 7.16 (ddd, *J* = 8.9, 6.7, 1.1 Hz, 1H); 6.78 (td, *J* = 6.8, 1.3 Hz, 1H); 4.66 (d, *J* = 0.6 Hz, 1H); 4.53 (d, *J* = 0.6 Hz, 1H); 0.77 (s, 9H); 0.01 (s, 6H).

¹³C NMR (101 MHz, CDCl₃) δ 151.4 (C); 150.2 (C); 139.7 (C); 133.4 (C); 128.8 (CH); 128.3 (CH); 128.16 (CH); 128.14 (CH); 123.7 (CH); 117.9 (CH); 112.0 (CH); 108.3 (C); 95.6 (CH₂); 25.5 (CH₃); -4.8 (CH₃).

HRMS: calculated for C₂₁H₂₇N₂OSi (M+H⁺): 351.1887, found 351.1880.

Synthesis of (Z)-1-(4-((*tert*-butyldimethylsilyloxy)-4-(4-fluorophenyl)but-3-en-1-yl)-4-(pyridin-2-yl)piperazine.



In an oven-dried two necked round bottom flask, azaperone (5 mmol, 1.637 g) was dissolved in dry THF (25 mL) and cooled to -78°C in a dry ice/acetone bath. A solution of NaHMDS (5.5 mmol, 5.5 mL of 1 M solution in THF, 1.1 equiv.) was added dropwise and the mixture stirred for 30 minutes, then warmed up to 0 °C for 30 minutes. The mixture was cooled down again to -78 °C and a solution of TBSCl (6 mmol, 904 mg) in dry THF (2 mL) was added dropwise. After 15 minutes stirring, the cold bath was removed and stirring continued overnight. Water and ethyl acetate were added, the mixture transferred into an extraction funnel and the organic layer was washed twice with a saturated solution of Na₂CO₃. The organic phase was then dried (MgSO₄) and concentrated to give a slightly yellow oil that was purified by flash column chromatography (hexanes/EtOAc gradient from 70:30 to 60:40 containing 1% of NEt₃ as eluent) to afford the product as a white crystalline solid (2.140 g, 97% yield).

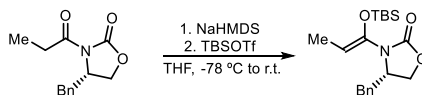
¹H NMR (500 MHz, CDCl₃) δ 8.22-8.19 (m, 1H); 7.52-7.46 (m, 1H); 7.44-7.37 (m, 2H); 7.03-6.95 (m, 2H); 6.69-6.60 (m, 2H); 5.06 (t, *J* = 6.7 Hz, 1H); 3.61-3.55 (m, 4H); 2.61-2.55 (m, 4H); 2.50-2.44 (m, 2H); 2.44-2.37 (m, 2H); 0.96 (s, 9H); -0.06 (s, 6H).

¹³C NMR (125 MHz, CDCl₃) δ 162.6 (d, *J* = 241 Hz, C); 159.9 (C); 149.7 (C); 148.3 (CH); 137.7 (CH); 136.1 (d, *J* = 3 Hz, C); 127.9 (d, *J* = 8 Hz, CH); 115.1 (d, *J* = 21 Hz, CH); 113.5 (CH); 109.2 (CH); 107.3 (CH); 58.5 (CH₂); 53.2 (CH₂); 45.6 (CH₂); 26.2 (CH₃); 24.1 (CH₂); 18.6 (C); -3.6 (CH₃).

¹⁹F NMR (376 MHz, CDCl₃) δ -114.48.

HRMS: calculated for C₂₅H₃₇FN₃OSi (M+H⁺): 442.2684, found 442.2679.

Synthesis of (S,Z)-4-benzyl-3-(1-((*tert*-butyldimethylsilyloxy)prop-1-en-1-yl)oxazolidin-2-one.



In oven dried round bottom flask kept under argon, (*S*)-4-benzyl-3-propionyloxazolidin-2-one (5.6 mmol, 1.32 g) was dissolved in dry THF (11.3 mL) and cooled down to -78°C. NaHMDS (1 M solution in THF, 6.2 mL) was then added dropwise via syringe and the reaction stirred for one hour at this temperature. TBSTf (5.9 mmol, 1.36 mL) was added dropwise, the reaction was stirred at this temperature for 30 minutes and then warmed up to ambient temperature over 30 minutes. Volatiles were evaporated under

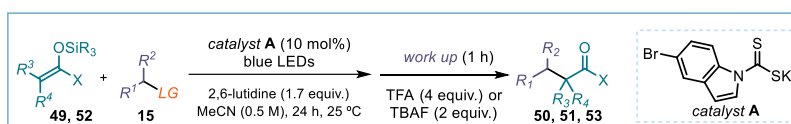
reduced pressure and diethyl ether (10 mL) was added to obtain a suspension, which was filtered quickly over Celite. The filtrate was concentrated and the crude purified by flash chromatography (gradient hexanes:EtOAc, from 95:5 to 9:1) with neutralized silica (treated with hexanes + 1% triethylamine) to give 1.640 g of a colorless oil. The isolated material consisted of a mixture of the product with a *N*-silylated oxazolidinone side-product arising from ketene elimination of the sodium enolate intermediate and subsequent *N*-silylation. The desired *N*-*O* silyl ketene acetal was judged 89% pure in weight by ^1H NMR analysis (1.47 g, 75% corrected yield). For characterization purposes, spectroscopic data of a fraction of the product (883 mg, 94% purity) are reported.

^1H NMR (400 MHz, CDCl_3) δ 7.36-7.30 (m, 2H); 7.30-7.24 (m, 1H); 7.19-7.14 (m, 2H); 4.93 (q, $J = 6.9$ Hz, 1H); 4.25-4.13 (m, 2H); 4.04 (dd, $J = 8.2, 5.3$ Hz, 1H); 3.20 (dd, $J = 13.4, 3.6$ Hz, 1H); 2.62 (dd, $J = 13.5, 9.4$ Hz, 1H); 1.69 (d, $J = 6.9$ Hz, 3H); 1.02 (s, 9H); 0.25 (s, 3H); 0.19 (s, 3H).

^{13}C NMR (101 MHz, CDCl_3) δ 155.5 (C); 137.9 (C); 135.7 (C); 129.1 (CH); 128.9 (CH); 127.1 (CH); 103.9 (CH); 66.6 (CH_2); 56.2 (CH); 38.3 (CH_2); 25.7 (CH_3); 18.1 (C); 11.0 (CH_3); -4.4 (CH_3); -4.7 (CH_3).

HRMS: calculated for $\text{C}_{19}\text{H}_{29}\text{NNaO}_3\text{Si}$ ($\text{M}+\text{Na}^+$): 370.1809, found 370.1807.

2.8.3 General procedure



In an oven dried Schlenk tube, **49** or **52** (0.75 mmol, 1.5 equiv.) was dissolved in acetonitrile (1 mL, HPLC grade), then 2,6-lutidine (99 μL , 0.85 mmol, 1.7 equiv.) was added, followed by catalyst **A** (15.5 mg, 0.05 mmol, 0.1 equiv.) and the alkyl electrophile **15** (0.5 mmol, 1 equiv.). The resulting yellow mixture was degassed via three cycles of freeze-pump-thaw. The Schlenk tube was then placed in the irradiation setup (see Figure 2.31), maintained at a temperature of 25 °C (25-26 °C measured in the central well), and the reaction, unless otherwise stated, was stirred for 24 hours under continuous irradiation from a blue LED strip. Chloroform (1 mL) was then added followed by trifluoroacetic acid (150 μL , 2 mmol, 4 equiv.) and the resulting mixture stirred until all the *O*-silylated product was hydrolyzed to the corresponding ketone product, as judged by TLC analysis. Volatiles were evaporated and the residue purified by column chromatography on silica gel to afford the corresponding product in the stated yield with >95% purity according to ^1H NMR analysis. The exact conditions for chromatography are reported for each compound.

2.8.4 Characterization Data

4-oxo-4-phenylbutanenitrile (50a)

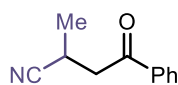
Prepared according to the general procedure using *tert*-butyldimethyl((1-phenylvinyl)oxy)silane (0.75 mmol, 176 mg) and chloroacetonitrile **15a** (0.5 mmol, 32 μL). Time of irradiation: 24 hours at 25 °C. Flash column chromatography (hexanes/EtOAc 80:20) to afford product **50a** as a yellowish solid (72 mg, 91% yield).

Characterization data matching data reported in the literature.⁵⁷

^1H NMR (400 MHz, CDCl_3) δ 7.94-7.88 (m, 2H); 7.60-7.54 (m, 1H); 7.48-7.41 (m, 2H); 3.33 (t, $J = 7.3$ Hz, 2H); 2.72 (t, $J = 7.3$ Hz, 2H).

⁵⁷ Xia, A.; Xie, X.; Chen, H.; Zhao, J.; Zhang, C.; Liu, Y. "Nickel-Catalyzed Cyanation of Unactivated Alkyl Chlorides or Bromides with $\text{Zn}(\text{CN})_2$ " *Org. Lett.* **2018**, *20*, 7735-7739.

¹³C NMR (101 MHz, CDCl₃) δ 195.8 (C); 135.9 (C); 134.2 (CH); 129.2 (CH); 128.3 (CH); 119.6 (C); 34.5 (CH₂); 12.1 (CH₂).



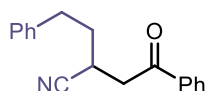
2-methyl-4-oxo-4-phenylbutanenitrile (50b).

Prepared according to the general procedure using *tert*-butyldimethyl((1-phenylvinyl)oxy)silane (0.75 mmol, 176 mg) and chloropropionitrile (0.5 mmol, 46 μL). Time of irradiation: 24 hours at 60 °C. Flash column chromatography (hexanes/EtOAc 80:20) to afford product **50b** as a slightly yellow oil (36 mg, 41% yield).

Characterization data matching data reported in the literature.⁵⁸

¹H NMR (400 MHz, CDCl₃) δ 7.96-7.90 (m, 2H); 7.62-7.55 (m, 1H); 7.50-7.43 (m, 2H); 3.39 (dd, *J* = 17.3, 6.3 Hz, 1H); 3.35-3.27 (m, 1H); 3.19 (dd, *J* = 17.3, 6.7 Hz, 1H); 1.40 (d, *J* = 7 Hz, 3H).

¹³C NMR (101 MHz, CDCl₃) δ 195.6 (C); 136.2 (C); 134.2 (CH); 129.2 (CH); 128.4 (CH); 122.9 (C); 42.6 (CH₂); 20.9 (CH); 18.2 (CH₃).



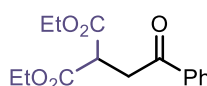
4-oxo-2-phenethyl-4-phenylbutanenitrile (50c)

Prepared according to the general procedure using *tert*-butyldimethyl((1-phenylvinyl)oxy)silane (0.75 mmol, 176 mg) and 1-cyano-3-phenylpropyl 4-nitrobenzenesulfonate (0.5 mmol, 173 mg). Time of irradiation: 24 hours at 60 °C. Flash column chromatography (hexanes/EtOAc 80:20, then a second chromatography with toluene as eluent) to afford product **50c** as a yellowish solid (55 mg, 42% yield).

¹H NMR (400 MHz, CDCl₃) δ 7.93-7.88 (m, 2H); 7.62-7.56 (m, 1H); 7.49-7.44 (m, 2H); 7.32-7.27 (m, 2H); 7.23-7.18 (m, 3H); 3.44-3.35 (m, 1H); 2.99-2.91 (m, 1H); 2.86-2.77 (m, 1H); 2.02-1.95 (m, 2H).

¹³C NMR (101 MHz, CDCl₃) δ 195.4 (C); 140.2 (C); 136.2 (C); 134.2 (CH); 129.2 (CH); 129.0 (CH); 128.8 (CH); 128.4 (CH); 126.8 (CH); 121.9 (C); 41.1 (CH₂); 33.9 (CH₂); 33.7 (CH₂); 26.3 (CH).

HRMS: calculated for C₁₈H₁₇NNaO (M+Na⁺): 286.1202, found 286.1198.



diethyl 2-(2-oxo-2-phenylethyl)malonate (50d)

Prepared according to the general procedure using *tert*-butyldimethyl((1-phenylvinyl)oxy)silane (0.75 mmol, 176 mg) and diethylchloromalonate (0.5 mmol, 85 μL). Time of irradiation: 24 hours at 25 °C. Flash column chromatography (hexanes/EtOAc gradient from 95:5 to 90:10) to afford product **50d** as a yellowish oil (131 mg, 94% yield).

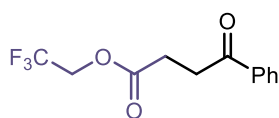
Characterization data matching data reported in the literature.⁵⁹

¹H NMR (400 MHz, CDCl₃) δ 7.98-7.94 (m, 2H); 7.58-7.53 (m, 1H); 7.48-7.42 (m, 2H); 4.27-4.16 (m, 4H); 4.04 (t, *J* = 7.1 Hz, 1H); 3.61 (d, *J* = 7.1 Hz, 2H); 1.27 (t, *J* = 7.2 Hz, 6H).

¹³C NMR (101 MHz, CDCl₃) δ 196.5 (C); 169.0 (C); 136.1 (C); 133.5 (CH); 128.6 (CH); 128.1 (CH); 61.7 (CH₂); 47.2 (CH); 37.7 (CH₂); 14.0 (CH₃).

⁵⁸ Yang, J.; Shen, Y.; Chen, F.-X. "Highly Efficient Cs₂CO₃-Catalyzed 1,4-Addition of Me₃SiCN to Enones with Water as the Additive" *Synthesis* **2010**, 1325-1333.

⁵⁹ Jiang, B.; Liang, Q.-J.; Han, Y.; Zhao, M.; Xu, Y.-H.; Loh, T.-P. "Copper-Catalyzed Dehydrogenative Diels-Alder Reaction" *Org. Lett.* **2018**, *20*, 3215-3219.



2,2,2-trifluoroethyl 4-oxo-4-phenylbutanoate (50e)

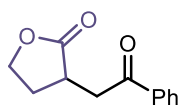
Prepared according to the general procedure using *tert*-butyldimethyl((1-phenylvinyl)oxy)silane (0.75 mmol, 176 mg) and 2,2,2-trifluoroethyl 2-chloroacetate (0.5 mmol, 88 mg). Time of irradiation: 24 hours at 60 °C. Flash column chromatography (hexanes/Toluene/DCM 50:20:30) to afford product **50e** as a yellow oil (48 mg, 37% yield).

¹H NMR (400 MHz, CDCl₃) δ 7.99-7.96 (m, 2H); 7.61-7.56 (m, 1H); 7.52-7.46 (m, 2H); 4.53 (q, *J* = 8.4 Hz, 2H); 3.38 (t, *J* = 6.6 Hz, 2H); 2.89 (t, *J* = 6.6 Hz, 2H).

¹³C NMR (101 MHz, CDCl₃) δ 197.6 (C); 171.6 (C); 136.4 (C); 133.6 (CH); 128.8 (CH); 128.2 (CH); 123.1 (q, *J* = 265 Hz, C); 61.2 (q, *J* = 37.9, CH₂); 33.3 (CH₂); 27.9 (CH₂).

¹⁹F NMR (376 MHz, CDCl₃) δ -73.88.

HRMS: calculated for C₁₂H₁₁F₃NaO₃ (M+Na⁺): 283.0552, found 283.0564.



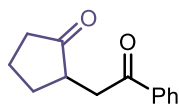
3-(2-oxo-2-phenylethyl)dihydrofuran-2(3H)-one (50f)

Prepared according to the general procedure using *tert*-butyldimethyl((1-phenylvinyl)oxy)silane (0.75 mmol, 176 mg) and 3-bromodihydrofuran-2(3H)-one (0.5 mmol, 82 mg). Time of irradiation: 24 hours at 25 °C. Flash column chromatography (hexanes/EtOAc gradient from 70:30 to 50:50) to afford product **50f** as an off-white solid (82 mg, 75% yield).

Characterization data matching data reported in the literature.⁶⁰

¹H NMR (400 MHz, CDCl₃) δ 8.00-7.94 (m, 2H); 7.63-7.55 (m, 1H); 7.52-7.44 (m, 2H); 4.44 (td, *J* = 9.0, 2.0 Hz, 1H); 4.32-4.24 (m, 1H); 3.72-3.61 (m, 1H); 3.24-3.09 (m, 2H); 2.69-2.59 (m, 1H); 2.05-1.92 (m, 1H).

¹³C NMR (101 MHz, CDCl₃) δ 196.9 (C); 179.2 (C); 136.2 (C); 133.5 (CH); 128.7 (CH), 128.0 (CH); 66.8 (CH₂); 39.3 (CH₂); 35.2 (CH); 29.0 (CH₂).



2-(2-oxo-2-phenylethyl)cyclopentan-1-one (50g)

Prepared according to the general procedure using *tert*-butyldimethyl((1-phenylvinyl)oxy)silane (0.75 mmol, 176 mg) 2-bromocyclopentan-1-one (0.5 mmol, 82 mg). Time of irradiation: 24 hours at 25 °C in DCE. Flash column chromatography (hexanes/Et₂O 60:40) to afford product **50g** as a yellow oil (83 mg, 82% yield).

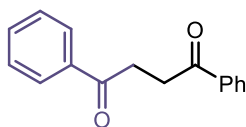
Characterization data matching data reported in the literature.⁶¹

¹H NMR (300 MHz, CDCl₃) δ 7.97-7.94 (m, 2H); 7.57-7.54 (m, 1H); 7.48-7.43 (m, 2H); 3.53 (dd, *J* = 18.1, 3.3 Hz, 1H); 3.05 (dd, *J* = 18.1, 8.0 Hz, 1H); 2.67-2.62 (m, 1H); 2.42-2.25 (m, 3H); 2.17-2.01 (m, 1H), 1.96-1.76 (m, 1H); 1.72-1.51 (m, 1H).

¹³C NMR (75 MHz, CDCl₃) δ 220.5 (C); 198.1 (C); 136.8 (C); 133.4 (CH); 128.8 (CH); 128.2 (CH); 45.2 (CH); 38.8(CH₂); 37.7 (CH₂); 29.9 (CH₂); 21.0 (CH₂).

⁶⁰ Cai, Y.; Roberts, B. P.; Tocher, D. A.; Barnett, S. A. "Carbon-carbon bond formation by radical addition-fragmentation reactions of O-alkylated enols" *Org. Biomol. Chem.* **2004**, *2*, 2517-2529.

⁶¹ Lan, X.-W.; Wang, N. X.; Zhang, W.; Wen, J.-L.; Bai, C.-B.; Xing, Y.; Li, Y. H. "Copper/Manganese Cocatalyzed Oxidative Coupling of Vinylarenes with Ketones" *Org. Lett.* **2015**, *17*, 4460-4463.



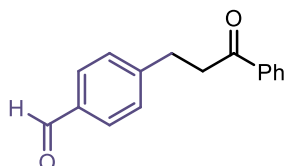
1,4-diphenylbutane-1,4-dione (50h)

Prepared according to the general procedure using *tert*-butyldimethyl((1-phenylvinyl)oxy)silane (0.75 mmol, 176 mg) and 2-chloro-1-phenylethan-1-one (0.5 mmol, 77 mg). Time of irradiation: 24 hours at 60 °C. Flash column chromatography (hexanes/AcOEt 96:4) to afford product **50h** as a white solid (57 mg, 47% yield).

Characterization data matching data reported in the literature.⁶¹

¹H NMR (400 MHz, CDCl₃) δ 8.06-8.03 (m, 4H); 7.58-7.56 (m, 2H); 7.51-7.47 (m, 4H); 3.47 (s, 4H).

¹³C NMR (101 MHz, CDCl₃) δ 198.8 (C); 136.9 (C); 133.3 (CH); 128.8 (CH); 128.3 (CH); 32.7(CH₂).



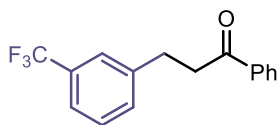
4-(3-oxo-3-phenylpropyl)benzaldehyde (50i)

Prepared according to the general procedure using *tert*-butyldimethyl((1-phenylvinyl)oxy)silane (0.75 mmol, 176 mg) and 4-formylbenzyl methanesulfonate (0.5 mmol, 107 mg). Time of irradiation: 24 hours at 25 °C. Flash column chromatography (hexanes/EtOAc gradient from 95:5 to 85:15) to afford product **50i** as a yellowish solid (70 mg, 59% yield).

Characterization data matching data reported in the literature.⁶²

¹H NMR (400 MHz, CDCl₃) δ 9.97 (s, 1H); 8.00-7.94 (m, 2H); 7.86-7.80 (m, 2H); 7.61-7.54 (m, 1H); 7.51-7.40 (m, 4H); 3.36 (t, *J* = 7.4 Hz, 2H); 3.17 (t, *J* = 7.4 Hz, 2H).

¹³C NMR (101 MHz, CDCl₃) δ 198.7 (C); 192.3 (CH); 148.9 (C); 136.6 (C); 134.6 (C); 133.3 (CH); 130.1 (CH); 129.2 (CH); 128.7 (CH); 128.0 (CH); 39.6 (CH₂); 30.2 (CH₂).



1-phenyl-3-(3-(trifluoromethyl)phenyl)propan-1-one (50j)

Prepared according to the general procedure using *tert*-butyldimethyl((1-phenylvinyl)oxy)silane (0.75 mmol, 176 mg) and 1-(bromomethyl)-3-(trifluoromethyl)benzene (0.5 mmol, 120 mg). Time of irradiation: 24 hours at 60 °C. Flash column chromatography (hexanes/DCM 60:40) to afford product **50j** as a white solid (83 mg, 60% yield).

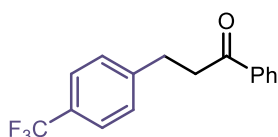
Characterization data matching data reported in the literature.⁶³

¹H NMR (400 MHz, CDCl₃) δ 7.97-7.95 (m, 2H); 7.59-7.47 (tt, *J* = 7.7, 1.3 Hz, 1H); 7.51 (bs, 1H); 7.48-7.38 (m, 5H); 3.33 (t, *J* = 7.5 Hz, 2H); 3.14 (t, *J* = 7.5 Hz, 2H).

¹³C NMR (101 MHz, CDCl₃) δ 198.7 (C); 142.3 (C); 136. (C); 133.3 (CH); 132.1 (CH); 130.9 (q, *J* = 32.2 Hz, C); 129.0 (CH); 128.8 (CH); 128.1 (CH); 124.2 (q, *J* = 270 Hz, C); 125.2 (q, *J* = 3.7 Hz, CH); 123.0 (q, *J* = 3.7 Hz, CH); 40.0 (CH₂); 29.8 (CH₂).

¹⁹F NMR (376 MHz, CDCl₃) δ -62.68.

HRMS: calculated for C₁₆H₁₄F₃O (M+H⁺): 279.0991, found 279.0999.



1-phenyl-3-(4-(trifluoromethyl)phenyl)propan-1-one (50k)

Prepared according to the general procedure using *tert*-butyldimethyl((1-phenylvinyl)oxy)silane (0.75 mmol, 176 mg) and 1-(bromomethyl)-3-(trifluoromethyl)benzene (0.5 mmol, 120 mg). Time of irradiation: 24 hours at

⁶² Jiang, Q.; Guo, T.; Wang, Q.; Wu, P.; Yu, Z. "Rhodium(I)-Catalyzed Arylation of β-Chloro Ketones and Related Derivatives through Domino Dehydrochlorination/ Conjugate Addition" *Adv. Synth. Catal.* **2013**, *355*, 1874-1880.

⁶³ Kuwahara, T.; Fukuyama, T.; Ryu, I. "RuHCl(CO)(PPh₃)₃-Catalyzed α-Alkylation of Ketones with Primary Alcohols" *Org. Lett.* **2012**, *14*, 4703-4705.

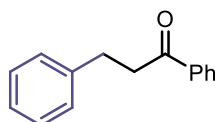
25 °C. Flash column chromatography (hexanes/Tol/DCM 50:10:40) to afford product **50k** as a white solid (51 mg, 37% yield).

Characterization data matching data reported in the literature.⁶⁴

¹H NMR (400 MHz, CDCl₃) δ 7.97-7.90 (m, 2H); 7.59-7.50 (m, 3H); 7.48-7.44 (m, 2H); 7.41-7.34 (m, 2H); 3.33 (t, *J* = 7.5 Hz, 2H); 3.15 (t, *J* = 7.5 Hz, 2H).

¹³C NMR (101 MHz, CDCl₃) δ 198.2 (C); 145.5 (C); 136.8 (C); 133.4 (CH); 129.1 (CH); 128.8 (CH); 128.7 (C); 128.1 (CH); 125.4 (q, *J* = 3.9 Hz, CH); 124.5 (q, *J* = 270 Hz, C); 39.9 (CH₂); 29.9 (CH₂).

¹⁹F NMR (376 MHz, CDCl₃) δ -62.49.



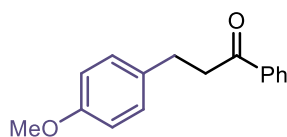
1,3-diphenylpropan-1-one (50l)

Prepared according to the general procedure using *tert*-butyldimethyl((1-phenylvinyl)oxy)silane (0.75 mmol, 176 mg) and (chloromethyl)benzene (0.5 mmol, 57.5 μL). Time of irradiation: 24 hours at 60 °C. Flash column chromatography (hexanes/Toluene/DCM 40:20:40) to afford product **50l** as a white solid (37 mg, 35% yield).

Characterization data matching data reported in the literature.⁶⁵

¹H NMR (400 MHz, CDCl₃) δ 8.97-7.95 (m, 2H); 7.58-7.54 (m, 1H); 7.47-7.44 (m, 2H); 7.32-7.23 (m, 4H); 7.22-7.18 (m, 1H); 3.33-3.29 (m, 2H); 3.09-3.06 (m, 2H).

¹³C NMR (101 MHz, CDCl₃) δ 199.4 (C); 141.4 (C); 137.0 (C); 133.2 (CH); 128.7 (CH); 128.7 (CH); 128.6 (CH); 128.2 (CH); 126.3 (CH); 40.6 (CH₂); 30.3 (CH₂).



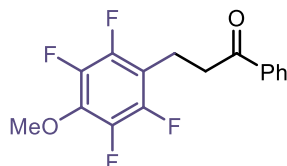
3-(4-methoxyphenyl)-1-phenylpropan-1-one (50m)

Prepared according to the general procedure using *tert*-butyldimethyl((1-phenylvinyl)oxy)silane (0.75 mmol, 176 mg) and 1-(chloromethyl)-4-methoxybenzene (0.5 mmol, 67.8 μL). Time of irradiation: 24 hours at 60 °C. Flash column chromatography (hexanes/EtOAc 96:4) to afford product **50m** as a white solid (36 mg, 30% yield).

Characterization data matching data reported in the literature.⁶⁶

¹H NMR (400 MHz, CDCl₃) δ 7.96-7.94 (m, 2H); 7.57-7.53 (m, 1H); 7.47-7.43 (m, 2H); 7.18 (d, *J* = 8.3 Hz, 2H); 6.84 (d, *J* = 8.7 Hz, 2H); 3.79 (s, 3H); 3.29-3.25 (m, 2H); 3.03-2.99 (m, 2H).

¹³C NMR (101 MHz, CDCl₃) δ 199.5 (C); 158.1 (C); 137.0 (C); 133.4 (C); 133.1 (CH); 129.5 (CH); 128.7 (CH); 128.1 (CH); 114 (CH); 55.4 (CH₃); 40.8 (CH₂); 29.4 (CH₂).



1-phenyl-3-(2,3,5,6-tetrafluoro-4-methoxyphenyl)propan-1-one (50n)

Prepared according to the general procedure using *tert*-butyldimethyl((1-phenylvinyl)oxy)silane (0.75 mmol, 176 mg) and 1-(bromomethyl)-2,3,5,6-tetrafluoro-4-methoxybenzene (0.5 mmol, 80 μL). Time of irradiation: 24 hours at 25 °C. Flash column chromatography (Toluene) to afford product **50n** as a white solid (153 mg, 98% yield).

⁶⁴ Prasanna, R.; Guha, S.; Sekar, G. "Proton-Coupled Electron Transfer: Transition-Metal-Free Selective Reduction of Chalcones and Alkynes Using Xanthate/Formic Acid" *Org. Lett.* **2019**, *21*, 2650-2653.

⁶⁵ Vellakkaran, M.; Andappan, M. M. S.; Kommu, N. "Replacing a stoichiometric silver oxidant with air: ligated Pd(ii)-catalysis to β-aryl carbonyl derivatives with improved chemoselectivity" *Green Chem.* **2014**, *16*, 2788-2797.

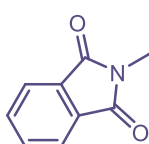
⁶⁶ Peña-López, M.; Piehl, P.; Elangovan, S.; Neumann, H.; Beller, M. "Manganese-Catalyzed Hydrogen-Autotransfer C-C Bond Formation: α-Alkylation of Ketones with Primary Alcohols" *Angew. Chem. Int. Ed.* **2016**, *55*, 14967-14971.

¹H NMR (400 MHz, CDCl₃) δ 7.96-7.94 (m, 2H); 7.57 (tt, *J* = 7.3, 1.3 Hz, 1H); 7.48-7.44 (m, 2H), 4.05 (t, *J* = 1.2 Hz, 3H); 3.30-3.26 (m, 2H); 3.14-3.10 (m, 2H)

¹³C NMR (101 MHz, CDCl₃) δ 198.1 (C); 146.5 (ddd, *J* = 244.0, 9.77, 4.0 Hz, C); 141.0 (ddt, *J* = 246.7, 15.4, 3.9 Hz, C); 136.9 (tt, *J* = 12.1, 3.8 Hz, C); 136.8 (C); 133.4 (CH); 128.8 (CH); 128.1 (CH); 112.6 (t, *J* = 18.5 Hz, C); 62.3 (t, *J* = 3.6 Hz, CH₃); 37.7 (CH₂); 17.2 (t, *J* = 1.8 Hz, CH₂).

¹⁹F NMR (376 MHz, CDCl₃) δ -145.4 - -145.5 (m, 2F), -158.49 - -158.57 (m, 2F).

HRMS: calculated for C₁₆H₁₂F₄O₂ (M+H⁺): 313.0846, found 313.0834.



2-(3-oxo-3-phenylpropyl)isoindoline-1,3-dione (50o)

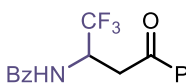
Prepared according to the general procedure using *tert*-butyldimethyl((1-phenylvinyl)oxy)silane (0.75 mmol, 176 mg) and 2-(chloromethyl)isoindoline-1,3-dione (0.5 mmol, 98 mg) in DCE. Time of irradiation: 24 hours at 25 °C.

Flash column chromatography (hexanes/EtOAc 90:10 to 85:15) to afford product **50o** as a slightly yellow oil (116 mg, 87% yield).

Characterization data matching data reported in the literature.⁶⁷

¹H NMR (400 MHz, CDCl₃) δ 7.93-7.87 (m, 2H); 7.83-7.77 (m, 2H); 7.70-7.64 (m, 2H); 7.55-7.48 (m, 1H); 7.44-7.37 (m, 2H); 4.10 (t, *J* = 7.4 Hz, 2H); 3.39 (t, *J* = 7.4 Hz, 2H).

¹³C NMR (101 MHz, CDCl₃) δ 197.6 (C); 168.5 (C); 136.7 (C); 134.3 (CH); 133.7 (CH); 132.4 (C); 129.0 (CH); 128.3 (CH); 123.6 (CH); 37.1 (CH₂); 33.9 (CH₂).



N-(1,1,1-trifluoro-4-oxo-4-phenylbutan-2-yl)benzamide (50p)

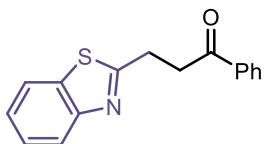
Prepared according to the general procedure using *tert*-butyldimethyl((1-phenylvinyl)oxy)silane (0.75 mmol, 176 mg) and *N*-(1-chloro-2,2,2-trifluoroethyl)benzamide (0.5 mmol, 119 mg) in DCE (1 mL). Time of irradiation: 24 hours at 25 °C. Flash column chromatography (hexanes/EtOAc 70:30) to afford product **50p** as an off-white solid (82 mg, 75% yield).

¹H NMR (400 MHz, CDCl₃) δ 8.01-7.94 (m, 2H); 7.88-7.82 (m, 2H); 7.68-7.61 (m, 1H); 7.59-7.44 (m, 6H); 5.52-5.37 (m, 1H); 3.67 (dd, *J* = 5.8, 17.3 Hz, 1H); 3.36 (dd, *J* = 5.8, 17.3 Hz, 1H).

¹³C NMR (101 MHz, CDCl₃) δ 196.5 (C); 166.9 (C); 136.1 (C); 134.1 (CH); 133.2 (C); 132.1 (CH); 128.9 (CH); 128.7 (CH); 128.2 (CH); 127.8 (q, *J* = 283 Hz, C); 127.2 (CH); 48.5 (q, *J* = 32 Hz, C); 35.7 (CH₂).

¹⁹F NMR (101 MHz, CDCl₃) δ -74.50.

HRMS: calculated for C₁₇H₁₃F₃NO₂ (M+H⁺): 320.0899, found 320.0904.



3-(benzo[d]thiazol-2-yl)-1-phenylpropan-1-one (50q)

Prepared according to the general procedure using *tert*-butyldimethyl((1-phenylvinyl)oxy)silane (0.75 mmol, 176 mg) and 2-(chloromethyl)benzothiazole (0.5 mmol, 92 mg) in DCE. Time of irradiation:

24 hours at 25 °C. Flash column chromatography (hexanes/EtOAc 90:10 to 85:15) to afford product **50q** as a slightly yellow oil (116 mg, 87% yield).

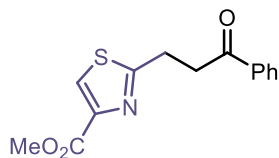
Characterization data matching data reported in the literature.⁶⁸

⁶⁷ Jie, X.; Shang, Y.; Zhang, X.; Su, W., "Cu-Catalyzed Sequential Dehydrogenation-Conjugate Addition for β -Functionalization of Saturated Ketones: Scope and Mechanism" *J. Am. Chem. Soc.* **2016**, *138*, 5623-5633.

⁶⁸ Lu, S.-C. Li, H.-S.; Xu, S.; Duan, G.-Y. "Silver-catalyzed C₂-selective direct alkylation of heteroarenes with tertiary cycloalkanol" *Org. Biomol. Chem.* **2017**, *15*, 324-327.

¹H NMR (400 MHz, CDCl₃) δ 8.05-8.01 (m, 1H); 8.00-7.96 (m, 2H); 7.86-7.81 (m, 1H); 7.57 (td, *J* = 7.3, 1.2 Hz, 1H); 7.52-7.44 (m, 3H); 7.43-7.39 (m, 1H); 3.65 (bs, 4H).

¹³C NMR (101 MHz, CDCl₃) δ 197.8 (C); 173.7 (C); 150.5 (C); 136.5 (C); 134.3 (C); 133.9 (CH); 129.1 (CH); 128.5 (CH); 127.2 (CH); 126.1 (CH); 122.1 (CH); 121.9 (CH); 37.9 (CH₂); 27.7 (CH₂).



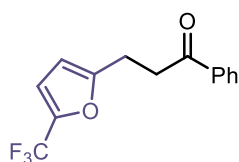
methyl 2-(3-oxo-3-phenylpropyl)thiazole-5-carboxylate (50r)

Prepared according to the general procedure using *tert*-butyldimethyl((1-phenylvinyl)oxy)silane (0.75 mmol, 176 mg) and methyl 2-(chloromethyl)thiazole-4-carboxylate (0.5 mmol, 96 mg). Time of irradiation: 24 hours at 25 °C in DCE. Flash column chromatography (hexanes/AcOEt 70:30) to afford product **50r** as a white solid (82 mg, 60% yield).

¹H NMR (400 MHz, CDCl₃) δ 8.07 (s, 1H); 8.01-7.95 (m, 2H); 7.60-7.55 (m, 1H); 7.49-7.44 (m, 2H); 3.93 (s, 3H); 3.60-3.55 (m, 2H); 3.53-3.48 (m, 2H).

¹³C NMR (101 MHz, CDCl₃) δ 197.9 (C); 170.8 (C); 162.0 (C); 146.5 (C); 136.5 (C); 133.6 (CH); 128.8 (CH); 128.2 (CH); 127.8 (CH); 52.6 (CH₃); 38.2 (CH₂); 27.6 (CH₂).

HRMS: calculated for C₁₄H₁₄NO₃S (M+H⁺): 276.0689, found 276.0699.



1-phenyl-3-(5-(trifluoromethyl)furan-2-yl)propan-1-one (50s)

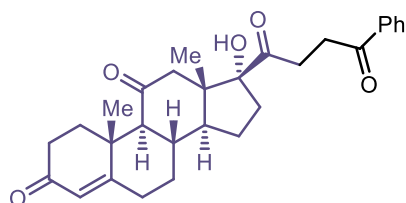
Prepared according to the general procedure using *tert*-butyldimethyl((1-phenylvinyl)oxy)silane (0.75 mmol, 176 mg) and 2-(bromomethyl)-5-(trifluoromethyl)furan (0.5 mmol, 69.0 μL). Time of irradiation: 24 hours at 60 °C in DCE. Flash column chromatography (hexanes/DCM 70:30) to afford product **50s** as a light brown solid (49 mg, 37% yield).

¹H NMR (400 MHz, CDCl₃) δ 7.98-7.96 (m, 2H); 7.60-7.56 (m, 1H); 7.50-7.46 (m, 2H); 6.68-6.67 (m, 1H); 6.15-6.14 (m, 1H); 3.37 (t, *J* = 7.7 Hz, 2H); 3.14 (t, *J* = 7.7 Hz, 2H).

¹³C NMR (101 MHz, CDCl₃) δ 198.1 (C); 158.0 (C); 140.6 (q, *J* = 43.3 Hz, C); 136.7 (C); 133.5 (CH); 128.8 (CH); 128.2 (CH); 119.3 (q, *J* = 269 Hz, CF₃); 112.6 (q, *J* = 3 Hz, CH); 106.8 (CH); 36.5 (CH₂); 22.5 (CH₂).

¹⁹F NMR (376 MHz, CDCl₃) δ -64.01.

HRMS: calculated for C₁₄H₁₁F₃NaO₂ (M+Na⁺): 291.0603, found 291.0604.



(8S,9S,10R,13S,14S,17R)-17-hydroxy-10,13-dimethyl-17-(4-oxo-4-phenylbutanoyl)-1,6,7,8,9,10,12,13,14,15,16,17-dodecahydro-3H-cyclopenta[a]phenanthrene-3,11(2H)-dione (50t)

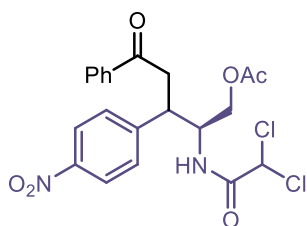
Prepared according to the general procedure using *tert*-butyldimethyl((1-phenylvinyl)oxy)silane (0.75 mmol, 176 mg) and 2-((8S,9S,10R,13S,14S,17R)-17-hydroxy-10,13-dimethyl-3,11-dioxo-2,3,6,7,8,9,10,11,12,13,14,15,16,17-tetradecahydro-1H-cyclopenta[a]phenanthren-17-yl)-2-oxoethyl methanesulfonate (0.5 mmol, 219 mg). Time of irradiation: 24 hours at 25 °C in DCE (20 mol% of catalyst). Flash column chromatography (Toluene/DCM/AcOEt 70:10:20 then 60:10:30) to afford product **50t** as a white solid (72 mg, 31% yield).

¹H NMR (400 MHz, CDCl₃) δ 7.98-7.95 (m, 2H); 7.59-7.57 (m, 1H); 7.47-7.45 (m, 2H); 5.74 (s, 1H); 3.54 (bs, 1H); 3.63-3.47 (m, 1H); 3.51-3.32 (m, 2H); 3.00 (d, *J* = 12.5 Hz, 1H); 2.84-2.75 (m, 2H); 2.52-2.45

(m, 3H); 2.35-2.29 (m, 3H); 2.19 (d, $J = 12.35$ Hz, 1H); 2.02 (s, 1H); 2.02-1.88 (m, 3H); 1.82-1.58 (m, 3H); 1.50-1.40 (m, 1H); 1.41 (s, 3H); 0.70 (s, 3H).

^{13}C NMR (101 MHz, CDCl_3) δ 211.8 (C); 210.0 (C); 199.9 (C); 199.8 (C); 168.8 (C); 136.0 (C); 133.7 (CH); 128.8 (CH); 128.4 (CH); 124.6 (CH); 89.6 (C); 62.7 (CH); 50.9 (C); 50.5 (CH_2); 49.8 (CH); 38.3 (C); 36.8 (CH); 34.9 (CH_2); 34.6 (CH_2); 34.2 (CH_2); 33.9 (CH_2); 32.4 (CH_2); 32.3 (CH_2); 31.9 (CH_2); 23.5 (CH_2); 17.4 (CH_3); 16.1 (CH_3).

HRMS: calculated for $\text{C}_{29}\text{H}_{34}\text{NaO}_5$ ($\text{M}+\text{Na}^+$): 485.2298, found 485.2300.



(2S)-2-(2,2-dichloroacetamido)-3-(4-nitrophenyl)-5-oxo-5-phenylpentyl acetate (50u)

Prepared according to the general procedure using *tert*butyldimethyl((1-phenylvinyl)oxy)silane (0.75 mmol, 176 mg) and (2*R*,3*R*)-2-(2,2-dichloroacetamido)-3-(4-nitrophenyl)-3-(((4-nitrophenyl)sulfonyl)oxy)propyl acetate (0.5 mmol, 275 mg). Time of irradiation: 24 hours at 25 °C. Flash column chromatography (DCM/hexanes/EtOAc 70:25:5) to afford product **50u** as a yellowish solid (53 mg, 23% yield, 1:1 mixture of diastereoisomers).

An analytical sample of each diastereoisomer could be obtained via further purification by preparative TLC (hexanes/AcOEt 60:40 as eluant)

Spectroscopic data for diastereoisomer 50uA ($R_f = 0.50$, hexanes/AcOEt 60:40)

^1H NMR (400 MHz, CDCl_3) δ 8.27-8.21 (m, 2H); 7.93-7.87 (m, 2H); 7.63-7.53 (m, 3H); 7.50-7.43 (m, 2H); 7.00 (br d, $J = 9.3$ Hz, 1H); 5.84 (s, 1H); 4.59-4.49 (m, 1H); 4.05-3.88 (m, 3H); 3.55 (dd, $J = 18.3, 6.6$ Hz, 1H); 3.37 (dd, $J = 18.3, 6.0$ Hz, 1H); 2.13 (s, 3H).

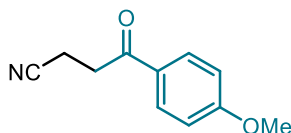
^{13}C NMR (101 MHz, CDCl_3) δ 197.9 (C); 170.8 (C); 164.8 (C); 148.5 (C); 147.3 (C); 136.0 (C); 133.8 (CH); 129.0 (CH); 128.7 (CH); 128.1 (CH); 124.3 (CH); 66.0 (CH); 63.7 (CH_2); 53.7 (CH); 42.3 (CH_2); 41.5 (CH); 20.6 (CH_3).

Spectroscopic data for diastereoisomer 50uB ($R_f = 0.42$, hexanes/AcOEt 60:40)

^1H NMR (400 MHz, CDCl_3) δ 8.24-8.18 (m, 2H); 7.95-7.87 (m, 2H); 7.63-7.56 (m, 1H); 7.53-7.47 (m, 4H); 6.49 (br s, $J = 9.5$ Hz, 1H); 5.88 (s, 1H); 4.72-4.62 (n, 1H); 4.25 (dd, $J = 11.8, 7.1$ Hz, 1H); 4.20-4.10 (m, 2H); 3.98-3.91 (m, 1H); 3.61 (dd, $J = 17.9, 6.0$ Hz, 1H); 3.48 (dd, $J = 17.9, 7.8$ Hz, 1H); 2.05 (s, 3H).

^{13}C NMR (101 MHz, CDCl_3) δ 197.0 (C); 171.2 (C); 164.8 (C); 147.7 (C); 147.3 (C); 136.6 (C); 134.0 (CH); 129.7 (CH); 129.1 (CH); 128.3 (CH); 124.3 (CH); 66.5 (CH); 64.2 (CH_2); 52.3 (CH); 42.4 (CH); 41.5 (CH_2); 21.0 (CH_3).

HRMS: calculated for $\text{C}_{21}\text{H}_{20}\text{Cl}_2\text{N}_2\text{NaO}_6$ ($\text{M}+\text{Na}^+$): 489.0591, found 489.0587.



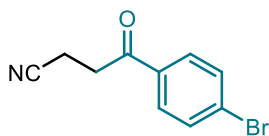
4-(4-methoxyphenyl)-4-oxobutanenitrile (51a)

Prepared according to the general procedure using *tert*-butyl((1-(4-methoxyphenyl)vinyl)oxy)dimethylsilane (0.75 mmol, 198 mg) and chloroacetonitrile (0.5 mmol, 32 μL). Time of irradiation: 24 hours at 25 °C. Flash column chromatography (hexanes/EtOAc 70:30) to afford product **51a** as a yellowish solid (63 mg, 66% yield).

Characterization data matching data reported in the literature.⁶⁹

¹H NMR (400 MHz, CDCl₃) δ 7.97-7.90 (m, 2H); 6.99-6.93 (m, 2H); 3.89 (s, 3H); 3.33 (t, *J* = 7.2 Hz, 2H); 2.77 (t, *J* = 7.4 Hz, 2H).

¹³C NMR (101 MHz, CDCl₃) δ 193.9 (C); 164.2 (C); 130.5 (CH); 128.9 (C); 119.5 (C); 114.2 (CH); 55.7 (CH₃); 34.0 (CH₂); 12.0 (CH₂).



4-(4-bromophenyl)-4-oxobutanenitrile (51b)

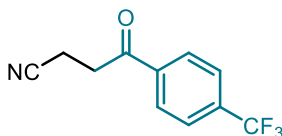
Prepared according to the general procedure using (1-(4-bromophenyl)vinyl)oxy(*tert*-butyl)dimethylsilane (0.75 mmol, 235 mg) and chloroacetonitrile (0.5 mmol, 32 μL). Time of irradiation: 24 hours at 25 °C.

Flash column chromatography (hexanes/EtOAc 80:20) to afford product **51b** as a white solid (102 mg, 86% yield).

Characterization data matching data reported in the literature.^{45b}

¹H NMR (400 MHz, CDCl₃) δ 7.8 (d, *J* = 8.5 Hz, 2H); 7.64 (d, *J* = 8.5 Hz, 2H); 3.35 (t, *J* = 7.3 Hz, 2H); 2.78 (t, *J* = 7.2 Hz, 2H)

¹³C NMR (101 MHz, CDCl₃) δ 194.4 (C); 134.4 (C); 132.4 (CH); 129.6 (CH); 129.4 (C); 119.1 (C); 34.3 (CH₂); 11.9 (CH₂).



4-oxo-4-(4-(trifluoromethyl)phenyl)butanenitrile (51c)

Prepared according to the general procedure using *tert*-butyldimethyl((1-(4-(trifluoromethyl)phenyl)vinyl)oxy)silane (0.75 mmol, 236 mg) and chloroacetonitrile (0.5 mmol, 32 μL). Time of irradiation: 24 hours at 25 °C.

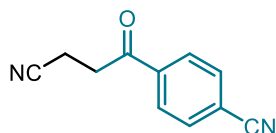
Flash column chromatography (hexanes/EtOAc 80:20) to afford product **51c** as a white solid (91.7 mg, 81% yield).

Characterization data matching data reported in the literature.^{45b}

¹H NMR (400 MHz, CDCl₃) δ 8.07 (d, *J* = 8.0 Hz, 2H); 7.77 (d, *J* = 8.0 Hz, 2H); 3.41 (t, *J* = 7.3 Hz, 2H); 2.80 (t, *J* = 7.3 Hz, 2H).

¹³C NMR (101 MHz, CDCl₃) δ 194.5 (C); 138.3 (C); 135.23 (q, *J* = 31.6 Hz, C); 128.5 (CH); 126.2 (q, *J* = 3.9 Hz, CH); 123.4 (q, *J* = 270.0 Hz, C); 118.9 (C); 33.8 (CH₂); 11.9 (CH₂).

¹⁹F NMR (376 MHz, CDCl₃) δ -63.35.



4-(3-cyanopropanoyl)benzonitrile (51d)

Prepared according to the general procedure using 4-(1-((*tert*-butyldimethylsilyl)oxy)vinyl)benzonitrile (0.75 mmol, 195 mg) and chloroacetonitrile (0.5 mmol, 32 μL). Time of irradiation: 24 hours at 25 °C.

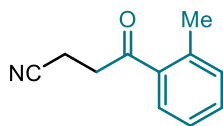
Flash column chromatography (hexanes/EtOAc 70:30) to afford product **51d** as a yellowish solid (68 mg, 74% yield).

Characterization data matching data reported in the literature.⁶⁹

¹H NMR (400 MHz, CDCl₃) δ 8.09-8.03 (m, 2H); 7.84-7.79 (m, 2H); 3.40 (t, *J* = 7.1 Hz, 2H); 2.80 (t, *J* = 7.1 Hz, 2H).

⁶⁹ Ociepa, M.; Baka, O.; Narodowicz, J.; Gryko, D. "Light-Driven Vitamin B₁₂-Catalysed Generation of Acyl Radicals from 2-S-Pyridyl Thioesters" *Adv. Synth. Catal.* **2017**, *359*, 3560-3565.

$^{13}\text{C NMR}$ (101 MHz, CDCl_3) δ 194.2 (C); 138.5 (C); 132.9 (CH); 128.6 (CH); 118.8 (C); 117.7 (C); 117.4 (C); 34.8 (CH_2); 11.9 (CH_2).



4-oxo-4-(o-tolyl)butanenitrile (51e)

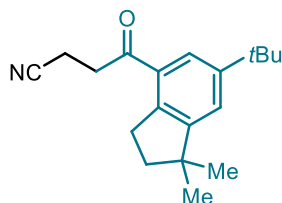
Prepared according to the general procedure using *tert*-butyldimethyl((1-(o-tolyl)vinyl)oxy)silane (0.75 mmol, 196 mg) and chloroacetonitrile (0.5 mmol, 32 μL). Time of irradiation: 24 hours at 25 $^\circ\text{C}$. Flash column chromatography (hexanes/ Et_2O 60:40) to afford product **51e** as a yellowish oil (80 mg, 92% yield).

Characterization data matching data reported in the literature.⁷⁰

$^1\text{H NMR}$ (500 MHz, CDCl_3) δ 7.69 (dd, $J = 7.7, 1.4$ Hz, 1H); 7.43 (dt, $J = 7.5, 1.6$ Hz, 1H); 7.32-7.28 (m, 2H); 3.32 (t, $J = 7.4$ Hz, 2H); 2.76 (t, $J = 7.4$ Hz, 2H), 2.54 (s, 3H).

$^{13}\text{C NMR}$ (126 MHz, CDCl_3) δ 198.5 (C); 139.4 (C); 135.9 (C); 132.6 (CH); 132.5 (CH); 128.9 (CH); 126.1 (CH); 119.4 (C); 36.6 (CH_2); 21.9 (CH_3); 12.2 (CH_2).

HRMS: calculated for $\text{C}_{11}\text{H}_{11}\text{NNaO}$ ($\text{M}+\text{Na}^+$): 196.0733, found 196.0732.



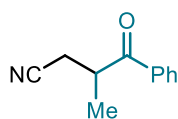
4-(6-(*tert*-butyl)-1,1-dimethyl-2,3-dihydro-1H-inden-4-yl)-4-oxobutanenitrile (51f)

Prepared according to the general procedure using *tert*-butyl((1-(6-(*tert*-butyl)-1,1-dimethyl-2,3-dihydro-1H-inden-4-yl)vinyl)oxy)dimethylsilane (0.75 mmol, 176 mg) and chloroacetonitrile (0.5 mmol, 32 μL). Time of irradiation: 24 hours at 25 $^\circ\text{C}$. Flash column chromatography (hexanes/ EtOAc 90:10) to afford product **51f** as a slightly brown solid (133 mg, 94% yield).

$^1\text{H NMR}$ (400 MHz, CDCl_3) δ 7.67 (d, $J = 1.8$ Hz, 1H); 7.39 (d, $J = 1.8$ Hz, 1H); 3.48-3.30 (t, $J = 7.5$ Hz, 2H), 3.17 (t, $J = 7.3$ Hz, 2H); 2.76 (t, $J = 7.5$ Hz, 2H); 1.96 (t, $J = 7.3$ Hz, 2H); 1.36 (s, 9H); 1.26 (s, 6H).

$^{13}\text{C NMR}$ (101 MHz, CDCl_3) δ 197.1 (C); 155.0 (C); 150.4 (C); 141.8 (C); 132.0 (C); 124.3 (CH); 123.9 (CH); 119.6 (C); 43.6 (C); 41.5 (CH_2); 35.8 (CH_2); 34.9 (C); 31.6 (CH_3); 31.0 (CH_2); 28.9 (CH_3); 12.0 (CH_2).

HRMS: calculated for $\text{C}_{19}\text{H}_{26}\text{NO}$ ($\text{M}+\text{H}^+$): 284,2009, found 284,2001.



3-methyl-4-oxo-4-phenylbutanenitrile (51g)

Prepared according to the general procedure using *tert*-butyldimethyl((1-phenylprop-1-en-1-yl)oxy)silane (0.75 mmol, 186 mg) and chloroacetonitrile (0.5 mmol, 32 μL). Time of irradiation: 24 hours at 25 $^\circ\text{C}$. Flash column chromatography (hexanes/ EtOAc slow gradient from 90:10 to 80:20) to afford product **51g** as a yellowish oil (67 mg, 90% yield).

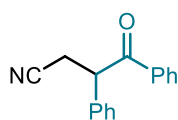
Characterization data matching data reported in the literature.⁷¹

$^1\text{H NMR}$ (400 MHz, CDCl_3) δ 7.98-7.92 (m, 2H); 7.65-7.58 (m, 1H); 7.55-7.47 (m, 2H); 3.88-3.76 (m, 1H); 2.75 (dd, $J = 16.9, 6.0$ Hz, 1H); 2.62 (dd, $J = 16.9, 7.8$ Hz, 1H); 1.40 (d, $J = 7.2$ Hz, 3H).

$^{13}\text{C NMR}$ (101 MHz, CDCl_3) δ 200.0 (C); 134.7 (C); 133.8 (CH); 128.9 (CH); 128.4 (CH); 118.6 (C); 38.0 (CH); 20.33 (CH_2); 18.0 (CH_3).

⁷⁰ Li, Y.; Shang, J.-Q.; Wang, X.-X.; Xia, W.-J.; Yang, T.; Xin, Y.; Li, Y. M. "Copper-Catalyzed Decarboxylative Oxyalkylation of Alkynyl Carboxylic Acids: Synthesis of γ -Diketones and γ -Ketonitriles" *Org. Lett.* **2019**, *21*, 2227-2230.

⁷¹ Miura, K.; Fujisawa, N.; Saito, H.; Wang, D.; Hosomi, A. "Synthetic Utility of Stannyl Enolates as Radical Alkylating Agents" *Org. Lett.* **2001**, *3*, 2591-2594.



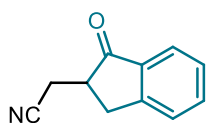
4-oxo-3,4-diphenylbutanenitrile (51h)

Prepared according to the general procedure using (*Z*)-*tert*-butyl((1,2-diphenylvinyl)oxy)dimethylsilane (0.75 mmol, 233 mg) and chloroacetonitrile (0.5 mmol, 32 μ L). Time of irradiation: 24 hours at 60 °C. The hydrolysis was performed with TBAF (1 M solution in THF, 1.0 mL, 1.0 mmol, 2.0 equiv.) for one hour. Flash column chromatography (hexanes/EtOAc gradient from 100:0 to 90:10) to afford product **51h** as a yellowish solid (97 mg, 82% yield).

Characterization data matching data reported in the literature.⁷²

¹H NMR (400 MHz, CDCl₃) δ 7.92 (d, *J* = 8.3 Hz, 2H); 7.50 (t, *J* = 7.3 Hz, 1H); 7.42-7.26 (m, 7H); 4.86 (dd, *J* = 7.8, 6.7 Hz, 1H); 3.09 (dd, *J* = 16.9, 6.6 Hz, 1H); 2.88 (dd, *J* = 16.9, 7.9 Hz, 1H).

¹³C NMR (101 MHz, CDCl₃) δ 196.1 (C); 136.6 (C); 135.2 (C); 133.8 (CH); 129.8 (CH); 129.1 (CH); 128.8 (CH); 128.6 (CH); 128.1 (CH); 118.4 (C); 50.6 (CH); 22.3 (CH₂).



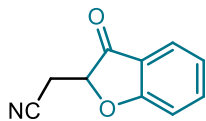
2-(1-oxo-2,3-dihydro-1H-inden-2-yl)acetonitrile (51i)

Prepared according to the general procedure using ((1*H*-inden-3-yl)oxy)(*tert*-butyl)dimethylsilane (0.75 mmol, 185 mg) and chloroacetonitrile (0.5 mmol, 32 μ L). Time of irradiation: 24 hours at 25 °C. Flash column chromatography (hexanes/EtOAc gradient from 80:20 to 75:25) to afford product **51i** as a yellowish solid (77 mg, 90% yield).

¹H NMR (400 MHz, CDCl₃) δ 7.78-7.72 (m, 1H); 7.66-7.59 (m, 1H); 7.51-7.46 (m, 1H); 7.42-7.36 (m, 1H); 3.52 (dd, *J* = 16.8, 7.5 Hz, 1H); 3.06-2.90 (m, 3H); 2.65-2.56 (m, 1H).

¹³C NMR (101 MHz, CDCl₃) δ 203.9 (C); 152.5 (C); 135.7 (CH); 135.4 (C); 128.0 (CH); 126.7 (CH); 124.3 (CH); 117.8 (C); 43.1 (CH); 32.1 (CH₂); 18.6 (CH₂).

HRMS: calculated for C₁₁H₉NNaO (M+Na⁺): 194.0576, found 194.0570.



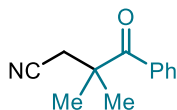
2-(3-oxo-2,3-dihydrobenzofuran-2-yl)acetonitrile (51j)

Prepared according to the general procedure using (benzofuran-3-yloxy)(*tert*-butyl)dimethylsilane (0.75 mmol, 186 mg) and chloroacetonitrile (0.5 mmol, 32 μ L). Time of irradiation: 24 hours at 25 °C. The hydrolysis was performed with TBAF (1 M solution in THF, 0.75 mL, 0.75 mmol, 1.5 equiv.) for two hours. Flash column chromatography (hexanes/EtOAc gradient from 80:20 to 75:25) to afford product **51j** as a yellowish solid (131 mg, 94% yield).

¹H NMR (400 MHz, CDCl₃) δ 7.75-7.65 (m, 2H); 7.25-7.13 (m, 2H); 4.75 (dd, *J* = 7.2, 4.4 Hz, 1H); 3.11 (dd, *J* = 17.1, 4.4 Hz, 1H); 2.83 (dd, *J* = 17.2, 7.2 Hz, 1H).

¹³C NMR (101 MHz, CDCl₃) δ 197.8 (C); 172.5 (C); 139.0 (CH); 124.7 (CH); 123.0 (CH); 119.8 (C); 115.1 (C); 113.8 (CH); 78.8 (CH); 20.1 (CH₂).

HRMS: calculated for C₁₀H₇NNaO₂ (M+Na⁺): 196.0369, found 196.0366.



3,3-dimethyl-4-oxo-4-phenylbutanenitrile (51k)

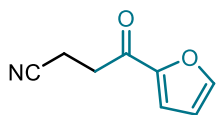
Prepared according to the general procedure using *tert*-butyldimethyl((2-methyl-1-phenylprop-1-en-1-yl)oxy)silane (0.75 mmol, 197 mg) and chloroacetonitrile (0.5 mmol, 32 μ L). Time of irradiation: 24 hours at 25 °C. Flash column chromatography (toluene) to afford product **51k** as a yellowish oil (47 mg, 50% yield).

⁷² Kong, D.; Li, M.; Wang, R.; Zi, G.; Hou, G. "Highly efficient asymmetric hydrogenation of cyano-substituted acrylate esters for synthesis of chiral γ -lactams and amino acids" *Org. Biomol. Chem.* **2016**, *14*, 1216-1220.

¹H NMR (400 MHz, CDCl₃) δ 7.78-7.72 (m, 2H); 7.57-7.51 (m, 1H); 7.49-7.42 (m, 2H); 2.72 (s, 2H); 1.58 (s, 6H).

¹³C NMR (101 MHz, CDCl₃) δ 204.5 (C); 136.5 (C); 131.9 (CH); 128.4 (CH); 128.1 (CH); 118.2 (C); 46.4 (C); 29.0 (CH₂); 25.3 (CH₃).

HRMS: calculated for C₁₂H₁₃NNaO (M+Na⁺): 210.0889, found 210.0887.



4-(furan-2-yl)-4-oxobutanenitrile (51l)

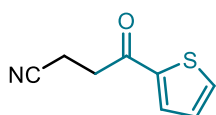
Prepared according to the general procedure using *tert*-butyl((1-(furan-2-yl)vinyl)oxy)dimethylsilane (0.75 mmol, 168 mg) and chloroacetonitrile (0.5 mmol, 32 μL). Time of irradiation: 24 hours at 25 °C. Flash column chromatography (hexanes/EtOAc 70:30) to afford product **51l** as a slightly brown solid (61.6 mg, 83% yield).

Characterization data matching data reported in the literature.⁶⁷

¹H NMR (400 MHz, CDCl₃) δ 7.61 (d, *J* = 1.5 Hz, 1H); 7.27 (d, *J* = 3.3 Hz, 1H); 6.58 (dd, *J* = 3.6, 1.8 Hz, 1H); 3.25 (t, *J* = 7.5 Hz, 2H); 2.75 (t, *J* = 7.5 Hz, 2H).

¹³C NMR (101 MHz, CDCl₃) δ 184.6 (C); 151. (C); 147.0 (CH); 119.0 (C); 117.8 (CH); 112.8 (CH); 34.0 (CH₂); 11.5 (CH₂).

HRMS: calculated for C₈H₈NO₂ (M+H⁺): 150.0550, found 150.0548.



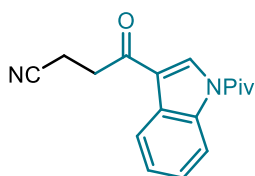
4-oxo-4-(thiophen-2-yl)butanenitrile (51m)

Prepared according to the general procedure using *tert*-butyldimethyl((1-(thiophen-2-yl)vinyl)oxy)silane (0.75 mmol, 176 mg) and chloroacetonitrile (0.5 mmol, 32 μL). Time of irradiation: 24 hours at 25 °C. Flash column chromatography (hexanes/EtOAc gradient from 90:10 to 80:20) to afford product **51m** as a yellowish solid (59 mg, 71% yield).

Characterization data matching data reported in the literature.⁶⁹

¹H NMR (500 MHz, CDCl₃) δ 7.73-7.70 (m, 1H); 7.68-7.65 (m, 1H); 7.15-7.11 (m, 1H); 3.29 (t, *J* = 7.2 Hz, 2H); 2.73 (t, *J* = 7.2 Hz, 2H).

¹³C NMR (101 MHz, CDCl₃) δ 188.6 (C); 142.9 (C); 134.9 (CH); 132.8 (CH); 128.8 (CH); 118.4 (C); 34.9 (CH₂); 12.1 (CH₂).



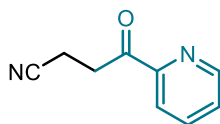
4-oxo-4-(1-pivaloyl-1H-indol-3-yl)butanenitrile (51n)

Prepared according to the general procedure using 1-(3-(1-((*tert*-butyldimethylsilyl)oxy)vinyl)-1H-indol-1-yl)-2,2-dimethylpropan-1-one (0.75 mmol, 268 mg) and chloroacetonitrile (0.5 mmol, 32 μL). Time of irradiation: 24 hours at 25 °C. Flash column chromatography (hexanes/EtOAc gradient from 80:20 to 70:30) to afford product **51n** as a yellowish solid (117 mg, 83% yield).

¹H NMR (400 MHz, CDCl₃) δ 8.46-8.41 (m, 1H); 8.35 (s, 1H); 8.28-8.23 (m, 1H); 7.44-7.36 (m, 2H); 3.31 (app t, *J* = 7.3 Hz, 2H); 2.81 (app t, *J* = 7.3 Hz, 2H); 1.56 (s, 9H).

¹³C NMR (101 MHz, CDCl₃) δ 190.9 (C); 177.1 (C); 137.3 (C); 131.2 (CH); 126.5 (CH); 125.8 (C); 125.3 (CH); 121.7 (CH); 119.6 (C); 119.3 (C); 117.0 (CH); 41.7 (C); 35.3 (CH₂); 28.7 (CH₃); 11.6 (CH₂).

HRMS: calculated for C₁₇H₁₉N₂O₂ (M+H⁺): 283.1441, found 283.1434.



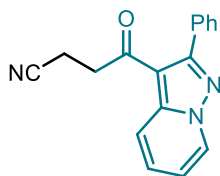
4-oxo-4-(pyridin-2-yl)butanenitrile (**51o**)

Prepared according to a slight modification of the general procedure using 2-(1-((*tert*-butyldimethylsilyl)oxy)vinyl)pyridine (0.75 mmol, 177 mg) and chloroacetonitrile (0.5 mmol, 32 μ L). Time of irradiation: 24 hours at 60 °C. The crude mixture was then treated with 1 mL of a 1 M solution of TBAF for one hour. The residue diluted with DCM and transferred to an extraction funnel containing saturated Na₂CO₃ solution. The aqueous layer was extracted three times, the combined organic phases dried (MgSO₄) and concentrated to a brown oil which was purified by flash column chromatography (hexanes/EtOAc 80:20) to afford product **51o** as a yellowish solid (44 mg, 55% yield).

¹H NMR (400 MHz, CDCl₃) δ 8.69 (qd, J = 4.8, 1.2 Hz, 1H); 8.07 (td, J = 7.8, 0.8 Hz, 1H); 7.88 (td, J = 7.8, 1.8 Hz, 1H); 7.53 (ddd, J = 7.8, 4.7, 1.2 Hz, 1H); 3.65 (t, J = 7.2 Hz, 2H); 2.77 (t, J = 7.2 Hz, 2H).

¹³C NMR (101 MHz, CDCl₃) δ 197.5 (C); 152.2 (C); 149.1 (CH); 137.1 (CH); 127.8 (CH); 121.9 (CH); 119.3 (C); 33.8 (CH₂); 11.7 (CH₂).

HRMS: calculated for C₉H₉N₂O (M+H⁺): 161.0709, found 161.0712.



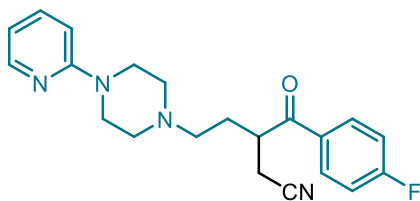
4-oxo-4-(2-phenylpyrazolo[1,5-*a*]pyridin-3-yl)butanenitrile (**51p**)

Prepared according to the general procedure using 3-(1-((*tert*-butyldimethylsilyl)oxy)vinyl)-2-phenylpyrazolo[1,5-*a*]pyridine (0.75 mmol, 263 mg) and chloroacetonitrile (0.5 mmol, 32 μ L). Time of irradiation: 24 hours at 25 °C. Flash column chromatography (hexanes/EtOAc gradient from 70:30 to 60:40) to afford product **51p** as an off-white solid (109 mg, 79% yield).

¹H NMR (500 MHz, CDCl₃) δ 8.53 (dt, J = 7.0, 1.0 Hz, 1H); 8.43 (dt, J = 9.0, 1.0 Hz, 1H); 7.56-7.50 (m, 6H); 7.06 (td, J = 7.0, 1.3 Hz, 1H); 2.71 (app t, 2H); 2.58 (app t, 2H).

¹³C NMR (125 MHz, CDCl₃) δ 190.8 (C); 157.0 (C); 142.6 (C); 133.5 (C); 130.0 (CH); 129.9 (CH); 129.5 (CH); 129.1 (CH); 120.5 (CH); 119.7 (C); 115.5 (CH); 110.8 (C); 37.1 (CH₂); 12.2 (CH₂). 1 aromatic CH signal not observed (overlapping signals).

HRMS: calculated for C₁₇H₁₃N₃NaO (M+Na⁺): 298.0951, found 298.0965.



3-(4-fluorobenzoyl)-5-(4-(pyridin-2-yl)piperazin-1-yl)pentanenitrile (**51q**)

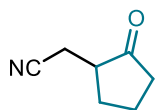
Prepared according to the general procedure using 1-(4-((*tert*-butyldimethylsilyl)oxy)-4-(4-fluorophenyl)but-3-en-1-yl)-4-(pyridin-2-yl)piperazine (0.75 mmol, 331 mg) and chloroacetonitrile (0.5 mmol, 32 μ L). Time of irradiation: 24 hours at 60 °C in dichloroethane as solvent. Flash column chromatography (hexanes/EtOAc 20:80) to afford product **51q** as a yellow oil (90 mg, 49% yield).

¹H NMR (500 MHz, CDCl₃) δ 8.19-8.15 (m, 1H); 8.10-8.02 (m, 2H); 7.50-7.43 (m, 1H); 7.20-7.12 (m, 2H); 6.65-6.57 (m, 2H); 3.97-3.88 (m, 1H); 3.42-3.34 (m, 2H); 3.34-3.25 (m, 2H); 2.75-2.62 (m, 2H); 2.51-2.33 (m, 6H); 2.19-2.08 (m, 1H); 1.94-1.84 (m, 1H).

¹³C NMR (125 MHz, CDCl₃) δ 198.0 (C); 165.9 (d, J = 256 Hz, C); 159.3 (C); 147.9 (CH); 137.4 (CH); 132.6 (d, J = 3 Hz, C); 131.1 (d, J = 9 Hz, CH); 118.4 (C); 116.0 (d, J = 21 Hz, CH); 113.4 (CH); 107.0 (CH); 55.3 (CH₂); 52.7 (CH₂); 44.8 (CH₂); 40.7 (CH); 29.8 (CH₂); 19.6 (CH₂).

^{19}F NMR (101 MHz, CDCl_3) δ -103.76.

HRMS: calculated for $\text{C}_{21}\text{H}_{24}\text{FN}_4\text{O}$ ($\text{M}+\text{H}^+$): 367.1929, found 367.1921.



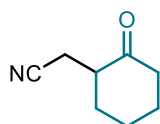
2-(2-oxocyclopentyl)acetonitrile (51r)

Prepared according to the general procedure using *tert*-butyl(cyclopent-1-en-1-yloxy)dimethylsilane (0.75 mmol, 149 mg) and chloroacetonitrile (0.5 mmol, 32 μL). Time of irradiation: 24 hours at 25 $^\circ\text{C}$ in DCE as solvent. Flash column chromatography (hexanes/EtOAc 80:20) to afford product **51r** as a yellowish oil (33.5 mg, 54% yield).

^1H NMR (300 MHz, CDCl_3) δ 2.77-2.69 (m, 1H); 2.50-2.36 (m, 4H); 2.24-2.05 (m, 2H); 1.93-1.85 (m, 2H)

^{13}C NMR (75 MHz, CDCl_3) δ 216.3 (C); 118.0 (C); 45.6 (CH); 37.2 (CH_2); 29.0 (CH_2); 20.3 (CH_2); 17.4 (CH_2).

HRMS: calculated for $\text{C}_7\text{H}_9\text{NNaO}$ ($\text{M}+\text{Na}^+$): 146.0576, found 146.0570.



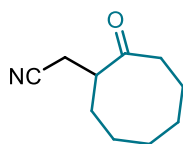
2-(2-oxocyclohexyl)acetonitrile (51s)

Prepared according to the general procedure using *tert*-butyl(cyclohex-1-en-1-yloxy)dimethylsilane (0.75 mmol, 159 mg) and chloroacetonitrile (0.5 mmol, 32 μL) in dichloroethane. Time of irradiation: 24 hours at 25 $^\circ\text{C}$. Flash column chromatography (hexanes/EtOAc gradient from 80:20 to 70:30) to afford product **51s** as a yellowish oil (57 mg, 83% yield).

^1H NMR (400 MHz, CDCl_3) δ 2.73-2.62 (m, 2H); 2.52-2.45 (m, 1H); 2.43-2.29 (m, 3H); 2.15 (ddq, J = 12.1, 5.9, 2.8 Hz, 1H); 2.01-1.93 (m, 1H); 1.81-1.62 (m, 2H); 1.49 (qd, J = 12.8, 3.6 Hz, 1H).

^{13}C NMR (101 MHz, CDCl_3) δ 208.7 (C), 118.7 (C), 47.0 (CH), 41.7 (CH_2), 33.5 (CH_2), 27.7 (CH_2), 25.0 (CH_2), 18.0 (CH_2).

HRMS: calculated for $\text{C}_8\text{H}_{11}\text{NNaO}$ ($\text{M}+\text{Na}^+$): 160.0733, found 160.0726.



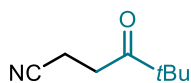
2-(2-oxocyclooctyl)acetonitrile (51t)

Prepared according to the general procedure using (*E*)-*tert*-butyl(cyclooct-1-en-1-yloxy)dimethylsilane (0.75 mmol, 180 mg) and chloroacetonitrile (0.5 mmol, 32 μL). Time of irradiation: 24 hours at 25 $^\circ\text{C}$ in DCE as solvent. Flash column chromatography (hexanes/EtOAc 80:20) to afford product **51t** as a yellowish oil (83 mg, 72% yield).

^1H NMR (400 MHz, CDCl_3) δ 3.01-2.99 (m, 1H); 2.70 (dd, J = 17.0, 6.2 Hz, 1H); 2.65-2.59 (m, 1H); 2.4 (dd, J = 17.0, 8.5 Hz, 1H); 2.36-2.32 (m, 1H); 2.23-2.22 (m, 1H); 2.05-2.02 (m, 1H); 1.82-1.67 (m, 5H); 1.52-1.46 (m, 2H); 0.99-0.97 (m, 1H)

^{13}C NMR (101 MHz, CDCl_3) δ 215.4 (C); 118.8 (C); 46.3 (CH); 42.0 (CH_2); 31.1 (CH_2); 27.3 (CH_2); 25.5 (CH_2); 24.5 (CH_2); 24.2 (CH_2); 18.6 (CH_2).

HRMS: calculated for $\text{C}_{10}\text{H}_{15}\text{NNaO}$ ($\text{M}+\text{Na}^+$): 188.1046, found 188.1051.



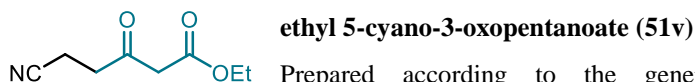
5,5-dimethyl-4-oxohexanenitrile (51u)

Prepared according to the general procedure using *tert*-butyl((3,3-dimethylbut-1-en-2-yl)oxy)dimethylsilane (0.75 mmol, 161 mg) and chloroacetonitrile (0.5 mmol, 32 μL). Time of irradiation: 24 hours at 25 $^\circ\text{C}$ in DCE as solvent. Flash column chromatography (hexanes/EtOAc 80:20) to afford product **51u** as a yellowish oil (64 mg, 92% yield).

Characterization data matching data reported in the literature.⁷³

¹H NMR (400 MHz, CDCl₃) δ 2.89 (t, *J* = 7.5 Hz, 2H); 2.58 (t, *J* = 7.5 Hz, 2H); 1.17 (s, 9H).

¹³C NMR (101 MHz, CDCl₃) δ 211.7 (C); 119.4 (C); 44.1 (C); 32.6 (CH₂); 26.5 (CH₃); 12.0 (CH₂).

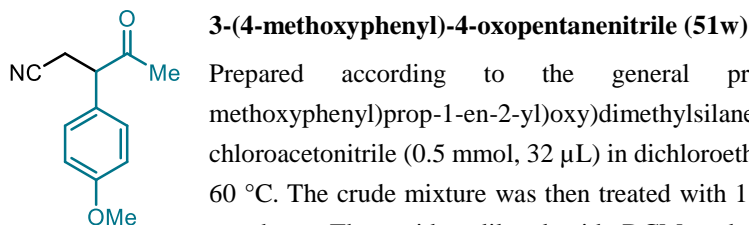


Prepared according to the general procedure using ethyl 3-((*tert*-butyldimethylsilyl)oxy)but-3-enoate (0.75 mmol, 183 mg) and chloroacetonitrile (0.5 mmol, 32 μL) in dichloroethane. Time of irradiation: 24 hours at 60 °C. Flash column chromatography (hexanes/EtOAc 70:30) to afford product **51v** as a yellowish solid (69 mg, 82% yield).

Characterization data matching data reported in the literature.⁷⁴

¹H NMR (400 MHz, CDCl₃) δ 4.22 (q, *J* = 7.2 Hz, 2H); 3.50 (s, 2H); 2.98 (t, *J* = 7.2 Hz, 2H); 2.63 (t, *J* = 7.2 Hz, 2H); 1.30 (t, *J* = 7.2 Hz, 3H).

¹³C NMR (101 MHz, CDCl₃) δ 198.6 (C); 166.5 (C); 118.5 (C); 61.8 (CH₂); 48.7 (CH₂); 38.0 (CH₂); 14.0 (CH₃); 11.3 (CH₂).

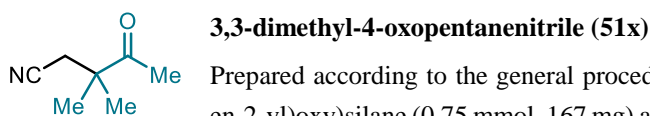


Prepared according to the general procedure using *tert*-butyl((1-(4-methoxyphenyl)prop-1-en-2-yl)oxy)dimethylsilane (0.75 mmol, 209 mg) and chloroacetonitrile (0.5 mmol, 32 μL) in dichloroethane. Time of irradiation: 24 hours at 60 °C. The crude mixture was then treated with 1 mL of a 1 M solution of TBAF for one hour. The residue diluted with DCM and transferred to an extraction funnel containing saturated Na₂CO₃ solution. The aqueous layer was extracted three times, the combined organic phases dried (MgSO₄) and concentrated to a brown oil which was purified by flash column chromatography (hexanes/EtOAc 80:20) to afford product **51w** as a yellowish solid (48 mg, 47% yield).

¹H NMR (400 MHz, CDCl₃) δ 7.17-7.09 (m, 2H); 6.96-6.90 (m, 2H); 3.93 (dd, *J* = 8.1, 6.5 Hz, 1H); 3.82 (s, 3H); 2.93 (dd, *J* = 16.9, 6.5 Hz, 1H); 2.68 (dd, *J* = 16.9, 8.1 Hz, 1H); 2.10 (s, 3H).

¹³C NMR (101 MHz, CDCl₃) δ 204.6 (C); 159.8 (C); 129.2 (CH); 127.4 (C); 118.3 (C); 115.0 (CH); 55.3 (CH₃); 54.6 (CH₃); 28.3 (CH); 20.5 (CH₂).

HRMS: calculated for C₁₂H₁₃NNaO₂ (M+Na⁺): 226.0838, found 226.0844.



Prepared according to the general procedure using *tert*-butyldimethyl((3-methylbut-2-en-2-yl)oxy)silane (0.75 mmol, 167 mg) and chloroacetonitrile (0.5 mmol, 32 μL). Time of irradiation: 24 hours at 25 °C in DCE as solvent. Flash column chromatography (hexanes/EtOAc 90:10) to afford product **51x** as a yellowish oil (23 mg, 37% yield).

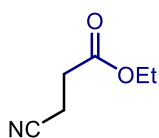
¹H NMR (400 MHz, CDCl₃) δ 2.53 (s, 2H); 2.21 (s, 3H); 1.35 (s, 6H).

¹³C NMR (101 MHz, CDCl₃) δ 209.0 (C); 118.2 (C); 46.5 (C); 26.9 (CH₃); 26.9 (CH₂); 24.7 (CH₃).

HRMS: calculated for C₇H₁₁NNaO (M+Na⁺): 148.0733, found 148.0730.

⁷³ Giese, B.; Thoma, G. "C-C Bond Formation via Carbon-Centered Radicals Generated from Dicarbonyl(η⁵-cyclopentadienyl) organoiron Complexes" *Helv. Chim. Acta* **1991**, *74*, 1143-1155.

⁷⁴ E. Holtz, E.; Langer, P. "Synthesis of 5-Cyano-1,3-dioxoalkanes by Reaction of 1,3-Dicarbonyl Dianions with Bromoacetonitrile" *Synth. Commun.* **2007**, *37*, 2959-2966.

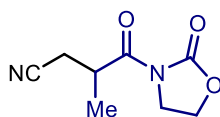


ethyl 3-cyanopropanoate (53a)

Prepared according to the general procedure using *tert*-butyl((1-ethoxyvinyl)oxy)dimethylsilane (0.75 mmol, 152 mg) and chloroacetonitrile (0.5 mmol, 32 μ L). Time of irradiation: 24 hours at 25 °C. Flash column chromatography (hexanes/EtOAc gradient from 80:20 to 70:30) to afford product **53a** as a yellowish oil (53 mg, 83% yield). Characterization data matching data reported in the literature.⁷⁵

¹H NMR (400 MHz, CDCl₃) δ 4.18 (q, J = 7.1 Hz, 2H); 2.70-2.60 (m, 4H); 1.27 (t, J = 7.1 Hz, 3H).

¹³C NMR (101 MHz, CDCl₃) δ 170.0 (C); 118.5 (C); 61.4 (CH₂); 29.9 (CH₂); 14.1 (CH₃); 12.9 (CH₂).



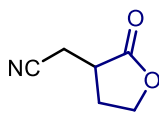
3-methyl-4-oxo-4-(2-oxooxazolidin-3-yl)butanenitrile (53b)

Prepared according to the general procedure using 3-(1-((*tert*-butyldimethylsilyl)oxy)prop-1-en-1-yl)oxazolidin-2-one (0.75 mmol, 193 mg) and chloroacetonitrile (0.5 mmol, 32 μ L). Time of irradiation: 24 hours at 25 °C. Flash column chromatography (hexanes/EtOAc gradient from 60:40 to 30:70) to afford product **53b** as a yellowish solid (81 mg, 89% yield).

¹H NMR (400 MHz, CDCl₃) δ 4.50-4.39 (m, 2H); 4.13-3.95 (m, 3H); 2.69 (dd, J = 16.8, 7.1 Hz, 1H); 2.55 (dd, J = 16.8, 7.1 Hz, 1H); 1.34 (d, J = 7.1 Hz, 3H).

¹³C NMR (101 MHz, CDCl₃) δ 173.5 (C); 153.0 (C); 117.9 (C); 62.3 (CH₂); 42.7 (CH₂); 35.1 (CH); 20.6 (CH₂); 17.2 (CH₃).

HRMS: calculated for C₈H₁₀N₂NaO₃ (M+Na⁺): 205.0584, found 205.0580.



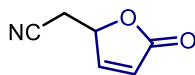
2-(2-oxotetrahydrofuran-3-yl)acetonitrile (53c)

Prepared according to the general procedure using *tert*-butyl((4,5-dihydrofuran-2-yl)oxy)dimethylsilane (0.75 mmol, 150 mg) and chloroacetonitrile (0.5 mmol, 32 μ L). Time of irradiation: 24 hours at 25 °C. Flash column chromatography (hexanes/acetone 80:20) to afford product **53c** as a yellowish oil (54 mg, 86% yield).

¹H NMR (300 MHz, CDCl₃) δ 4.48 (td, J = 9.0, 1.7 Hz, 1H); 4.33-4.22 (m, 1H); 2.97-2.85 (m, 2H); 2.67-2.57 (m, 2H); 2.29-2.22 (m, 1H).

¹³C NMR (126 MHz, CDCl₃) δ 175.6 (C); 117.0 (C); 66.5 (CH); 36.6 (CH₂); 28.3 (CH₂); 18.6 (CH₂).

HRMS: calculated for C₆H₇NNaO₂ (M+Na⁺): 148.0369, found 148.0368.



2-(5-oxo-2,5-dihydrofuran-2-yl)acetonitrile (53d)

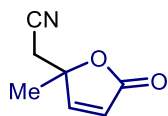
Prepared according to the general procedure using *tert*-butyl(furan-2-yloxy)dimethylsilane (0.75 mmol, 186 mg) and chloroacetonitrile (0.5 mmol, 32 μ L). Time of irradiation: 48 hours at 25 °C. Flash column chromatography (hexanes/EtOAc 40:60) to afford product **53d** as a yellowish liquid (54 mg, 88% yield).

¹H NMR (400 MHz, CDCl₃) δ 7.54 (dd, J = 5.7, 1.6 Hz, 1H); 6.33 (dd, J = 5.7, 2.0 Hz, 1H); 5.26 (ddt, J = 6.4, 5.5, 1.7 Hz, 1H); 2.93 (dd, J = 16.9, 5.5 Hz, 1H); 2.87 (dd, J = 16.9, 6.5 Hz, 1H).

¹³C NMR (101 MHz, CDCl₃) δ 171.1 (C); 152.8 (CH); 124.2 (CH); 114.3 (C); 76.9 (CH); 22.5 (CH₂).

⁷⁵ Laroche, C.; Harakat, D.; Bertus, F.; Szymoniak, J. "Studies on the titanium-catalyzed cyclopropanation of nitriles" *Org. Biomol. Chem.* **2005**, *3*, 3482-3487.

HRMS: calculated for C₆H₆NO₂ (M+H⁺): 124.0393, found 124.0393.



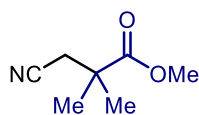
2-(2-methyl-5-oxo-2,5-dihydrofuran-2-yl)acetonitrile (53e)

Prepared according to the general procedure using *tert*-butyldimethyl((5-methylfuran-2-yl)oxy)silane (0.75 mmol, 159 mg) and chloroacetonitrile (0.5 mmol, 32 μL). Time of irradiation: 24 hours at 25 °C for 2 days. Flash column chromatography (hexanes/acetone 80:20) to afford product **53e** as a yellowish oil (44 mg, 64% yield).

¹H NMR (400 MHz, CDCl₃) δ 7.49 (d, *J* = 5.6 Hz, 1H); 6.22 (d, *J* = 5.6 Hz, 1H); 2.89 (d, *J* = 16.6 Hz, 1H); 2.82 (d, *J* = 16.6 Hz, 1H); 1.64 (s, 3H).

¹³C NMR (101 MHz, CDCl₃) δ 170.5 (C); 157.0 (CH); 122.8 (CH); 114.8 (C); 84.0 (C); 28.4 (CH₂); 23.7 (CH₃).

HRMS: calculated for C₇H₇NNaO₂ (M+Na⁺): 160.0369, found 160.0368.



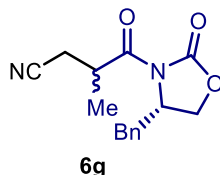
methyl 3-cyano-2,2-dimethylpropanoate (53f)

Prepared according to the general procedure using *tert*-butyl((1-methoxy-2-methylprop-1-en-1-yl)oxy)dimethylsilane (0.75 mmol, 173 mg) and chloroacetonitrile (0.5 mmol, 32 μL). Time of irradiation: 24 hours at 25 °C. Flash column chromatography (hexanes/EtOAc gradient from 100:0 to 90:10) to afford product **53f** as a yellowish liquid (23 mg, 32% yield).

Characterization data matching data reported in the literature.⁷⁶

¹H NMR (300 MHz, CDCl₃) δ 3.74 (s, 3H); 2.60 (s, 2H); 1.37 (s, 6H).

¹³C NMR (101 MHz, CDCl₃) δ 175.6 (C); 117.6 (C); 52.8 (CH₃); 41.1 (C); 28.2 (CH₂); 25.0 (CH₃).



4-((S)-4-benzyl-2-oxooxazolidin-3-yl)-3-methyl-4-oxobutanenitrile (53g)

Prepared according to the general procedure using (*S,Z*)-4-benzyl-3-(1-((*tert*-butyldimethylsilyl)oxy)prop-1-en-1-yl)oxazolidin-2-one (1.5 mmol, 621 mg) and chloroacetonitrile (0.5 mmol, 32 μL). Time of irradiation: 24 hours at 25 °C. The d.r. was determined to be 2.8:1 by ¹H NMR analysis of the crude mixture, which was purified by flash column chromatography (hexanes/EtOAc gradient from 80:20 to 70:30) to afford product **53g** as a yellowish liquid (94.8 mg, 70% yield).

Spectroscopic data for the major diastereoisomer:

¹H NMR (400 MHz, CDCl₃) δ 7.38-7.30 (m, 3H); 7.24-7.19 (m, 2H); 4.68 (ddt, *J* = 9.5, 6.9, 3.4 Hz, 1H); 4.26 (dd, *J* = 9.2, 6.9 Hz, 1H); 4.23 (dd, *J* = 9.2, 3.5 Hz, 1H); 4.09 (sextet, *J* = 6.8 Hz, 1H); 3.32 (dd, *J* = 13.4, 3.3 Hz, 1H); 2.82 (dd, *J* = 13.4, 9.6 Hz, 1H); 2.74 (dd, *J* = 16.7, 7.0 Hz, 1H); 2.60 (dd, *J* = 16.7, 6.6 Hz, 1H); 1.37 (d, *J* = 7.0 Hz, 3H).

¹³C NMR (101 MHz, CDCl₃) δ 173.5 (C); 152.9 (C); 134.9 (C); 129.4 (CH); 129.0 (CH); 127.5 (CH); 117.9 (C); 66.5 (CH₂); 55.4 (CH); 37.7 (CH₂); 35.3 (CH); 20.9 (CH₂); 17.0 (CH₃).

Spectroscopic data for the minor diastereoisomer:

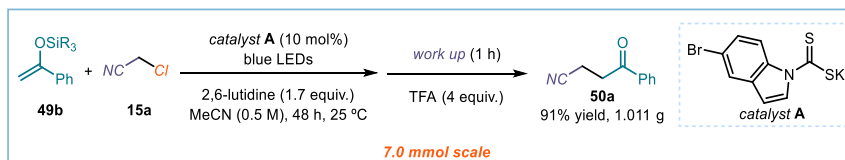
¹H NMR (400 MHz, CDCl₃) δ 7.33-7.26 (m, 3H); 7.22-7.17 (m, 2H); 4.74 (ddt, *J* = 9.5, 7.9, 3.4 Hz, 1H); 4.29 (dd, *J* = 9.2, 7.9 Hz, 1H); 4.28-4.23 (m, 1H); 4.04 (sextet, *J* = 7.2 Hz, 1H); 3.24 (dd, *J* = 13.5, 3.5 Hz, 1H); 2.81 (dd, *J* = 13.5, 9.4 Hz, 1H); 2.72 (dd, *J* = 16.8, 7.4 Hz, 1H); 2.56 (dd, *J* = 16.7, 6.5 Hz, 1H); 1.40 (d, *J* = 7.0 Hz, 3H).

⁷⁶ Reddy, P. A.; Hsiang, B. C. H.; Latifi, T. N.; Hill, M. W.; Woodward, K. E.; Rothman, S. M.; Ferrendelli, J. A.; Covey, D. F. "3,3-Dialkyl- and 3-Alkyl-3-Benzyl-Substituted 2-Pyrrolidinones: A New Class of Anticonvulsant Agents" *J. Med. Chem.* **1996**, *39*, 1898-1906.

$^{13}\text{C NMR}$ (101 MHz, CDCl_3) δ 173.5 (C); 152.9 (C); 134.8 (C); 129.4 (CH); 128.9 (CH); 127.5 (CH); 118.1 (C); 66.6 (CH_2); 55.0 (CH); 37.8 (CH_2); 35.6 (CH); 20.5 (CH_2); 17.5 (CH_3).

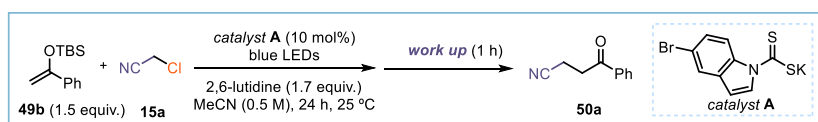
HRMS: calculated for $\text{C}_{15}\text{H}_{16}\text{N}_2\text{NaO}_3$ ($\text{M}+\text{Na}^+$): 295.1053, found 295.1052.

2.8.5 Gram scale reaction (7.0 mmol)



The model photochemical reaction can be scaled-up up to 7.0 mmol scale by using the same experimental set-up described in Figure S2. In an oven dried Schlenk tube (length x diameter = 22 x 2 cm), the silyl enol ether **49b** (2.46 g, 10.5 mmol, 1.5 equiv.) was dissolved in acetonitrile (7 mL), then 2,6-lutidine (1.4 mL, 11.9 mmol, 1.7 equiv.) and DTC catalyst **A** (217 mg, 0.7 mmol, 0.1 equiv.) were added with stirring, followed by chloroacetonitrile **15a** (443 μL , 7 mmol, 1 equiv.). An additional volume of acetonitrile (7 mL) was added to the reaction tube, washing the sides from residual solids. The resulting mixture was stirred for 10 min and then degassed via three cycles of freeze-pump-thaw. The Schlenk tube was then placed in the irradiation setup, maintained at a temperature of 25 °C (25-26 °C measured in the central well), and the reaction was stirred for 48 hours under continuous irradiation. Chloroform (5 mL) was then added followed by trifluoroacetic acid (2.2 mL, 28 mmol, 4 equiv.) and the resulting mixture stirred for 1 hour. Complete conversion of the *O*-silylated product **50a'** to the ketone product **50a** was assessed by TLC analysis. Volatiles were evaporated, water (70 mL) was added and the product was extracted with EtOAc (4x50 mL). The organic phase was dried over anhydrous MgSO_4 , filtered and the solvent evaporated under reduced pressure. The crude was purified by column chromatography (Hex:EtOAc, 80:20) to afford the corresponding product **50a** as an off-white solid (1.011g, 91% yield) with >95% purity according to ^1H NMR analysis.

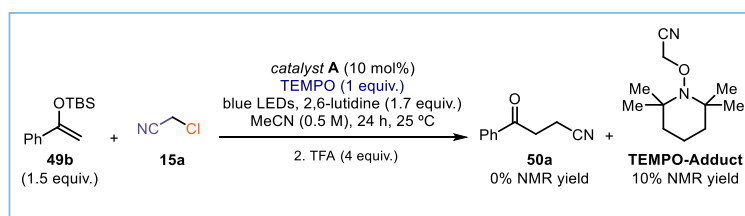
2.8.6 Screening of hydrolysis conditions



Entry	Work up	Yield (%) ^a
1	TFA (4 equiv.)	quant.
2	TBAF 1 M in THF (2 equiv.)	quant.
3	H ₂ SO ₄ (4 equiv.)	40%
4	CH ₃ SO ₃ H (4 equiv.)	quant.
5	HCl 36% in H ₂ O (4 equiv.)	quant.

Table 3. The optimization reactions were performed following the General procedure on 0.2 mmol scale. After the irradiation, CDCl₃ (400 μL) was added followed by the desilylating agent. The mixture was stirred for 1 h at room temperature and then an aliquot was analyzed by ¹H NMR. ^a Yield of **50a** determined by ¹H NMR analysis of the crude mixture using trichloroethylene as the internal standard.

2.8.7. Mechanistic Investigations



In an oven dried Schlenk tube, **49b** (70 mg, 0.3 mmol, 1.5 equiv.) was dissolved in acetonitrile (400 μL), then chloroacetonitrile **15a** (13 μL, 0.2 mmol, 1 equiv.) was added followed by 2,6-lutidine (40 μL, 0.34 mmol, 1.7 equiv.), catalyst **A** (6.2 mg, 0.02 mmol, 0.1 equiv.), and TEMPO (31 mg, 0.2 mmol, 1 equiv.). The resulting orange mixture was degassed via three cycles of freeze-pump-thaw. The Schlenk tube was then placed in the irradiation setup and irradiated at 25 °C for 24 hours. Then, trichloroethylene (18 μL, 1 equiv.) was added as internal standard, the residue was diluted with CDCl₃ and an aliquot analyzed by ¹H NMR spectroscopy to determine conversion and yield. To the crude mixture TFA (4 equiv.) was added and a second aliquot analyzed by ¹H NMR spectroscopy. Product **50a** was not formed, whereas the cyanomethyl-TEMPO adduct can be observed in the crude NMR spectra before hydrolysis (10% NMR yield, matching reported data).⁷⁷

⁷⁷ Wu, X.; Riedel, J.; Dong, V. M. "Transforming Olefins into γ,δ-Unsaturated Nitriles through Copper Catalysis" *Angew. Chem. Int. Ed.* **2017**, *56*, 11589–11593.

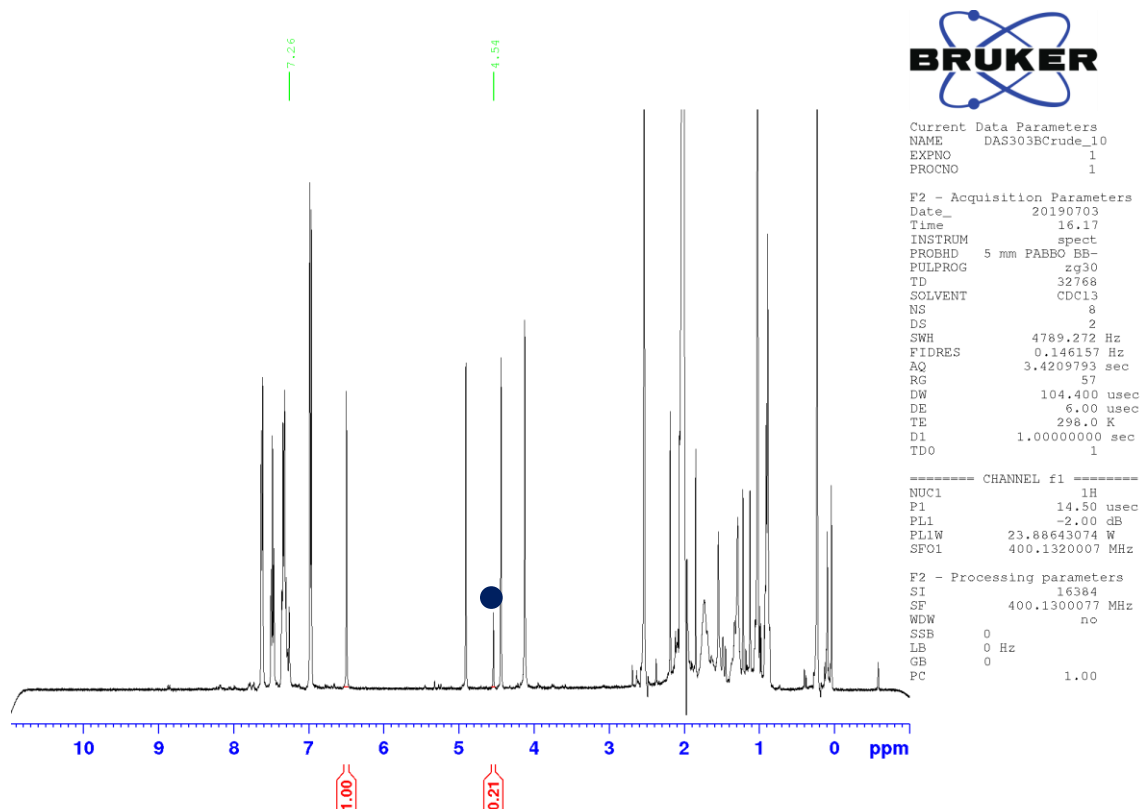
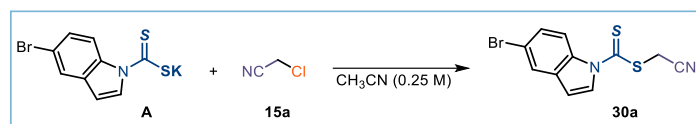


Figure 2.34. ^1H NMR spectrum of the crude reaction mixture after 24 h of irradiation in presence of TEMPO. The cyanomethyl-TEMPO adduct was formed in 10% yield as determined by using trichloroethylene as internal standard. The diagnostic signal of TEMPO adduct is indicated by the blue circle.

2.8.7.1 Synthesis and characterization of dithiocarbamate intermediate **30a**



In a round bottom flask, the dithiocarbamate anion catalyst **A** (3 mmol, 931 mg) was dissolved in acetonitrile (12 mL). Then chloroacetonitrile **15a** (3 mmol, 190 μL) was added and the resulting mixture stirred for one hour at ambient temperature. The mixture was transferred to an extraction funnel containing water (25 mL) and extracted with ethyl acetate (25 mL). The organic phase was further washed with brine (25 mL), dried over anhydrous MgSO_4 , filtered and concentrated to dryness to obtain pure cyanomethyl 5-bromo-1*H*-indole-1-carbodithioate **30a** as an ochre powder (894 mg, 96% yield).

^1H NMR (300 MHz, CDCl_3) δ 8.82 (d, J = 8.9 Hz, 1H), 7.95 (d, J = 3.9 Hz, 1H), 7.71 (d, J = 2.0 Hz, 1H), 7.45 (dd, J = 9.0, 2.0 Hz, 1H), 6.69 (d, J = 3.9 Hz, 1H), 4.22 (s, 2H).

^{13}C NMR (101 MHz, CDCl_3) δ 191.4 (C), 136.2 (C), 133.8 (C), 128.9 (CH), 127.5 (CH), 124.5 (CH), 118.4 (C), 118.3 (CH), 114.7 (C), 110.5 (CH), 22.3 (CH_2).

HRMS: calculated for $\text{C}_{11}\text{H}_8\text{BrN}_2\text{S}_2$ ($\text{M}+\text{Na}^+$): 310.9307, found 310.9306.

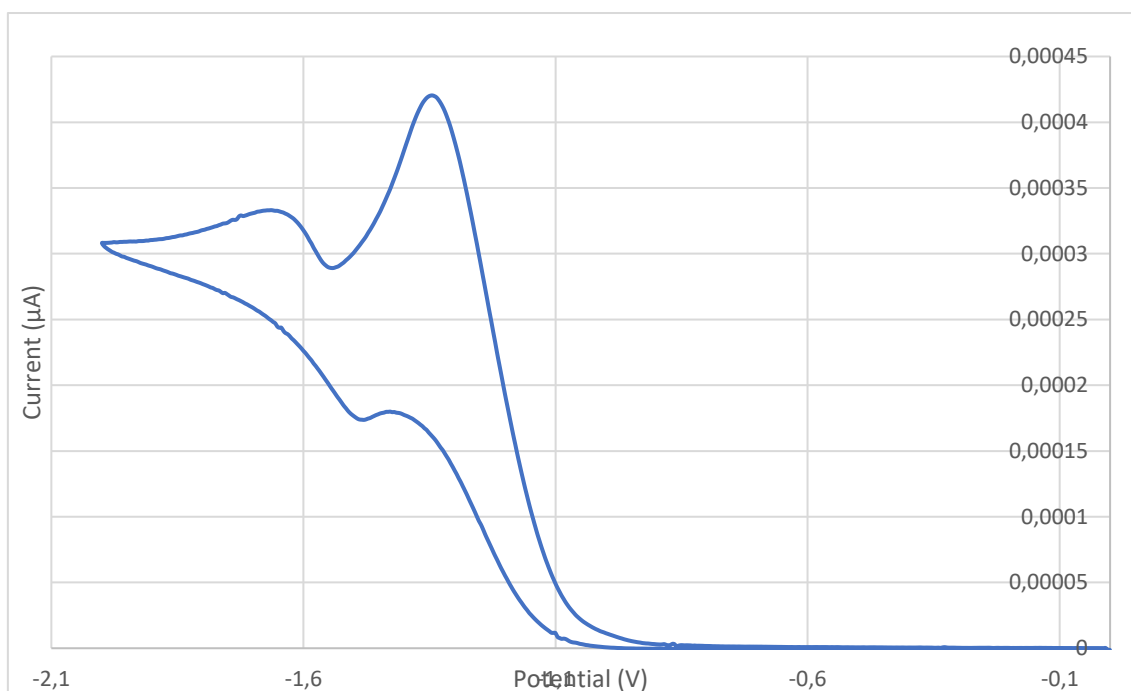
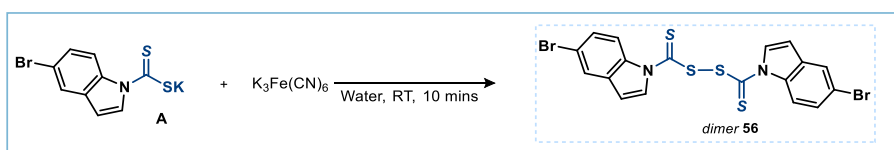


Figure 2.35. Cyclic voltammogram of **30a**: [0.02M] in [0.1 M] TBAPF₆ in CH₃CN. Sweep rate: 500 mV/s. Pt electrode working electrode, Ag/AgCl (KCl 3.5 M) reference electrode, Pt wire auxiliary electrode. Irreversible reduction, $E_{\text{red}}(\mathbf{30a}/\mathbf{30a}^{\cdot-}) = -1.34$ V.

2.8.7.2 Synthesis and characterization of the dimer **56**



An excess of K₃[Fe(CN)₆] aqueous solution (3 mL, 0.5 mol/L) was slowly added to the aqueous solution of potassium potassium 5-bromo-1H-indole-1-carbodithioate (115 mg, 0.371 mmol, 1 eq) with a vigorous magnetic stirring for 5 minutes at room temperature. A yellow powder precipitates during the addition. The mixture was stirred for 10 minutes more, then filtered, washed first with deionized water, then MeOH, and then air dried. The resulting solid was placed under high vacuum to remove water and MeOH traces. A fine yellow powder was obtained, 89 mg, 89% yield.⁷⁸

¹H NMR (500 MHz, CDCl₃) δ 8.82 (d, $J = 9.0$ Hz, 2H), 8.29 (d, $J = 3.8$ Hz, 2H), 7.75 (d, $J = 2.0$ Hz, 2H), 7.48 (dd, $J = 9.0, 2.0$ Hz, 2H), 6.77 (dd, $J = 3.8$ Hz, 2H).

⁷⁸ On smaller scale the compound can be purified by standard flash column chromatography using a 9:1 Hex/AcOEt as eluent.

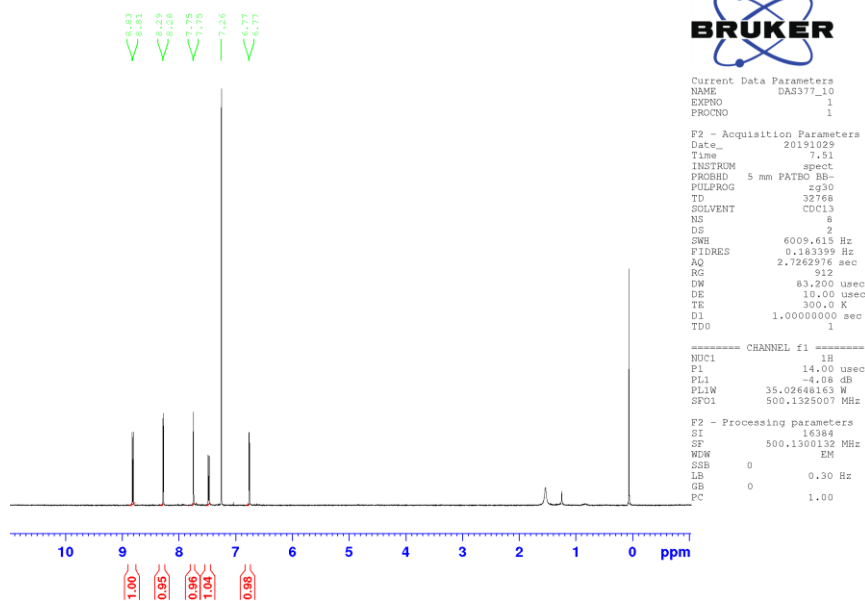


Figure 2.36. ¹H-NMR spectrum of the dimer **56**

¹³C NMR (101 MHz, CDCl₃) δ 189.7 (C), 136.8 (C), 133.7 (C), 128.8 (CH), 128.1 (CH), 124.4 (CH), 118.5 (C), 118.3 (CH), 110.3 (CH).

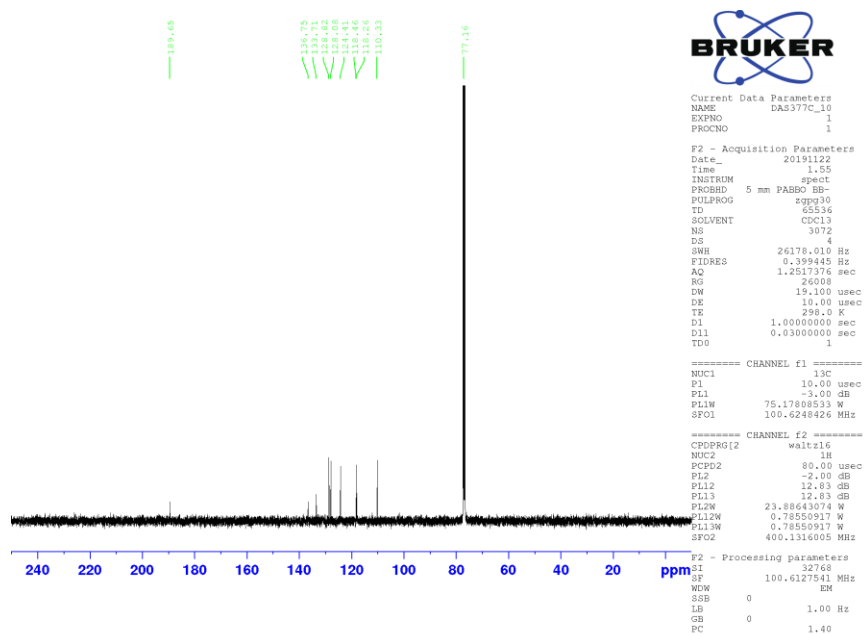


Figure 2.37. ¹³C-NMR spectrum of the dimer **56**.

HRMS: calculated for C₁₈H₁₀Br₂N₂NaS₄ (M+Na⁺): 562.7986, found 562.7986.

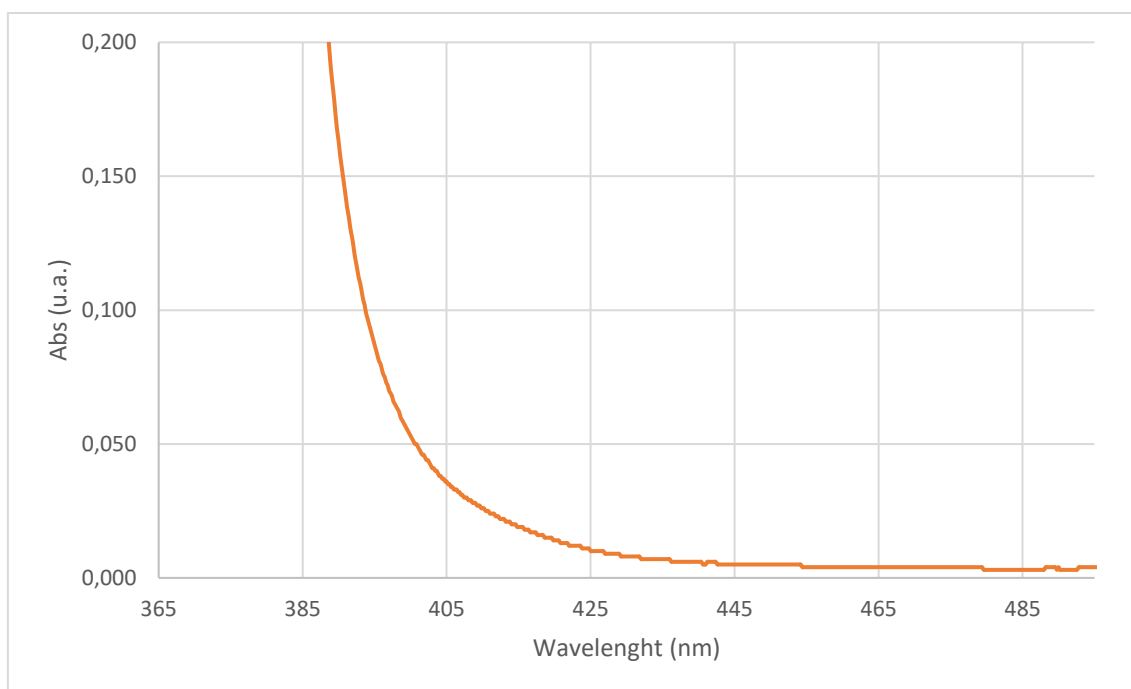


Figure 2.38. UV-Vis absorption spectrum of the dimer **56** recorded at $2 \cdot 10^{-4}$ M concentration in THF.

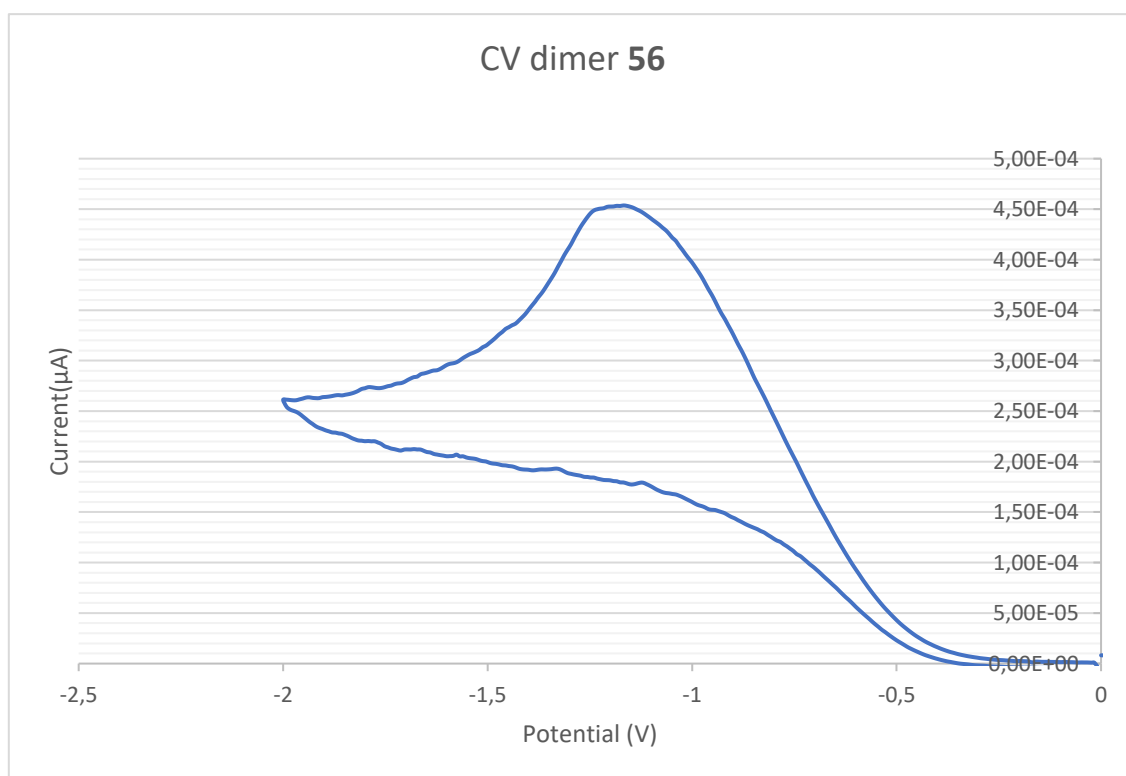
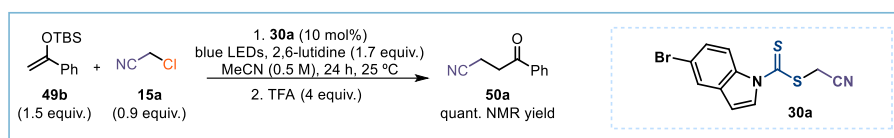


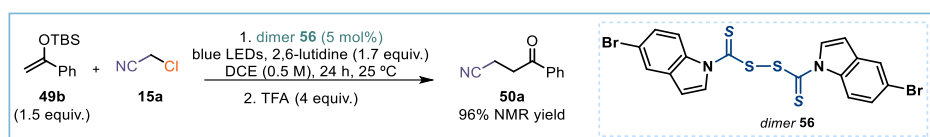
Figure 2.39. Cyclic voltammogram of the dimer **56**. [0.02M] in [0.1 M] TBAPF₆ in THF. Sweep rate: 500 mV/s. Pt electrode working electrode, Ag/AgCl (KCl 3.5 M) reference electrode, Pt wire auxiliary electrode. Irreversible reduction, $E_{\text{red}}(\mathbf{56}/\mathbf{56}^{\cdot-}) = -1.18$ V.

2.8.7.3 Involvement of **30a** in the catalytic cycle



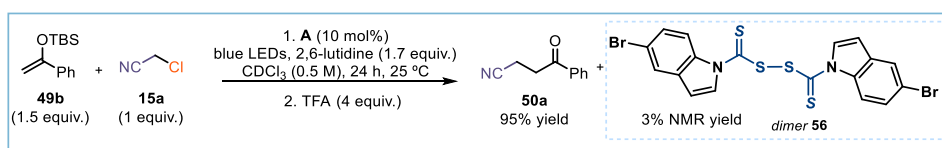
In an oven dried Schlenk tube, silyl enol ether **49b** (0.3 mmol, 70 mg, 1.5 equiv.) was dissolved in acetonitrile (400 μ L, HPLC grade), then 2,6-lutidine (0.34 mmol, 40 μ L, 1.7 equiv.) was added, followed by cyanomethyl 5-bromo-1*H*-indole-1-carbodithioate **30a** (6.2 mg, 0.02 mmol, 0.1 equiv.) and chloroacetonitrile **15a** (0.18 mmol, 11 μ L, 0.9 equiv.). The resulting yellow mixture was degassed via three cycles of freeze-pump-thaw. The Schlenk tube was then placed in the irradiation setup, maintained at a temperature of 25 $^{\circ}$ C and the reaction was stirred under irradiation for 24 hours. Trichloroethylene (0.2 mmol, 18 μ L, 1 equiv.) was added, the residue dissolved in CDCl_3 and an aliquot analyzed by ^1H NMR, which showed quantitative formation of the desired product **50a**.

2.8.7.4 Involvement of dimer **56** in the catalytic cycle



In an oven dried Schlenk tube, silyl enol ether **49b** (0.3 mmol, 70 mg, 1.5 equiv.) was dissolved in DCE (400 μ L), then 2,6-lutidine (0.34 mmol, 40 μ L, 1.7 equiv.) was added, followed by DTC-dimer (5.4 mg, 0.02 mmol, 0.05 equiv.) and chloroacetonitrile **15a** (0.2 mmol, 13 μ L, 1 equiv.). The resulting yellow mixture was degassed via three cycles of freeze-pump-thaw. The Schlenk tube was then placed in the irradiation setup, maintained at a temperature of 25 $^{\circ}$ C and the reaction was stirred under irradiation for 24 hours. Trichloroethylene (0.2 mmol, 18 μ L, 1 equiv.) was added, the residue dissolved in CDCl_3 and an aliquot analyzed by ^1H NMR, which showed formation of the desired product **50a** (96% yield). Importantly, no reaction was observed when the same experiment was performed in the dark.

2.8.7.5 Detection of dimer **56** in the reaction mixture



In an oven dried Schlenk tube, silyl enol ether **49b** (0.15 mmol, 35 mg, 1.5 equiv.) was dissolved in CDCl_3 (200 μ L), then 2,6-lutidine (0.17 mmol, 20 μ L, 1.7 equiv.) was added, followed by catalyst **A** (3.10 mg, 0.01 mmol, 0.1 equiv.) and chloroacetonitrile **15a** (0.1 mmol, 6.5 μ L, 1 equiv.). The resulting yellow mixture was degassed via three cycles of freeze-pump-thaw. The Schlenk tube was then placed in the irradiation setup, maintained at a temperature of 25 $^{\circ}$ C and the reaction was stirred under irradiation for 24 hours. Trichloroethylene (0.1 mmol, 9 μ L, 1 equiv.) was added, the residue dissolved in CDCl_3 and an aliquot analyzed by ^1H NMR, which showed the formation of the dimer **56** (3% yield, see Figures 2.38 and 2.39).

Diagnostic signals: ^1H NMR (400 MHz) δ (ppm): 8.82 (d, $J = 9.0$ Hz, 2H), 8.28 (d, $J = 3.8$ Hz, 2H), 7.75 (d, $J = 2.0$ Hz, 2H), 6.77 (dd, $J = 3.8$ Hz, 2H).

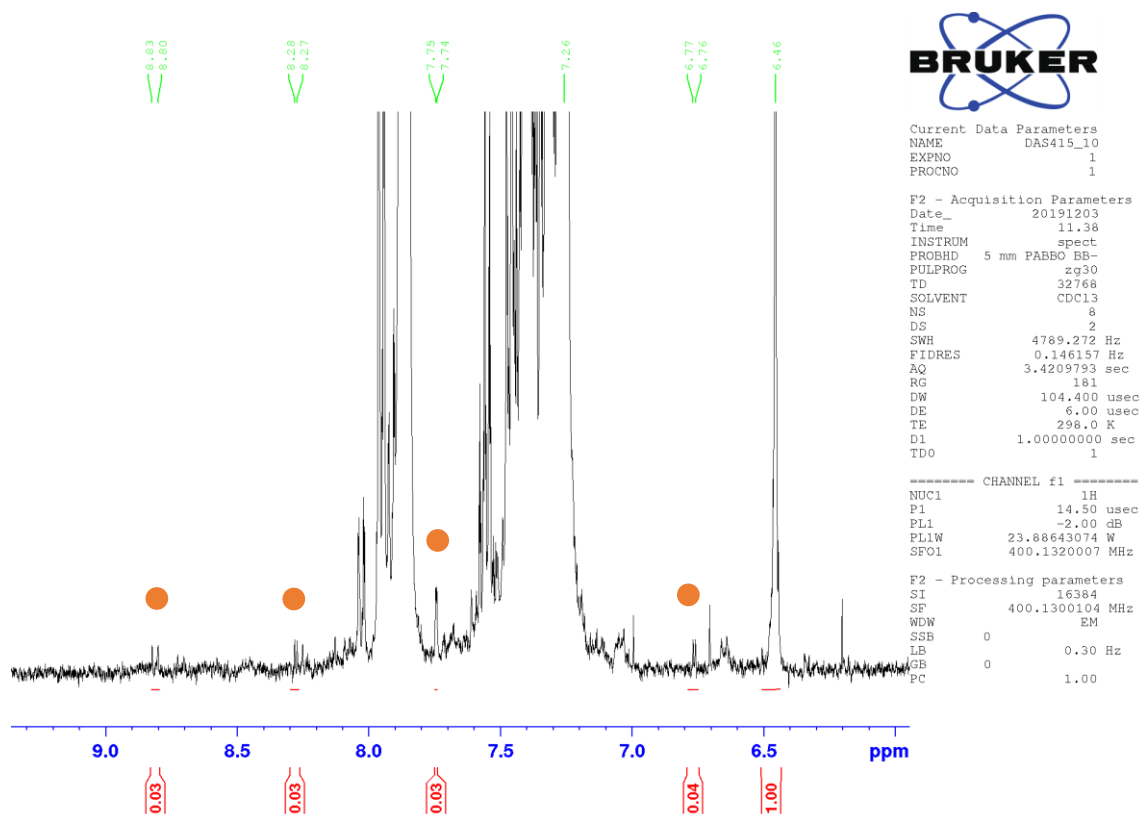


Figure 2.40. ^1H NMR spectrum of the crude reaction mixture after 24 h of irradiation.

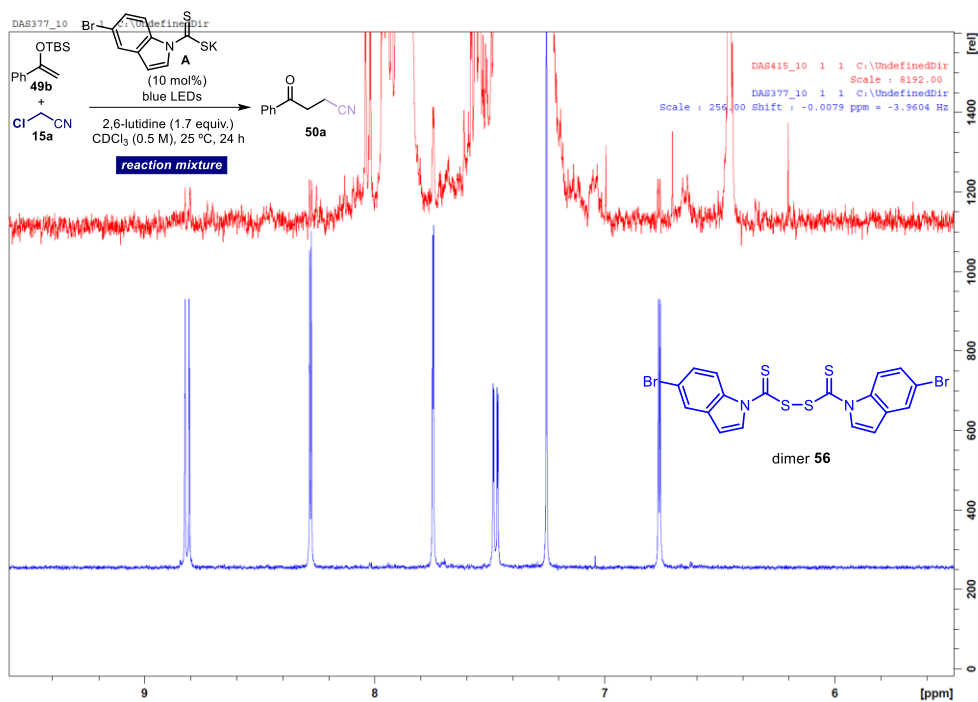
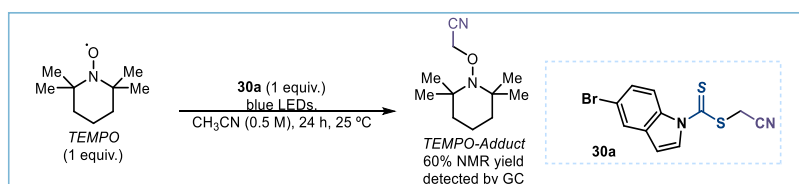


Figure 2.41. ^1H NMR analysis of the model catalytic reaction. *Red spectrum*: crude reaction mixture; *Blue spectrum*: authentic sample of an isolated dimer **56**.

2.8.7.6 Involvement of **30a** as radical precursor



In an oven-dried Schlenk tube, cyanomethyl 5-bromo-1*H*-indole-1-carbodithioate **30a** (0.2 mmol, 62 mg) and 2,2,6,6-tetramethylpiperidine 1-oxyl (TEMPO) (0.2 mmol, 31 mg) were dissolved in acetonitrile (400 μL). The resulting mixture was degassed via three cycles of freeze-pump-thaw and the Schlenk tube was then placed in the irradiation setup at a temperature of 25 °C and irradiated for 24 hours. Then trichloroethylene (0.2 mmol, 18 μl) was added as internal standard, the mixture diluted with CDCl₃ (400 μL), and an aliquot analyzed by ¹H NMR spectroscopy, which revealed the formation of the cyanomethyl-TEMPO adduct (77% conversion, 60% yield). The spectroscopic data are in agreement with those already reported in the literature.

Diagnostic signals: ¹H NMR (400 MHz) δ (ppm): 4.47 (s, 2H), 1.14 (s, CH₃), 1.05 (s, CH₃).

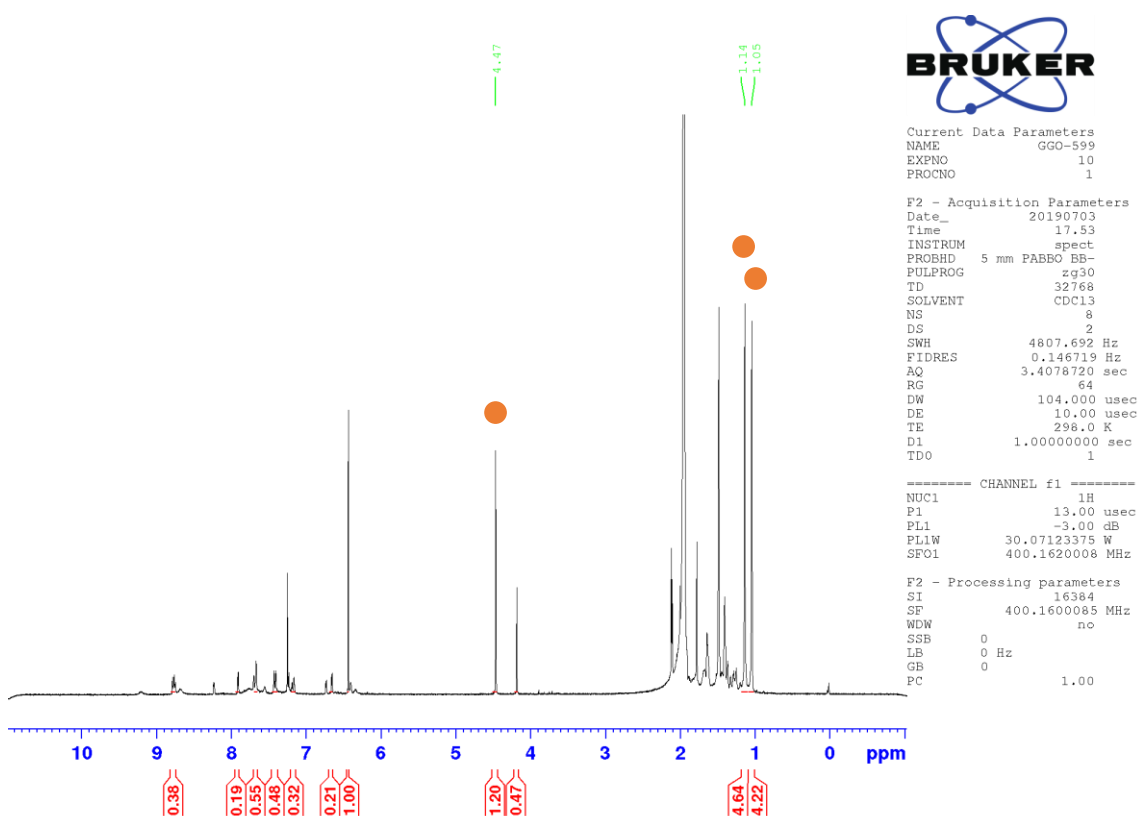


Figure 2.42. ¹H NMR spectrum of the crude reaction mixture after 24 h of irradiation in presence of TEMPO. The cyanomethyl-TEMPO adduct was formed in 60% yield as determined by using trichloroethylene as internal standard. The diagnostic signals of TEMPO adduct are indicated by the orange circles.

The presence of the cyanomethyl-TEMPO adduct was further confirmed by GC-MS analysis: 5 min at 50 °C, followed by a gradient until 300 °C in 6.25 min, then 10 min at 300 °C; τ = 8.128 min. Diagnostic MS peaks: *m/z* (%) 196.2 (2), 181.1 (85), 156.1 (100).

A control experiment in the absence of light showed no formation of the cyanomethyl-TEMPO adduct product.

2.8.7.7 Quantum Yield Measurement

A ferrioxalate actinometer solution was prepared by following the Hammond variation of the Hatchard and Parker procedure outlined in the Handbook of Photochemistry.⁷⁹ The ferrioxalate actinometer solution measures the decomposition of ferric ions to ferrous ions, which are complexed by 1,10-phenanthroline and monitored by UV/Vis absorbance at 510 nm. The moles of iron-phenanthroline complex formed are related to moles of photons absorbed.

The following solutions were prepared and stored in a dark laboratory (red light):

1. Potassium ferrioxalate solution: 294.8 mg of potassium ferrioxalate (commercially available from Alfa Aesar) and 139 μ L of sulfuric acid (96%) were added to a 50 mL volumetric flask, and filled to the mark with water (HPLC grade).
2. Phenanthroline solution: 0.2% by weight of 1,10-phenanthroline in water (100 mg in 50 mL volumetric flask).
3. Buffer solution: 2.47 g of NaOAc and 0.5 mL of sulfuric acid (96%) were added to a 50 mL volumetric flask, and filled to the mark with water (HPLC grade).
4. Model reaction solution: silyl enol ether **49b** (7.5 mmol), chloroacetonitrile **15a** (4.5 mmol), intermediate **30a** (0.5 mmol), and 2,6-Lutidine (8.5 mmol) were sequentially added to a 5 mL volumetric flask and filled to the mark with acetonitrile (HPLC grade).

The actinometry measurements were done as follows:

1 mL of the actinometer solution was added to a Schlenk tube (diameter = 12 mm). The Schlenk tube was placed in a single HP LED 1.5 cm away from the light source. The solution was irradiated at 460 nm (irradiance 10 mW/cm²). This procedure was repeated 4 times, quenching the solutions after different time intervals: 10 sec, 20 sec, 30 sec, and 40 sec. Then 1 mL of the reaction mixture of the stock solution has been placed in a Schlenk tube, degassed via three cycles of freeze-pump-thaw, placed in the irradiation set up and it has been irradiated for 60 minutes. This procedure has been performed other three times with different irradiation times (120 min, 180 min, 240 min).

After irradiation, the actinometer solutions were removed and placed in a 10 mL volumetric flask containing 0.5 mL of 1,10-phenanthroline solution and 2 mL of buffer solution. These flasks were filled to the mark with water (HPLC grade).

The UV-Vis spectra of the complexed actinometer samples were recorded for each time interval. The absorbance of the complexed actinometer solution was monitored at 510 nm.

⁷⁹ Murov, S. L. Ed. *Handbook of Photochemistry* **1973**, Marcel Dekker, New York.

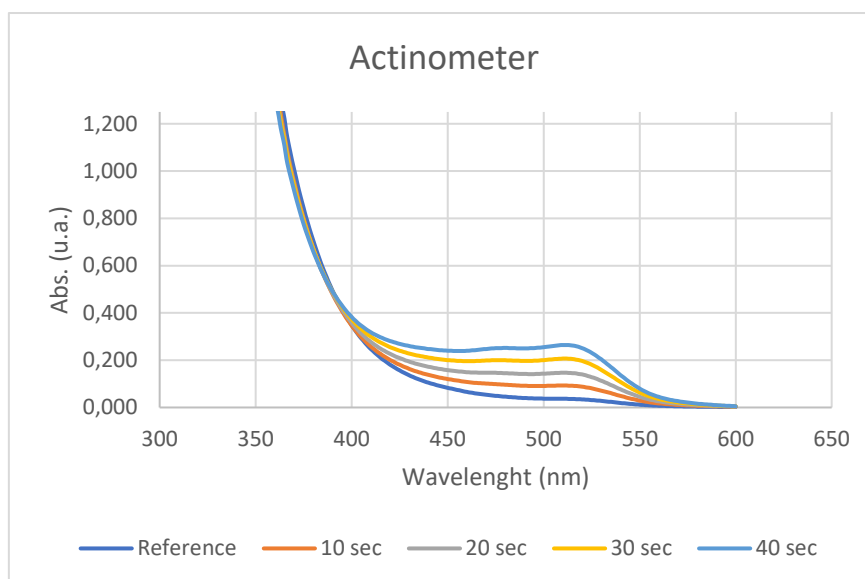


Figure 2.43. Actinometer

The moles of Fe^{2+} formed for each sample is determined using Beers' Law (Eq. 1) :

$$\text{Mols of Fe(II)} = V_1 \times V_3 \times \Delta A(510 \text{ nm}) / 10^3 \times V_2 \times l \times \varepsilon(510 \text{ nm}) \quad (\text{Eq. 1})$$

where V_1 is the irradiated volume (1 mL), V_2 is the aliquot of the irradiated solution taken for the determination of the ferrous ions (1 mL), V_3 is the final volume after complexation with phenanthroline (10 mL), l is the optical path-length of the irradiation cell (1 cm), $\Delta A(510 \text{ nm})$ is the optical difference in absorbance between the irradiated solution and the one stored in the dark, $\varepsilon(510 \text{ nm})$ is the extinction coefficient the complex $\text{Fe}(\text{phen})_3^{2+}$ at 510 nm ($11100 \text{ L mol}^{-1} \text{ cm}$). The moles of Fe^{2+} formed (x) are plotted as a function of time (t). The slope of this line was correlated to the moles of incident photons by unit of time ($q_0 \text{ n,p}$) by the use of the following Equation 2:

$$\Phi(\lambda) = dx/dt \cdot q_{n,p} \cdot 0 [1 - 10^{-A(\lambda)}] \quad (\text{Eq. 2})$$

where dx/dt is the rate of change of a measurable quantity (spectral or any other property), the quantum yield (Φ) for Fe^{2+} at 458 nm is 1.1,⁸⁰ $[1 - 10^{-A(\lambda)}]$ is the ratio of absorbed photons by the solution, and $A(\lambda)$ is the absorbance of the actinometer at the wavelength used to carry out the experiments (460 nm). The absorbance at 460 nm $A(460)$ was measured using a Shimadzu 2401PC UV-Vis spectrophotometer in a 10 mm path quartz cuvette, obtaining an absorbance of 0.146. $q_{n,p}^0$, which is the photon flux, was determined to be $3,36 \times 10^{-08}$.

⁸⁰ C. A. Holubov, C. A.; Langford, C. H. "Wavelength and Temperature Dependence in the Photolysis of the Chemical Actinometer, Potassium Trisoxalatoferrate(III), at longer Wavelengths" *Inorg. Chim. Acta.* **1981**, 53, 59-60.

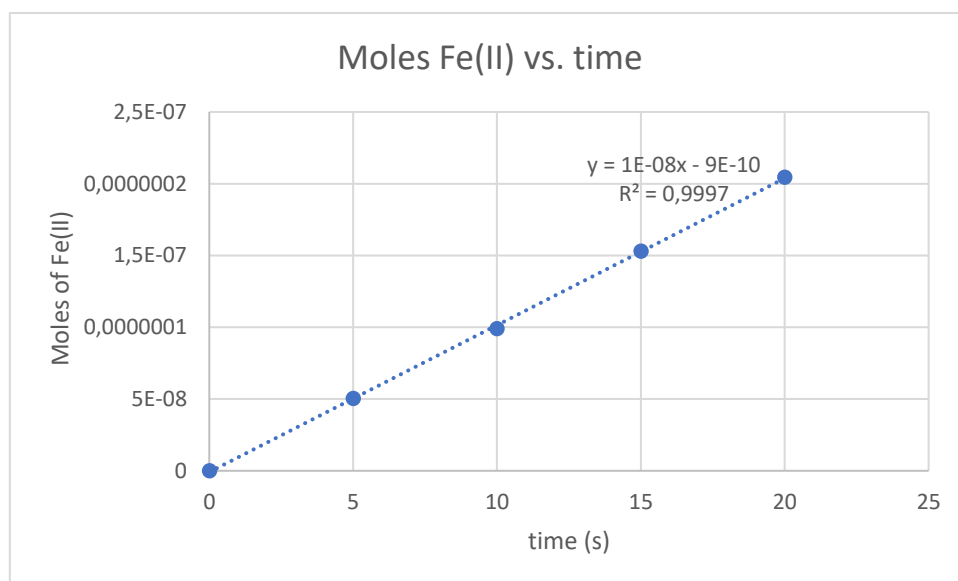


Figure 2.44. Moles of Fe(II) over time.

The moles of product **50a** formed for the model reaction were determined by GC measurement (FID detector) using 1,3,5-trimethoxybenzene as internal standard. The moles of product per unit of time are related to the number of photons absorbed. The photons absorbed are correlated to the number of incident photons by the use of Equation 1. According to this, if we plot the moles of product (x) versus the moles of incident photons ($q_0 n, p \cdot dt$), the slope is equal to: $\Phi \cdot (1 - 10^{-A(460 \text{ nm})})$, where Φ is the quantum yield to be determined and $A(460 \text{ nm})$ is the absorption of the reaction under study. $A(460 \text{ nm})$ was measured using a Shimadzu 2401PC UV-Vis spectrophotometer in 10 mm path quartz. An absorbance of 1.5 was determined for the model reaction mixture. The quantum yield (Φ)_{cat.} of the photochemical transformation was measured to be 0.053. The procedure was repeated a second time to provide a similar value: quantum yield (Φ)_{cat.} at 460 nm of 0.054.

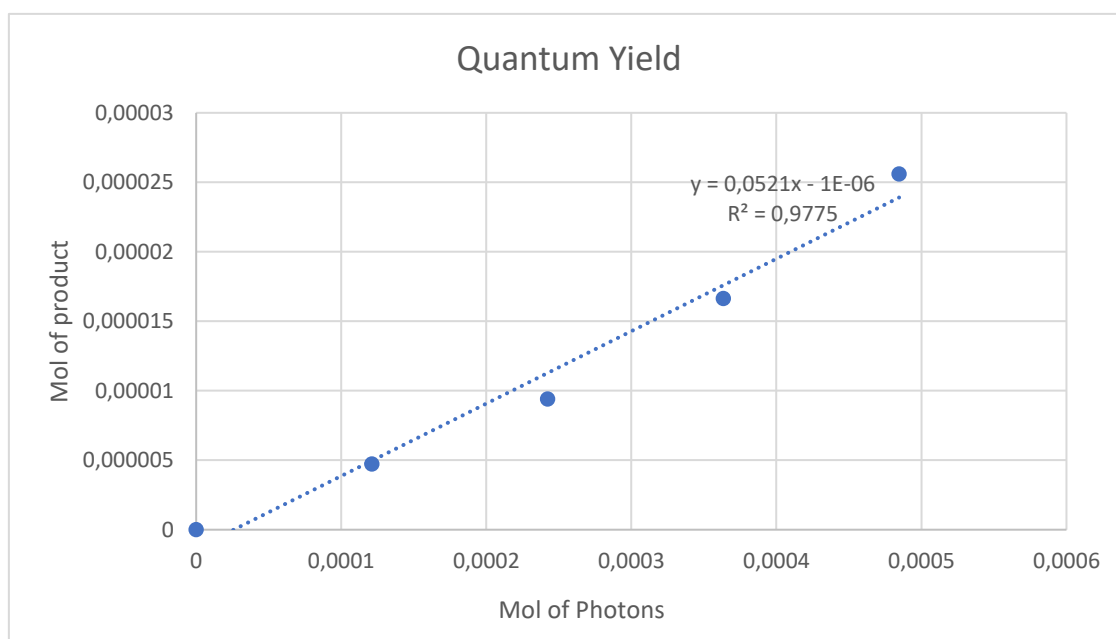


Figure 2.45. Quantum yield.

Using the very same approach the quantum yield under stoichiometric conditions has been measured: quantum yield (Φ)_{stoichiometric} at 460 nm of 0.061.

2.8.7.8 Mechanistic Alternatives

We considered the possibility of an alternative pathway enabled by a group transfer mechanism (Figure 2.46 below).

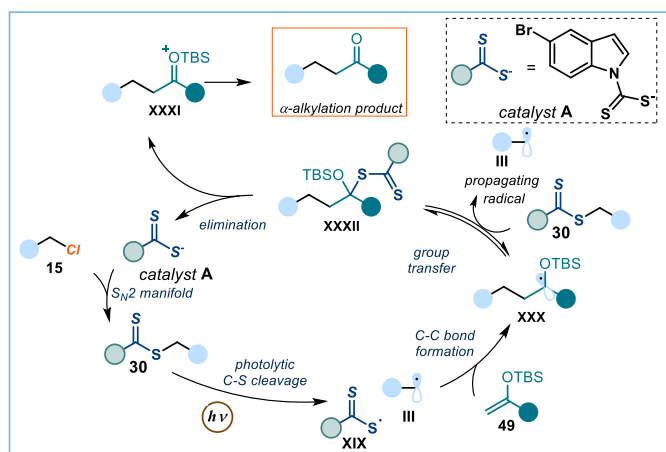
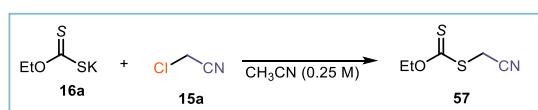


Figure 2.46. A possible group transfer-based mechanism following a radical chain propagation.

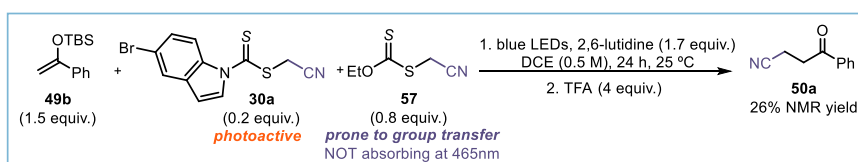


Preparation of intermediate 57. In a round bottom flask, the potassium O-ethyl carbonodithioate **16a** (9.05 mmol, 1.45 g) was dissolved in acetonitrile (36 mL). Then chloroacetonitrile **15a** (9.05 mmol, 572 μ L) was added and the resulting mixture stirred for one hour at ambient temperature. The mixture was transferred to an extraction funnel containing water (75 mL) and extracted with ethyl acetate (75 mL). The organic phase was further washed with brine (25 mL), dried over anhydrous MgSO_4 , filtered and concentrated to dryness to obtain pure cyanomethyl S-(cyanomethyl) O-ethyl carbonodithioate **52** as a yellow oil (1.3 g, 89% yield).

¹H NMR (400 MHz, CDCl_3) δ 4.72 (q, J = 7.1 Hz, 2H), 3.89 (s, 1H), 1.47 (t, J = 6.8 Hz, 3H).

¹³C NMR (126 MHz, CDCl_3) δ 209.1 (C), 115.3 (C), 71.6 (CH_2), 21.41 (CH_2), 13.8 (CH_3).

Characterization data matching data reported in the literature.⁸¹



In an oven-dried Schlenk tube, silyl enol ether **49b** (0.15 mmol, 35 mg, 1.5 equiv.) was dissolved in DCE (200 μ L), then 2,6-lutidine (0.17 mmol, 20 μ L, 1.7 equiv.) was added, followed by cyanomethyl 5-bromo-1H-indole-1-carbodithioate **30a** (0.02 mmol, 6.22 mg) and S-(cyanomethyl) O-ethyl carbonodithioate **57**

⁸¹ V. Liautard, F. Robert, Y. Landais "Free-Radical Carboalkynylation and Carboalkenylation of Olefins" *Org. Lett.* **2011**, *13*, 10, 2658-2661.

(0.08 mmol, 13 mg). The resulting mixture was degassed via three cycles of freeze-pump-thaw and the Schlenk tube was then placed in the irradiation setup at a temperature of 25 °C and irradiated for 24 hours. Then trichloroethylene (0.2 mmol, 18 μ l) was added as internal standard, the mixture diluted with CDCl_3 (400 μ L). Finally, the reaction mixture was treated with TFA (0.4 mmol) and an aliquot analyzed by ^1H NMR spectroscopy which revealed the formation of the desired product **50a** (26% yield).

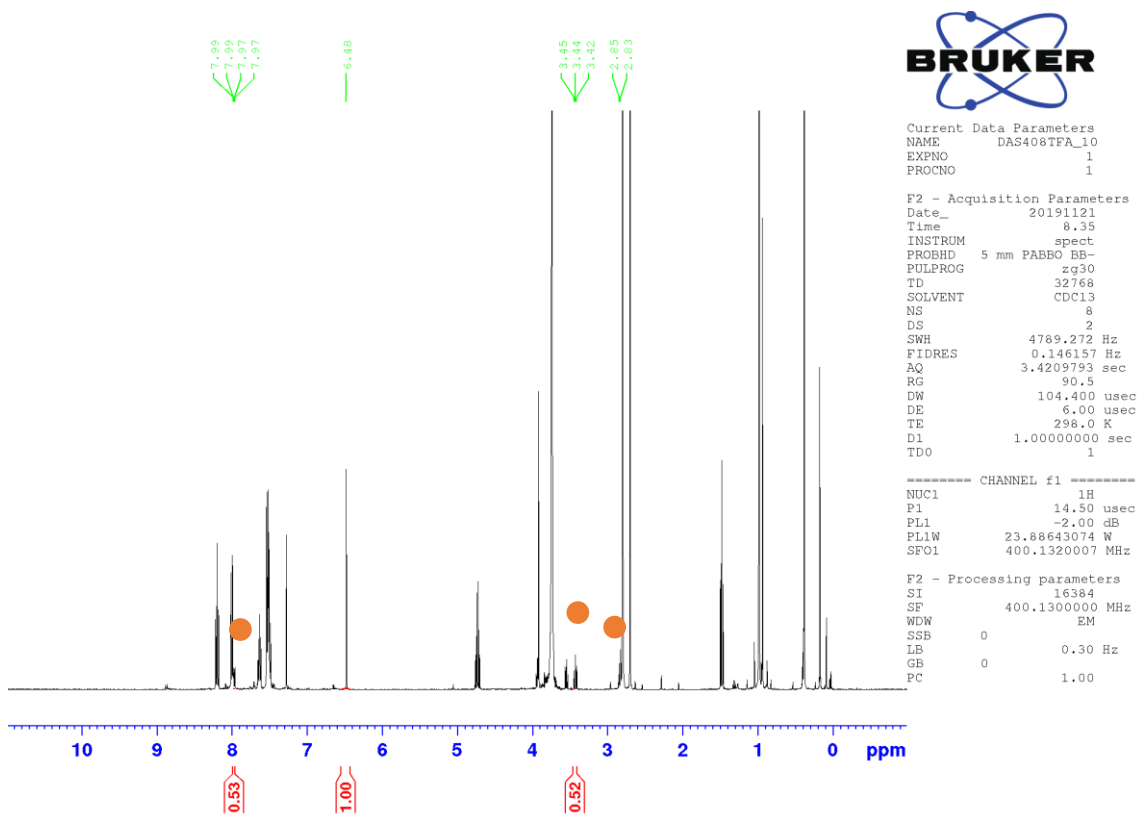


Figure 2.47. ^1H NMR spectrum of the crude reaction mixture after 24 h. Product **50a** was formed in 26% yield as determined by using trichloroethylene as internal standard.

We also considered the possibility of an alternative mechanism based on a single-electron transfer (SET) event between radical **XXX** and the intermediate **30**, as depicted in Figure 2.47. Here the radical intermediate **XXX** reduces **30**, leading to intermediate **XXXI** while generating catalyst **A** and the propagating radical **III**.

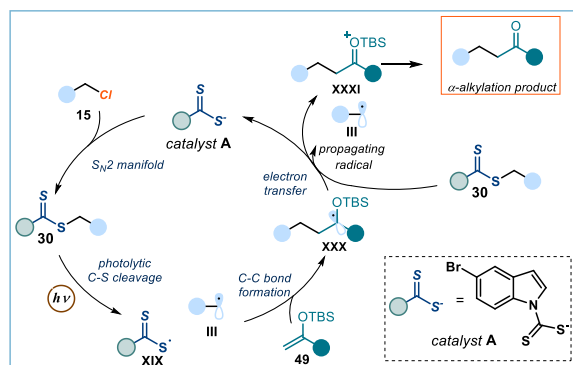


Figure 2.48. A possible SET(**XXX**-and **30**)-based mechanism following a chain propagation.

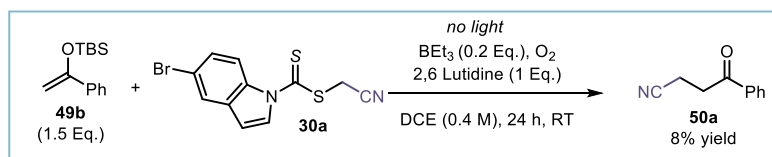


Figure 2.49. (a) Triethylborane/O₂ as an initiation system.

In an oven-dried Schlenk tube, silyl enol ether **49b** (0.130 mmol, 30 mg, 1.3 equiv.) was dissolved in DCE (250 μ L), then 2,6-lutidine (0.1 mmol, 12 μ L, 1 equiv.) was added, followed by cyanomethyl 5-bromo-1H-indole-1-carbodithioate **30a** (0.1 mmol, 31 mg), and a solution of BEt₃ in hexane (20 μ L, 1M). The resulting mixture was left stirring vigorously at a temperature of 25 $^{\circ}$ C for 24 hours. Then trichloroethylene (0.1 mmol, 9 μ l) was added as internal standard, the mixture diluted with CDCl₃ (400 μ L), and an aliquot analyzed by ¹H NMR spectroscopy which revealed the formation of the desired product **50a** (8% yield).

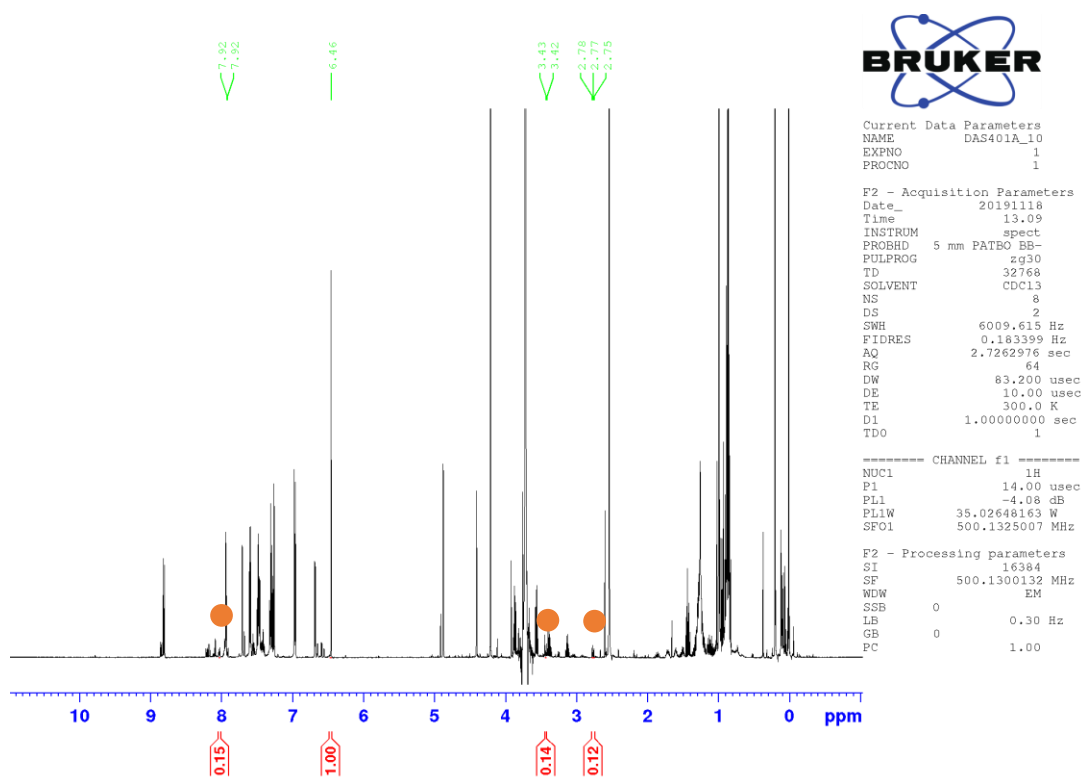
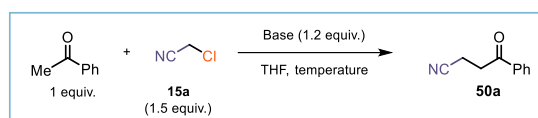


Figure 2.50. ¹H NMR spectrum of the crude reaction mixture after 24 h. Product **50a** was formed in 8% yield as determined by using trichloroethylene as internal standard.

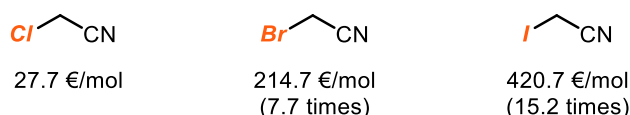
2.8.8 α -Alkylation of Acetophenone by Enolate Chemistry



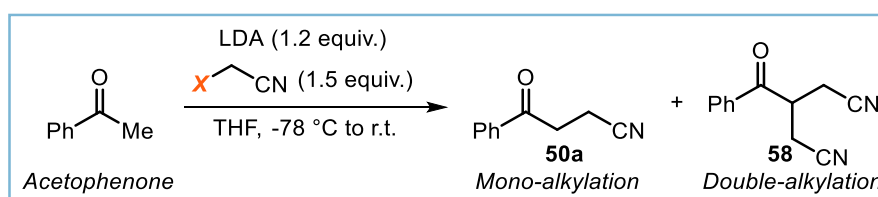
Entry	base	Temperature	yield
1	LDA (commercial)	-78°C (30 min) to r.t. (1 h)	Complex mixture
2	LDA (freshly prepared)	-78°C (30 min) to r.t. (1 h)	Complex mixture
3	LDA (freshly prepared)	-78°C (3h)	Unreacted SM
4	LiHMDS	-78°C (30 min) to r.t. (1 h)	Complex mixture
5	NaHMDS	-78°C (30 min) to r.t. (1 h)	Complex mixture
6	KHMDS	-78°C (30 min) to r.t. (1 h)	Unreacted SM

Table S4. Screening of lithium enolates for the alkylation of acetophenone with chloroacetonitrile.

In an oven dried Schlenk tube under argon cooled at -78°C in a dry ice/acetone bath, the base (commercial or freshly prepared, 1.2 mmol, 1.2 equiv.) was diluted to 0.25 M concentration with dry THF (4 mL), then a solution of acetophenone (117 μ L, 1 mmol) in dry THF (0.5 mL) was added dropwise. After 15 minutes stirring at this temperature, the solution was allowed to warm up to room temperature and stirred for 30 minutes. The mixture was cooled back to -78°C and a solution of chloroacetonitrile (95 μ L, 1.5 mmol) in dry THF (0.5 mL) was added dropwise. The mixture was then stirred for an additional 30 minutes and allowed to warm up to room temperature. Water (0.5 mL) was then added and the mixture transferred to an extraction funnel containing ether (10 mL) and 1M HCl (10 mL). The aqueous layer was extracted with ether (2x 10 mL), the combined organic fractions were then washed with brine (5 mL), dried (MgSO_4) and solvents removed under reduced pressure. The residue was then diluted with 1 mL of CDCl_3 , trichloroethylene (90 μ L, 1 equivalent) added as internal standard and an aliquot analyzed by ^1H NMR.



Price of the electrophiles as supplied by Sigma-Aldrich (09/07/2019).



Entry	X	Conversion (%)	50a (%)	58 (%)
1	Cl	96	0	0
2	Br	68	9	8
3	I	89	5	3

Table S5. Screening of electrophiles for the alkylation of acetophenone derived lithium enolate.

In an oven dried Schlenk flask under argon cooled at -78°C in a dry ice/acetone bath, diisopropylamine (1.2 mmol, 168 μ L) was diluted to 0.25 M concentration with dry THF (4 mL), then a solution of *n*-butyllithium

2.5 M in hexane (480 μ L) was added dropwise. The solution was stirred for 15 min, then a solution of acetophenone (1 mmol, 117 μ L) in dry THF (0.5 mL) was added dropwise. After 15 minutes stirring at this temperature, the solution was allowed to warm up to room temperature and stirred for 30 minutes. The mixture was cooled back to -78°C and the electrophile (1.5 mmol, 1.5 equiv.) was added dropwise. The mixture was then stirred for an additional 30 minutes and allowed to warm up to room temperature. Water (0.5 mL) was then added and the mixture transferred to an extraction funnel containing a 1M HCl aqueous solution (10 mL). The aqueous layer was extracted with ether (2x10 mL), the organic fractions were dried over anhydrous MgSO_4 and the solvent removed under reduced pressure. The residue was then diluted with 1mL of CDCl_3 , trichloroethylene (90 μ L, 1 equivalent) was added as internal standard and an aliquot analyzed by ^1H NMR to determine conversion and yield.

The crude mixture arising from reaction with iodoacetonitrile was submitted to flash chromatography (gradient from Hex to Hex:EtOAc,1:1) which allowed to identify the double alkylated side product **9**.

^1H NMR (400 MHz, CDCl_3) δ 7.95 (d, $J= 8.0$ Hz, 2H), 7.69 (t, $J= 7.4$ Hz, 1H), 7.56 (t, $J= 7.8$ Hz, 2H), 4.08 (quint., $J= 6.6$ Hz, 1H), 2.93 (dd, $J= 17.1, 6.2$ Hz, 2H), 2.82 (dd, $J= 17.1, 7.0$ Hz, 2H).

HRMS: calculated for $\text{C}_{12}\text{H}_{10}\text{N}_2\text{NaO}$ ($\text{M}+\text{Na}^+$): 221.0685, found 221.0684.

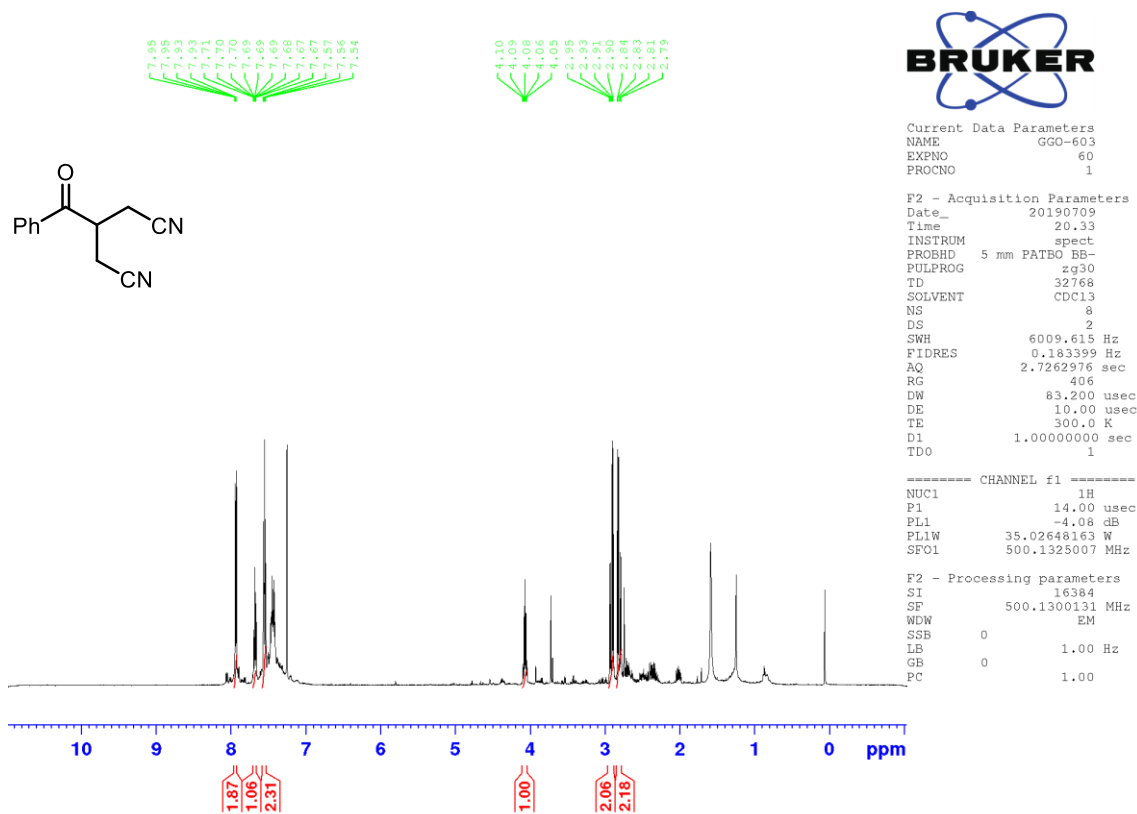
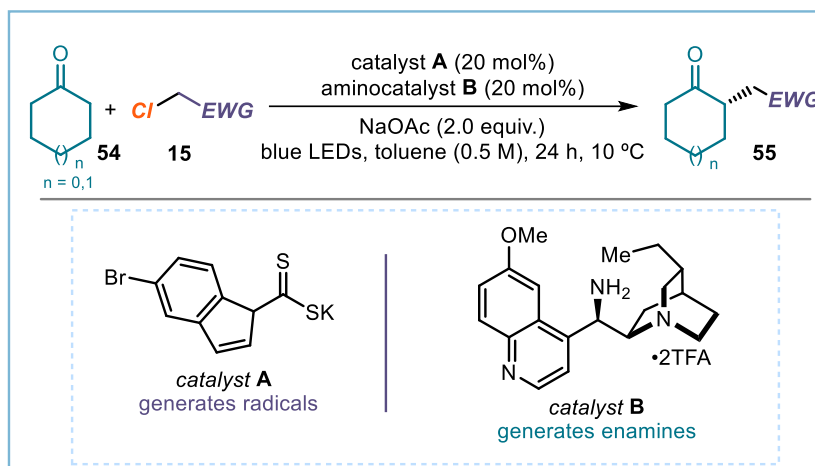


Figure 2.51. ^1H NMR spectrum of the isolated double alkylated side product **58**.

2.8.9 Enantioselective Radical α -Alkylation of Cyclic Ketones

2.8.9.1 General procedure



In an oven dried 10 mL Schlenk tube, catalyst **A** (0.04 mmol, 20 mol%) and sodium acetate (0.4 mmol, 2 equiv.) were added at once to a stirred solution of catalyst **B** (0.04 mmol, 20 mol%) and the cyclic ketone **54** (2.0 mmol, 10 equiv.) in toluene (1.0 mL). After addition of the alkyl halide (0.2 mmol, 1 equiv.), the reaction mixture was degassed via freeze pump thaw (3 cycles; thawing in ice-water to avoid warming the mixture above 0 °C) and backfilled with argon. The Schlenk tube was sealed, positioned into the photoreactor (see Figure S3) and irradiated with a blue LED strip for 24 hours at the specified temperature, then warmed to ambient temperature. The crude mixture was directly purified by flash column chromatography to afford the title compound **55** in the stated yield and enantiomeric purity. Unless otherwise noted, yields and enantiomeric excesses refer to an average of two independent runs.

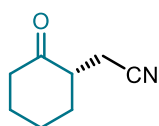
Note: Epimerization of the α -chiral center within product **55** was commonly observed upon chromatography on silica gel. As such, chromatographic purifications have to be performed under high flow and generally conducted as quickly as possible.

Determination of Enantiomeric Purity: HPLC analysis on chiral stationary phase was performed on an Agilent 1200-series instrument, employing Daicel Chiralpak IA, IB, ID, IC and IC-3 columns, or a Waters ACQUITY® UPC² instrument, using Trefoil AMY1, CEL1, and CEL2 and Daicel Chiralpak IC chiral columns. The exact conditions for the analyses are specified within the characterisation section. HPLC traces were compared to racemic samples prepared performing the reaction in the presence of pyrrolidine.

In most cases, the products are lacking a suitable chromophore to allow analysis by HPLC or UPC² methods. Derivatization into the corresponding tosyl hydrazone was therefore performed.

Derivatization of enantioenriched chiral ketones **55** with *p*-toluenesulfonyl hydrazide for UPC²/HPLC analysis. *p*-Toluenesulfonyl hydrazide (1.2 equiv.) was added at once to a solution of pure enantioenriched ketone **835** in MeOH (0.2 M). After stirring for 3 hours at ambient temperature, an analytical sample of the corresponding hydrazone was obtained by preparative TLC (1:1 CH₂Cl₂/EtOAc as eluent).

2.8.9.2 Characterization data



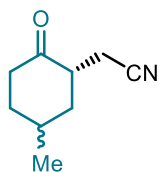
(S)-2-(2-oxocyclohexyl)acetonitrile (**55a**)

Prepared according to the general procedure using chloroacetonitrile (0.2 mmol, 13 μ L), cyclohexanone (2.0 mmol, 0.21 mL), catalyst **A** (0.04 mmol, 12 mg), catalyst **B** (0.04 mmol, 22 mg) and sodium acetate (0.4 mmol, 33 mg). Time of irradiation: 24 hours at 10 $^{\circ}$ C. The crude mixture was purified by flash column chromatography (hexane/EtOAc gradient from 10:1 to 1:1), concentrated and repurified by flash column chromatography (DCM/EtOAc gradient from 100:1 to 20:1) to afford product **55a** as a yellowish oil (21 mg, 76% yield, 90% *ee*). The enantiomeric excess was determined, after derivatization of the isolated ketone with *p*-toluenesulfonyl hydrazide to afford the corresponding hydrazone, to be 90% by UPC² analysis on Acquity Trefoil CEL1 column: 92:8 CO₂/*i*PrOH, flow rate 3.00 mL/min, λ = 230 nm; τ_{Major} = 7.20 min, τ_{Minor} = 9.46 min. $[\alpha]_D^{25}$ = -15.3 (*c* = 0.43, MeOH, 90% *ee*). Absolute configuration determined in comparison to the data reported in the literature.⁸²

¹H NMR (400 MHz, CDCl₃) δ 2.73-2.62 (m, 2H); 2.52-2.45 (m, 1H); 2.43-2.29 (m, 3H); 2.15 (ddq, *J* = 12.1, 5.9, 2.8 Hz, 1H); 2.01-1.93 (m, 1H); 1.81-1.62 (m, 2H); 1.49 (qd, *J* = 12.8, 3.6 Hz, 1H).

¹³C NMR (101 MHz, CDCl₃) δ 208.7 (C); 118.7 (C); 47.0 (CH); 41.7 (CH₂); 33.5 (CH₂); 27.7 (CH₂); 25.0 (CH₂); 18.0 (CH₂).

HRMS: calculated for C₈H₁₁NNaO (M+Na⁺): 160.0733, found 160.0726.



2-((1S)-5-methyl-2-oxocyclohexyl)acetonitrile (**55b**)

Prepared according to the general procedure using chloroacetonitrile (0.2 mmol, 13 μ L), 4-methylcyclohexanone (2.0 mmol, 0.25 mL), catalyst **A** (0.04 mmol, 12 mg), catalyst **B** (0.04 mmol, 22 mg) and sodium acetate (0.4 mmol, 33 mg). Time of irradiation: 24 hours at 10 $^{\circ}$ C. The crude mixture was purified by flash column chromatography (hexane/EtOAc gradient from 10:1 to 2:1), concentrated and repurified by flash column chromatography (DCM/EtOAc gradient from 100:1 to 40:1) to afford product **55b** as a yellowish oil (23 mg, 76% yield, 5.1:1 mixture of diastereoisomers). The relative stereochemistry was determined by selective 1D-NOESY. The major diastereoisomer was determined as the *trans* isomer by correlation between the methyl group in position 4 and the substituted α -proton [when 4-Me is irradiated the CO-CH(CH₂CN) is correlated]. The enantiomeric excess of the major diastereoisomer was determined, after derivatization of the isolated ketone with *p*-toluenesulfonyl hydrazide to afford the corresponding hydrazone, to be 93% by HPLC analysis on Daicel Chiralpak IA: 20 $^{\circ}$ C, 95:5 hexane/*i*PrOH, flow rate 1.0 mL/min, λ = 230 nm; τ_{Major} = 65.0 min, τ_{Minor} = 72.6 min. $[\alpha]_D^{28}$ = -24.4 (*c* = 0.29, MeOH, 5.1:1 dr, 91% *ee*_{major}, product obtained from the parallel experiment).

¹H NMR_{major diastereoisomer} (500 MHz, CDCl₃) δ 2.91-2.79 (m, 1H); 2.68 (dd, *J* = 17.1, 5.2 Hz, 1H); 2.52 (ddd, *J* = 14.4, 12.6, 6.4 Hz, 1H); 2.43-2.30 (m, 2H); 2.22 (qp, *J* = 7.4, 3.9 Hz, 1H); 2.11 (ddt, *J* = 13.3, 5.9, 2.9 Hz, 1H); 1.98-1.83 (m, 2H); 1.76 (td, *J* = 12.9, 4.8 Hz, 1H); 1.24 (d, *J* = 7.2 Hz, 3H).

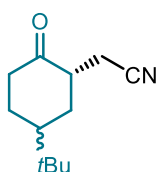
¹³C NMR_{major diastereoisomer} (126 MHz, CDCl₃) δ 209.2 (C); 118.6 (C); 42.3 (CH); 38.8 (CH₂); 37.1 (CH₂); 32.8 (CH₂); 26.9 (CH); 18.0 (CH₂); 17.8 (CH₃).

¹H NMR_{minor diastereoisomer} (500 MHz, CDCl₃) δ 1.46-1.35 (m, 1H); 1.04 (d, *J* = 6.4 Hz, 3H).

¹³C NMR_{minor diastereoisomer} (126 MHz, CDCl₃) δ 208.9; 118.7; 46.0; 41.3; 40.9; 35.6; 31.8; 21.1; 17.9.

HRMS: calculated for C₉H₁₃NNaO (M+Na⁺): 174.0889, found 174.0891.

⁸² Koul, S.; Crout, D. H. G.; Errington, W.; Tax, J. "Biotransformation of $\alpha\beta$ -unsaturated carbonyl compounds: sulfides, sulfoxides, sulfones, nitriles and esters by yeast species: carbonyl group and carbon-carbon double bond reduction" *J. Chem. Soc., Perkin Trans. 1* **1995**, 2969-2988.



2-((1S)-5-(tert-butyl)-2-oxocyclohexyl)acetonitrile (55c)

Prepared according to the general procedure using chloroacetonitrile (0.2 mmol, 13 μ L), 4-tert-butylcyclohexanone (2.0 mmol, 309 mg), catalyst **A** (0.04 mmol, 12 mg), catalyst **B** (0.04 mmol, 22 mg) and sodium acetate (0.4 mmol, 33 mg). Time of irradiation: 24 hours at 10 $^{\circ}$ C. The crude mixture was purified by flash column chromatography (hexane/EtOAc gradient from 10:1 to 2:1), concentrated and repurified by flash column chromatography (DCM/EtOAc gradient from 100:1 to 40:1) to afford product **55c** as a yellowish oil (33 mg, 85% yield, 2.2:1 mixture of diastereoisomers). The relative stereochemistry was determined by analogy with compounds **55b** and **55d**. The enantiomeric excesses were determined, after derivatization of the isolated ketone with *p*-toluenesulfonyl hydrazide to afford the corresponding hydrazone, by UPC² analysis on Acquity Trefoil AMY1 column: 89:11 CO₂/EtOH, flow rate 3.00 mL/min, λ = 230 nm; major diastereoisomer (79% ee): τ_{Major} = 4.27 min, τ_{Minor} = 5.97 min; minor diastereoisomer (71% ee): τ_{Major} = 7.53 min, τ_{Minor} = 6.88 min. $[\alpha]_D^{27}$ = -44.1 (c = 0.40, CHCl₃, 2.2:1 dr, 79% *ee*_{major}, 71% *ee*_{minor}).

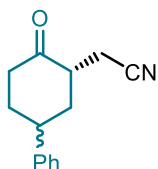
¹H NMR_{major diastereoisomer} (500 MHz, CDCl₃) δ 2.74-2.64 (m, 2H); 2.54-2.46 (m, 1H); 2.45-2.31 (m, 3H); 2.15 (ddq, *J* = 12.4, 6.1, 3.1 Hz, 1H); 1.76-1.61 (m, 1H); 1.55-1.42 (m, 1H); 1.31 (q, *J* = 12.7 Hz, 1H); 0.94 (s, 9H).

¹³C NMR_{major diastereoisomer} (126 MHz, CDCl₃) δ 209.0 (C); 118.7 (C); 46.9 (CH); 46.3 (CH); 41.0 (CH₂); 34.6 (CH₂); 32.7 (C); 28.5 (CH₂); 27.7 (CH₃); 18.1 (CH₂).

¹H NMR_{minor diastereoisomer} (500 MHz, CDCl₃) δ 2.82-2.75 (m, 1H); 2.27 (ddd, *J* = 18.1, 12.5, 6.0 Hz, 1H); 2.08 (dt, *J* = 14.0, 8.1 Hz, 1H); 1.95-1.89 (m, 1H); 0.93 (s, 9H).

¹³C NMR_{minor diastereoisomer} (126 MHz, CDCl₃) δ 211.3 (C); 118.3 (C); 43.2 (CH); 42.6 (CH); 38.5 (CH₂); 33.2 (C); 28.8 (CH₂); 27.1 (CH₃); 23.1 (CH₂); 18.2 (CH₂).

HRMS: calculated for C₁₂H₁₉NNaO (M+Na⁺): 216.1359, found 216.1365.



(S)-2-(2-oxo-5-phenylcyclohexyl)acetonitrile (55d)

Prepared according to the general procedure using chloroacetonitrile (0.2 mmol, 13 μ L), 4-phenylcyclohexanone (2.0 mmol, 348 mg), catalyst **A** (0.04 mmol, 12 mg), catalyst **B** (0.04 mmol, 22 mg) and sodium acetate (0.4 mmol, 33 mg). Time of irradiation: 24 hours at 10 $^{\circ}$ C. The crude mixture was purified by flash column chromatography (hexane/EtOAc gradient from 10:1 to 2:1), concentrated and repurified by flash column chromatography (DCM/EtOAc gradient from 100:1 to 40:1) to afford product **55d** as a yellowish oil (35 mg, 83% yield, 2.5:1 mixture of diastereoisomers). The relative stereochemistry was determined by selective 1D-NOESY. The major diastereoisomer was determined as the *trans* isomer by absence of correlation between the benzylic proton and the substituted α -proton [when the benzylic proton was irradiated the CO-CH(CH₂CN) is not correlated]. The minor diastereoisomer was determined as the *cis* isomer by correlation between the benzylic proton and the substituted α -proton [when the benzylic proton was irradiated the CO-CH(CH₂CN) is correlated]. The enantiomeric excesses were determined by UPC² analysis on Acquity Trefoil CEL1 column: gradient from 100% CO₂ to 60:40 CO₂/*i*PrOH over 5 minutes, curve 6, flow rate: 3.00 mL/min, λ = 210 nm; major diastereoisomer (93% ee): τ_{Major} = 4.08 min, τ_{Minor} = 3.96 min; minor diastereoisomer (80% ee): τ_{Major} = 4.57 min, τ_{Minor} = 4.47 min. $[\alpha]_D^{27}$ = +10.6 (c = 0.36, CHCl₃, 2.5:1 dr, 92% *ee*_{major}, 78% *ee*_{minor}, product obtained from the parallel experiment).

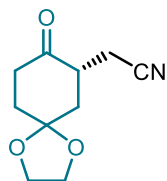
¹H NMR_{major diastereoisomer} (500 MHz, CDCl₃) δ 7.45-7.37 (m, 3H); 7.31-7.21 (m, 2H); 3.30 (p, *J* = 4.7 Hz, 1H); 2.82 (ddt, *J* = 11.3, 7.9, 5.5 Hz, 1H); 2.78-2.72 (m, 1H); 2.69 (dd, *J* = 17.0, 5.1 Hz, 1H); 2.62-2.40 (m, 4H); 2.22-2.13 (m, 1H); 2.06 (ddd, *J* = 13.8, 11.5, 5.2 Hz, 1H).

¹³C NMR *major diastereoisomer* (126 MHz, CDCl₃) δ 208.9 (C); 141.7 (C); 129.1(CH); 126.8 (CH); 126.7(CH); 118.3 (C); 43.0 (CH); 38.0 (CH₂); 36.5 (CH₂); 36.2 (CH); 30.5 (CH₂); 18.1 (CH₂).

¹H NMR *minor diastereoisomer* (500 MHz, CDCl₃) δ 7.44-7.37 (m, 2H); 7.36-7.31 (m, 2H); 7.30-7.21 (m, 1H); 3.18 (tt, *J* = 12.3, 3.4 Hz, 1H); 2.90 (ddt, *J* = 11.0, 7.4, 5.3 Hz, 1H); 2.78-2.72 (m, 1H); 2.62-2.41 (m, 4H); 2.33-2.26 (m, 1H); 1.97 (qd, *J* = 12.6, 5.8 Hz, 1H); 1.80 (q, *J* = 12.9 Hz, 1H).

¹³C NMR *minor diastereoisomer* (126 MHz, CDCl₃) δ 207.9 (C); 143.5 (C); 128.9 (CH); 127.1 (CH); 126.7 (CH); 118.4 (C); 46.4 (CH); 43.0 (CH); 41.1 (CH₂); 40.4 (CH₂); 34.6 (CH₂); 17.9 (CH₂).

HRMS: calculated for C₁₄H₁₅NNaO (M+Na⁺): 236.1046, found 236.1047.



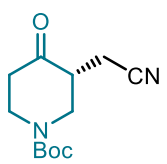
(R)-2-(8-oxo-1,4-dioxaspiro[4.5]decan-7-yl)acetonitrile (55e)

Prepared according to the general procedure using chloroacetonitrile (0.2 mmol, 13 μL), 3,3-dimethylcyclohexanone (2.0 mmol, 312 mg), catalyst **A** (0.04 mmol, 12 mg), catalyst **B** (0.04 mmol, 22 mg) and sodium acetate (0.4 mmol, 33 mg). Time of irradiation: 24 hours at 10 °C. The crude mixture was purified by flash column chromatography (hexane/EtOAc gradient from 10:1 to 1:1), concentrated and repurified by flash column chromatography (DCM/EtOAc gradient from 100:1 to 10:1) to afford product **55e** as a yellowish solid (34 mg, 87% yield, 89% *ee*). The enantiomeric excess was determined, after derivatization of the isolated ketone with *p*-toluenesulfonyl hydrazide to afford corresponding hydrazone, to be 89% by UPC² analysis on Acquity Trefoil CEL1 column: gradient from 100% CO₂ to 60:40 CO₂/*i*PrOH over 5 minutes, curve 6, flow rate 3.00 mL/min, λ = 230 nm; τ_{Major} = 4.91 min, τ_{Minor} = 5.64 min. [α]_D²⁷ = +1.2 (c = 0.54, MeOH, 89% *ee*). Absolute configuration determined in comparison to compound **55a**.

¹H NMR (400 MHz, CDCl₃) δ 4.11-4.00 (m, 4H); 3.12-2.96 (m, 1H); 2.76-2.63 (m, 2H); 2.48-2.41 (m, 1H); 2.41 (dd, *J* = 17.1, 8.0 Hz, 1H); 2.30 (ddd, *J* = 13.0, 5.8, 3.5 Hz, 1H); 2.11-1.94 (m, 2H); 1.85 (t, *J* = 13.3 Hz, 1H).

¹³C NMR (101 MHz, CDCl₃) δ 207.3 (C); 118.2 (C); 106.8 (C); 65.1 (CH₂); 64.9 (CH₂); 43.2 (CH); 40.0 (CH₂); 37.7 (CH₂); 34.7 (CH₂); 17.6 (CH₂).

HRMS: calculated for C₁₀H₁₃NNaO₃ (M+Na⁺): 218.0788, found 218.0782.



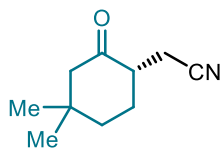
tert-butyl (R)-3-(cyanomethyl)-4-oxopiperidine-1-carboxylate (55f)

Prepared according to the general procedure using chloroacetonitrile (0.2 mmol, 13 μL), *N*-Boc-4-piperidone (2.0 mmol, 399 mg), catalyst **A** (0.04 mmol, 12 mg), catalyst **B** (0.04 mmol, 22 mg) and sodium acetate (0.4 mmol, 33 mg). Time of irradiation: 24 hours at 10 °C. The crude mixture was purified by flash column chromatography (hexane/EtOAc gradient from 8:1 to 1:1), concentrated and repurified by flash column chromatography (DCM/EtOAc gradient from 80:1 to 5:1) to afford product **55f** as a white solid (21 mg, 45% yield, 77% *ee*). The enantiomeric excess was determined to be 71% (average of two runs, 77% and 64% *e.e.*, respectively) by UPC² analysis on Acquity Trefoil CEL1 column: 95:5 CO₂/*i*PrOH, flow rate 3.00 mL/min, λ = 220 nm; τ_{Major} = 1.45 min, τ_{Minor} = 1.69 min. [α]_D²⁶ = +13.6 (c = 0.33, CHCl₃, 64% *ee*, product obtained from the parallel experiment). Absolute configuration determined in comparison to compound **55a**.

¹H NMR (500 MHz, CDCl₃) δ 4.56 (bs, 1H); 4.38 (bs, 1H); 3.20-3.07 (m, 1H); 2.90 (bs, 1H); 2.80 (dq, *J* = 12.0, 6.1 Hz, 1H); 2.67 (bs, 1H); 2.60-2.39 (m, 3H); 1.50 (s, 9H).

¹³C NMR (126 MHz, CDCl₃) δ 205.1 (C); 154.3 (C); 117.4 (C); 81.4 (C); 48.0 (CH₂); 46.1 (CH); 44.0 (CH₂); 41.0 (CH₂); 28.4 (CH₃); 15.1 (CH₂).

HRMS: calculated for C₁₂H₁₈N₂NaO₃ (M+Na⁺): 261.1210, found 261.1210.



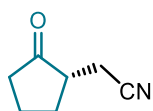
(S)-2-(4,4-dimethyl-2-oxocyclohexyl)acetonitrile (55g)

Prepared according to the general procedure using chloroacetonitrile (0.2 mmol, 13 μ L), 3,3-dimethylcyclohexanone (2.0 mmol, 0.28 mL), catalyst **A** (0.04 mmol, 12 mg), catalyst **B** (0.04 mmol, 22 mg) and sodium acetate (0.4 mmol, 33 mg). Time of irradiation: 24 hours at 10 $^{\circ}$ C. The crude mixture was purified by flash column chromatography (hexane/EtOAc gradient from 10:1 to 2:1), concentrated and repurified by flash column chromatography (DCM/EtOAc gradient from 100:1 to 40:1) to afford product **55g** as a clear oil (9 mg, 26% yield, 84% *ee*). The enantiomeric excess was determined, after derivatization of the isolated ketone with *p*-toluenesulfonyl hydrazide to afford corresponding hydrazone, to be 85% by UPC² analysis on Acquity Trefoil CEL2 column: gradient from 100% CO₂ to 60:40 CO₂/EtOH over 5 minutes, curve 6, flow rate 3.00 mL/min, λ = 230 nm; τ_{Major} = 4.88 min, τ_{Minor} = 5.07 min. $[\alpha]_D^{24}$ = 9.00 (*c* = 0.19, CHCl₃, 84% *ee*, product obtained from the parallel experiment). Absolute configuration determined in comparison to compound **55a**.

¹H NMR (500 MHz, CDCl₃) δ 2.68 (dd, *J* = 16.9, 5.0 Hz, 1H); 2.63-2.55 (m, 1H); 2.40 (dd, *J* = 16.9, 7.9 Hz, 1H); 2.31-2.23 (m, 2H); 2.19 (dd, *J* = 13.1, 2.4 Hz, 1H); 1.79-1.60 (m, 3H); 1.10 (s, 3H); 0.88 (s, 3H).

¹³C NMR (126 MHz, CDCl₃) δ 208.5 (C); 118.6 (C); 54.6 (CH₂); 46.0 (CH); 37.9 (CH₂); 37.1 (C); 32.0 (CH₃); 29.2 (CH₂); 25.1 (CH₃); 17.8 (CH₂).

HRMS: calculated for C₁₀H₁₅NNaO (M+Na⁺): 188.1046, found 188.1048.



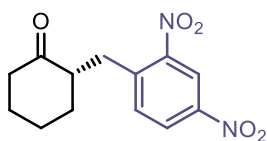
(S)-2-(2-oxocyclopentyl)acetonitrile (55h)

Prepared according to the general procedure using chloroacetonitrile (0.2 mmol, 13 μ L), cyclopentanone (2.0 mmol, 0.18 mL), catalyst **A** (0.04 mmol, 12 mg), catalyst **B** (0.04 mmol, 22 mg) and sodium acetate (0.4 mmol, 33 mg). Time of irradiation: 24 hours at 25 $^{\circ}$ C. The crude mixture was purified by flash column chromatography (hexane/EtOAc gradient from 10:1 to 1:1), concentrated and repurified by flash column chromatography (DCM/EtOAc gradient from 100:1 to 20:1) to afford product **55h** as a yellowish oil (9 mg, 35% yield, 40% *ee*). The enantiomeric excess was determined, after derivatization of the isolated ketone with *p*-toluenesulfonyl hydrazide to afford corresponding hydrazone, to be 40% by UPC² analysis on Acquity Trefoil AMY1 column: gradient from 100% CO₂ to 60:40 CO₂/EtOH over 5 minutes, curve 6, flow rate 3.00 mL/min, λ = 230 nm; τ_{Major} = 4.78 min, τ_{Minor} = 4.57 min. $[\alpha]_D^{24}$ = +78.4 (*c* = 0.14, CHCl₃, 40% *ee*). Absolute configuration determined in comparison to compound **55a**.

¹H NMR (500 MHz, CDCl₃) δ 2.75-2.70 (m, 1H); 2.50-2.35 (m, 4H); 2.25-2.08 (m, 2H); 1.96-1.82 (m, 1H); 1.81-1.67 (m, 1H).

¹³C NMR (126 MHz, CDCl₃) δ 216.2 (C); 118.0 (C); 45.5 (CH); 37.2 (CH₂); 29.0 (CH₂); 20.3 (CH₂); 17.4 (CH₂).

HRMS: calculated for C₇H₉NNaO (M+Na⁺): 146.0576, found 146.0570.



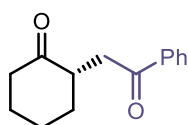
(S)-2-(2,4-dinitrobenzyl)cyclohexan-1-one (55i)

Prepared according to the general procedure using 2,4-dinitrobenzyl chloride (0.2 mmol, 43 mg), cyclohexanone (2.0 mmol, 0.21 mL), catalyst **A** (0.04 mmol, 12 mg), catalyst **B** (0.04 mmol, 22 mg) and sodium acetate (0.4 mmol, 33 mg). Time of irradiation: 24 hours at 10 $^{\circ}$ C. The crude mixture was purified by flash column chromatography (hexane/EtOAc gradient from 10:1 to 1:1), concentrated and repurified by flash column chromatography (DCM/EtOAc gradient from 100:1 to 20:1) to afford product **55i** as a yellowish solid (39

mg, 70% yield, 90% *ee*). The enantiomeric excess was determined to be 90% by UPC² analysis on Acquity Trefoil AMY1 column: gradient from 100% CO₂ to 60:40 CO₂/EtOH over 5 minutes, curve 6, flow rate 3.00 mL/min, $\lambda = 240$ nm; $\tau_{Major} = 4.15$ min, $\tau_{Minor} = 4.37$ min. $[\alpha]_D^{25} = -64.7$ ($c = 0.35$, CHCl₃, 90% *ee*). Absolute configuration determined in comparison to the data reported in the literature.⁸³

¹H NMR (500 MHz, CDCl₃) δ 8.76 (d, $J = 2.3$ Hz, 1H); 8.33 (dd, $J = 8.5, 2.4$ Hz, 1H); 7.77 (d, $J = 8.5$ Hz, 1H); 3.51 (dd, $J = 13.6, 7.6$ Hz, 1H); 2.85 (dd, $J = 13.6, 5.1$ Hz, 1H); 2.72 (dtd, $J = 11.9, 7.6, 5.4, 1.1$ Hz, 1H); 2.45-2.37 (m, 1H); 2.29 (tdd, $J = 13.4, 6.1, 1.2$ Hz, 1H); 2.18 (ddq, $J = 13.1, 5.9, 3.0$ Hz, 1H); 2.14-2.08 (m, 1H); 1.98-1.86 (m, 1H); 1.75-1.61 (m, 2H); 1.52 (qd, $J = 12.7, 3.7$ Hz, 1H).

¹³C NMR (126 MHz, CDCl₃) δ 211.2 (C); 149.5 (C); 146.5 (C); 143.1 (C); 135.1 (CH); 126.7 (CH); 120.4 (CH); 51.8 (CH); 42.4 (CH₂); 35.1 (CH₂); 33.2 (CH₂); 28.2 (CH₂); 25.5 (CH₂).



(S)-2-(2-oxo-2-phenylethyl)cyclohexan-1-one (55j)

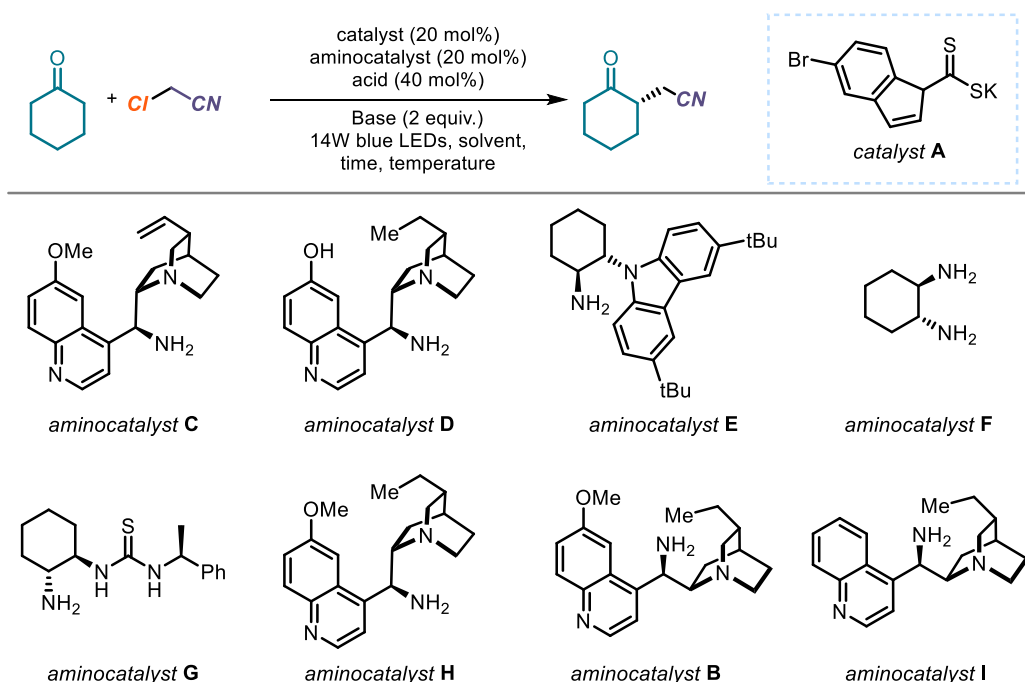
Prepared according to the general procedure using 2-chloroacetophenone (0.2 mmol, 31 mg), cyclohexanone (2.0 mmol, 0.21 mL), catalyst **A** (0.04 mmol, 12 mg), catalyst **B** (0.04 mmol, 22 mg) and sodium acetate (0.4 mmol, 33 mg). Time of irradiation: 24 hours at 10°C. The crude mixture was purified by flash column chromatography (hexane/EtOAc gradient from 10:1 to 4:1), concentrated and repurified by flash column chromatography (DCM/EtOAc gradient from 100:1 to 60:1) to afford product **55j** as a white solid (18 mg, 41% yield, 95% *ee*). The enantiomeric excess was determined to be 95% by UPC² analysis on Daicel Chiralpak IC column: gradient from 100% CO₂ to 60:40 CO₂/MeOH over 5 minutes, curve 6, flow rate 3.00 mL/min, $\lambda = 240$ nm; $\tau_{Major} = 2.55$ min, $\tau_{Minor} = 2.69$ min. $[\alpha]_D^{24} = -67.2$ ($c = 0.21$, CHCl₃, 94% *ee*, product obtained from the parallel experiment). Absolute configuration determined in comparison to the data reported in the literature.⁵⁰

¹H NMR (500 MHz, CDCl₃) δ 8.01-7.94 (m, 2H); 7.58-7.53 (m, 1H); 7.50-7.42 (m, 2H); 3.60 (dd, $J = 17.7, 6.6$ Hz, 1H); 3.17 (dq, $J = 12.2, 6.0$ Hz, 1H); 2.68 (dd, $J = 17.7, 5.7$ Hz, 1H); 2.48-2.38 (m, 2H); 2.24-2.17 (m, 1H); 2.17-2.08 (m, 1H); 1.93-1.86 (m, 1H); 1.78 (qt, $J = 13.1, 3.5$ Hz, 1H); 1.73-1.60 (m, 1H); 1.45 (qd, $J = 12.9, 3.8$ Hz, 1H).

¹³C NMR (126 MHz, CDCl₃) δ 211.6 (C); 198.8 (C); 137.2 (C); 133.1 (CH); 128.7 (CH); 128.2 (CH); 46.6 (CH); 42.1 (CH₂); 38.5 (CH₂); 34.5 (CH₂); 28.1 (CH₂); 25.5 (CH₂).

⁸³ Arceo, E., Bahamonde, A.; Bergonzini, G.; Melchiorre, P. "Enantioselective direct α -alkylation of cyclic ketones by means of photo-organocatalysis" *Chem. Sci.* **2014**, *5*, 2438-2442.

2.8.9.3 Optimization studies



entry	Amino-catalyst	acid	base	solvent	temperature	time	yield ^a	<i>e.e.</i> ^b
1	C	TFA	NaOAc	toluene	30-35 °C	16 h	43%	77%
2	C	TFA	NaOAc	toluene	30-35 °C	16 h	0% ^c	
3	C	TFA	NaOAc	toluene	30-35°C	16 h	7% ^d	
4	C	TFA	NaOAc	MTBE	30-35°C	16 h	5%	-
5	C	TFA	NaOAc	DCM	30-35°C	16 h	traces	-
6	C	TFA	NaOAc	MeCN	30-35°C	16 h	10%	-
7	C	TFA	NaOAc	PhCl	30-35°C	16 h	37%	-
8	C	TFA	NaOAc	PhCF ₃	30-35°C	15 h	31%	-
9	C	BA	NaOAc	toluene	30-35°C	16 h	23%	-
10	C	<i>p</i> -NO ₂ BA	NaOAc	toluene	30-35°C	16 h	15%	-
11	C	<i>p</i> -CF ₃ BA	NaOAc	toluene	30-35°C	16 h	10%	-
12	C	MsOH	NaOAc	toluene	30-35°C	22 h	23%	-
13	C	TsOH	NaOAc	toluene	30-35°C	22 h	29%	-
14	C	-	NaOAc	toluene	30-35°C	16 h	traces	-
15	C	TFA (20%)	NaOAc	toluene	30-35°C	16 h	7%	-
16	C	TFA (60%)	NaOAc	toluene	30-35°C	16 h	22%	-
17	C	TFA (80%)	NaOAc	toluene	30-35°C	16 h	15%	-
18	C	TFA	lutidine	toluene	30-35°C	15 h	5%	-
19	C	TFA	NaHCO ₃	toluene	30-35°C	23 h	25%	-
20	C	TFA	K ₂ CO ₃	toluene	30-35°C	23 h	traces	-
21	C	TFA	-	toluene	30-35°C	16 h	traces	-

22	D	TFA	NaOAc	toluene	30-35°C	16 h	23%	80%
23	E	BA (20%)	NaOAc	toluene	30-35°C	16 h	traces	-
24	F	TFA	NaOAc	toluene	30-35°C	19 h	13%	-
25	G	TFA	NaOAc	toluene	30-35°C	15 h	29%	-
26	C	TFA	NaOAc	toluene	30-35°C	15 h	56% ^e	73%
27	H	TFA	NaOAc	toluene	30-35°C	15 h	74%	73%
28	B	TFA	NaOAc	toluene	30-35°C	15 h	64%	-81%
29	I	TFA	NaOAc	toluene	30-35°C	15 h	47%	-71%
30	H	TFA	NaOAc	toluene	30-35°C	15 h	81% ^e	78%
31	H	TFA	NaOAc	toluene	10°C	15 h	60%	86%
32	H	TFA	NaOAc	toluene	0°C	15 h	49% ^e	90%
33	H	TFA	NaOAc	toluene	10°C	15 h	80% ^e	88%
34	H	TFA	NaOAc	toluene	20°C	15 h	81% ^e	84%
35	H	TFA	NaOAc	toluene	10°C	24 h	83% ^e	87%
36	B	TFA	NaOAc	toluene	10°C	15 h	75% ^e	-91%
37	B	TFA	NaOAc	toluene	10°C	24 h	82% ^e	-91%

Table S6. Optimization studies for the asymmetric α -alkylation of ketones. Reactions performed on a 0.2 mmol scale, using 4 equivalents of cyclohexanone and 2 equivalents of base in 1 mL of solvent; a) yield determined on the crude mixture by ¹H NMR or GC analysis using 1,3,5-trimethoxybenzene as an internal standard; b) Enantiomeric excess determined on the corresponding hydrazone by chiral UPC²; c) Reaction performed without light; d) 5W 460nm LED was used as a light source; e) using 10 equivalents of cyclohexanone.

Chapter III

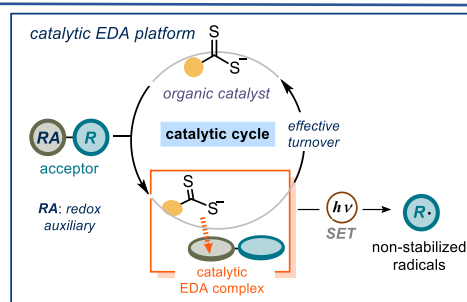
A General Organocatalytic System for Electron Donor–Acceptor Complex Photoactivation and its Use in Radical Processes

Target

To develop a catalytic electron donor-acceptor (EDA) complex platform, based on the use of dithiocarbamates as catalytic donors, for the activation of a wide variety of electron-poor radical precursors.

Tool

Exploiting the electronic features of dithiocarbamates and xanthates, and their potential as catalytic donors in EDA complex photochemistry for the generation of carbon-centered radicals.¹



3.1 Introduction

As discussed in Chapter 2, our research laboratory has used dithiocarbamate and xanthate anions as nucleophilic organocatalysts for the photochemical generation of radicals from commercially available alkyl(pseudo) halides.² Central to this catalytic platform was the ability of the organocatalyst to trigger an S_N2 reaction with simple C(sp³) alkyl electrophiles and form a photoactive intermediate **I** (Figure 3.1a); upon light excitation, radicals were generated and engaged in a range of transformations.³ Besides developing synthetically useful processes, detailed investigations were performed to understand the mechanism of catalyst turnover and to define the limitations of this catalytic platform. Regarding catalyst turnover, we found that the sulphur-centered radical **II**, which is formed upon photo-mediated homolytic cleavage of the weak C–S bond within intermediate **I**, could dimerize to form the stable intermediate **III**.^{3c,d} Dimer **III**, which can absorb in the visible region, is in a light-controlled equilibrium with the progenitor **II**. This dimerization manifold effectively extends the lifetime of radical **II**,⁴ which acquires a persistent character, thereby enabling an effective catalyst turnover. Furthermore, we showed that the sulphur-

¹ The project discussed in this chapter was conducted in collaboration with Dr. Eduardo de Pedro Beato and Wei Zhou. I was mainly involved in the design, optimization, and scope evaluation of the alkylation of enol ethers in a two and three-component approach and the development of the trifluoromethylation procedure. I also performed most of the mechanistic studies. This work has been published, see: De Pedro Beato, E.; Spinnato, D.; Zhou, W.; Melchiorre, P. "A General Organocatalytic System for Electron Donor–Acceptor Complex Photoactivation and Its Use in Radical Processes" *J. Am. Chem. Soc.* **2021**, *143*, 12304–12314.

² Schweitzer-Chaput, B.; Horwitz, M. A.; de Pedro Beato, E.; Melchiorre, P. "Photochemical generation of radicals from alkyl electrophiles using a nucleophilic organic catalyst" *Nat. Chem.* **2019**, *11*, 129–135.

³ (a) Mazzarella, D.; Magagnano, G.; Schweitzer-Chaput, B.; Melchiorre, P. "Photochemical Organocatalytic Borylation of Alkyl Chlorides, Bromides, and Sulfonates" *ACS Catal.* **2019**, *9*, 5876–5880. (b) Cuadros, S.; Horwitz, M. A.; Schweitzer-Chaput, B.; Melchiorre, P. "A visible-light mediated three-component radical process using dithiocarbamate anion catalysis" *Chem. Sci.* **2019**, *10*, 5484–5488. (c) Spinnato D.; Schweitzer-Chaput B.; Goti G.; M. Ošek; Melchiorre P. "A Photochemical Organocatalytic Strategy for the α -Alkylation of Ketones by using Radicals" *Angew. Chem. Int. Ed.* **2020**, *59*, 9485–9490. (d) de Pedro Beato, E.; Mazzarella, D.; Balletti, M.; Melchiorre, P. "Photochemical generation of acyl and carbamoyl radicals using a nucleophilic organic catalyst: applications and mechanism thereof" *Chem. Sci.* **2020**, *11*, 6312–6324. (e) Balletti, M.; Marcantonio, E.; Melchiorre, P. "Photochemical organocatalytic enantioselective radical γ -functionalization of α -branched enals" DOI: 10.1039/D2CC01638A.

⁴ (a) Leifert, D.; Studer, A. "The Persistent Radical Effect in Organic Synthesis" *Angew. Chem. Int. Ed.* **2020**, *59*, 74–108. (b) Frenette, M.; Aliaga, C.; Font-Sanchis, E.; Scaiano, J. C. "Bond Dissociation Energies for Radical Dimers Derived from Highly Stabilized Carbon-Centered Radicals" *Org. Lett.* **2004**, *6*, 2579–2582.

centered radical **II** can use two different mechanisms for turnover, since it can be reduced back to its catalytic active form in two ways: *i*) via single-electron transfer (SET) from an open-shell intermediate of the catalytic cycle; *ii*) via hydrogen atom transfer (HAT) from an external hydrogen atom donor, such as γ -terpinene.

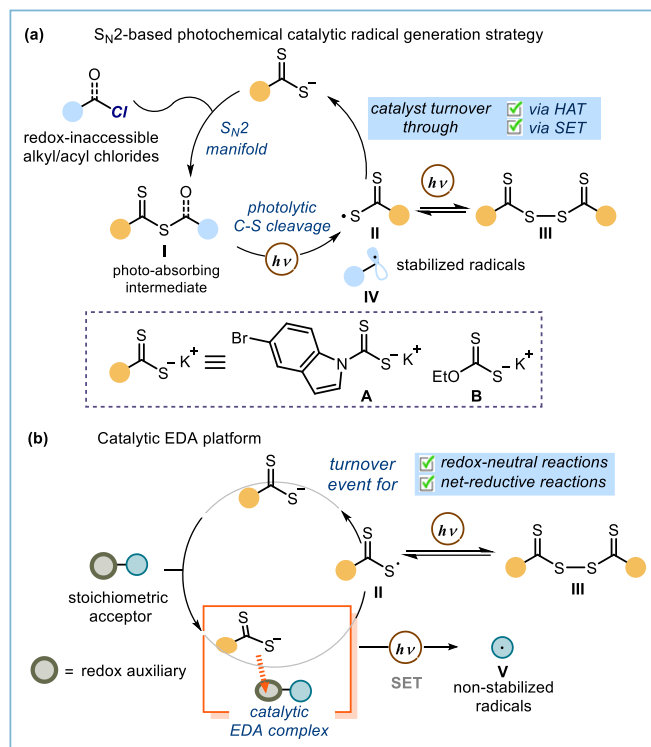


Figure 3.1. Dithiocarbamates as organocatalysts for radical generation: (a) S_N2 -based mechanism; (b) catalytic EDA platform.

Based on this knowledge, we wondered whether it would be possible to develop an alternative organocatalytic system based on dithiocarbamates (**A** or **B**, Figure 3.1a), which could overcome the main limitation found in our previous approach: namely, the inability to generate non-stabilized radicals. We surmised that the localized electron-density on the dithiocarbamate or xanthate anion's sulphur atom could offer an alternative catalytic pathway for radical generation where the organocatalyst acted as an electron donor (**D**). Upon association with electron-poor radical precursors (**A**), a photo-active electron donor-acceptor (EDA) complex would be generated that, upon excitation, would generate the target radical **V**.⁵ In this scenario, the generation of radicals would not be dependent on the electrophilic character of the radical precursor nor on the bond dissociation energy of the C-S bond within **I**, but only on the ability of the catalyst to engage the radical precursor in productive EDA complex formation (Figure 3.1b). This catalytic strategy could therefore offer a way to access non-stabilized radicals.

In this chapter, our efforts to develop a catalytic EDA complex strategy that exploits dithiocarbamate anions as catalytic donors is discussed. The following section offers an overview of radical generation methods based on the photoexcitation of EDA complexes.

⁵ Crisenza, G. E. M.; Mazzearella, D.; Melchiorre, P. "Synthetic Methods Driven by the Photoactivity of Electron Donor-Acceptor Complexes" *J. Am. Chem. Soc.* **2020**, *142*, 5461-5476.

3.2 Electron donor-acceptor complexes

The last decade has witnessed the flourishing of new mild and efficient radical generation strategies, mostly based on photoredox and electrochemical processes.⁶ This has resulted in the increased use of radical reactivity in organic synthesis.⁷ The majority of methods for making radicals rely on the use of precious transition metal-based photocatalysts. Organic dyes have been extensively investigated as potentially advantageous replacements for typical rare metal-based photocatalysts (such as Ru and Ir).⁸ A different approach obviates the need for any photocatalyst: it is based on the ground-state formation of photoactive EDA complexes. An EDA complex is a new ground-state complex generally formed by the association of an electron-rich species with an electron-poor one (Figure 3.2). This new chemical entity possesses unique physical properties derived from new molecular orbitals (Ψ_{GS} and Ψ_{ES}) generated through the hybridization of the frontier orbitals of the two partners: the highest occupied molecular orbital (HOMO) of the *donor* (**D**), and the lowest unoccupied molecular orbital (LUMO) of the *acceptor* (**A**).^{5, 9} Occasionally, photoexcitation of this new chemical entity promotes an SET from the electron-rich species (donor) to the electron-poor (acceptor). This SET delivers a radical ion pair that can then undergo chemical transformations to furnish the desired radical used for the forgery of new covalent bonds.

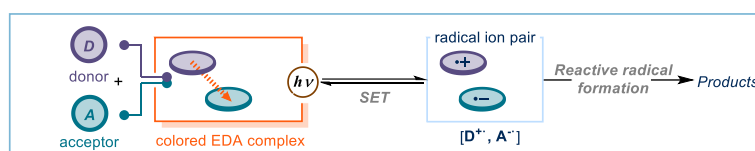


Figure 3.2. Radical formation promoted by photoactive EDA complex.

The first observation of an EDA complex dates back to 1909, when Hildebrand and Glascock observed that iodine-containing solutions possessed different spectroscopic features depending on the solvent system used.¹⁰ Forty years later, Hildebrand concluded that a ground-state association between one molecule of iodine and one molecule of benzene (or mesitylene) was responsible for the observed color change in those solvents.¹¹ It was proposed that the Lewis basicity of the aromatic partner and the relative Lewis acidity of iodine promoted this association. Later on, Mulliken rationalized the formation of these complexes using the principles of quantum mechanics.¹² Specifically, the association of an electron-rich substance characterized by a high-in-energy HOMO (the donor) and an electron-poor molecule with a low-in-energy

⁶ For reviews on photoredox radical generation strategies see: a) Shaw, M. H.; Twilton, J.; MacMillan, D. W. C. "Photoredox Catalysis in Organic Chemistry" *J. Org. Chem.* **2016**, *81*, 6808–6926. b) Romero, N.; Nicewicz, D. "Organic Photoredox Catalysis" *Chem. Rev.* **2016**, *116*, 10075–10166. c) Matsui, J. K.; Lang, S. B.; Heitz, D. R.; Molander, G. A. "Photoredox-mediated routes to radicals: the value of catalytic radical generation in synthetic methods development" *ACS Catal.* **2017**, *7*, 2563–2575. For a review on electrochemical radical generation strategies see: d) Kingston, C.; Palkowitz, M. D.; Takahira, Y.; Vantourout, J. C.; Peters, B. K.; Kawamata, Y.; Baran, P. S. A Survival Guide for the "Electro-curious". *Acc. Chem. Res.* **2020**, *53*, 72–83.

⁷ (a) Blakemore, D. C.; Castro, L.; Churcher, I.; Rees, D. C.; Thomas, A. W.; Wilson, D. M.; Wood, A. "Organic synthesis provides opportunities to transform drug discovery" *Nat. Chem.* **2018**, *10*, 383–394. (b) Douglas, J. J.; Sevrin, M. J.; Stephenson, C. R. J. "Visible Light Photocatalysis: Applications and New Disconnections in the Synthesis of Pharmaceutical Agents" *Organic Process Research & Development* **2016**, *20*, 1134–1147. (c) Sambiagio, C.; Noël, T. "Flow Photochemistry: Shine Some Light on Those Tubes!" *Trends in Chemistry* **2020**, *2*, 92–106.

⁸ Vega-Penalzo, A.; Mateos, J.; Company, X.; Escudero-Casao, M.; Dell'Amico, L. "A Rational Approach to Organo-Photocatalysis: Novel Designs and Structure-Property Relationships" *Angew. Chem. Int. Ed.* **2021**, *60*, 1082–1097.

⁹ Lima, C. G. S.; de M. Lima, T.; Duarte, M.; Jurberg, I. D.; Paixão, M. W. "Organic Synthesis Enabled by Light-Irradiation of EDA Complexes: Theoretical Background and Synthetic Applications" *ACS Catalysis* **2016**, *6*, 1389–1407.

¹⁰ Hildebrand, J. H.; Glascock, B. L. "The Color of Iodine Solutions" *J. Am. Chem. Soc.* **1909**, *31*, 26–31.

¹¹ Benesi, H. A.; Hildebrand, J. H. "A Spectrophotometric Investigation of the Interaction of Iodine with Aromatic Hydrocarbons" *J. Am. Chem. Soc.* **1949**, *71*, 2703–2707.

¹² (a) Mulliken, R. S. "Structures of Complexes Formed by Halogen Molecules with Aromatic and with Oxygenated Solvents" *J. Am. Chem. Soc.* **1950**, *72*, 600–608. (b) Mulliken, R. S. "Molecular Compounds and their Spectra. II" *J. Am. Chem. Soc.* **1952**, *74*, 811–824. (c) Mulliken, R. S. "Molecular Compounds and their Spectra. III. The Interaction of Electron Donors and Acceptors" *J. Phys. Chem.* **1952**, *56*, 801–822.

LUMO (the acceptor) can deliver a new complex in the ground state. When the frontier orbitals of the two partners possess similar energy and symmetry, the association is promoted through rehybridization of the molecular frontier orbitals, generating a new chemical entity with singular chemical and physical properties (Figure 3.3). The new electronic distribution is described by Ψ_{GS} and Ψ_{ES} (Ψ = wave-function, associated with ground and excited states) and the energy difference between the two states can be spectroscopically observed by the appearance of a new charge-transfer band in the absorption spectrum ($h\nu_{CT}$), corresponding to the $\Psi_{GS} \rightarrow \Psi_{ES}$ electronic transition (Figure 3.3b). Usually, the energy gap between Ψ_{GS} and Ψ_{ES} lies within the visible light region. Upon light-promoted excitation of the EDA complex (orange box in Figure 3.3a), the Ψ_{ES} is populated, which promotes an SET from **D** to **A** to generate a radical ion pair (Figure 3.3a light blue box).

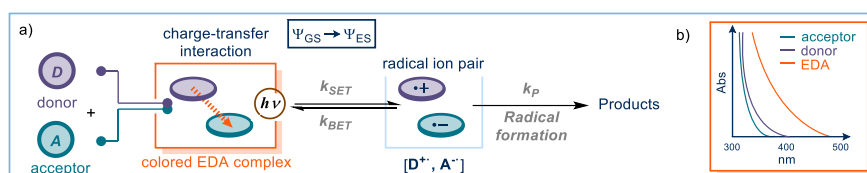


Figure 3.3. a) General scheme of EDA complex activation. b) Uv-Vis analysis of an EDA complex.

3.2.1 Synthetic applications of stoichiometric EDA complexes

Beside few seminal studies in the 20th century, the use of photoactive EDA complexes in organic synthesis has been limited until recently.⁵ This was probably linked to the reversible nature of the SET event that hampers the formation of the reactive open-shell intermediates.^{5,13} In particular, when the back-electron transfer (BET) from the radical ion pair (Figure 3.4, light blue box) is kinetically favored (faster than the formation of the desired radicals), productive photoactivation of the EDA complex cannot be realized. However, if a leaving group (LG) is present within the acceptor's scaffold, an irreversible fragmentation event occurs. In this way, the unfavorable equilibrium between SET and BET is bypassed and the irreversible fragmentation drives the formation of a radical **R**[•], which can then engage in synthetic processes (Figure 3.4).

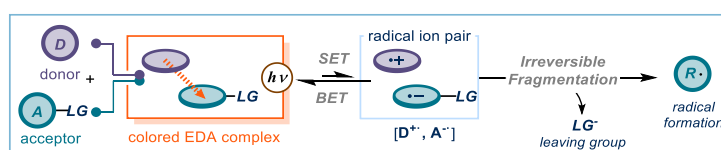


Figure 3.1. Exploitation of acceptors containing a leaving group in EDA complex chemistry.

In 1987, Kornblum observed that, when mixing a solution of colorless *p*-nitrocumyl chloride **1** with colorless quinuclidine **2**, an orange-yellow solution was produced immediately.¹⁴ Spectroscopic analysis showed the formation of a new charge-transfer band, suggesting the formation of an EDA aggregate as responsible for the observed color change. When the colored EDA complex (Figure 3.2, orange box) was excited by light irradiation, an SET between the partners occurred. The fast and irreversible fragmentation obviated the BET process, delivering benzyl radical **VIII**. The open-shell species **VIII** was then intercepted by another molecule of quinuclidine **2**, which was present in significantly higher concentration than **VII**,

¹³ Rathore, R.; Kochi, J. K. "Donor/Acceptor Organizations and the Electron-Transfer Paradigm for Organic Reactivity" *Adv. Phys. Org. Chem.* **2000**, *35*, 193–318.

¹⁴ Wade, P. A.; Morrison, H. A.; Kornblum, N. "The Effect of Light on Electron-Transfer Substitution at a Saturated Carbon Atom" *J. Org. Chem.* **1987**, *52*, 3102–3107.

forming the C-N bond within **IX** (Figure 3.2). Finally, a second molecule of **1** was reduced by **IX** to form the coupling product **4** and propagate the chain process by generating another molecule of benzyl radical **VIII**. Under these conditions, the photo-excitation of the EDA aggregate initiated an efficient radical chain process. The quantum yield for the overall process was determined to be higher than 1, proving the chain-based nature of the transformation.

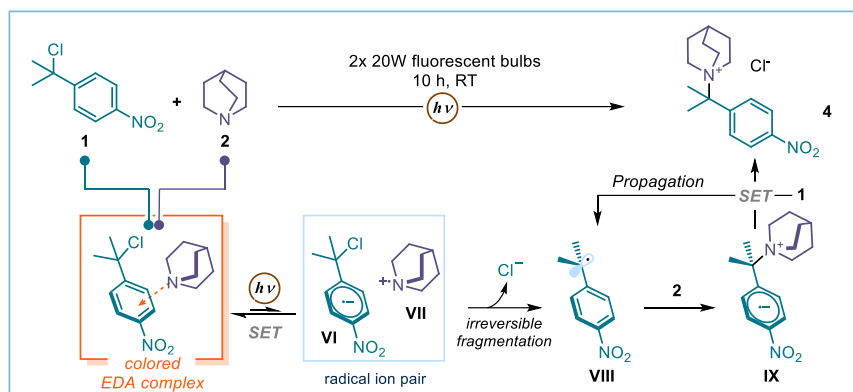


Figure 3.2. Reaction promoted by a photo-active EDA complex in a stoichiometric regime.

Despite few key studies in the 1970's and 1980's,¹⁵ the synthetic potential of EDA complex photoactivation was not been fully realized. More than twenty years later, the renaissance of EDA complex photochemistry took place. While developing a photoredox protocol for the arylation of heteroaromatics with iodonium salts (**6**) as radical precursors (Figure 3.6), Chatani and co-workers observed that, when electron-rich pyrroles (**5**) were employed as substrates, the reaction mixture turned orange. It turned out that product formation was not dependent on the presence of an external photocatalyst.¹⁶ Indeed, simple visible light irradiation was enough to trigger the desired arylation reaction. The striking change in color upon mixing the two reactants and the observed reactivity prompted the authors to perform spectroscopic analysis of the reaction mixture. The UV-vis absorption spectrum of a mixture of the pyrrole **5** and iodonium salt **6** showed a new charge-transfer band, which provided evidence that the observed reactivity was promoted by the formation of an EDA complex. Photo-activation of the colored EDA aggregate (Figure 3.6, orange box), followed by irreversible extrusion of aryl iodide, promoted the formation of the reactive radicals **X** and **XI**, which, upon radical-radical cross-coupling and deprotonation, delivered the arylated product **7** in high yields.^{16,5}

¹⁵ (a) Cantacuzene, D.; Wakselman, C.; Dorme, R. "Condensation of Perfluoroalkyl Iodides with Unsaturated Nitrogen Compounds" *J. Chem. Soc., Perkin Trans. 1* **1977**, 1365–1371. (b) Russell, G. A.; Wang, K. "Homolytic Alkylation of Enamines by Electrophilic Radicals" *J. Org. Chem.* **1991**, *56*, 3475–3479. (c) Bunnett, J. F. "Aromatic Substitution by the $S_{RN}1$ Mechanism" *Acc. Chem. Res.* **1978**, *11*, 413–420. (d) Sankararaman, S.; Haney, W. A.; Kochi, J. K. "Annihilation of Aromatic Cation Radicals by Ion-Pair and Radical-Pair Collapse. Unusual Solvent and Salt Effects in the Competition for Aromatic Substitution" *J. Am. Chem. Soc.* **1987**, *109*, 7824–7838. (e) Fukuzumi, S.; Mochida, K.; Kochi, J. K. "A Unified Mechanism for Thermal and Photochemical Activation of Charge-Transfer Processes with Organometals. Steric Effects in the Insertion of Tetracyanoethylene" *J. Am. Chem. Soc.* **1979**, *101*, 5961–5972. (f) Gotoh, T.; Padias, A. B.; Hall, J. H. K. "An Electron Donor/Acceptor Complex and Thermal Triplex as Intermediates in the Cycloaddition Reaction of N-Vinylcarbazole with Dimethyl 2,2-Dicyanoethylene-1,1-dicarboxylate" *J. Am. Chem. Soc.* **1991**, *113*, 1308–1312. (g) Fox, M. A.; Younathan, J.; Fryxell, G. E. "Photoinitiation of the $S_{RN}1$ Reaction by Excitation of Charge-Transfer Complexes" *J. Org. Chem.* **1983**, *48*, 3109–3112. ¹⁶ Tobisu, M.; Furukawa, T.; Chatani, N. "Visible Light-mediated Direct Arylation of Arenes and Heteroarenes Using Diaryliodonium Salts in the Presence and Absence of a Photocatalyst" *Chem. Lett.* **2013**, *42*, 1203–1205.

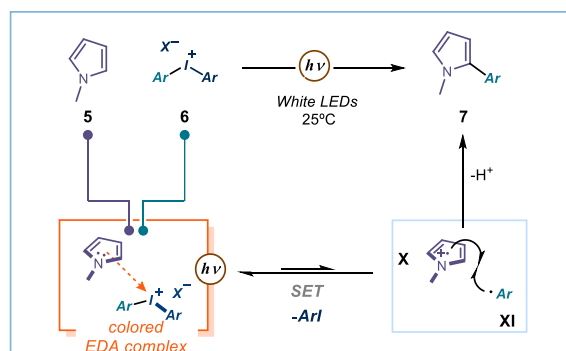


Figure 3.6. Arylation of electron-rich heteroaromatics driven by stoichiometric EDA complex activation.

In 2019, Yang and co-workers developed a catalyst-free methodology for the synthesis of S-aryl dithiocarbamates which was promoted by a photoactive EDA complex activation manifold (Figure 3.7).¹⁷ Specifically, light irradiation of a mixture of aryl iodide **8** (the acceptor) and dithiocarbamate **9** (the donor) and promoted a single electron transfer from the electron-rich dithiocarbamate anion to the electron-accepting aryl iodide, delivering a radical ion pair (Figure 3.7, light blue box). Irreversible fragmentation of the iodide drove the formation of the aryl radical **XII** which coupled with **XIII** delivering the desired cross-coupling product **10**.

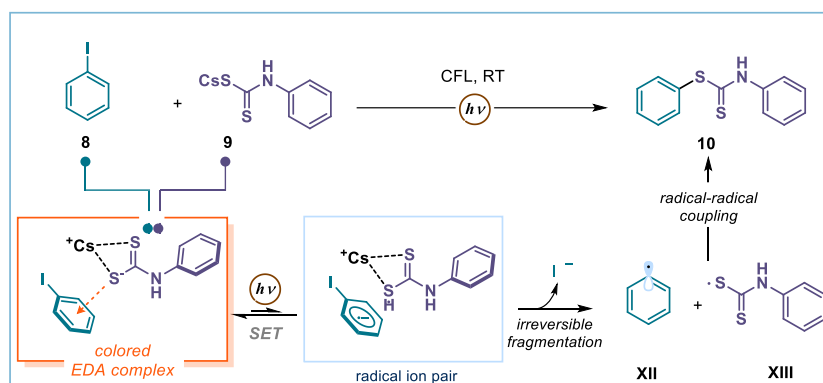


Figure 3.7. Synthesis of aryl dithiocarbamate via stoichiometric EDA complex activation.

This report represented the first approach in which a dithiocarbamate anion participated in an EDA complex-mediated radical transformation.

3.2.2 EDA complex with substoichiometric amount of donors

Simultaneously to Chatani's discovery, our group was investigating the organocatalytic enantioselective α -alkylation of aldehydes **11** with electron-deficient alkyl bromides **12** as electrophiles (Figure 3.7).¹⁸ The transformation was previously reported to require a photocatalyst to generate the desired carbon-centered radical **XVII** from **12**.¹⁹ However, control experiments confirmed that, when using the organic catalyst **13**, the photocatalyst was not needed to trigger the transformation. Importantly, the desired product **14** was not observed in the dark, suggesting that a photo-active specie was responsible for the observed reactivity.

¹⁷ Li, G.; Yan, Q.; Gan, Z.; Li, Q.; Dou, X.; Yang, D. "Photocatalyst-Free Visible-Light-Promoted C(sp²)-S Coupling: A Strategy for the Preparation of S-Aryl Dithiocarbamates" *Org. Lett.* **2019**, *21*, 7938–7942.

¹⁸ Arceo, E.; Jurberg, I. D.; Álvarez-Fernandez, A.; Melchiorre, P. "Photochemical activity of a key donor-acceptor complex can drive stereoselective catalytic α -alkylation of aldehydes" *Nat. Chem.* **2013**, *5*, 750–756.

¹⁹ Nicewicz, D. A.; MacMillan, D. W. C. "Merging Photoredox Catalysis with Organocatalysis: The Direct Asymmetric Alkylation of Aldehydes" *Science* **2008**, *322*, 77–80.

Mechanistic studies revealed the ability of the electron-rich enamine intermediate **XIV** to form a colored EDA complex with electron-deficient bromides **12**. Visible-light excitation of the EDA complex promoted an SET from the donor **XIV** to the acceptor **12**, delivering a radical ion pair (Figure 3.8, light blue box). The irreversible extrusion of bromide prevents the unproductive BET while leading to a benzylic radical **XVII**. By measuring the quantum yield of the reaction (which was major than 1), it was established that the reaction proceeded through a radical chain mechanism, in which the photoactive EDA aggregate acted as an initiator to generate the initial radical.²⁰ The efficient propagation step relied on the strong reducing ability of α -amino radical **XIX**.²¹ Indeed, when the benzyl radical **XVII** reacted with the ground-state enamine **XVIII**, the α -amino radical intermediate **XIX** that was formed could reduce substrate **12**, propagating the chain by formation of radical **XVII** while delivering the enantioenriched product **14**.

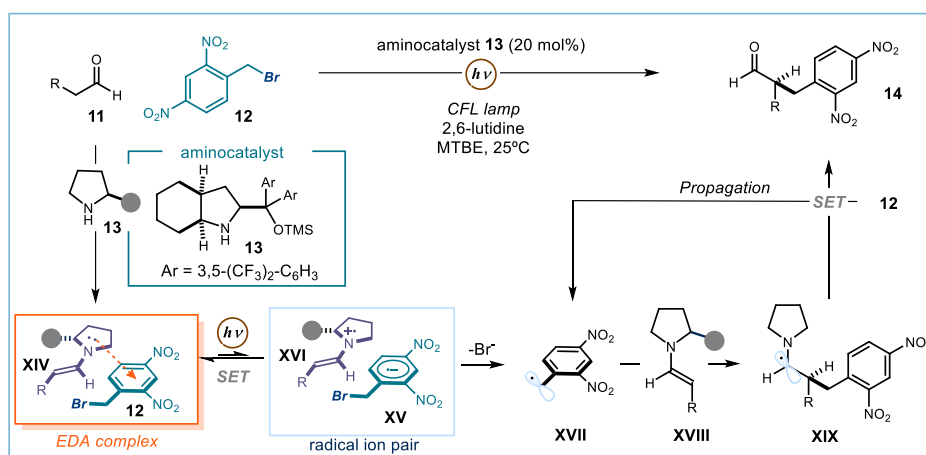


Figure 3.8. Enantioselective alkylation of aldehydes initiated by a visible-light absorbing enamine-based EDA complex.

This was the first report where the ability of *catalytically* formed chiral *donor* species, such as enamines **XIV**, participated in a transformation governed by a photoactive EDA complex, enabling stereoselective transformations through open-shell intermediates without the need of a photoredox system.²² Since that report, several asymmetric organocatalytic transformations, in which a chiral catalytic intermediate acted as an EDA complex *donor*, were developed. For example, a catalytic phase-transfer approach was developed for the EDA complex-mediated enantioselective perfluoroalkylation of β -ketoesters where a chiral enolate acted as catalytic entity.²³

3.2.3 EDA complex chemistry using sacrificial donors and redox auxiliaries

The methodologies described up to this point function to ultimately couple the two substrates involved in the EDA aggregate. Therefore, the need for highly polarized reagents with donor and acceptor properties is somehow restricting the applicability of this approach.⁵ In order to overcome this limitation, two different approaches have been purposely designed: *i*) the employment of a sacrificial donor (**SD**), able to elicit the formation of a photoactive EDA complex upon aggregation with an electron-poor substrate (Figure 3.9a);

²⁰ Bahamonde, A.; Melchiorre, P. Mechanism of the Stereoselective α -Alkylation of Aldehydes Driven by the Photochemical Activity of Enamines. *J. Am. Chem. Soc.* **2016**, *138*, 8019–8030.

²¹ Alvarez, E. M.; Karl, T.; Berger, F.; Torkowski, L.; Ritter, T. "Late-Stage Heteroarylation of Hetero(aryl)sulfonium Salts Activated by α -Amino Alkyl Radicals" *Angew. Chem. Int. Ed.* **2021**, *60*, 13609–13613.

²² Silvi, M.; Melchiorre, P. Enhancing the potential of enantioselective organocatalysis with light. *Nature* **2018**, *554*, 41–49.

²³ Woźniak, Ł.; Murphy, J. J.; Melchiorre, P. Photo-organocatalytic Enantioselective Perfluoroalkylation of β -Ketoesters. *J. Am. Chem. Soc.* **2015**, *137*, 5678–5681.

ii) the installation of a redox-auxiliary within the substrate, which can act as an electron acceptor unit that is ultimately lost upon fragmentation (Figure 3.9b).

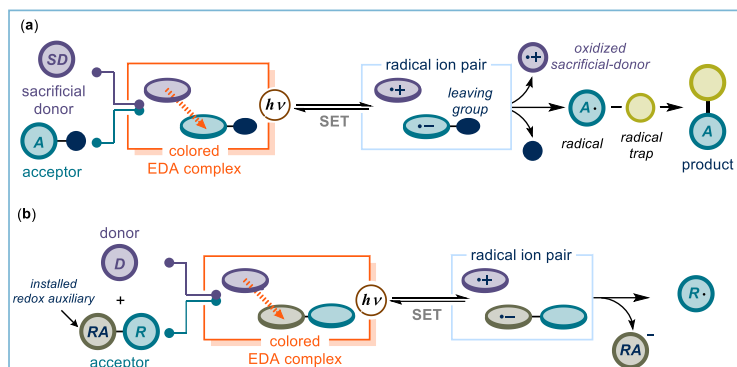


Figure 3.9. a) Sacrificial donor in EDA complex. b) Redox auxiliaries in EDA chemistry.

In the first strategy (Figure 3.9a), upon aggregation of an electron-poor substrate with stoichiometric amounts of an electron-rich sacrificial donor **SD**, irradiation with visible light triggers a single-electron transfer (SET) from the **SD** to the substrate, promoting the formation of a radical ion pair. After *mesolysis* (heterolytic cleavage leading to a radical and an ionic species), a radical intermediate is generated which can then react with an external radical trap. One example of this strategy was developed by Yu and co-workers, who used stoichiometric amounts of secondary amines **15** as a sacrificial donor to form an EDA complex with perfluoroalkyl iodides **16**.²⁴ Visible light irradiation triggered the formation of perfluoroalkyl radicals **XX**, which added on isocyanide **17**, delivering radical **XXI**. The ensuing intermediate **XXI** promoted a cyclization to afford radical **XXII**, which abstracted an iodine from **16** to form the quinoxaline product **18** while propagating a chain reaction through generation of a second equivalent of **XX**.

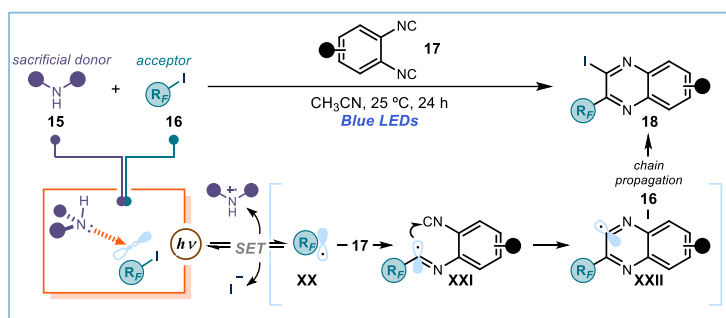


Figure 3.10. Sacrificial donor-based EDA in radical cyclization.

This approach demonstrated the potential of EDA complex-based photochemistry to provide a more general activation mode, since the donor did not form part of the final product. Yet, in this scenario, the formation of the EDA complex still required specific electronic properties of the substrates. For example, in the radical-based cyclization presented in Figure 3.10, it was the electron-poor nature of the perfluoroalkyl iodide **16** that ensured EDA complex formation, while the iodide acted only as a leaving group. As a

²⁴ Sun, X.; Wang, W.; Li, Y.; Ma, J.; Yu, S. "Halogen-Bond-Promoted Double Radical Isocyanide Insertion under Visible-Light Irradiation: Synthesis of 2-Fluoroalkylated Quinoxalines" *Org. Lett.* **2016**, *18*, 4638–4641.

limitation, the “philicity”²⁵ of the radical that could be generated by this approach is restricted to highly electrophilic open-shell species, such as perfluoroalkyl radicals **XX**.

The second strategy developed to increase the synthetic importance of EDA photochemistry was to install a redox auxiliary into one of the EDA partners (Figure 3.9b). The auxiliary had two functions: firstly, unique steric and electronic properties could be implemented to permit more favorable EDA complex formation and SET; secondly, it also underwent rapid fragmentation after the SET, acting as an effective leaving group. In this manner, the electronic properties of the substrate were not essential for effective EDA complex formation. In turn, the radical emerging from the intracomplex SET could be either nucleophilic or electrophilic. One of the first examples that capitalized on the use of a redox auxiliary to promote EDA complex photochemistry was reported by Leonori and co-workers (Figure 3.11).²⁶ In this work, a radical 5-*exo-trig* cyclization was reported for the synthesis of nitrogen-containing heterocycles **20-21**. Highly electron-poor *O*-aryl oximes **19** were designed as bench-stable EDA acceptors to engage with simple tertiary amines, such as triethylamine, as sacrificial donors (Figure 3.11, orange box). Light-promoted SET delivered the radical ion pair (Figure 3.11, light blue box), which, upon extrusion of the phenoxide **22**, afforded the reactive imidyl radical **XXV** (Figure 3.11, dashed box). This underwent 5-*exo-trig* cyclization onto the terminal alkene to give the primary carbon-centered radical **XXVI**, which either underwent hydrogen atom transfer from cyclohexadiene (CHD) to give **20**, or was oxidized by **22** to deliver cyclic imine product **21**.

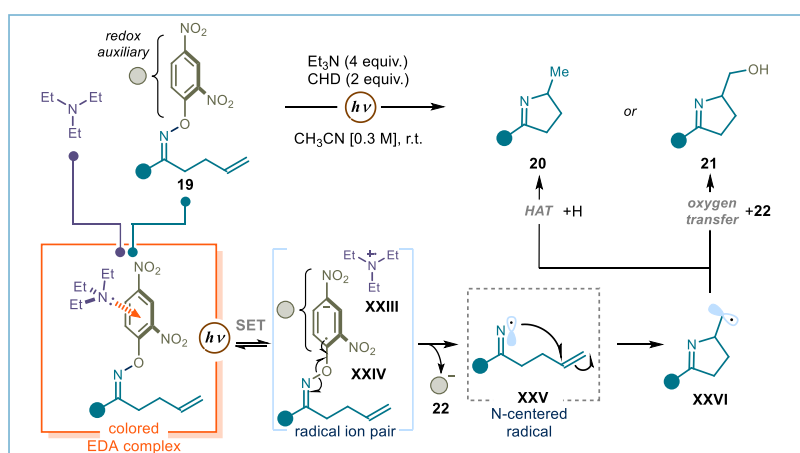


Figure 3.11. Dinitro-substituted *O*-aryl oximes as redox auxiliaries in EDA complex chemistry.

In the following years, the exploitation of redox auxiliaries in EDA complex chemistry has been studied in greater detail, in particular through the use of redox-auxiliary-activation of carboxylic acids (redox-active esters **23**, Figure 3.12 bottom) or aliphatic amines (pyridinium salts **24**, Figure 3.12 bottom).²⁷ For example, Aggarwal and co-workers reported the ability of **23** and **24** to participate as EDA electron acceptor partners

²⁵ Parsaee, F.; Senarathna, M. C.; Kannangara, P. B.; Alexander, S. N.; Arche, P. D. E.; Welin, E. R. “Radical philicity and its role in selective organic transformations” *Nature Reviews Chemistry* **2021**, *5*, 486–499.

²⁶ Davies, J.; Booth, S. G.; Essafi, S.; Dryfe, R. A. W.; Leonori, D. “Visible-Light-Mediated Generation of Nitrogen-Centered Radicals: Metal-Free Hydroimination and Iminohydroxylation Cyclization Reactions” *Angew. Chem. Int. Ed.* **2015**, *54*, 14017–14021.

²⁷ (a) Zhang, J.; Li, Y.; Xu, R.; Chen, Y. “Donor-Acceptor Complex Enables Alkoxy Radical Generation for Metal-Free C(sp³)-C(sp³) Cleavage and Allylation/Alkenylation” *Angew. Chem. Int. Ed.* **2017**, *56*, 12619–12623. (b) Li, Y.; Zhang, J.; Li, D.; Chen, Y. “Metal-Free C(sp³)-H Allylation via Aryl Carboxyl Radicals Enabled by Donor/Acceptor Complex” *Org. Lett.* **2018**, *20*, 3296–3299. (c) Fawcett, A.; Pradeilles, J.; Wang, Y.; Mutsuga, T.; Myers, E. L.; Aggarwal, V. K. “Photoinduced decarboxylative borylation of carboxylic acids” *Science* **2017**, *357*, 283–286. (d) Wu, J.; Grant, P. S.; Li, X.; Noble, A.; Aggarwal, V. K. “Catalyst Free Deaminative Functionalizations of Primary Amines by Photoinduced Single-Electron Transfer” *Angew. Chem. Int. Ed.* **2019**, *58*, 5697–5701. Wu, J.; Bär, R. M.; Guo, L.; Noble, A.; Aggarwal V. K. “Photoinduced Deoxygenative Borylations of Aliphatic Alcohols” *Angew. Chem. Int. Ed.* **2019**, *58*, 18830–18834.

in borylation reactions. These protocols readily converted available carboxylic acids or amines into valuable boronic esters through the *in-situ* formation of a ternary photoactive aggregate (Figure 3.12, orange box), which upon light irradiation generated nucleophilic carbon-centered radical **XXVIII**. These open-shell species were eventually trapped by the DMA-B₂Cat₂ aggregate delivering the desired product **26** and a strongly reducing boron-centered radical **XXIX**, which promoted an efficient radical chain propagation by reducing a molecule of radical precursor **23** or **24**.^{27c, d}

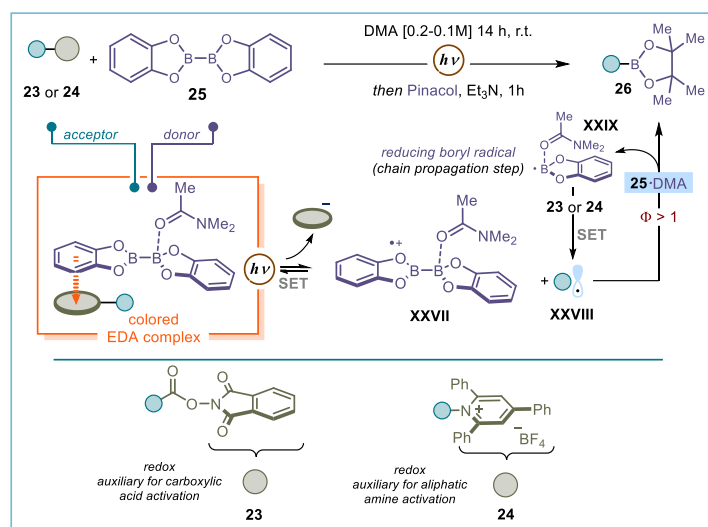


Figure 3.12. Redox auxiliaries in EDA chemistry for efficient radical borylation.

3.2.4 Catalytic EDA complexes

The development of new EDA-based processes taking advantage of sacrificial donors has demonstrated the synthetic potential of this chemistry. However, these approaches still necessitate of stoichiometric additives. Developing a catalytic EDA complex activation would represent a significant advance in the field. As discussed in Section 3.2.2, the Melchiorre group showed that some organocatalytic intermediates, such as enamines,²⁸ iminium ions,²⁹ and enolates,²³ could engage in photoactive EDA complexes to generate radicals while also serving as chiral radical traps. Mechanistic experiments demonstrated how the EDA complex was responsible for the initiation of radical chain-based processes. Therefore, the requirement for specific catalysts and reagents were essential to effectively initiate and propagate the chain reactions. Hence, the development of a general catalytic EDA complex strategy would considerably expand the generality of the chemistry. In the general strategy illustrated in Figure 3.13a, an electron-rich catalyst would deliver an EDA aggregate with an electron-poor substance. Light-promoted SET would produce a radical ion pair. Fragmentation of the radical anion would give a neutral radical that could be intercepted by a radical trap to form the desired product. On the other hand, the catalyst radical cation would need to be reduced through SET in order to render the process catalytic. Since 2019, a few light-driven catalytic

²⁸ Arceo, E.; Bahamonde, A.; Bergonzini, G.; Melchiorre, P. "Enantioselective direct α -alkylation of cyclic ketones by means of photo-organocatalysis" *Chem. Sci.* **2014**, *5*, 2438–2442.

²⁹ Cao, Z.-Y.; Ghosh, T.; Melchiorre, P. "Enantioselective radical conjugate additions driven by a photoactive intramolecular iminium-ion-based EDA complex" *Nat. Commun.* **2018**, *9*, 3274.

EDA strategies have been reported in which the donor is regenerated after SET, demonstrating catalysis of an EDA partner is feasible (Figure 3.13b).^{30,31}

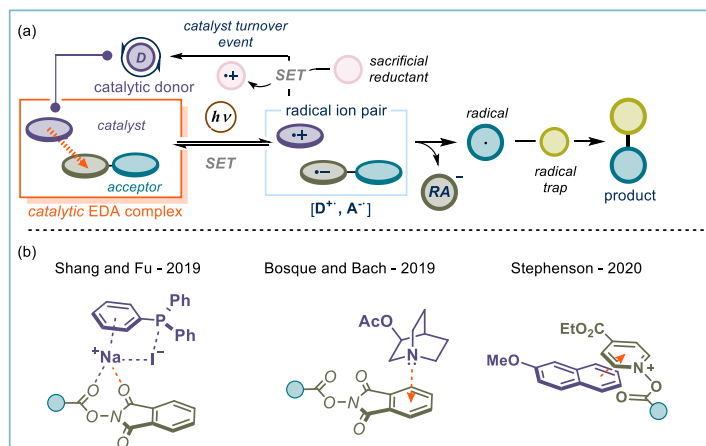


Figure 3.13. Catalytic donor in EDA-based strategies.

The first catalytic EDA report was disclosed in 2019 by Shang, Fu and co-workers.^{30a} In their work, the ability of alkali iodides, such as NaI, and triphenyl phosphine (PPh₃) to deliver a ternary EDA aggregate with different radical precursors, such as phthalimide esters **23**, was exploited for the generation of carbon-centered radicals **XXXII** (Figure 3.14). Upon light excitation, SET from the catalytic donor partner (NaI–PPh₃) to phthalimide ester **23** promotes the formation of carbon-centered radical **XXXII**, which could be trapped by different substrates. For example, the use of quinolines **27** in the presence of acids led to an efficient Minisci reaction to deliver C-H functionalized heteroarematies **28**. The radical cation **XXXIII**, generated upon C–C bond formation, was oxidized by the Ph₃P–I•⁺ delivering the desired product **28** and turning over the catalytic entity. Use of triphenylphosphine was critical for effective catalyst turnover, due to stabilization of the iodine radical with PPh₃. Quantum yield determination ($\Phi = 0.15$) supported a closed catalytic cycle being operative. This catalytic system could also be applied to an array of radical precursors bearing electron-deficient auxiliary moieties, including pyridinium salts **24** and hypervalent iodine reagent **30**.^{30a} Finally, the same NaI/PPh₃ catalytic system was employed to perform the α -alkylation of enol ethers (**31**), Heck-type reaction with **32** as radical trap, and an enantioselective Minisci reaction, originally developed by the Phipps group under photoredox conditions.³² While this catalytic system is

³⁰ (a) Fu, M.-C.; Shang, R.; Zhao, B.; Wang, B.; Fu, Y. Photocatalytic decarboxylative alkylations mediated by triphenylphosphine and sodium iodide. *Science* **2019**, *363*, 1429–1434. (b) Wang, Y.-T.; Fu, M.-C.; Zhao, B.; Shang, R.; Fu, Y. Photocatalytic decarboxylative alkenylation of α -amino and α -hydroxy acid-derived redox active esters by NaI/PPh₃ catalysis. *Chem. Commun.* **2020**, *56*, 2495–2498. (c) Fu, M.-C.; Wang, J. X.; Shang, R. Triphenylphosphine-Catalyzed Alkylative Iododecarboxylation with Lithium Iodide under Visible Light. *Org. Lett.* **2020**, *22*, 8572–8577. (d) Bosque, I.; Bach, T. 3-Acetoxyquinuclidine as Catalyst in Electron Donor-Acceptor Complex-Mediated Reactions Triggered by Visible Light. *ACS Catal.* **2019**, *9*, 9103–9109. (e) McClain, E. J.; Monos, T. M.; Mori, M.; Beatty, J. W.; Stephenson, C. R. J. Design and Implementation of a Catalytic Electron Donor–Acceptor Complex Platform for Radical Trifluoromethylation and Alkylation. *ACS Catalysis* **2020**, *10*, 12636–12641.

³¹ (a) Quint, V.; Morlet-Savary, F.; Lohier, J.-F.; Lalevée, J.; Gaumont, A.-C.; Lakhdar, S. “Metal-Free, Visible Light-Photocatalyzed Synthesis of Benzo[b]phosphole Oxides: Synthetic and Mechanistic Investigations” *J. Am. Chem. Soc.* **2016**, *138*, 7436–7441. (b) Emmanuel, M. A.; Greenberg, N. R.; Oblinsky, D. G.; Hyster, T. K. “Accessing non-natural reactivity by irradiating nicotinamide-dependent enzymes with light” *Nature* **2016**, *540*, 414–417. (c) Biegasiewicz, K. F.; Cooper, S. J.; Gao, X.; Oblinsky, D. G.; Kim, J. H.; Garfinkle, S. E.; Joyce, L. A.; Sandoval, B. A.; Scholes, G. D.; Hyster, T. K. “Photoexcitation of flavoenzymes enables a stereoselective radical cyclization” *Science* **2019**, *364*, 1166–1169. (d) Clayman, P. D.; Hyster, T. K. “Photoenzymatic Generation of Unstabilized Alkyl Radicals: An Asymmetric Reductive Cyclization” *J. Am. Chem. Soc.* **2020**, *142*, 15673–15677. (e) Page, C. G.; Cooper, S. J.; DeHovitz, J. S.; Oblinsky, D. G.; Biegasiewicz, K. F.; Antropow, A. H.; Armbrust, K. W.; Ellis, J. M.; Hamann, L. G.; Horn, E. J.; Oberg, K. M.; Scholes, G. D.; Hyster, T. K. “Quaternary Charge-Transfer Complex Enables Photoenzymatic Intermolecular Hydroalkylation of Olefins” *J. Am. Chem. Soc.* **2021**, *143*, 97–102.

³² Proctor, R. S. J.; Davis, H. J.; Phipps, R. J. “Catalytic enantioselective Minisci-type addition to heteroarenes” *Science* **2018**, *360*, 419–422.

characterized by broad applicability in terms of radical precursors, the methodology could be applied to redox-neutral transformations only, since catalyst turnover could only be realized via SET reduction from radical intermediates generated during the process (e.g. intermediate **XXXI**, Figure 3.14). A net-reductive process would instead require the use of an external reductant in order to deliver the desired product and to turn over the catalytically active entity.

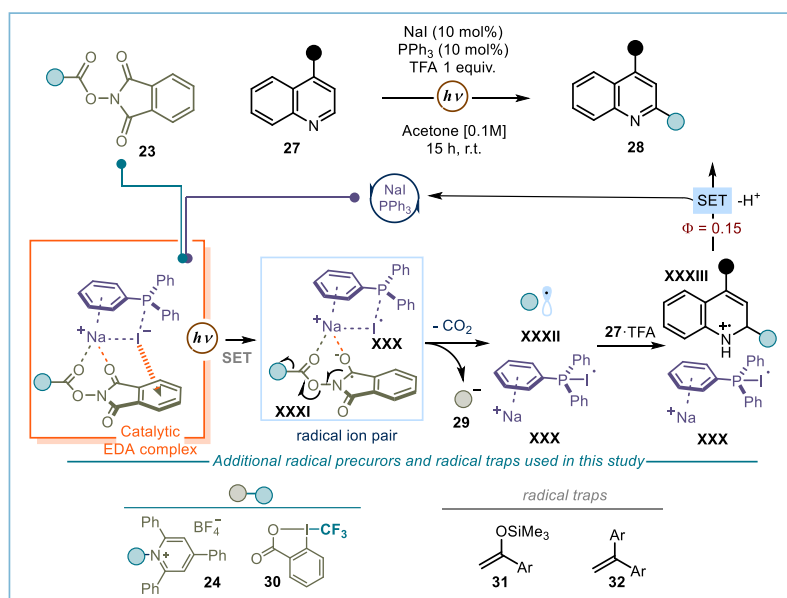


Figure 3.14. Decarboxylative Minisci reaction promoted by a catalytic ternary EDA complex.

In the same year, another example of catalytic donors in EDA-promoted processes was reported by Bosque and Bach.^{30d} They used the geometrically-strained structure of 3-acetoxyquinuclidine **34** for the catalytic photoactivation of electron-poor tetrachlorophthalimide esters **33** (Figure 3.15). The combination of the two partners **33** and **34** delivered a photoactive EDA aggregate that, upon irradiation at 455 nm, promoted the formation of the aminated product **36**. Mechanistically, the formation of the EDA complex (Figure 3.15, orange box) and its irradiation triggered an SET from the catalyst to tetrachlorophthalimide moiety to deliver a radical ion pair (Figure 3.15, light blue box). Decarboxylation from the radical anion **XXXIV** formed the highly reducing α -amino radical **XXXVI** which was oxidized through SET by **XXXV**, turning over the catalyst and forming the iminium ion **XXXVII**. Finally, 1,2-addition of free tetrachlorophthalimide anion **35** to **XXXVII** delivered product **36**. The quantum yield measurement, found to be as low as 0.02, did not support a radical chain mechanism. Crucial for the successful implementation of this system was the geometrical restriction of the catalyst's scaffold, which avoided the α -deprotonation of the radical cation **XXXV** that would result in the degradation of the catalyst.^{30d}

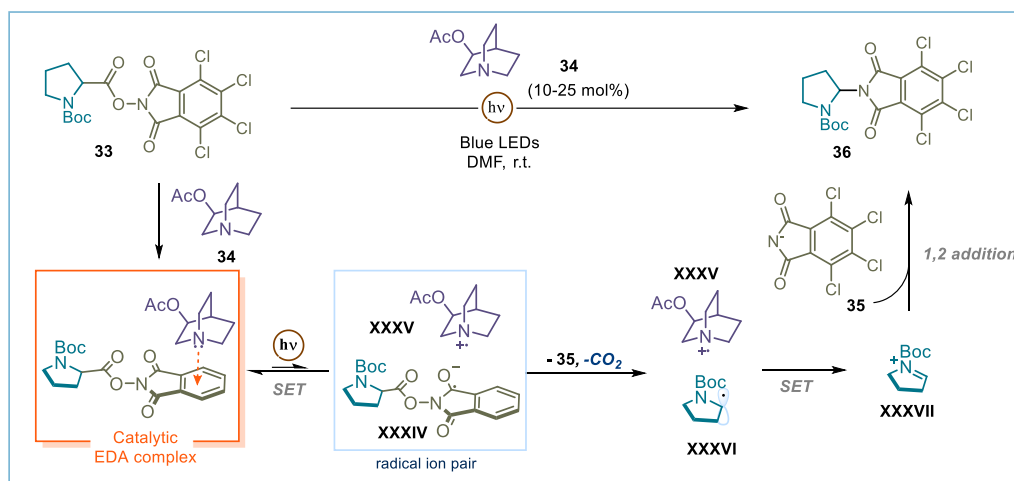


Figure 3.15. 3-Acetoxyquinuclidine as catalytic donor in EDA chemistry.

The latest example of catalytic donor in EDA-based processes was developed by the Stephenson group.^{30e} The authors used electron-rich 2-methoxynaphthalene **39** as a catalytic donor partner in combination with pyridinium salt **XXXVIII**, which is formed *in situ* by the condensation of trifluoroacetic anhydride (TFAA) and *N*-oxide **37** (Figure 3.16). Light excitation of the photoactive EDA complex (Figure 3.16, orange box) triggered an intra-complex SET resulting in the formation of a radical ion pair, constituted by **XL** and **XXXIX**. Radical-based fragmentation of the labile N-O bond in **XL** promoted the formation of trifluoromethyl radical **XLI** and **40**. The highly electrophilic trifluoromethyl radical was then trapped by electron-rich heteroarene compounds **38**, forging a new C-C bond. In the last step, the ensuing radical **XLII** was oxidized by the kinetically stable radical cation **XXXIX**, providing the desired trifluoromethylated product **41** and regenerating the catalyst **39**.

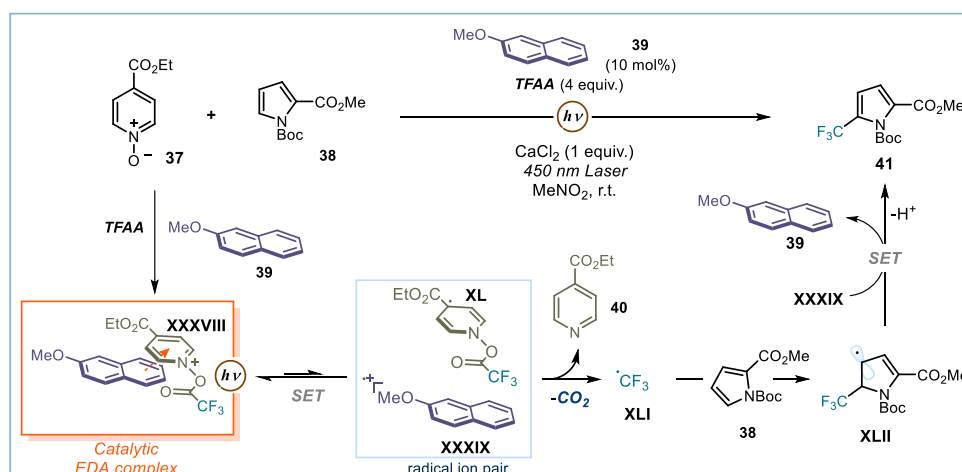


Figure 3.16. Radical trifluoromethylation of heteroarenes driven by catalytic EDA.

3.3 Target of the Project

The target of this project was to show that the dithiocarbamate-based organic catalysts, previously employed to activate alkyl(pseudo)halides through an S_N2 -based mechanism, can act as a general and modular class of electron-donor organocatalysts for the formation of photoactive EDA complexes with different electron-poor radical precursors (Figure 3.17b).¹ In particular, we aimed to use commercially available dithiocarbamate and xanthogenate catalysts **A** and **B** to promote the formation of those radicals we could not generate with the approach described in Chapter II, namely non-stabilized primary and secondary carbon radicals, tertiary radicals, and nitrogen-centered radicals. In principle, the modular nature of our organocatalysts would help us to tune their properties (e.g. catalyst turnover or stability in acidic media) offering a powerful and versatile EDA catalytic strategy. Furthermore, we wanted to exploit this flexibility to develop both net-reductive and redox-neutral photo-induced radical processes. The former reactivity was not achievable with previously reported catalytic EDA strategies due the inability of the catalyst to be turned over via hydrogen atom transfer. We were also keen to use mechanistic investigations to determine if a closed catalytic cycle was operational in the developed reactions, thus providing evidence of the catalysts' ability to turn over and iteratively drive every catalytic cycle.

3.3.1 Design plan

In chapter II, I described how the nucleophilic dithiocarbamate anion **A** could be used for the activation of alkyl electrophiles via a nucleophilic substitution pathway (Figure 3.17a). Blue light irradiation of the photon-absorbing S_N2 adduct **I** delivered open-shell species upon homolytic cleavage of the weak C-S bond. The radicals generated in this manner were eventually used to forge new C-C and C-B bonds.³ One feature of this strategy was to rely on the electrophilic character of the precursors and not on their redox properties or bond dissociation energies of specific bonds within the precursors' core. The mechanistically distinct strategy offered the possibility to generate radicals in a catalytic manner from precursors that were inert towards previously reported radical generation methods. However, it granted access to radicals only from substrates able to undergo nucleophilic substitution. Furthermore, effective homolytic cleavage of the C-S bond within **I** occurred only when stabilized radicals could be generated (including benzyl, allyl, or radicals with a stabilizing group at their α -position).³ Since 2019, when the first report on dithiocarbamate anion catalyst was published,² investigations were performed in our group to elucidate the mechanism of catalyst turnover. Specifically, as discussed in Chapter II and in the introduction of this chapter, I found that the sulphur radical **II**, which is formed after photo-promoted homolytic cleavage of intermediate **I**, dimerizes under the reaction conditions to afford **III**.^{3c} Dimer **III**, which can absorb light in the visible region, is in a light-regulated equilibrium with the progenitor sulphur-centred radical **II**. This dimerization manifold confers kinetic stability to **II**,⁴ and permits an effective catalyst turnover. Further investigations demonstrated that the sulphur-centred **II** can be effectively reduced by both SET or HAT processes (Figure 3.17b).^{3d}

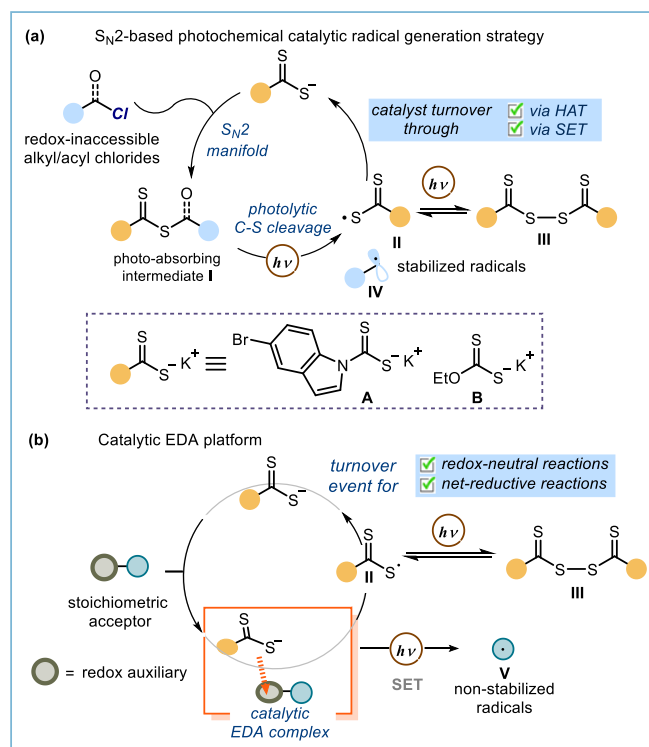


Figure 3.17. (a) A radical generation strategy based on nucleophilic substitution path. (b) Design of a catalytic EDA complex platform.

Considering the ability of catalyst **A** and **B** to be turned over through two possible manifold (HAT from an external hydrogen donor or SET from an intermediate of the catalytic cycle) and their electron-rich nature, we thought that the development of a general photo-organocatalytic EDA platform using **A** and **B** as catalytic donors could be feasible (Figure 3.17b). Synthetically, it would be interesting to have a catalytic EDA platform based on the use of commercially available catalysts that allows the generation of a wide range of radicals and to engage them in mechanistically distinct reaction pathways.

3.4 Results and discussion

We started our investigation by testing the feasibility of the EDA complex catalytic strategy by employing *N*-(acyloxy)phthalimide esters as suitable EDA acceptors.^{27a,30} The Giese addition between cyclohexyl *N*-(acyloxy)phthalimide (NHPI) **23a** and phenylvinyl sulphone **42a** promoted by the catalytic donors **A** or **B** was selected as the benchmark transformation (Figure 3.18a). This process required the generation of a non-stabilized secondary radical **XLIII**, which was not accessible via the previously reported S_N2 -based strategy (Figure 3.18).^{2,3} From a mechanistic standpoint, the resulting Giese-type addition of the cyclohexyl radical **XLIII** to the Michael acceptor **42a** necessitates a reductive step in order to proceed. Figure 3.18 shows a plausible mechanism of the overall process. The aggregation in the ground state between the selected electron-rich donor catalyst (**A** or **B**) and the electron-poor redox active ester **23a** would lead to a photo-absorbing EDA complex (Figure 3.18, orange box). The formation of the EDA aggregate should be achievable by considering the tendency of thiolates and dithiocarbonyl anions to serve as donor partners in

stoichiometric EDA complexes.³³ A light-promoted intracomplex SET would then deliver the desired carbon-centered radical **XLIII** together with the sulphur-centered radical **II**.

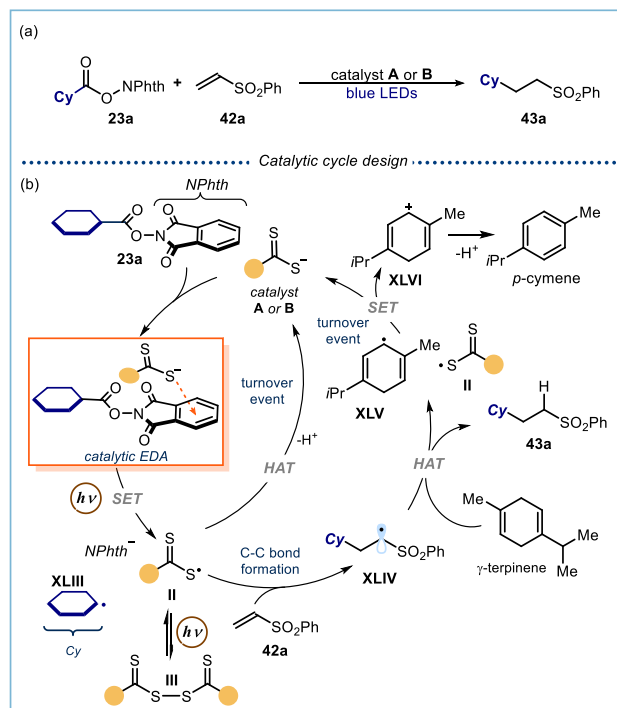


Figure 3.18. Original plan for a net-reductive Giese-type addition reaction driven by a catalytic photoactive EDA complex.

Interception of the nucleophilic radical by **42a** forges a new C-C bond, while the ensuing electrophilic radical **XLIV** is quenched by a HAT event from γ -terpinene (external H donor). This step would deliver the desired product **43a** and the cyclohexadienyl radical **XLV**. Overall, this constitutes a net-reductive process since the radical precursor **23a** and its Giese-addition radical intermediate **XLIV** are to be reduced. To turnover the dithiocarbonyl radical **II** ($E_{\text{ox}} = 0.45\text{--}0.75$ V vs. SCE), an SET or HAT from the reductive additive must take place to reform the catalytic anion. Both reductive steps would eventually close the catalytic cycle by returning the organic catalyst to its original oxidation state. The propensity of the catalyst to be turned over by using an external reductant (e.g. γ -terpinene) increases the versatility of this EDA catalytic system. Indeed, none of the previously developed catalytic EDA approaches could realize the turnover event in this manner.³⁰

3.4.1 Developing redox-neutral transformations³⁴

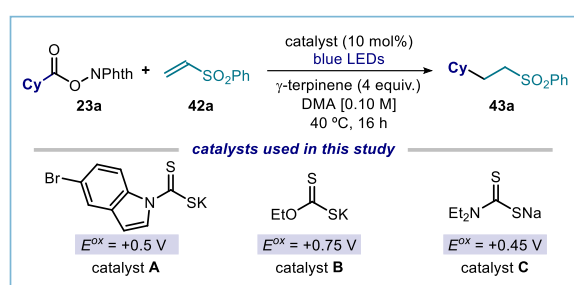
The initial screening for the development of a Giese-type addition reaction was performed by reacting phthalimide ester **23a** and phenylvinyl sulfone **42a** in the presence of an excess of γ -terpinene as the H donor (4 equiv.), and a catalytic amount of the anion donor (Table 3.1). Under blue LEDs irradiation (460 nm), the dithiocarbamate **A** (containing a bromoindole moiety), the more nucleophilic xanthogenate **B** and dithiocarbamate **C** all showed competency as catalytic donors, providing the desired product **43a** in good

³³ (a) Liu, B.; Lim, C.-H.; Miyake, G. M. "Visible-Light-Promoted C-S Cross-Coupling via Intermolecular Charge Transfer" *J. Am. Chem. Soc.* **2017**, *139*, 13616–13619. (b) Yang, M.; Cao, T.; Xu, T.; Liao, S. "Visible-Light-Induced Deaminative Thioesterification of Amino Acid Derived Katritzky Salts via Electron Donor–Acceptor Complex Formation" *Org. Lett.* **2019**, *21*, 8673–8678. (c) Sundaravelu, N.; Nandy, A.; Sekar, G. "Visible Light Mediated Photocatalyst Free C-S Cross Coupling: Domino Synthesis of Thiochromane Derivatives via Photoinduced Electron Transfer" *Org. Lett.* **2021**, *23*, 3115–3119.

³⁴ The design, scope and optimization of the reaction detailed in this section was performed by Eduardo de Pedro Beato. Quantum yield measurement, spectroscopic analysis and catalyst stability studies were performed by Davide Spinnato.

yields (entries 1-3). These results showed the feasibility of our hypothesis: regardless of the specific properties of each dithiocarbonyl anions, they could efficiently promote the generation of non-stabilized alkyl radicals upon SET with phthalimide esters **23a**. The versatility of the dithiocarbamate/xanthogenate scaffolds should allow us to select the best catalyst depending on the required photophysical and chemical properties of the reaction in study, offering greater generality for the catalytic EDA complex strategy. Due to its superior performance and lower price, xanthate anion **B** was selected for further studies. Interestingly, catalyst **B** is also effective under green light irradiation ($\lambda_{\text{max}} = 520$ nm, entry 4), delivering the desired product in comparable yields to the optimal conditions (blue LEDs). Control experiments established the necessity for light illumination and for the donor catalyst (entries 6 and 7), whereas the addition of a radical scavenger, such as 2,2,6,6-tetramethylpiperidine 1-oxyl (TEMPO), completely inhibited the reaction (entry 8, the cyclohexyl-TEMPO adduct was detected).

Table 3.1. Optimization studies.



entry	catalyst	deviation	yield (%) ^a
1	A	none	81
2	B	none	95 (86) ^b
3	C	none	85
4	B	green LED (520 nm)	95
5	B	under air	0
6	B	no light	0
7	none	none	0
8	B	TEMPO (1.5 equiv.)	0

Reactions performed under an argon atmosphere on a 0.1 mmol scale at 40 °C for 16 h using 465 nm LEDs strip. Stoichiometry: 1.5 equiv. of **42a** and 4 equiv. of γ -terpinene. For details on cyclic voltammetry measurements see the Experimental Section. ^a ¹H NMR yields were calculated using trimethoxybenzene as the internal standard. ^b Yield referring to purified product **43a**. LED: Light-emitting diode. NPhth: phthalimide.

We then performed further mechanistically diagnostic investigations. UV/Vis spectroscopic measurements under the reaction conditions confirmed the formation of the key EDA aggregate (Figure 3.19). When catalyst **B** and the NHPI substrate **23a** were mixed, the colorless solutions turned to a strong yellow color, while the appearance of a new charge-transfer band at higher wavelengths was diagnostic of a ground-state EDA complex (orange line).

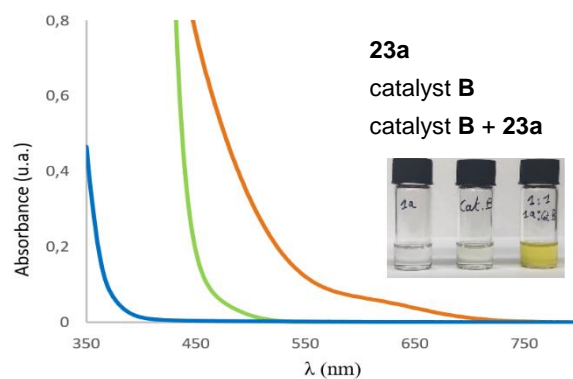


Figure 3.19. UV-Vis analysis performed in dimethylacetamide in 1 mm path quartz cuvettes, and appearance of the single reaction components and of the colored EDA complex between catalyst **B** and **23a**. [**23a**] = 0.10 M, [catalyst **B**] = 0.01 M.

In addition, we performed transient absorption spectroscopy (TAS) studies to detect the formation of the sulphur-centered radical **IIb** (Figure 3.20). When a 1:1 mixture of catalyst **B** and ester **23a** was irradiated by means of laser flash photolysis, a transient species absorbing at 620 nm was detected (half lifetime = 0.1 ± 0.01 ms), and its decay was in agreement with the characteristic line shape of xanthyl radical **IIb** (Figure 3.20).^{34,35} This observation supports the notion that the photoinduced intracomplex SET is the central event for radical generation.

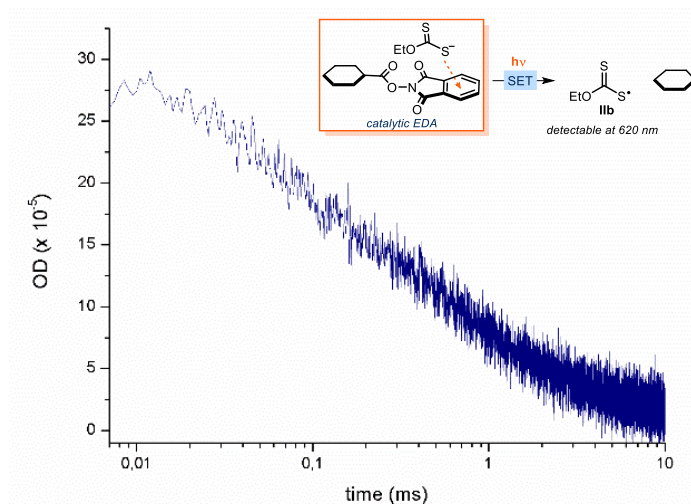


Figure 3.20. Absorption of the transient xanthyl radical **IIb** at 620 nm generated upon 355 nm laser excitation of a 1:1 mixture of **23a** and catalyst **B** 30 mM in DMA.

To elucidate whether a closed catalytic cycle or a chain propagation mechanism was operative, we measured the quantum yield (Φ) of the reaction between **23a** and **42a** catalyzed by **B**. The measured quantum yield was found to be as low as 0.01 ($\lambda = 460$ nm, using potassium ferrioxalate as the actinometer), which supports the proposed closed catalytic cycle depicted in Figure 3.17. This result substantiates our original hypothesis that dithiocarbonyl anions **B** can serve as catalytic donors for EDA complex photochemistry and not as a mere initiator for radical chain processes.

³⁵ Kaga, A.; Wu, X.; Lim, J. Y. J.; Hayashi, H.; Lu, Y.; Yeow, E. K. L.; Chiba, S. "Degenerative xanthate transfer to olefins under visible-light photocatalysis" *Beilstein J. Org. Chem.* **2018**, *14*, 3047-3058.

The robustness of the protocol was tested by implementing a two-step telescoped sequence to synthesize the active ester **23a** *in situ* from its corresponding carboxylic acid, and use it without isolation (Figure 3.20a). This one-pot telescoped procedure delivered the desired product **43a** without any significant decrease in yield, thus showing that isolation of intermediate **23a** was not required. In addition, the desired product **43a** could be obtained in 70% yield also by using a *domino* protocol, where all the reagents were included at the onset of the reaction (Figure 3.20b). This highlights the strength of the catalytic protocol, since byproducts derived from the generation of the active ester **23a** did not interfere with the reaction.

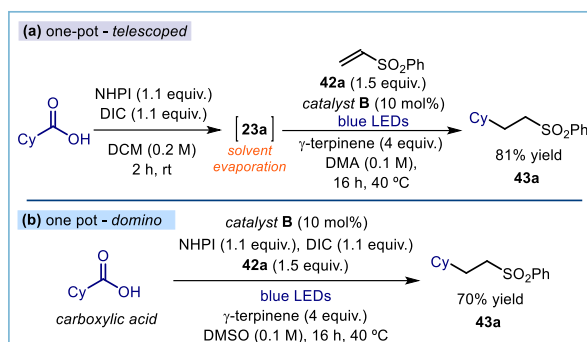


Figure 3.21. (a) Telescoped procedure to functionalize the carboxylic acid. (b) Domino procedure, where all reagents were added at the same time. Yields refer to the isolated product **43a**. DIC: *N,N'*-diisopropylcarbodiimide; NHPI: *N*-(hydroxy)phthalimide.

Using the telescoped procedure, we evaluated the scope of the decarboxylative Giese-type addition using the optimized conditions depicted in Figure 3.22. A wide range of carboxylic acids could be used as radical precursors. Primary (products **43b**, **43e**), secondary (product **43c**), and tertiary radicals (product **43d**) were effectively trapped by electron-poor olefins **42** with modest to excellent yields. Several functional groups were compatible with our strategy, including free alcohols (product **43j**) and carbamates (products **43f-i**). The selective formation of product **43e** was achieved in the presence of an electrophilic alkyl chloride, which suggests that EDA complex aggregation is more efficient than the formation of S_N2 intermediates of type **I** (Figure 3.17a). α -Amino radicals could be generated also from the corresponding amino acids, affording products **43f-i** in good to excellent yield. Biorelevant compounds, including *dehydrocholic acid*, *oleanolic acid*, and *biotin*, were directly functionalized delivering products **43g**, **43h** and **43i** without the need for additional protection/deprotection steps.

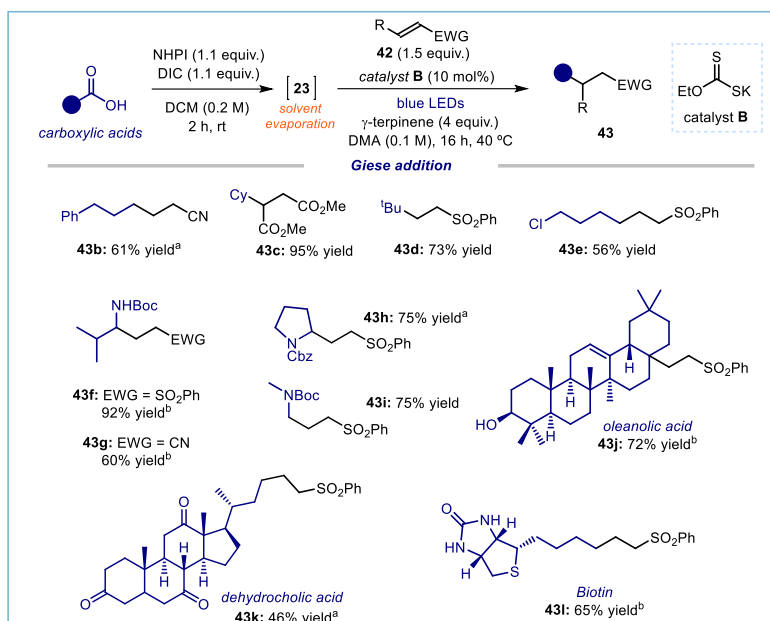
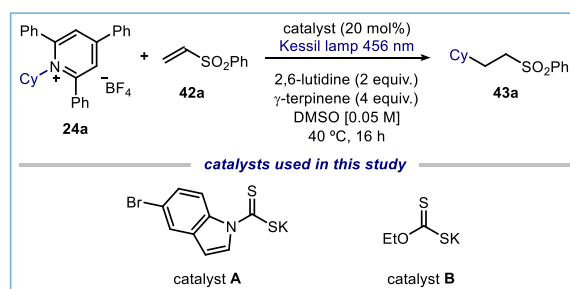


Figure 3.22. Giese-type addition using carboxylic acids as radical precursors. Reactions performed on a 0.2 mmol scale using 1 equiv. of acid; yields of isolated products **43**. ^aUsing the preformed redox-active ester **23** as the radical precursor. ^bOne-pot domino procedure according to the conditions in Figure 3.21.

To further explore the potential of our photochemical catalytic radical generation method, we investigated the activation of *N*-alkylpyridinium salts **24** as a source of carbon-centered radicals (Table 3.2), since they have been already shown to participate in EDA-based chemistry (see Sections 3.3.2 and 3.3.3).^{27d, 30a} In this case, the indole-based dithiocarbamate catalyst **A** (entry 1) showed better performance than catalyst **B** (entry 2). This result highlights how the modular nature of these donor catalysts can be leveraged to optimize the activation of electronically different radical precursors. Light irradiation (entry 6) and catalyst (entry 7) were, once again, essential for the success of the reaction.

Table 3.2. Giese addition with pyridinium salts as radical precursors



entry	catalyst	deviation	yield (%) ^a
1	A	none	83 (67) ^b
2	B	none	70
3	A	green light	24
4	B	green light	20
5	A	under air	0
6	A	no light	0
7	-	no catalyst	0

Reactions performed under inert atmosphere on a 0.1 mmol scale. ^a ¹H NMR yields were calculated using trimethoxybenzene as the internal standard. ^b Yield of the isolated product **43a** on a 0.2 mmol scale.

Non-stabilized carbon-centered radicals were effectively generated upon light-promoted intracomplex SET and they could be intercepted by electron-poor olefins **42** (Figure 3.23a). In a similar fashion to the decarboxylative Giese-type addition, a telescoped one-pot procedure could be developed since the isolation of *N*-alkylpyridinium salts **24** could be circumvented through *in situ* formation from the corresponding alkyl primary amines (Figure 3.23b).

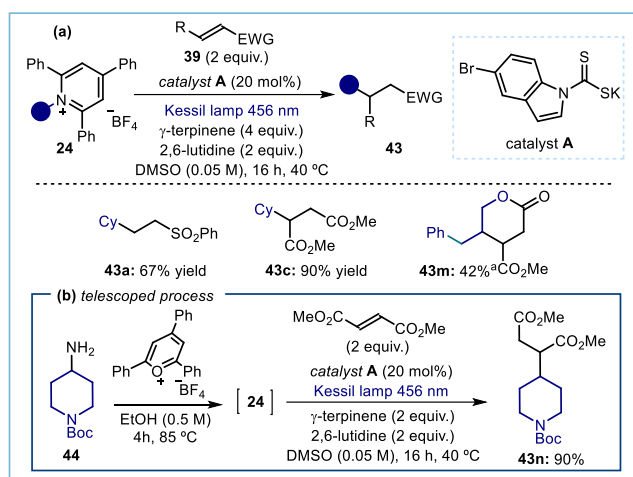


Figure 3.23. (a) Giese-type addition starting from aliphatic amines derivatives. ^a Product **43m** was formed in a 3.8:1 ratio with the regio-isomeric five-member ring adduct, see the Experimental section for details. (b) One-pot telescoped Giese addition from pyridinium salts.

Conscious of the ability of our catalytic system to generate radicals from redox-active derivatives of carboxylic acids **23**, we wondered if the same approach used for the decarboxylative Giese-type addition could be implemented to promote a safer alternative to the Barton decarboxylation reaction simply by removing the olefin trap **42** (Figure 3.24). The Barton decarboxylation, in which alkyl carboxylic acids are converted into simple alkanes through overall replacement of the carboxylate group with a hydrogen atom, is a robust and well-known synthetic reaction.³⁶ However, toxic tin-based reagents and harsh conditions are often required to carry out this transformation. As anticipated, removal of the Michael acceptor from the conditions depicted in Table 3.1 afforded the desired reduced product **45**. Once again, the synthetic utility of our method was demonstrated by developing the desired radical decarboxylation in a one-pot domino reaction (Figure 3.23). The use of catalytic amounts of xanthogenate anion **B** (10 mol%) enabled the decarboxylation of primary (product **45a**), secondary (product **45b**) and tertiary (product **45c**) carboxylic acids. The protocol could be applied in the reduction of pharmaceutically active compounds and in the decarboxylation of biologically relevant carboxylic-acid-containing molecules. For example, *Gibberellic acid* and a *baclofen* derivative afforded the desired products **45f** and **45g** in 60% and 74% yield, respectively. The synthetic usefulness of the process was further highlighted by large-scale (4 mmol) defunctionalization of *dehydrocholic acid*, which delivered adduct **45d** in 55% yield.

³⁶ (a) Barton, D. H. R.; Crich, D.; Motherwell, W. B. "New and Improved Methods for the Radical Decarboxylation of Acids" *J. Chem. Soc., Chem. Commun.* **1983**, 939–941. (b) Barton, D. H. R.; Crich, D.; Motherwell, W. B. "The invention of new radical chain reactions. Part VIII. Radical chemistry of thiohydroxamic esters; A new method for the generation of carbon radicals from carboxylic acids" *Tetrahedron* **1985**, *41*, 3901–3924. For a recent application: (c) Qin, T.; Malins, L. R.; Edwards, J. T.; Merchant, R. R.; Novak, A. J. E.; Zhong, J. Z.; Mills, R. B.; Yan, M.; Yuan, C.; Eastgate, M. D.; Baran, P. S. "Nickel-Catalyzed Barton Decarboxylation and Giese Reactions: A Practical Take on Classic Transforms" *Angew. Chem., Int. Ed.* **2017**, *56*, 260–265.

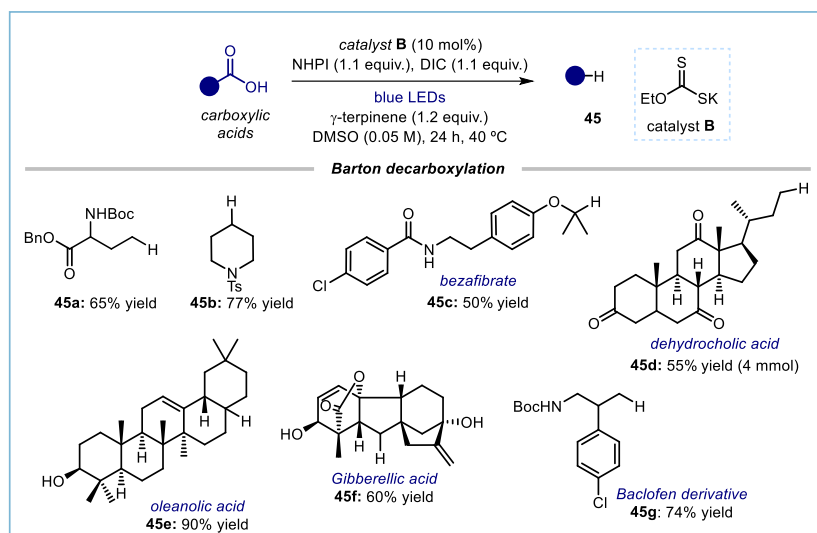


Figure 3.24. EDA complex catalysis for the Barton decarboxylation. (a) Reactions performed on 0.2 mmol scale using a one-pot domino process; yields refer to isolated products **45** after purification. NHPI: *N*-Hydroxyphthalimide, DIC: *N,N'*-diisopropylcarbodiimide, Boc: *tert*-Butyloxycarbonyl; Bn: benzyl.

Exploiting the previously demonstrated tendency of *N*-alkylpyridinium salts to participate in EDA complex formation with our dithiocarbonyl anion catalysts **A** and **B**, we envisioned that our method could permit deleting a strong C-N bond while replacing it with a C-H bond (Figure 3.24). Once again, the indole-based catalyst **A** performed better when *N*-alkylpyridinium salts **24** were used as radical precursors.

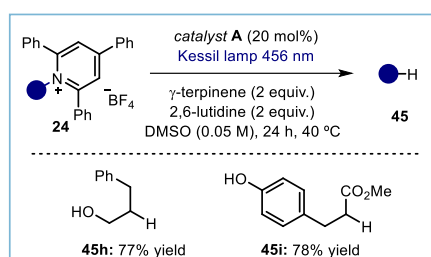


Figure 3.25. EDA complex catalysis for deaminative reduction.

From a mechanistic standpoint, these reductive defunctionalization reactions are proposed to occur in a similar way to the net-reductive Giese addition depicted in Figure 3.18. Specifically, the open-shell species of type **XLIII**, generated upon light-promoted excitation of the EDA aggregate, can abstract a hydrogen atom from γ -terpinene, while the sulphur-centered radical **II** is turned over to the corresponding anion catalyst by SET from bis-allylic radical **XLV**. The low value obtained for the quantum yield measurement ($\Phi = 0.01$) for the transformation leading to product **45b** disfavored a mechanistic scenario based on a radical chain propagation mechanism.

3.4.2 Redox-neutral process³⁷

So far, we have demonstrated that our catalytic EDA complex platform could be exploited to develop net-reductive transformations (Section 3.4.1). This represented the first catalytic EDA approach where the turnover event does not necessitate an SET with an open-shell intermediate which is a progenitor of the reaction product. However, in order to test the synthetic versatility of our system, we wanted to challenge

³⁷ The design, optimization, scope evaluation, and mechanistic studies detailed in this section were performed by Davide Spinnato.

the ability of dithiocarbamate anions to promote mechanistically distinct organic transformations under catalytic EDA conditions. While the Giese addition and the Barton decarboxylation were net-reductive processes, we were keen to test the potential of our catalytic system to promote redox-neutral transformations, where one intermediate of the catalytic cycle can master the turnover event of the sulphur-centered radical via an SET. Intermediates of type **XLVIII** have been already shown to engage intermediate of type **II** in SET event ensuring the regeneration of catalyst **A** (see Chapter II).^{3c} Consequently, we realized that the α -alkylation of silyl enol ethers **46** might represent a suitable reaction to implement our hypothesis. The catalytic cycle depicted in Figure 3.26 can be dissected in four fundamental steps: *i*) formation of a photoactive EDA complex between the catalytic anion donor and pyridinium salt **24**; *ii*) generation of radicals of type **XLVII** via blue light-promoted intracomplex SET; *iii*) interception of the open-shell electrophilic species by the nucleophilic silyl enol ether **46** to forge the new C-C bond; *iv*) SET from the ensuing α -oxo radical **XLVIII** to the sulphur-centered radical **II** that ensures catalyst turnover and formation of oxocarbenium ion **XLIX**, which eventually undergoes water-assisted desilylation to deliver the desired product. As already discussed, this SET step becomes kinetically feasible due to the stabilization of the sulphur-centered radical **II** via the light-controlled dimerization mechanism. Overall, the reaction is characterized by one reduction event for the formation of the reactive radical **XLVII** and one oxidation for product formation and catalyst turnover. Therefore, the process constitutes a redox-neutral transformation.

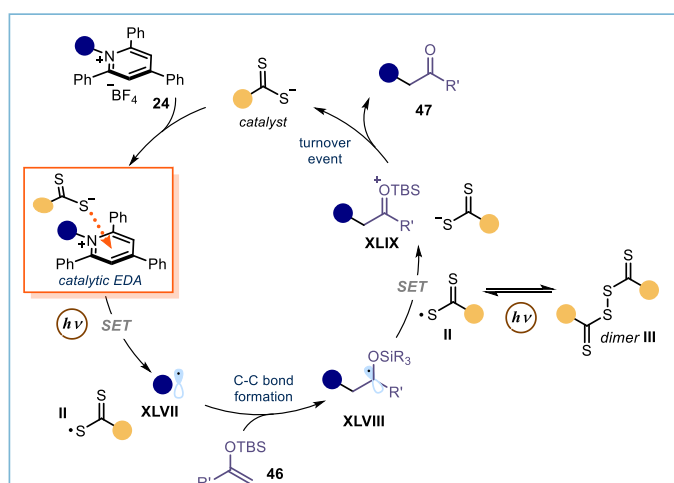
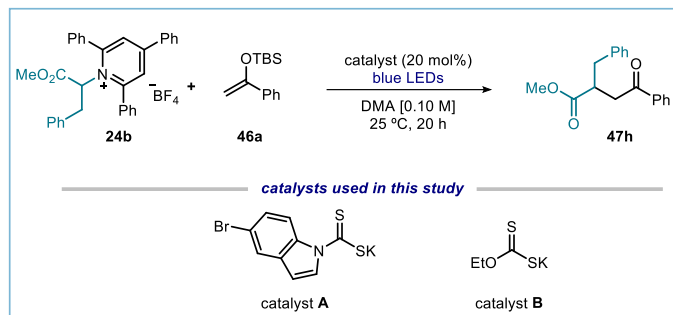


Figure 3.26. Mechanistic plan for a redox neutral transformation catalyzed by the excitation of a catalytic EDA complex.

We started the investigation for the α -alkylation of silyl enol ethers employing pyridinium salt **24b**, since it delivers an electrophilic radical upon SET and fragmentation (Table 3.3). This electrophilic radical has the right polarity to undergo addition to nucleophilic silyl enol ether **46a**. Performing the reaction described in Table 3.3 using a catalytic amount of dithiocarbonyl anion **A** (20 mol%) in the presence of a slight excess of silyl enol ether **46a** (1.5 equiv.) afforded only 16% of the desired product **47h** (Table 3.3, entry 1). The yield was comparable to the amount of catalyst used, thus suggesting that acid-mediated degradation of the organocatalyst might be occurring, since for each molecule of product formed one equivalent of HBF_4 is liberated. Therefore, we decided to add an external base (2,6-lutidine) to counterbalance the increasing acidity of the solution upon product formation. Gratifyingly, the addition of the base improved the reaction efficiency and the desired product **47h** was obtained in 89% after flash chromatography. Xanthate anion **B** also proved a competent catalyst for this transformation, however lower yield of product **47h** was observed. Therefore, we continued our investigations using catalyst **A**. Use of green light irradiation instead of blue light also promoted the reaction, albeit with lower efficiency (entry 4, 45% NMR yield). Attempts to reduce

the catalyst loading to 10% resulted in a lower yield of 62% (entry 5). Finally, control reactions indicated that an inert atmosphere (entry 6), light irradiation (entry 7), and presence of the catalyst (entry 8) were essential for the success of the reaction.

Table 3.3 α -alkylation of silyl enol ethers.



entry	catalyst	Base	deviation	yield (%) ^a
1	A	-	none	16
2	A	2,6-lutidine (1 equiv.)	none	95 (89) ^b
3	B	2,6-lutidine (1 equiv.)	none	80
4	B	2,6-lutidine (1 equiv.)	green light	45
5	A	2,6-lutidine (1 equiv.)	cat. 10 mol%	62
6	A	2,6-lutidine (1 equiv.)	under air	0
7	A	2,6-lutidine (1 equiv.)	no light	0
8	none	2,6-lutidine (1 equiv.)	none	0

Reactions performed under inert atmosphere on a 0.1 mmol scale. ^a ¹H NMR yields were calculated using trimethoxybenzene as the internal standard. ^b Yield of the isolated product on a 0.2 mmol scale.

With the optimized conditions in hand (Table 3.3, entry 2), we evaluated the scope of the radical-mediated α -alkylation of silyl enol ethers (Figure 3.27). A wide range of electrophilic radicals can be installed at the α -position of silyl enol ethers **46a** in high yields. Pyridinium salts **24**, delivering primary (products **47a-b**) and secondary (products **47c-d**) radicals, were competent substrates for the alkylation reaction. Importantly, nitrogen-containing heterocycles, which are often found in drug candidates, were well tolerated (products **47e-f**). Electronically and structurally different silyl enol ethers **46** could effectively intercept an electrophilic secondary α -ester radical, offering products **47g-m** in modest to excellent yields. Last, non-stabilized and nucleophilic primary and secondary radicals, generated from phthalimide esters **23**, were successfully intercepted by **46a** delivering products **47n** and **47o** in moderate yields. The lower yields can be attributed to the partially unmatched polarity between the two reaction partners.

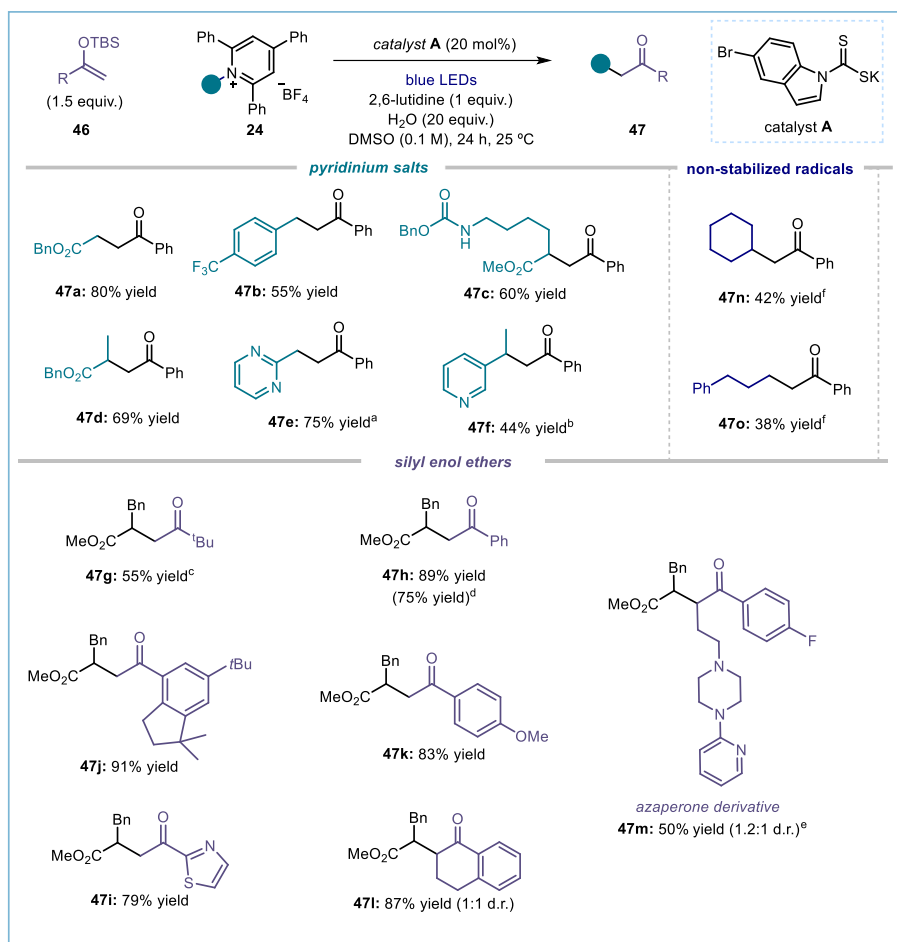


Figure 3.27. Redox-neutral addition of alkyl radicals to silyl enol ethers. Reactions performed on 0.2 mmol scale using 2.0 mL of DMSO; yields refer to isolated products **47** after purification. Unless otherwise indicated, all entries were performed at 25 °C. ^a40 °C; ^b60 °C; ^c1:1 mixture of DMSO/DCE used as solvent; ^ein the absence of water; ^fusing alkyl *N*-(acyloxy)phthalimides **23** as radical precursors. TBS: *tert*-butyldimethylsilyl.

Considering the different reaction mechanism of this redox-neutral transformation with respect to the previously described net-reductive transformations, we found it pertinent to measure the quantum yield of the reaction leading to product **47h**. The low quantum yield ($\Phi = 0.02$, $\lambda = 460$ nm) supported the mechanism depicted in Figure 3.25, where catalyst **A** can effectively deliver the product and be turned over.

Capitalizing on the unmatched polarity between the nucleophilic radical traps **43** and the nucleophilic radicals derived from redox active ester **23**, we questioned if we could develop an unreported three-component α -alkylation of enol ethers (Figure 3.28). The reaction would work as follows: upon light-promoted EDA activation of **23**, the nucleophilic radical would be trapped selectively by the electron-deficient olefin **42** forging the first new C-C bond. The ensuing electrophilic radical would then possess the right polarity to engage in a second C-C bond formation event with the electron-rich silyl enol ether **46**, affording the complex three-component product **48**. Eventually, the turn-over of the catalyst would rely on the same SET depicted in Figure 3.25. In this cascade reaction, catalyst **B** offered the best performance, allowing for the efficient construction of structurally complex products **48** from readily available redox-active derivatives of carboxylic acids.

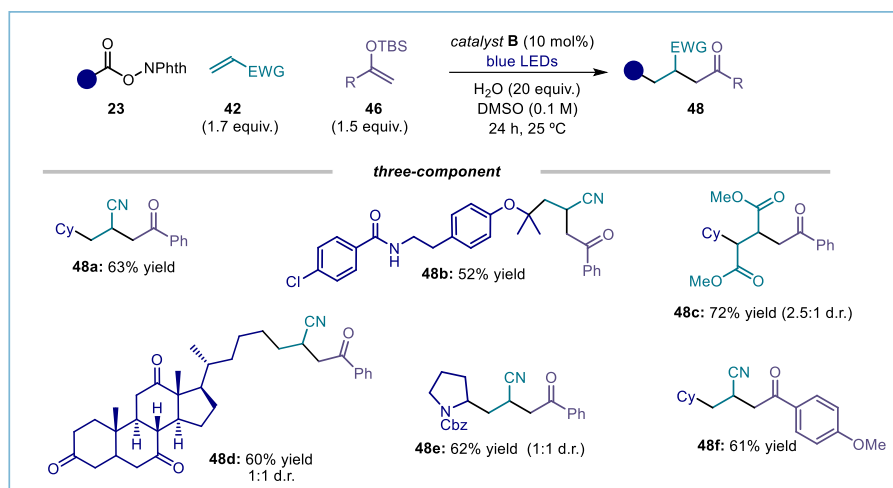


Figure 3.28. Three-component process under EDA complex catalysis; NPhth: phthalimide.

3.4.3 Minisci reaction³⁸

We also wondered if we could apply our system to develop a second redox-neutral transformation, namely the venerable Minisci reaction.³⁹ This process could not be realized with our nucleophilic substitution activation mechanism, due to the inability to generate highly reactive nucleophilic carbon-centered radicals. The Minisci reaction requires the addition of nucleophilic carbon-centered radicals **L** to electron-poor heteroaromatics **49**, and it represents one of the most useful approaches to directly modify heterocyclic pharmaceutical building blocks. Mechanistically, in analogy to the alkylation of enol ethers, a final oxidation step is required after radical addition to obtain the desired product **50** (Figure 3.29).⁴⁰ This oxidation step would be based on an exergonic SET between the sulphur radical **II** ($E^{\text{ox}} = 0.45$ V vs. SCE) and intermediate **LII** ($E^{\text{red}} = -1.01$ V vs. SCE).⁴¹ This step would also eventually regenerate the catalytically active anion **A**.

³⁸ The scope and optimization of the reaction detailed in this section has been performed by Wei Zhou. I performed the quantum yield measurement for this reaction.

³⁹ (a) Minisci, F.; Bernardi, R.; Bertini, F.; Galli, R.; Perchinummo, M. "Nucleophilic character of alkyl radicals—VI: A new convenient selective alkylation of heteroaromatic bases" *Tetrahedron* **1971**, *27*, 3575–3580. (b) Minisci, F.; Fontana, F.; Vismara, E. "Substitutions by nucleophilic free radicals: A new general reaction of heteroaromatic bases" *J. Heterocycl. Chem* **1990**, *27*, 79. (c) Duncton, M. A. J. "Minisci reactions: Versatile CH-functionalizations for medicinal chemists" *Med. Chem. Commun.* **2011**, *2*, 1135–1161. d) Wang, W. G.; Wang, S. F. "Recent Advances in Minisci-type Reactions and Applications in Organic Synthesis" *Cur. Org. Chem.* **2021**, *25*, 894–934.

⁴⁰ Proctor, R. S. J.; Phipps, R. J. "Recent Advances in Minisci-Type Reactions" *Angew. Chem. Int. Ed.* **2019**, *58*, 13666–13699.

⁴¹ Bieszczad, B.; Perego, L. A.; Melchiorre, P. "Photochemical C–H Hydroxyalkylation of Quinolines and Isoquinolines" *Angew. Chem. Int. Ed.* **2019**, *58*, 16878–16883.

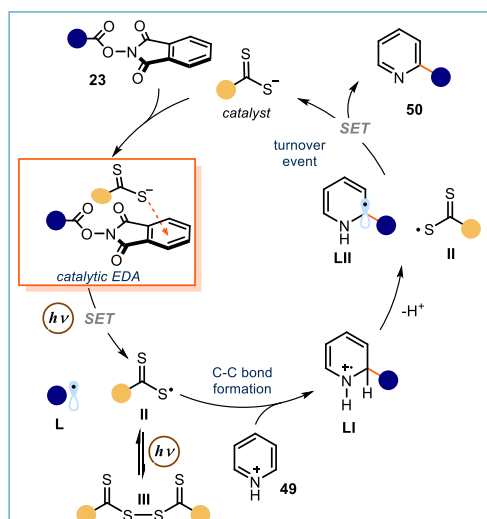


Figure 3.29. Mechanistic proposal for the EDA-complex-catalyzed Minisci reaction.

Based on the higher stability of catalyst **A** under the acidic conditions typically used for the activation of the heteroaromatic partner, this catalyst was selected as EDA catalytic donor. When the reaction between phthalimide esters **23** and 4-methyl quinoline was tested using 10 mol% of catalyst **A** in the presence of 0.75 equivalents of triflic acid, the desired product **50a** was isolated in 80% (Figure 3.30). We then surveyed the heterocycles that could undergo efficiently the desired Minisci reaction. The process worked for a broad range of compounds, allowing for the functionalization of quinolines (products **50a-c**), isoquinolines (product **50d**), and pyridines (product **50e**). Interestingly, a wide number of functional groups could be accommodated within the heterocycle scaffold without substantial erosion in efficiency. For example, protected amines (product **50g**), unprotected alcohols (product **50h-j**), and esters (products **50h-i**), were well tolerated. In addition, pharmaceutical relevant compounds, such as HIF prolyl-hydroxylase inhibitor *roxadustat*⁴² (products **50h-i**), the anti-cancer agent *camptothecin*⁴³ (product **50j**), and the neuroleptic drug azaperone (product **50k**), could be functionalized in good yields. Finally, by employing the redox-active ester derived from acetic acid, we managed to selectively methylate several heteroaromatic compounds (products **50c**, **50g**, and **50i**) by simply switching the solvent system from dimethylsulfoxide (DMSO) to dimethylacetamide (DMA).⁴⁴ Primary, secondary, and tertiary carbon-centered radicals could be installed easily into 2-methylquinoline using redox active ester **23** as radical precursor (products **50l-p**).

⁴² Dhillon, S. "Roxadustat: First Global Approval" *Drugs*, **2019**, *79*, 563–572.

⁴³ Tavangar, F.; Sepehri, H.; Jazi, S. M.; Asadi, J. "Amphotericin B potentiates the anticancer activity of doxorubicin on the MCF-7 breast cancer cells" *J Chem Biol*, **2017**, *10*, 143–150.

⁴⁴ For a review on the importance of methylation in medicinal chemistry: Aynetdinova, D.; Callens, M. C.; Hicks, H. B.; Poh, C. Y. X.; Shennan, B. D. A.; Boyd, A. M.; Lim, Z. H.; Leitch, J. A.; Dixon, D. J. "Installing the "magic methyl" – C–H methylation in synthesis" *Chem. Soc. Rev.* **2021**, *50*, 5517–5563.

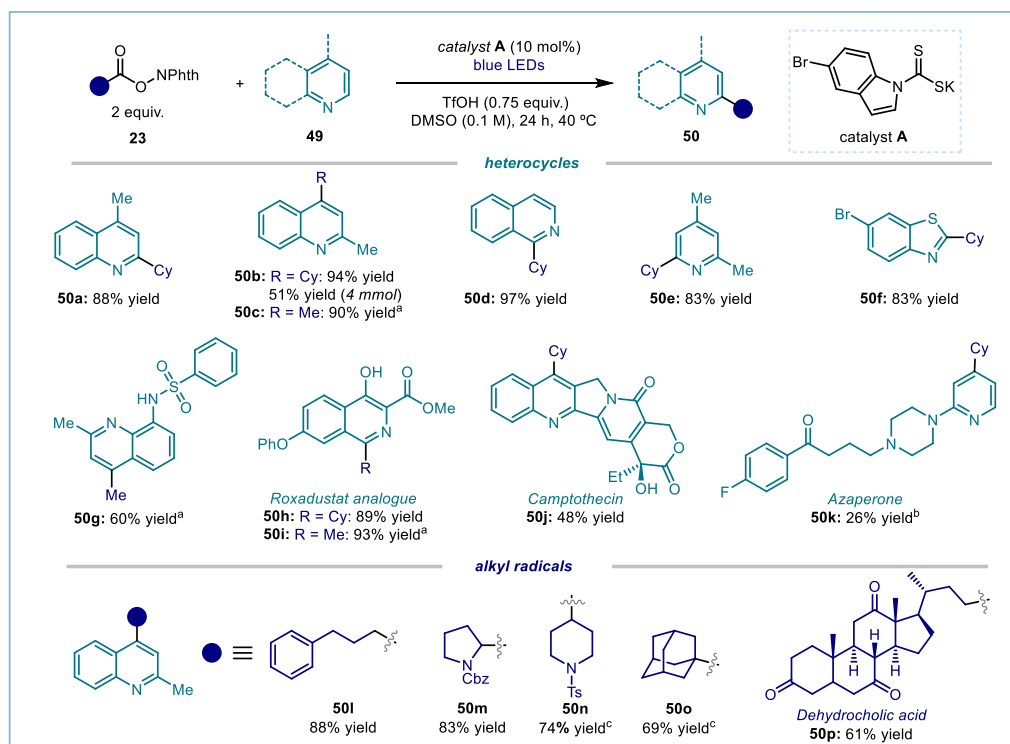


Figure 3.30. Minisci reaction. Reactions performed on 0.2 mmol scale in DMSO 0.1 M; yields refer to isolated products **50** after purification. ^aPerformed in NMP as solvent; ^b3 equiv. of TfOH; ^cperformed at 60 °C. Cy: cyclohexyl.; Ts: tosyl; NPhth: phthalimide.

In agreement with the other transformations developed using this catalytic EDA approach, also the quantum yield for the Minisci reaction leading to product **50b** was found to be lower than 0.01 ($\lambda = 460$ nm, using potassium ferrioxalate as the actinometer).

The combination of catalytic radical generation strategies with a second chiral catalyst that can induce stereocontrol over the bond formation event is becoming a common tool in organic chemistry for the development of new stereoselective transformations.^{3c, 45} To expand the synthetic potential of our methodology, we combined our catalytic EDA strategy for radical generation with the power of Brønsted acid catalysis to promote a stereoselective Minisci reaction. In 2018, Phipps and co-workers developed a stereoselective approach for Minisci reaction where the combination of a photoredox catalyst and a chiral phosphoric acid ((*R*)-TRIP) could promote the first example of this challenging transformation.³¹ Specifically, the photoredox system served to deliver prochiral radicals from α -amino acid derivatives of type **23** (Figure 3.31), while the chiral phosphoric acid exerted the double function to activate the heterocycle partner and to control the stereoselective C-C bond formation by coordinating the fleeting prochiral radical via hydrogen bonding interactions. When performing this transformation using catalyst **A** instead of a photoredox catalyst (Figure 3.31), we obtained the desired products (**50q** and **50r**) in high yield and enantioselectivity.

⁴⁵ (a) Le Saux, E.; Ma, D.; Bonilla, P.; Holden, C. M.; Lustosa, D.; Melchiorre, P. "A General Organocatalytic System for Enantioselective Radical Conjugate Additions to Enals" *Angew. Chem. Int. Ed.* **2021**, *60*, 5357–5362. (b) Li, Y.; Han, C.; Wang, Y.; Huang, X.; Zhao, X.; Qiao, B.; Jiang, Z. "Catalytic Asymmetric Reductive Azaarylation of Olefins via Enantioselective Radical Coupling" DOI: 10.1021/jacs.2c01458.

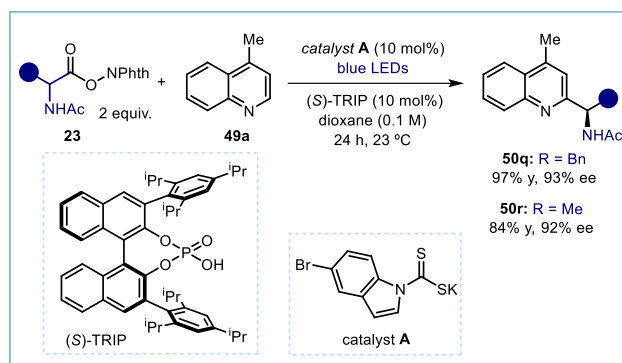


Figure 3.31 Application in enantioselective radical catalysis; Ac: acetyl; NPhth: phthalimide.

3.4.4 Further application of the EDA catalytic system⁴⁶

We further decided to explore the potential of our EDA catalytic radical generation approach by investigating other radical precursors that can engage in EDA complex formation. Specifically, we targeted the formation of a trifluoromethyl radical (Figure 3.32). Trifluoromethylation was accomplished using catalyst **A**, the Togni reagent **51** as the EDA complex acceptor, and the silyl enol ether **46a** as an effective trap, affording the α -trifluoromethylated ketone **52**.⁴⁷

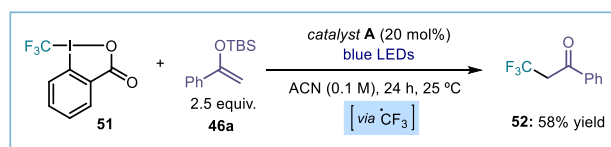


Figure 3.32. Trifluoromethylation of ketones via EDA complex catalysis.

We also used the xanthate catalyst **B** to generate an amidyl radical upon EDA complex activation of the dinitrophenoxy amide **19** (Figure 3.33).²⁶ Radical cyclization afforded the lactam product **53** in high yield.

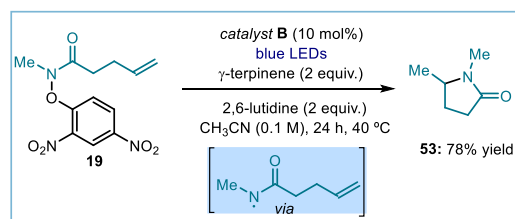


Figure 3.33 Amidyl radical formation and cyclization.

3.5 Conclusions

In summary, we have developed the first general catalytic EDA complex system based on our previously developed organic catalysts, which here acted as catalytic donors. This class of compounds could form photoactive EDA aggregates with a wide array of electron-poor redox-active radical precursors. Light-promoted intracomplex SET induced the formation of stabilized and non-stabilized radicals with different

⁴⁶ The optimization and isolation of products **52** and **53** was performed by Davide Spinnato.

⁴⁷ (a) Cheng, Y.; Yu, S. Hydrotrifluoromethylation of Unactivated Alkenes and Alkynes Enabled by an Electron-Donor-Acceptor Complex of Togni's Reagent with a Tertiary Amine. *Org. Lett.* **2016**, *18*, 2962–2965. (b) Tu, H.-Y.; Zhu, S.; Qing, F.-L.; Chu, L. A four-component radical cascade trifluoromethylation reaction of alkenes enabled by an electron-donor-acceptor complex. *Chem. Commun.* **2018**, *54*, 12710–12713.

electronic properties. The radicals generated in this way were then used in mechanistically different processes. Our previous knowledge of the catalyst behavior allowed us to develop redox neutral and net-reductive radical transformations. The ability of the catalyst to turn over and iteratively drive every catalytic cycle has been proven by quantum yield measurements for all the developed transformations. We also highlighted how the catalysts' stability and the method's high functional group tolerance could be advantageous for the direct radical functionalization of abundant functional groups, including aliphatic carboxylic acids and amines, and for applications in the late-stage elaboration of biorelevant compounds and enantioselective radical catalysis. Overall, all these aspects hint at the generality of the newly developed catalytic EDA complex platform and suggest that our approach might be useful to develop new synthetic transformations. This method is complementary to our previously reported methodology based on the same catalysts, since it relies on a different property of the radical precursor (redox properties instead of electrophilicity). In addition, also the radical generation event is different (SET vs C-S bond homolysis). These crucial differences granted access to stabilized and non-stabilized alkyl radicals, including heteroatom-centered radicals, and allowed us to perform reactions unachievable with the previous strategy.

3.6 Experimental section⁴⁸

3.6.1 General information

The NMR spectra were recorded at 400 MHz and 500 MHz for ¹H and 100 or 125 MHz for ¹³C. The chemical shift (δ) for ¹H and ¹³C are given in ppm relative to residual signals of the solvents (CHCl₃ @ 7.26 ppm ¹H NMR and 77.16 ppm ¹³C NMR, and tetramethylsilane @ 0 ppm). Coupling constants are given in Hertz. The following abbreviations are used to indicate the multiplicity: s, singlet; d, doublet; q, quartet; m, multiplet; bs, broad signal; app, apparent.

High resolution mass spectra (HRMS) were obtained from the ICIQ HRMS unit on MicroTOF Focus and Maxis Impact (Bruker Daltonics) with electrospray ionization. (ESI). UV-vis measurements were carried out on a Shimadzu UV-2401PC spectrophotometer equipped with photomultiplier detector, double beam optics and D₂ and W light sources or an Agilent Cary60 spectrophotometer. Emission spectra of light sources were recorded on Ocean Optics USB4000 fiber optic spectrometer.

Yields of isolated products refer to materials of >95% purity as determined by ¹H NMR.

General Procedures. All reactions were set up under an argon atmosphere in oven-dried glassware. Synthesis grade solvents were used as purchased, anhydrous solvents were taken from a commercial SPS solvent dispenser. Chromatographic purification of products was accomplished using forced-flow chromatography (FC) on silica gel (35-70 mesh). For thin layer chromatography (TLC) analysis throughout this work, Merck pre-coated TLC plates (silica gel 60 GF₂₅₄, 0.25 mm) were employed, using UV light as the visualizing agent and an acidic mixture of vanillin or basic aqueous potassium permanganate (KMnO₄) stain solutions, and heat as developing agents. Organic solutions were concentrated under reduced pressure on a Büchi rotatory evaporator.

Determination of Enantiomeric Purity. HPLC analysis on chiral stationary phase was performed on an Agilent 1200-series instrument, employing Daicel Chiralpak IC column.

⁴⁸ The ¹H NMR, ¹⁹F NMR, ¹³C NMR spectra and UPC² traces are available in the literature¹ and are not reported in the present dissertation.

Materials. Most of the starting materials used in this study are commercial and were purchased in the highest purity available from Sigma-Aldrich, Fluka, Alfa Aesar, Fluorochem, and used as received, without further purifications.

3.6.2 Substrate synthesis

The following substrates were synthesized according to reported procedures (Figure 3.34).⁴⁹

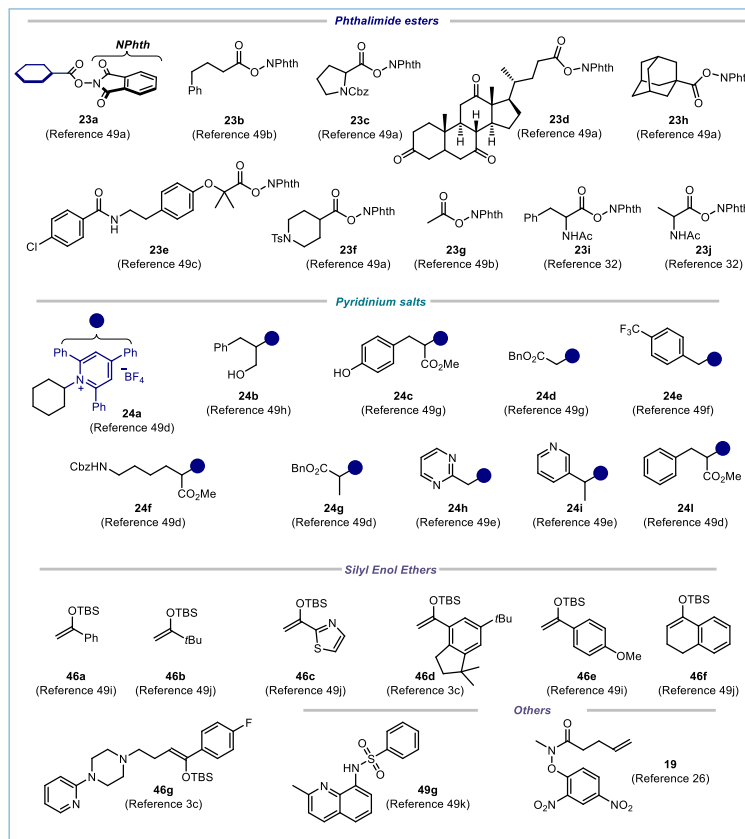


Figure 3.34. Starting materials synthesised according to known procedures.

⁴⁹ (a) Qin, T.; Malins, L. R.; Edwards, J. T.; Merchant, R. R.; Novak, A. J. E.; Zhong, J. Z.; Mills, R. B.; Yan, M.; Yuan, C.; Eastgate, M. D.; Baran, P. S. "Nickel-Catalyzed Barton Decarboxylation and Giese Reactions: A Practical Take on Classic Transforms" *Angew. Chem., Int. Ed.* **2017**, *56*, 260-265. (b) Huihui, K. M. M.; Caputo, J. A.; Melchor, Z.; Olivares, A. M.; Spiewak, A. M.; Johnson, K. A.; DiBenedetto, T. A.; Kim, S.; Ackerman, L. K. G.; Weix, D. J. "Decarboxylative Cross-Electrophile Coupling of N-Hydroxyphthalimide Esters with Aryl Iodides" *J. Am. Chem. Soc.* **2016**, *138*, 5016-5019. (c) Ishii, T.; Kakeno, Y.; Nagao, K.; Ohmiya, H. "N-Heterocyclic Carbene-Catalyzed Decarboxylative Alkylation of Aldehydes" *J. Am. Chem. Soc.* **2019**, *141*, 3854-3858. (d) Klauk F. J. R.; James M. J.; Glorius F. "Deaminative Strategy for the Visible-Light-Mediated Generation of Alkyl Radicals" *Angew. Chem., Int. Ed.* **2017**, *56*, 12336-12339. (e) Liao J.; Guan W.; Boscoe B. P.; Tucker J. W.; Tomlin J. W.; Garnsey M. R.; Watson M. P. "Transforming Benzylic Amines into Diarylmethanes: Cross-Couplings of Benzylic Pyridinium Salts via C-N Bond Activation" *Org. Lett.* **2018**, *20*, 3030-3033. (f) Xia Q.; Li Y.; Wang X.; Dai P.; Deng H.; Zhang W.-H. "Visible Light-Driven α -Alkylation of N-Aryl tetrahydroisoquinolines Initiated by Electron Donor-Acceptor Complexes" *Org. Lett.* **2020**, *22*, 7290-7294. (g) Laroche B.; Tang X.; Archer G.; Di Sanza R.; Melchiorre P. "Photochemical Chemoselective Alkylation of Tryptophan-Containing Peptides" *Org. Lett.* **2021**, *23*, 285-289. (h) Lai S.-Z.; Yang Y.-M.; Xu H.; Tang Z.-Y.; Luo Z. "Photoinduced Deaminative Coupling of Alkylpyridinium Salts with Terminal Arylalkynes" *J. Org. Chem.* **2020**, *85*, 15638-15644. (i) Perrotta D.; Racine S.; Vuilleumier J.; de Nanteuil F.; Waser J. "[4 + 2]-Annulations of Aminocyclobutanes" *Org. Lett.* **2015**, *17*, 1030-1033. (j) Li Y.; Liu J.; Zhao S.; Du X.; Guo M.; Zhao W.; Tang X.; Wang G. "Copper-Catalyzed Fluoroolefination of Silyl Enol Ethers and Ketones toward the Synthesis of β -Fluoroenones" *Org. Lett.* **2018**, *20*, 917-920. (k) Perez C.; Barkley-Levenson A. M.; Dick B. L.; Glatt P. F.; Martinez Y.; Siegel D.; Momper J. D.; Palmer A. A.; Cohen S. M. "Metal-Binding Pharmacophore Library Yields the Discovery of a Glyoxalase 1 Inhibitor" *J. Med. Chem.* **2019**, *62*, 1609-1625.

3.6.3 Experimental setups

3.6.3.1 Set-up 1 - 3D printed reactor with LED strip

For reactions performed using a blue LED strip as the light source, a 3D-printed photoreactor was used, consisting of a 9 cm diameter crystallizing dish with a 3D printed support of 6 positions, and a hole of 22 mm in the middle to allow ventilation (Figure 3.35, left). A commercial 1-meter LED strip was wrapped around the crystallizing dish, while a fan was used to cool down the reactor (the reaction temperature was measured to be between 35-40 °C). Each of the positions could be used to fit a standard 16 mm diameter vial with a Teflon screw cap. Experiments at 465 nm were conducted using a 1m strip, 14.4W “LEDXON MODULAR 9009083 LED, SINGLE 5050” purchased from Farnell, catalog number 9009083. The emission spectrum of these LEDs is shown in Figure 3.35, right panel.

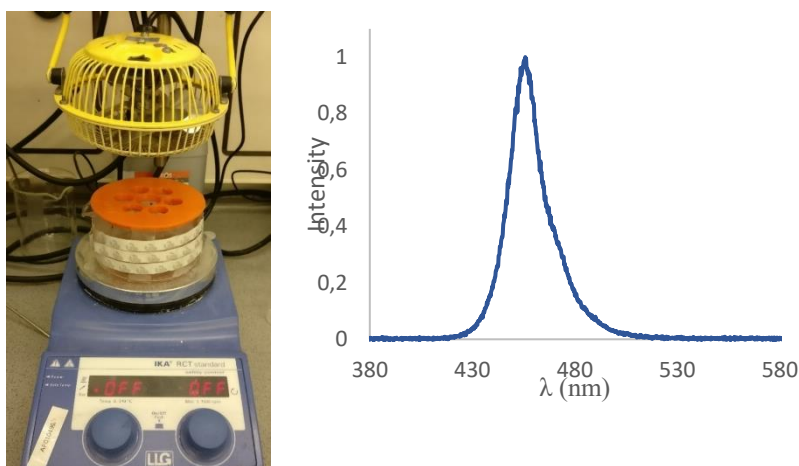


Figure 3.35. Blue LEDs photoreactor used for reactions where temperature control was not needed (*left*). Emission spectrum of the 465 nm LED strip used in this reactor (*right*).

3.6.3.2 Set-up 2 - Kessil lamp setup

For reactions performed with a Kessil lamp, the irradiation set-up consisted of a 50 W Kessil blue LED lamp (PR160L-456, 100% intensity, 2-3 cm away –Figure 3.35).

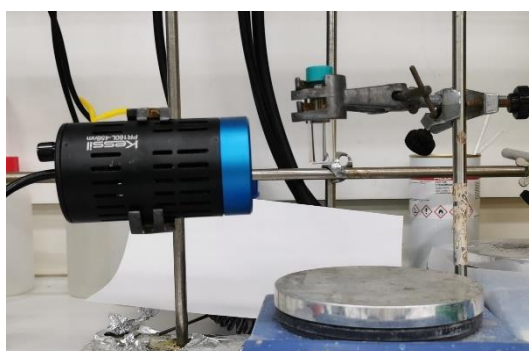


Figure 3.36. Kessil lamp set-up.

3.6.3.3 Set-up 3 - Temperature-controlled 4-position reactor with LED strip

For reactions where temperature control was employed, the photoreactor consisted of a 12.5 cm diameter jar fitted with 4 standard B29 size quickfit-glass joints arranged around a central B29 size joint. A

commercial 1-meter LED strip was wrapped around the jar, followed by a layer of aluminium foil and cotton for insulation (Figure 3.37).

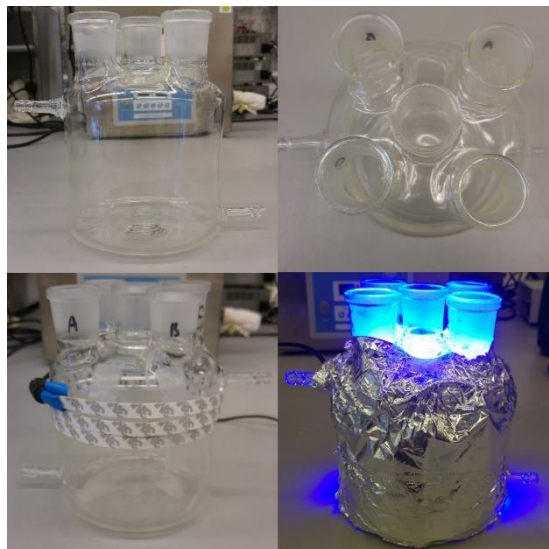


Figure 3.37. Photoreactor used for temperature-controlled reactions - pictures taken at different stages of the set-up assembly.

Each of the joints could be used to fit a standard 16 mm or 25 mm diameter Schlenk tube with a Teflon adaptor (Figure 3.37).



Figure 3.38. Teflon adaptors to use Schlenk tubes in the photoreactor.

An inlet/outlet system provided circulation of liquid (ethylene glycol/water mixture) from a Huber Minichiller 300 inside the jar. This setup allowed the performance of reactions at temperatures ranging from $-20\text{ }^{\circ}\text{C}$ to $80\text{ }^{\circ}\text{C}$ with accurate control of the reaction temperature ($\pm 1^{\circ}\text{C}$, Figure 3.38).

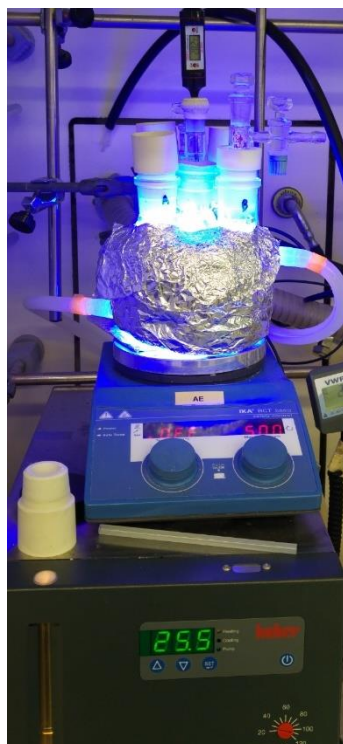


Figure 3.39. Fully assembled temperature-controlled photoreactor in operation.

In order to maintain consistent illumination between different experiments, only the four external positions were used to perform reactions. The central position was used to monitor the temperature using a thermometer inside another inserted Schlenk tube identical to those used to perform reactions, ensuring that the reaction mixtures were at the desired temperature.

3.6.3.4 Set-up 4 - Temperature controlled one-position reactor with LED strip

The set up for the enantioselective version of the Minisci reaction consisted of a consisted of a 4 cm diameter jar fitted with a standard 29 sized ground glass joint. A commercial 1 meter LED strip was wrapped around the jar, followed by a layer of aluminium foil and cotton for insulation. An inlet and an outlet allow the circulation of liquid from a Huber Minichiller 300 inside the jar. This setup allows to perform reactions at temperatures ranging from -20 °C to 80 °C with accurate control of the reaction temperature (± 1 °C). An inlet and an outlet allow the circulation of liquid from a Huber Minichiller 300 inside the jar. This setup allows to perform reactions at temperatures ranging from -20 °C to 80 °C with accurate control of the reaction temperature (± 1 °C, Figure 3.40).

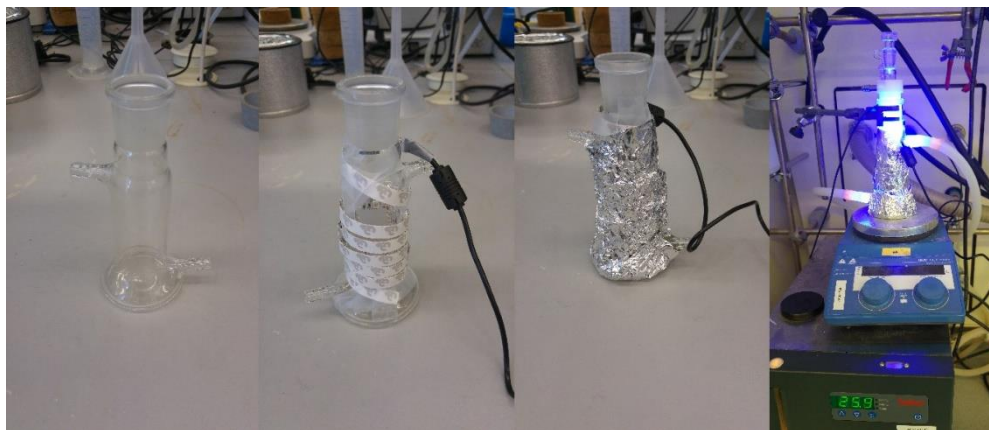
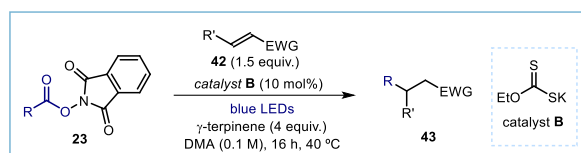


Figure 3.40. Fully assembled controlled temperature photoreactor in operation for enantioselective Minisci reaction.

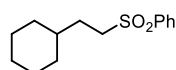
3.6.4 Giese addition

3.6.4.1 General procedure A



Reactions performed using *set-up 1* in Figure 3.34. In an oven dried vial with a Teflon septum screw cap, potassium ethyl xanthogenate **B** (3.2 mg, 0.02 mmol, 0.1 equiv.), *N*-hydroxyphthalimide ester **23** (0.2 mmol, 1 equiv.) and the electron-poor olefin **42** (0.3 mmol, 1.5 equiv., *if solid*), were dissolved in DMA (2 mL, synthesis grade solvent). Then, γ -terpinene (128 μ L, 0.8 mmol, 4 equiv.) was added. The resulting orange mixture was degassed with argon sparging for 60 seconds. If the electron-poor olefin **42** was *liquid*, it was added via syringe after the argon sparging. The vial was then placed in the 3D printed support photoreactor and irradiated under stirring for 16 hours, unless otherwise specified. The mixture was transferred to an extraction funnel, NaOH 1M solution was added, and the organic layer was extracted with DCM. The organic layer was washed with brine twice. The combined organic layers were dried over anhydrous $MgSO_4$, filtered, and concentrated to dryness. The crude residue was purified by column chromatography to afford the corresponding product **43** in the stated yield with >95% purity according to 1H NMR analysis.

3.6.4.2 Characterization of products with general procedure A

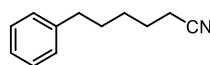


2-cyclohexylethyl)sulfonyl)benzene (33a): Synthesized according to General Procedure A using 1,3-dioxoisindolin-2-yl cyclohexanecarboxylate **23a** (54.5 mg, 0.2 mmol, 1 equiv.) and phenyl vinyl sulfone **42a** (50.4 mg, 0.3 mmol, 1.5 equiv.). The crude mixture was purified by flash column chromatography on silica gel (5% AcOEt in hexanes as eluent) to afford **33a** (43.5 mg, 86% yield) as a white solid.

1H NMR (500 MHz, $CDCl_3$) δ 7.94 – 7.85 (m, 2H), 7.69 – 7.61 (m, 1H), 7.61 – 7.52 (m, 2H), 3.13 – 3.05 (m, 2H), 1.71 – 1.54 (m, 7H), 1.28 (ddt, $J = 14.6, 7.5, 3.8$ Hz, 1H), 1.23 – 1.06 (m, 3H), 0.92 – 0.76 (m, 2H).

^{13}C NMR (126 MHz, $CDCl_3$) δ 139.4, 133.7, 129.4, 128.2, 54.5, 36.8, 32.9, 29.7, 26.4, 26.1.

Matching reported literature data.⁵⁰



6-phenylhexanenitrile (43b): Synthesized according to General Procedure A using 5 equiv. of γ -terpinene, 1,3-dioxoisindolin-2-yl 4-phenylbutanoate **23b** (62 mg, 0.2 mmol, 1 equiv.) and acrylonitrile **42b** (26.3 μ L, 0.4 mmol, 2 equiv.). The crude mixture was purified by flash column chromatography on silica gel (5% AcOEt in hexanes as eluent) to afford **43b** (21 mg, 61% yield) as a yellow oil.

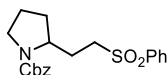
1H NMR (400 MHz, $CDCl_3$) δ 7.33 – 7.24 (m, 2H), 7.23 – 7.14 (m, 3H), 2.64 (t, $J = 7.6$ Hz, 2H), 2.33 (t, $J = 7.1$ Hz, 2H), 1.75 – 1.62 (m, 4H), 1.54 – 1.42 (m, 2H).

^{13}C NMR (101 MHz, $CDCl_3$) δ 142.1, 128.5, 128.5, 126.0, 119.9, 35.7, 30.7, 28.4, 25.4, 17.2.

Matching reported literature data.⁵¹

⁵⁰ Chen, X.; Luo, X.; Peng, X.; Guo, J.; Zai, J.; Wang, P. "Catalyst-Free Decarboxylation of Carboxylic Acids and Deoxygenation of Alcohols by Electro-Induced Radical Formation" *Chem. Eur. J.* **2020**, *26*, 3226-3230.

⁵¹ Bhunia, A.; Bergander, K.; Studer, A., Cooperative Palladium/Lewis Acid-Catalyzed Transfer Hydrocyanation of Alkenes and Alkynes Using 1-Methylcyclohexa-2,5-diene-1-carbonitrile. *J. Am. Chem. Soc.* **2018**, *140*, 16353-16359.

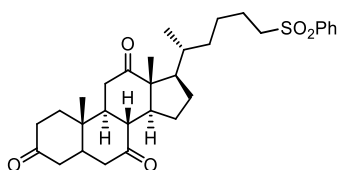


Benzyl 2-(2-(phenylsulfonyl)ethyl)pyrrolidine-1-carboxylate (43h): Synthesized according to General Procedure A using 1-benzyl 2-(1,3-dioxoisindolin-2-yl)pyrrolidine-1,2-dicarboxylate **23c** (54.5 mg, 0.2 mmol, 1 equiv.) and phenyl vinyl sulfone **42a** (50.4 mg, 0.3 mmol, 1.5 equiv.). The crude mixture was purified by flash column chromatography on silica gel (20% AcOEt in hexanes as eluent) to afford **43h** (56 mg, 75% yield) as a white solid.

¹H NMR (400 MHz, CDCl₃) mixture of rotamers: δ 7.96 – 7.77 (m, 2H), 7.68 – 7.60 (m, 1H), 7.54 (d, *J* = 7.5 Hz, 2H), 7.40 – 7.20 (m, 5H), 5.05 (d, *J* = 7.6 Hz, 2H), 3.94 (d, *J* = 9.9 Hz, 1H), 3.58 – 3.28 (m, 2H), 3.27 – 2.91 (m, 2H), 2.23 – 1.74 (m, 5H), 1.63 (ddd, *J* = 11.3, 5.5, 3.0 Hz, 1H).

¹³C NMR (101 MHz, CDCl₃) mixture of rotamers: δ 155.5, 139.3, 136.9, 133.8, 129.4, 128.6, 128.1, 127.9, 67.2, 66.9, 56.5, 55.9, 54.0, 53.7, 46.9, 46.5, 31.2, 30.7, 27.9, 23.8, 23.1.

Matching reported literature data.⁵²



((5S,8R,9S,10S,13R,14S,17R)-10,13-dimethyl-17-(6-(phenylsulfonyl)hexan-2-yl)dodecahydro-3H-cyclopenta[a]phenanthrene-3,7,12(2H,4H)-trione (43k): Synthesized according to General Procedure A using 1,3-dioxoisindolin-2-yl 4-((5S,8R,9S,10S,13R,14S,17R)-10,13-dimethyl-3,7,12-

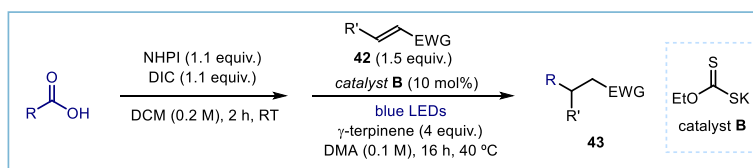
trioxohexadecahydro-1H-cyclopenta[a]phenanthren-17-yl)pentanoate **23d** (54.5 mg, 0.2 mmol, 1 equiv.) and phenyl vinyl sulfone **42a** (50.4 mg, 0.3 mmol, 1.5 equiv.). The crude mixture was purified by flash column chromatography on silica gel (50% AcOEt in hexanes as eluent) to afford **43k** (48.0 mg, 46% yield) as a white solid.

¹H NMR (400 MHz, CDCl₃) δ 7.95 – 7.85 (m, 2H), 7.70 – 7.61 (m, 1H), 7.61 – 7.53 (m, 2H), 3.16 – 3.00 (m, 2H), 2.95 – 2.78 (m, 3H), 2.38 – 2.17 (m, 6H), 2.16 – 2.06 (m, 2H), 2.02 – 1.90 (m, 4H), 1.88 – 1.52 (m, 5H), 1.47 – 1.30 (m, 1H), 1.39 (s, 3H), 1.32 – 1.12 (m, 5H), 1.04 (s, 3H), 0.78 (d, *J* = 6.6 Hz, 3H).

¹³C NMR (101 MHz, CDCl₃) δ 212.1, 209.1, 208.9, 139.4, 133.8, 129.4, 128.2, 57.0, 56.5, 51.9, 49.1, 47.0, 45.8, 45.7, 45.1, 42.9, 38.8, 36.6, 36.2, 35.9, 35.4, 34.9, 28.0, 25.4, 25.3, 23.1, 22.0, 19.0, 12.0.

Matching reported literature data.^{49a}

3.6.4.3 General procedure B (one-pot telescoped from carboxylic acids)

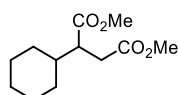


Reactions performed using *set-up 1* in Figure 3.34. In an oven dried vial with a Teflon septum screw cap, carboxylic acid (0.2 mmol, 1 equiv.) and *N*-hydroxyphthalimide (NHPI, 35.8 mg, 0.22 mmol, 1.1 equiv.) were dissolved in CH₂Cl₂ (1 mL, HPLC grade) and *N,N'*-diisopropylcarbodiimide (DIC, 34 μL, 0.22 mmol, 1.1 equiv.) was added via syringe. The reaction was stirred at ambient temperature until complete consumption of the carboxylic acid was observed by TLC (usually 1-2 hours). The crude reaction mixture was concentrated under vacuum to obtain the crude phthalimide ester, which was used without further purification in the next step.

⁵² Chu, L.; Ohta, C.; Zuo, Z.; MacMillan, D. W. C., Carboxylic Acids as A Traceless Activation Group for Conjugate Additions: A Three-Step Synthesis of (±)-Pregabalin. *J. Am. Chem. Soc.* **2014**, *136*, 10886-10889.

In the same vial containing the crude phthalimide ester, xanthogenate **B** (3.2 mg, 0.02 mmol, 0.1 equiv.) and the electron-poor olefin **42** (0.3 mmol, 1.5 equiv., *if solid*) were dissolved in DMA (2 mL, synthesis grade). Next, γ -terpinene (128 μ L, 0.8 mmol, 4 equiv.) was added and the resulting orange mixture was degassed with argon sparging for 60 seconds. If the electron-poor olefin **42** was *liquid*, it was added via syringe after the argon sparging. The vial was then placed in the 3D printed support photoreactor and irradiated under stirring for 16 hours, if not otherwise specified. The mixture was transferred to an extraction funnel, NaOH 1M solution was added and the organic layer was extracted with CH_2Cl_2 . The organic layer was washed with brine twice. The combined organic layers were dried over anhydrous MgSO_4 , filtered, and concentrated to dryness. The crude residue was purified by column chromatography to afford the corresponding product in the stated yield with >95% purity according to ^1H NMR analysis.

3.6.4.4 Characterization of products with general procedure B

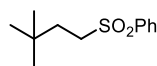


dimethyl 2-cyclohexylsuccinate (43c): Synthesized according to General Procedure B using 2 equiv. of γ -terpinene, cyclohexanecarboxylic acid (25.6 mg, 0.2 mmol, 1 equiv.) and dimethyl fumarate **42c** (43 mg, 0.3 mmol, 1.5 equiv.). The crude mixture was purified by flash column chromatography on silica gel (5% AcOEt in hexanes as eluent) to afford **43c** (44 mg, 95% yield) as a yellow oil.

^1H NMR (500 MHz, CDCl_3) δ 3.69 (s, 3H), 3.66 (s, 3H), 2.78 – 2.66 (m, 2H), 2.45 (dt, $J = 13.1, 8.9$ Hz, 1H), 1.78 – 1.69 (m, 2H), 1.69 – 1.52 (m, 4H), 1.31 – 1.15 (m, 2H), 1.15 – 1.07 (m, 1H), 1.06 – 0.92 (m, 2H).

^{13}C NMR (126 MHz, CDCl_3) δ 175.1, 173.1, 51.9, 51.7, 47.2, 40.1, 33.4, 30.8, 30.3, 26.4, 26.3.

Matching reported literature data.⁵⁰

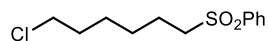


((3,3-dimethylbutyl)sulfonyl)benzene (43d): Synthesized according to General Procedure B using pivalic acid (20.4 mg, 0.2 mmol, 1 equiv.) and phenyl vinyl sulfone **42a** (50.4 mg, 0.3 mmol, 1.5 equiv.). The crude mixture was purified by flash column chromatography on silica gel (7% AcOEt in hexanes as eluent) to afford **43d** (33.0 mg, 73% yield) as a yellow oil.

^1H NMR (400 MHz, CDCl_3) δ 7.98 – 7.85 (m, 2H), 7.71 – 7.62 (m, 1H), 7.65 – 7.53 (m, 2H), 3.10 – 3.01 (m, 2H), 1.64 – 1.55 (m, 2H), 0.86 (s, 9H).

^{13}C NMR (101 MHz, CDCl_3) δ 142.1, 128.5, 128.5, 126.0, 119.9, 35.7, 30.7, 28.4, 25.4, 17.2.

Matching reported literature data.⁵⁰



((7-chloroheptyl)sulfonyl)benzene (43e): Synthesized according to General Procedure B using 5-Chlorovaleric acid (27.3 mg, 0.2 mmol, 1 equiv.) and phenyl vinyl sulfone **42a** (50.4 mg, 0.3 mmol, 1.5 equiv.). The crude mixture was purified by flash column chromatography on silica gel (20% DCM in hexanes as eluent) to afford **43e** (29.1 mg, 56% yield) as a white solid.

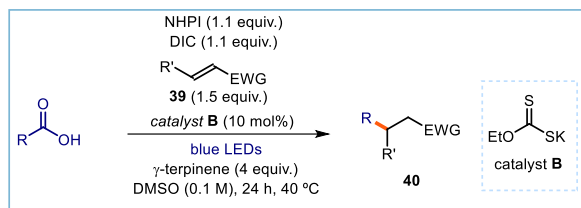
^1H NMR (400 MHz, CDCl_3) δ 7.95 – 7.88 (m, 2H), 7.69 – 7.64 (m, 1H), 7.61 – 7.55 (m, 2H), 3.50 (t, $J = 6.5$ Hz, 2H), 3.12 – 3.05 (m, 2H), 1.77 – 1.71 (m, 4H), 1.44 – 1.39 (m, 4H).

^{13}C NMR (101 MHz, CDCl_3) δ 139.3, 133.8, 129.4, 128.2, 56.3, 44.9, 32.2, 29.8, 27.7, 26.4, 22.7.

Matching reported literature data.⁵³

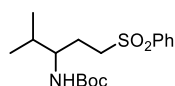
⁵³ Li, D.; Ma, T.-K.; Scott, R. J.; Wilden, J. D. "Electrochemical radical reactions of alkyl iodides: a highly efficient, clean, green alternative to tin reagents" *Chem. Sci.* **2020**, *11*, 5333-5338.

3.6.4.5 General procedure C (one-pot domino from carboxylic acids)



Reactions performed using *set-up 1*. In an oven dried vial with a Teflon septum screw cap, carboxylic acid (0.2 mmol, 1 equiv.), *N*-hydroxyphthalimide (NHPI, 35.8 mg, 0.22 mmol, 1.1 equiv.), xanthogenate catalyst **B** (3.2 mg, 0.02 mmol, 0.1 equiv.), and the electron-poor olefin **42** (0.3 mmol, 1.5 equiv., *if solid*) were dissolved in DMSO (2 mL) and *N,N'*-diisopropylcarbodiimide (DIC, 34 μ L, 0.22 mmol, 1.1 equiv.) was added via syringe. Next, γ -terpinene (128 μ L, 0.8 mmol, 4 equiv.) was added and the resulting orange mixture was degassed with argon sparging for 60 seconds. If the electron-poor olefin **32** were *liquid*, it was added via syringe after the argon sparging. The vial was then placed in the 3D printed support photoreactor and irradiated under stirring for 24 hours, unless otherwise specified. The mixture was transferred to an extraction funnel, NaOH 1M solution was added and the organic layer was extracted with CH_2Cl_2 . The organic layer was washed with brine twice. The combined organic layers were dried over anhydrous MgSO_4 , filtered, and concentrated to dryness. The crude residue was purified by column chromatography to afford the corresponding product in the stated yield with >95% purity according to ^1H NMR analysis.

3.6.4.6 Characterization of products with general procedure C

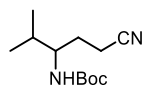


tert-butyl (4-methyl-1-(phenylsulfonyl)pentan-3-yl)carbamate (43f): Synthesized according to General Procedure C using NMP as solvent, L-valine (43.5 mg, 0.2 mmol, 1 equiv.) and phenyl vinyl sulfone **42a** (50.4 mg, 0.3 mmol, 1.5 equiv.). The crude mixture was purified by flash column chromatography on silica gel (25% AcOEt in hexanes as eluent) to afford **43f** (63 mg, 92% yield) as a white solid.

^1H NMR (500 MHz, CDCl_3) δ 7.93 – 7.88 (m, 2H), 7.69 – 7.63 (m, 1H), 7.57 (dd, J = 8.4, 7.1 Hz, 2H), 4.32 (d, J = 10.1 Hz, 1H), 3.42 (td, J = 10.4, 4.8 Hz, 1H), 3.15 (ddd, J = 9.1, 6.1, 1.7 Hz, 2H), 1.93 (tdd, J = 12.1, 7.4, 3.4 Hz, 1H), 1.82 – 1.61 (m, 2H), 1.40 (s, 9H), 0.87 (dd, J = 10.0, 6.8 Hz, 6H).

^{13}C NMR (126 MHz, CDCl_3) δ 156.1, 139.4, 133.9, 129.5, 128.1, 79.7, 54.7, 54.1, 32.8, 28.5, 25.9, 19.2, 17.8.

Matching reported literature data.⁵⁴



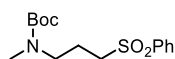
tert-butyl (1-cyano-4-methylpentan-3-yl)carbamate (43g): Synthesized according to General Procedure C using 5 equiv. of γ -terpinene, L-valine (43.5 mg, 0.2 mmol, 1 equiv.) and acrylonitrile **42b** (26.3 μ L, 0.4 mmol, 2 equiv.). The crude mixture was purified by flash column chromatography on silica gel (15% AcOEt in hexanes as eluent) to afford **43g** (27 mg, 60% yield) as a yellow oil.

^1H NMR (400 MHz, CDCl_3) δ 4.34 (d, J = 9.9 Hz, 1H), 3.45 (tdd, J = 10.4, 5.5, 3.4 Hz, 1H), 2.49 – 2.30 (m, 2H), 1.90 (td, J = 11.7, 9.8, 5.5 Hz, 1H), 1.72 (dt, J = 13.0, 6.5 Hz, 1H), 1.62 (td, J = 15.0, 14.5, 9.7 Hz, 1H), 1.44 (s, 9H), 0.91 (dd, J = 10.4, 6.8 Hz, 6H).

^{13}C NMR (101 MHz, CDCl_3) δ 156.1, 119.9, 79.7, 55.4, 32.5, 29.4, 28.5, 19.2, 17.9, 14.7.

⁵⁴ Yoshimi, Y.; Masuda, M.; Mizunashi, T.; Nishikawa, K.; Maeda, K.; Koshida, N.; Itou, T.; Morita, T.; Hatanaka, M. "Inter- and Intramolecular Addition Reactions of Electron-Deficient Alkenes with Alkyl Radicals, Generated by SET-Photochemical Decarboxylation of Carboxylic Acids, Serve as a Mild and Efficient Method for the Preparation of γ -Amino Acids and Macrocylic Lactones" *Org. Lett.* **2009**, *11*, 4652-4655.

Matching reported literature data.⁵¹



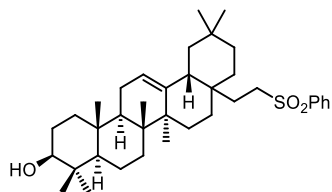
tert-butyl methyl(3-(phenylsulfonyl)propyl)carbamate (43i): Synthesized according to General Procedure C using *N*-(tert-butoxycarbonyl)-*N*-methylglycine (38 mg, 0.2

mmol, 1 equiv.) and phenyl vinyl sulfone **42a** (50.4 mg, 0.3 mmol, 1.5 equiv.). The crude mixture was purified by flash column chromatography on silica gel (20% AcOEt in hexanes as eluent) to afford **43i** (47 mg, 75% yield) as a yellow oil.

¹H NMR (400 MHz, CDCl₃) mixture of rotamers: δ 7.94 – 7.86 (m, 2H), 7.70 – 7.62 (m, 1H), 7.57 (dd, *J* = 8.3, 6.8 Hz, 2H), 3.29 (t, *J* = 6.8 Hz, 2H), 3.11 – 2.99 (m, 2H), 2.79 (s, 3H), 1.99 – 1.87 (m, 2H), 1.40 (s, 9H).

¹³C NMR (101 MHz, CDCl₃) mixture of rotamers: δ 155.9, 139.2, 133.9, 129.5, 128.1, 79.9, 53.9, 47.4, 34.3, 28.5, 21.0.

HRMS: calculated for C₁₅H₂₃NNaO₄S (M+Na⁺): 336.1240, found 336.1236 (+1.2 ppm).



(3*S*,4*aR*,6*aR*,6*bS*,12*aR*,14*aR*,14*bR*)-4,4,6*a*,6*b*,11,11,14*b*-heptamethyl-8*a*-(2-(phenylsulfonyl)ethyl)-1,2,3,4,4*a*,5,6,6*a*,6*b*,7,8,8*a*,9,10,11,12,12*a*,14,14*a*,14*b*-

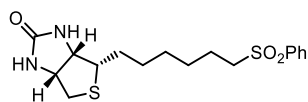
icosahydricen-3-ol (43j): Synthesized according to General Procedure C using NMP as solvent, oleanolic acid (91 mg, 0.2 mmol, 1

equiv) and phenyl vinyl sulfone **42a** (50.4 mg, 0.3 mmol, 1.5 equiv.). The crude mixture was purified by flash column chromatography on silica gel (40% AcOEt in hexanes as eluent) to afford **43j** (84 mg, 72% yield) as light-yellow solid.

¹H NMR (400 MHz, CDCl₃) δ 7.90 – 7.84 (m, 2H), 7.67 – 7.59 (m, 1H), 7.58 – 7.50 (m, 2H), 5.15 (t, *J* = 3.6 Hz, 1H), 3.19 (dd, *J* = 10.7, 4.8 Hz, 1H), 3.01 (dtd, *J* = 37.9, 13.5, 4.3 Hz, 2H), 2.01 – 1.76 (m, 7H), 1.66 (t, *J* = 13.5 Hz, 1H), 1.62 – 1.36 (m, 7H), 1.37 – 1.26 (m, 3H), 1.23 – 1.11 (m, 4H), 1.09 (s, 3H), 1.02 (dd, *J* = 13.7, 2.1 Hz, 1H), 0.97 (s, 3H), 0.94 – 0.90 (m, 1H), 0.88 (s, 3H), 0.85 (s, 3H), 0.82 (s, 3H), 0.77 (s, 3H), 0.68 (dd, *J* = 11.5, 1.9 Hz, 1H), 0.60 (s, 3H).

¹³C NMR (101 MHz, CDCl₃) δ 143.6, 139.3, 133.6, 129.4, 128.1, 123.1, 79.0, 55.2, 51.6, 47.6, 46.9, 46.5, 41.6, 39.7, 38.9, 38.7, 37.0, 34.7, 34.3, 33.2, 32.9, 32.5, 31.9, 31.0, 29.8, 28.2, 27.3, 26.1, 25.5, 23.6, 23.3, 18.4, 16.5, 15.7, 15.6.

Matching reported literature data.^{49a}



(3*aS*,4*S*,6*aR*)-4-(6-(phenylsulfonyl)hexyl)tetrahydro-1*H*-thieno[3,4-*d*]imidazol-2(3*H*)-one (43l): Synthesized according to General Procedure C using 4 mL of DMSO, biotin (49 mg, 0.2 mmol, 1 equiv.) and phenyl

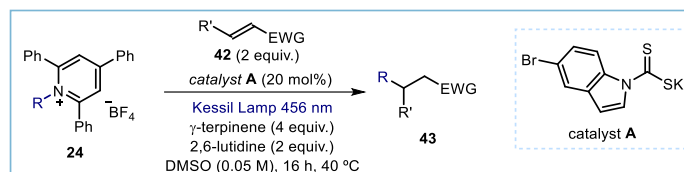
vinyl sulfone **42a** (50.4 mg, 0.3 mmol, 1.5 equiv.). The crude mixture was purified by flash column chromatography on silica gel (2-5% MeOH in DCM as eluent) to afford **43l** (48 mg, 65% yield) as a yellow oil.

¹H NMR (500 MHz, Methanol-*d*₄) δ 7.99 – 7.89 (m, 2H), 7.77 – 7.70 (m, 1H), 7.72 – 7.58 (m, 2H), 4.53 – 4.46 (m, 1H), 4.29 (ddd, *J* = 12.2, 7.9, 4.5 Hz, 1H), 3.24 – 3.19 (m, 2H), 3.19 – 3.14 (m, 1H), 2.92 (dt, *J* = 12.7, 5.1 Hz, 1H), 2.70 (dd, *J* = 12.7, 4.4 Hz, 1H), 1.66 (tdd, *J* = 15.3, 8.3, 4.4 Hz, 3H), 1.53 (ddd, *J* = 16.8, 8.8, 5.5 Hz, 1H), 1.45 – 1.27 (m, 6H).

¹³C NMR (101 MHz, CDCl₃) δ 164.5, 139.2, 133.8, 129.4, 128.1, 62.4, 60.8, 56.1, 55.8, 40.6, 31.4, 31.0, 28.8, 28.7, 28.4, 27.9, 22.7, 22.5, 14.1.

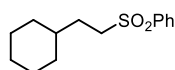
HRMS: calculated for $C_{17}H_{24}N_2NaO_3S_2$ ($M+Na^+$): 391.1120, found 391.1121 (-0.3 ppm).

3.6.4.7 General procedure D (using pyridinium salts)



Reactions performed using **set-up 2** in Figure 3.35. In an oven dried vial, with a Teflon septum screw cap, dithiocarbamate **A** (12.4 mg, 0.04 mmol, 0.2 equiv.), pyridinium salt **24** (0.2 mmol, 1 equiv.) and the electron-poor olefin **42** (0.4 mmol, 2 equiv.), were dissolved in DMSO (4 mL). Then, γ -terpinene (128 μ L, 0.8 mmol, 4 equiv.) and 2,6-lutidine (46 μ L, 0.4 mmol, 2 equiv.) were added. The resulting orange mixture was degassed with argon sparging for 60 seconds. The vial was then placed at 2-3 cm of a 50 W Kessil blue LED lamp and irradiated under stirring for 16 hours. The mixture was transferred to an extraction funnel, $NaHCO_3$ sat. solution was added and the organic layer was extracted with EtOAc. The organic layer was washed with brine twice. The combined organic layers were dried over anhydrous $MgSO_4$, filtered, and concentrated to dryness. The crude residue was purified by column chromatography to afford the corresponding product in the stated yield with >95% purity according to 1H NMR analysis.

3.6.4.8 Characterization of products with general procedure D

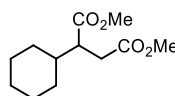


((2-cyclohexylethyl)sulfonyl)benzene (43a): Synthesized according to General Procedure D using 1-cyclohexyl-2,4,6-triphenylpyridin-1-ium tetrafluoroborate **24a** (95 mg, 0.2 mmol, 1 equiv.) and phenyl vinyl sulfone **42a** (67 mg, 0.4 mmol, 2 equiv.). The crude mixture was purified by flash column chromatography on silica gel (10% AcOEt in hexanes as eluent) to afford **43a** (34 mg, 67% yield) as a white solid.

1H NMR (500 MHz, $CDCl_3$) δ 7.94 – 7.85 (m, 2H), 7.69 – 7.61 (m, 1H), 7.61 – 7.52 (m, 2H), 3.13 – 3.05 (m, 2H), 1.71 – 1.54 (m, 7H), 1.28 (ddt, $J = 14.6, 7.5, 3.8$ Hz, 1H), 1.23 – 1.06 (m, 3H), 0.92 – 0.76 (m, 2H).

^{13}C NMR (126 MHz, $CDCl_3$) δ 139.4, 133.7, 129.4, 128.2, 54.5, 36.8, 32.9, 29.7, 26.4, 26.1.

Matching reported literature data.⁴⁷

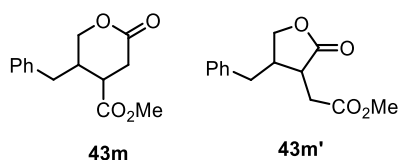


dimethyl 2-cyclohexylsuccinate (43c): Synthesized according to General Procedure D using 2 equiv. of γ -terpinene, 1-cyclohexyl-2,4,6-triphenylpyridin-1-ium tetrafluoroborate **24a** (95 mg, 0.2 mmol, 1 equiv.) and dimethyl fumarate **42c** (57 mg, 0.4 mmol, 2 equiv.). The crude mixture was purified by flash column chromatography on silica gel (5% AcOEt in hexanes as eluent) to afford **43c** (41 mg, 90% yield) as a yellow oil.

1H NMR (400 MHz, $CDCl_3$) δ 3.69 (s, 3H), 3.66 (s, 3H), 2.78 – 2.66 (m, 2H), 2.45 (dt, $J = 13.1, 8.9$ Hz, 1H), 1.78 – 1.69 (m, 2H), 1.69 – 1.52 (m, 4H), 1.31 – 1.15 (m, 2H), 1.15 – 1.07 (m, 1H), 1.06 – 0.92 (m, 2H).

^{13}C NMR (126 MHz, $CDCl_3$) δ 175.1, 173.1, 51.9, 51.7, 47.2, 40.1, 33.4, 30.8, 30.3, 26.4, 26.3.

Matching reported literature data.⁴⁷



methyl 5-benzyl-2-oxotetrahydro-2H-pyran-4-carboxylate (43m): Synthesized according to General Procedure D using 2 equiv. of γ -terpinene, 1-(1-hydroxy-3-phenylpropan-2-yl)-2,4,6-triphenylpyridin-1-ium tetrafluoroborate **24b** (106 mg, 0.2 mmol, 1 equiv.) and dimethyl fumarate **42c** (57 mg, 0.4 mmol, 2 equiv.).

The crude mixture was purified by flash column chromatography on silica gel (10% AcOEt in hexanes as eluent) to afford an unseparable mixture of regioisomers **43m/43m'** (**3.8:1**) (27 mg, 54% yield) as a yellow oil. Corrected yield for **43m** (42% yield)

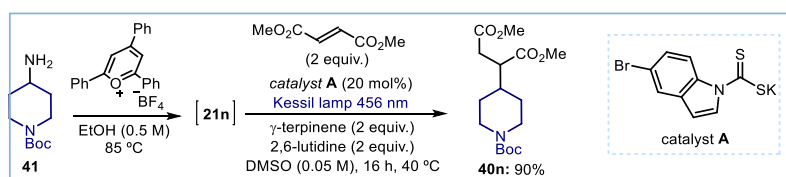
Products formed upon intramolecular esterification promoted by the acidic conditions delivered by the silica during purification.

¹H NMR (400 MHz, CDCl₃) mixture of regioisomers δ 7.35 – 7.28 (m, 2.5H), 7.28 – 7.21 (m, 1.25H), 7.19 – 7.10 (m, 2.5H), 4.35 – 4.28 (m, 1H), 4.14 – 4.06 (m, 0.5H), 3.96 – 3.88 (m, 1H), 3.74 (s, 0.75H), 3.69 (s, 3H), 3.31 – 3.23 (m, 0.25H), 3.05 – 2.85 (m, 1.5H), 2.85 – 2.66 (m, 3.25H), 2.63 (d, $J = 10.2$ Hz, 0.25H), 2.61 – 2.55 (m, 2H), 2.34 (dd, $J = 13.7, 11.9$ Hz, 0.25H).

¹³C NMR (101 MHz, CDCl₃) mixture of regioisomers: δ 177.8, 171.6, 137.8, 129.1, 129.0, 129.0, 128.7, 127.1, 126.9, 71.4, 70.1, 52.3, 52.2, 42.4, 42.0, 40.8, 39.7, 38.4, 33.6, 33.3, 30.2, 29.8.

HRMS: calculated for C₁₄H₁₆NaO₄ (M+Na⁺): 271.0941, found 271.0939 (+0.7 ppm).

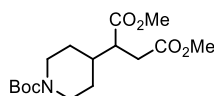
3.6.4.9 General procedure E (telescoped reaction from amine)



Reactions performed using *set-up 2* in Figure 3.35. In an oven dried vial, with a Teflon septum screw cap, primary amine (0.22 mmol, 1.1 equiv.) and 2,4,6-triphenylpyridinium tetrafluoroborate (79.2 mg, 0.2 mmol, 1 equiv.) were dissolved in ethanol (0.4 mL, HPLC grade). The reaction was stirred at 80 °C for 4 hours. In the same vial without evaporating the solvent, dithiocarbamate **A** (12.4 mg, 0.04 mmol, 0.2 equiv.), electron-poor olefin **42** (0.4 mmol, 2 equiv.), DMSO (4 mL), γ -terpinene (64 μ L, 0.4 mmol, 2 equiv.) and 2,6-lutidine (46 μ L, 0.4 mmol, 2 equiv.) were added sequentially. The resulting orange mixture was degassed with argon sparging for 60 seconds. The vial was then placed at 2-3 cm of a 50 W Kessil blue LED lamp and irradiated under stirring for 16 hours. The mixture was transferred to an extraction funnel, saturated aqueous NaHCO₃ was added, and the organic layer extracted with EtOAc. The organic layer was washed with brine twice. The combined organic layers were dried over anhydrous MgSO₄, filtered, and concentrated to dryness. The crude residue was purified by column chromatography to afford the corresponding product in the stated yield with >95% purity according to ¹H NMR analysis.

A control experiment without catalyst **A** delivered no conversion of the pyridinium salt upon irradiation.

3.6.4.10 Characterization of products with general procedure E



dimethyl 2-(1-(tert-butoxycarbonyl)piperidin-4-yl)succinate (43n): Synthesized according to General Procedure E using 2 equiv. of γ -terpinene, *tert*-butyl 4-aminopiperidine-1-carboxylate (40 mg, 0.2 mmol, 1 equiv.) and dimethyl fumarate

42c (57 mg, 0.4 mmol, 2 equiv.). The crude mixture was purified by flash column chromatography on silica gel (0-40% AcOEt in hexanes as eluent) to afford **43n** (59 mg, 90% yield) as a yellow oil.

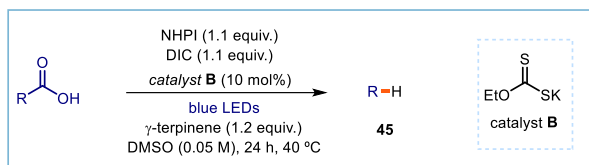
¹H NMR (400 MHz, CDCl₃) δ 4.12 (d, *J* = 13.3 Hz, 2H), 3.70 (s, 3H), 3.66 (s, 3H), 2.81 – 2.68 (m, 2H), 2.63 (tt, *J* = 13.0, 3.0 Hz, 2H), 2.52 – 2.41 (m, 1H), 1.73 (tdd, *J* = 12.3, 6.1, 3.6 Hz, 1H), 1.57 (ddt, *J* = 23.3, 13.0, 3.0 Hz, 2H), 1.44 (s, 9H), 1.34 – 1.15 (m, 2H).

¹³C NMR (126 MHz, CDCl₃) δ 174.7, 172.9, 155.1, 79.9, 52.2, 46.6, 44.2, 38.7, 33.6, 33.6, 29.9, 29.7, 28.8, 28.8.

HRMS: calculated for C₁₆H₂₇NNaO₆ (M+Na⁺): 352.1731, found 352.1726. (+1.4 ppm).

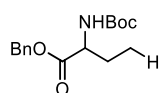
3.6.5 Reduction

3.6.5.1 General procedure F (Barton decarboxylation)



Reactions performed using **set-up 1** in Figure 3.34. In an oven dried vial, with a Teflon septum screw cap, carboxylic acid (0.2 mmol, 1 equiv.), *N*-hydroxyphthalimide (NHPI, 35.8 mg, 0.22 mmol, 1.1 equiv.) and xanthogenate **B** (3.2 mg, 0.02 mmol, 0.1 equiv.) were dissolved in DMSO (4 mL) and *N,N'*-diisopropylcarbodiimide (DIC, 34 μL, 0.22 mmol, 1.1 equiv.) was added via syringe. Then, γ-terpinene (38 μL, 0.24 mmol, 1.2 equiv.) was added. The resulting orange mixture was degassed with argon sparging for 60 seconds. The vial was then placed in the 3D printed support photoreactor and irradiated under stirring for 24 hours, unless otherwise specified. The mixture was transferred to an extraction funnel, NaOH 1M solution was added and the organic layer was extracted with CH₂Cl₂. The organic layer was washed with brine twice. The combined organic layers were dried over anhydrous MgSO₄, filtered, and concentrated to dryness. The crude residue was purified by column chromatography to afford the corresponding product in the stated yield with >95% purity according to ¹H NMR analysis.

3.6.5.2 Characterization of products with general procedure F

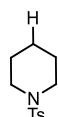


benzyl (*S*)-2-((tert-butoxycarbonyl)amino)butanoate (45a): Synthesized according to General Procedure F using (*S*)-5-(benzyloxy)-4-((tert-butoxycarbonyl)amino)-5-oxopentanoic acid (67 mg, 0.2 mmol, 1 equiv.). The crude mixture was purified by flash column chromatography on silica gel (25% AcOEt in hexanes as eluent) to afford **45a** (38 mg, 65% yield) as a yellow oil.

¹H NMR (400 MHz, CDCl₃) δ 7.41 – 7.28 (m, 5H), 5.24 – 5.10 (m, 2H), 5.04 (d, *J* = 8.3 Hz, 1H), 4.30 (t, *J* = 7.1 Hz, 1H), 1.93 – 1.80 (m, 1H), 1.69 (dt, *J* = 14.2, 7.2 Hz, 1H), 1.44 (s, 9H), 0.90 (t, *J* = 7.5 Hz, 3H).

¹³C NMR (101 MHz, CDCl₃) δ 172.8, 155.5, 135.6, 128.7, 128.5, 128.4, 79.9, 67.1, 54.8, 28.5, 26.1, 9.7.

Matching reported literature data.^{49a}

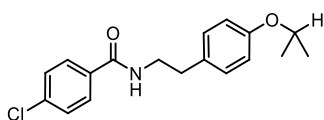


1-tosylpiperidine (45b): Synthesized according to General Procedure F using 1-tosylpiperidine-4-carboxylic acid (57 mg, 0.2 mmol, 1 equiv.). The crude mixture was purified by flash column chromatography on silica gel (10% AcOEt in hexanes as eluent) to afford **45b** (37 mg, 77% yield) as a white solid.

¹H NMR (500 MHz, CDCl₃) δ 7.66 – 7.60 (m, 2H), 7.34 – 7.28 (m, 2H), 2.99 – 2.93 (m, 4H), 2.42 (s, 3H), 1.63 (p, *J* = 5.9 Hz, 4H), 1.40 (tt, *J* = 8.2, 4.7 Hz, 2H).

¹³C NMR (126 MHz, CDCl₃) δ 143.4, 133.5, 129.7, 127.8, 47.1, 25.3, 23.7, 21.6.

Matching reported literature data.^{49a}



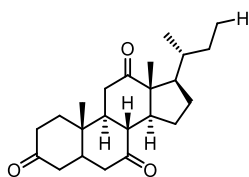
4-chloro-N-(4-isopropoxyphenethyl)benzamide (45c): Synthesized according to General Procedure F using Bezafibrate (72 mg, 0.2 mmol, 1 equiv.). The crude mixture was purified by flash column chromatography on silica gel (25% AcOEt in hexanes as eluent) to afford **45c** (32 mg, 50%

yield) as a white solid.

¹H NMR (400 MHz, CDCl₃) mixture of rotamers: δ 7.65 – 7.59 (m, 2H), 7.37 (dd, *J* = 8.6, 2.0 Hz, 2H), 7.15 – 7.04 (m, 2H), 6.89 – 6.79 (m, 2H), 6.13 (s, 1H), 4.52 (p, *J* = 6.1 Hz, 1H), 3.67 (qd, *J* = 6.7, 6.3, 3.7 Hz, 2H), 2.85 (t, *J* = 6.9 Hz, 2H), 1.33 (d, *J* = 6.1 Hz, 6H).

¹³C NMR (101 MHz, CDCl₃) mixture of rotamers: δ 166.6, 156.8, 137.8, 133.1, 130.6, 130.0, 129.9, 129.0, 128.4, 116.3, 115.8, 70.1, 41.5, 34.8, 22.2.

HRMS: calculated for C₁₆H₁₈ClN₄NaO (M+Na⁺): 340.1061, found 340.1075 (+4.1 ppm).



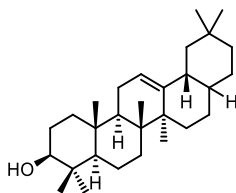
(5S,8R,9S,10S,13R,14S,17R)-17-(sec-butyl)-10,13-dimethyldodecahydro-3H-cyclopenta[a]phenanthrene-3,7,12(2H,4H)-trione (45d): Synthesized according to General Procedure F using dehydrocholic acid (81 mg, 0.2 mmol, 1 equiv.). The crude mixture was purified by flash column chromatography on silica gel (30% AcOEt in hexanes as eluent) to afford **45d** (37 mg, 51% yield) as

a light-yellow solid.

¹H NMR (400 MHz, CDCl₃) δ 2.96 – 2.80 (m, 3H), 2.39 – 2.17 (m, 6H), 2.13 (dd, *J* = 12.5, 4.8 Hz, 2H), 2.09 – 1.90 (m, 4H), 1.85 (td, *J* = 11.2, 7.0 Hz, 1H), 1.68 – 1.56 (m, 2H), 1.52 – 1.44 (m, 1H), 1.40 (s, 3H), 1.35 – 1.20 (m, 3H), 1.20 – 1.10 (m, 1H), 1.07 (s, 3H), 0.85 (dd, *J* = 15.9, 6.9 Hz, 6H).

¹³C NMR (101 MHz, CDCl₃) δ 212.2, 209.2, 208.9, 57.0, 52.0, 49.2, 47.0, 45.7, 45.6, 45.1, 42.9, 38.8, 37.6, 36.6, 36.2, 35.4, 28.0, 27.8, 25.4, 22.1, 18.6, 12.0, 11.0.

Matching reported literature data.^{49a}



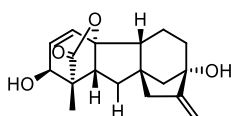
(3S,4aR,6aR,6bS,12aR,14aR,14bR)-4,4,6a,6b,11,11,14b-heptamethyl-1,2,3,4,4a,5,6,6a,6b,7,8,8a,9,10,11,12,12a,14,14a,14b-icosahydropicen-3-ol (45e): Synthesized according to General Procedure F using oleanolic acid (91 mg, 0.2 mmol, 1 equiv.). The crude mixture was purified by flash column chromatography on silica gel (15% AcOEt in hexanes as eluent) to afford **45e** (74

mg, 90% yield) as white solid.

¹H NMR (400 MHz, CDCl₃) δ 5.19 (t, *J* = 3.7 Hz, 1H), 3.22 (ddz, *J* = 11.0, 5.0 Hz, 1H), 2.34 (dt, *J* = 13.7, 4.8 Hz, 1H), 1.91 – 1.83 (m, 2H), 1.83 – 1.75 (m, 1H), 1.74 – 1.65 (m, 2H), 1.65 – 1.58 (m, 4H), 1.5 – 1.54 (m, 2H), 1.50 – 1.31 (m, 6H), 1.29 – 1.17 (m, 4H), 1.11 (d, *J* = 0.9 Hz, 3H), 1.08 – 1.04 (m, 1H), 1.02 – 0.96 (m, 4H), 0.93 (s, 3H), 0.89 (s, 3H), 0.87 (s, 6H), 0.79 (s, 3H), 0.77 – 0.70 (m, 1H).

¹³C NMR (101 MHz, CDCl₃) δ 146.1, 121.2, 79.2, 55.4, 47.9, 45.1, 42.6, 41.1, 39.3, 38.9, 38.6, 37.3, 35.9, 33.8, 33.8, 33.2, 31.3, 31.2, 29.9, 28.3, 28.1, 27.4, 25.2, 24.0, 23.5, 22.4, 18.6, 17.6, 15.8, 15.5.

Matching reported literature data.^{49a}



(1S,2S,4aR,4bR,7S,9aR,10aR)-2,7-dihydroxy-1-methyl-8-methylene-1,2,4b,5,6,7,8,9,10,10a-decahydro-4a,1-(epoxymethano)-7,9a-methanobenzo[a]azulen-13-one (45f): Synthesized according to General

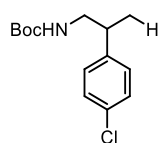
Procedure F using gibberellic acid (69 mg, 0.2 mmol, 1 equiv.). The crude mixture was purified by flash

column chromatography on silica gel (40% AcOEt in hexanes as eluent) to afford **45f** (36 mg, 60% yield) as a white solid.

¹H NMR (400 MHz, Acetone-*d*₆) δ 6.34 (dd, *J* = 9.3, 0.9 Hz, 1H), 5.85 (dd, *J* = 9.3, 3.7 Hz, 1H), 5.16 (td, *J* = 2.5, 1.1 Hz, 1H), 4.81 (tt, *J* = 2.1, 1.0 Hz, 1H), 4.56 – 4.50 (m, 1H), 4.01 (dd, *J* = 6.4, 3.6 Hz, 1H), 3.71 (s, 1H), 2.85 – 2.74 (m, 1H), 2.40 (q, *J* = 2.0 Hz, 2H), 2.03 – 2.00 (m, 1H), 1.91 (dd, *J* = 13.6, 8.2 Hz, 1H), 1.87 – 1.80 (m, 2H), 1.79 – 1.65 (m, 3H), 1.61 (dd, *J* = 13.6, 11.0 Hz, 1H), 1.53 – 1.47 (m, 1H), 1.21 (s, 3H).

¹³C NMR (101 MHz, Acetone-*d*₆) δ 179.6, 160.6, 134.0, 133.3, 105.7, 92.8, 78.9, 70.2, 54.5, 52.3, 50.2, 48.2, 45.9, 40.1, 36.4, 30.2, 17.6, 15.2.

HRMS: calculated for C₁₈H₂₂NaO₄ (M+Na⁺): 325.1410, found 325.1400 (–3.3 ppm).



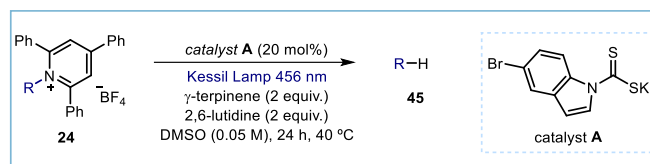
tert-butyl (2-(4-chlorophenyl)propyl)carbamate (45g): Synthesized according to General Procedure F using 4-((*tert*-butoxycarbonyl)amino)-3-(4-chlorophenyl)butanoic acid (63 mg, 0.2 mmol, 1 equiv.). The crude mixture was purified by flash column chromatography on silica gel (10% AcOEt in hexanes as eluent) to afford **45g** (40 mg, 74% yield) as colorless oil.

¹H NMR (400 MHz, CDCl₃) δ 7.34 – 7.20 (m, 2H), 7.17 – 7.07 (m, 2H), 4.41 (s, 1H), 3.35 (s, 1H), 3.15 (dd, *J* = 13.6, 8.3 Hz, 1H), 2.91 (q, *J* = 7.1 Hz, 1H), 1.41 (s, 9H), 1.24 (d, *J* = 7.0 Hz, 3H).

¹³C NMR (101 MHz, CDCl₃) δ 156.0, 142.9, 132.4, 129.8, 128.8, 128.8, 128.6, 47.4, 39.8, 28.5, 28.5, 19.2, 1.2.

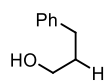
Matching reported literature data.⁵⁵

3.6.5.3 General procedure G (deaminative reduction)



Reactions performed using **set-up 2** in Figure 3.35. In an oven dried vial, with a Teflon septum screw cap, dithiocarbamate **A** (12.4 mg, 0.04 mmol, 0.2 equiv.) and pyridinium salt **24** (0.2 mmol, 1 equiv.) were dissolved in DMSO (4 mL). Then, γ -terpinene (64 μ L, 0.4 mmol, 2 equiv.) and 2,6-lutidine (46 μ L, 0.4 mmol, 2 equiv.) were added. The resulting orange mixture was degassed with argon sparging for 60 seconds. The vial was then placed at 2-3 cm of a 50 W Kessil blue LED lamp and irradiated under stirring for 16 hours. The mixture was transferred to an extraction funnel, NaHCO₃ sat. solution was added and the organic layer was extracted with EtOAc. The organic layer was washed with brine twice. The combined organic layers were dried over anhydrous MgSO₄, filtered, and concentrated to dryness. The crude residue was purified by column chromatography to afford the corresponding product in the stated yield with >95% purity according to ¹H NMR analysis.

3.6.5.4 Characterization of products with general procedure G



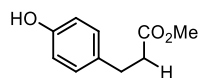
3-phenylpropan-1-ol (45h): Synthesized according to General Procedure G using 1-(1-hydroxy-3-phenylpropan-2-yl)-2,4,6-triphenylpyridin-1-ium tetrafluoroborate **24b** (106 mg, 0.2 mmol, 1 equiv.). The crude mixture was purified by flash column chromatography on silica gel (15% AcOEt in pentane as eluent) to afford **45h** (21 mg, 77% yield) as a colorless oil.

⁵⁵ Steiman, T. J.; Liu, J.; Mengiste, A.; Doyle, A. G., Synthesis of β -Phenethylamines via Ni/Photoredox Cross-Electrophile Coupling of Aliphatic Aziridines and Aryl Iodides. *J. Am. Chem. Soc.* **2020**, *142*, 7598-7605.

¹H NMR (400 MHz, CDCl₃) δ 7.33 – 7.26 (m, 2H), 7.23 – 7.17 (m, 3H), 3.68 (t, *J* = 6.4 Hz, 2H), 2.72 (dd, *J* = 8.7, 6.8 Hz, 2H), 1.96 – 1.85 (m, 2H).

¹³C NMR (101 MHz, CDCl₃) δ 141.9, 128.6, 128.5, 126.0, 62.4, 34.4, 32.2.

Matching reported literature data.⁵⁶



methyl 3-(4-hydroxyphenyl)propanoate (45i): Synthesized according to General Procedure G using 1-(3-(4-hydroxyphenyl)-1-methoxy-1-oxopropan-2-yl)-2,4,6-triphenylpyridin-1-ium tetrafluoroborate **24c** (115 mg, 0.2 mmol, 1 equiv.). The crude mixture was purified by flash column chromatography on silica gel (0–40% AcOEt in hexanes as eluent) to afford **45i** (28 mg, 78% yield) as a colorless oil.

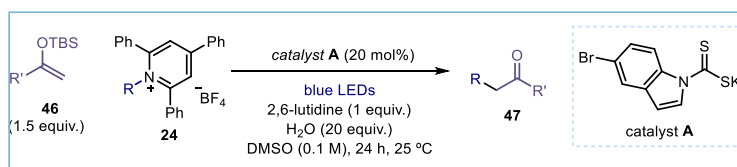
¹H NMR (400 MHz, CDCl₃) δ 7.04 (d, *J* = 8.4 Hz, 2H), 6.79 – 6.71 (m, 2H), 5.74 (s, 1H), 3.67 (s, 3H), 2.88 (t, *J* = 7.7 Hz, 2H), 2.61 (dd, *J* = 9.0, 6.5 Hz, 2H).

¹³C NMR (101 MHz, CDCl₃) δ 174.1, 154.4, 132.4, 129.5, 115.5, 51.9, 36.2, 30.2.

Matching reported literature data.⁵⁷

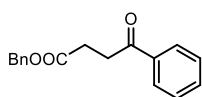
3.6.6 α -Alkylation of silyl enol ethers

3.6.6.1 General procedure H



Reactions performed using *set-up 3* in Figure 3.36. In an oven dried vial with a Teflon septum screw cap, silyl enol ether **43** (0.3 mmol, 1.5 equiv.) was dissolved in DMSO (2 mL), followed by addition of 2,6-lutidine (23 μ L, 0.2 mmol, 1.0 equiv.), pyridinium salt **24** (0.2 mmol, 1.0 equiv.), catalyst **A** (12.4 mg, 0.04 mmol, 0.2 equiv.) and water (4.0 mmol, 20 equiv.). The resulting orange mixture was degassed by bubbling argon for 60 seconds. The vial was then placed in the irradiation setup, maintained at a temperature of 25 °C (25–26 °C measured in the central well), and the reaction was stirred for 24 hours under continuous irradiation from a blue LED strip, unless otherwise stated. The crude mixture was diluted with EtOAc and brine was added. The layers were separated, and the aqueous layer extracted with EtOAc ($\times 3$). The combined organic fractions were dried over anhydrous MgSO₄, filtered, and concentrated to dryness. The crude residue was purified by column chromatography on silica gel to afford the corresponding product in the stated yield with >95% purity according to ¹H NMR analysis.

3.6.6.2 Characterization of products with general procedure H



Benzyl 4-oxo-4-phenylbutanoate (47a): Prepared according to General Procedure H using *set-up 3* (75% intensity). 2,6-lutidine (46 μ L, 0.4 mmol, 2 equiv.), *tert*-butyldimethyl((1-phenylvinyl)oxy)silane **42a** (70 mg, 0.4 mmol, 2 equiv.) and 1-(2-(benzyloxy)-2-oxoethyl)-2,4,6-triphenylpyridin-1-ium tetrafluoroborate **24d** (109 mg, 0.2 mmol, 1 equiv.). Flash column chromatography (hexanes/EtOAc 95:5) to afford product **47a** as an off-white oil (43 mg, 80% yield).

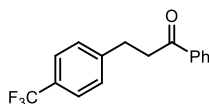
⁵⁶ Vechorkin, O.; Proust, V.; Hu, X., Functional Group Tolerant Kumada–Corriu–Tamao Coupling of Nonactivated Alkyl Halides with Aryl and Heteroaryl Nucleophiles: Catalysis by a Nickel Pincer Complex Permits the Coupling of Functionalized Grignard Reagents. *J. Am. Chem. Soc.* **2009**, *131*, 9756–9766.

⁵⁷ Percec, V.; Peterca, M.; Sienkowska, M. J.; Ilies, M. A.; Aqad, E.; Smidkral, J.; Heiney, P. A., Synthesis and Retrostructural Analysis of Libraries of AB₃ and Constitutional Isomeric AB₂ Phenylpropyl Ether-Based Supramolecular Dendrimers. *J. Am. Chem. Soc.* **2006**, *128*, 3324–3334.

¹H NMR (300 MHz, CDCl₃) δ 8.03 – 7.94 (m, 2H), 7.56 (m, 1H), 7.46 (m, 2H), 7.40 – 7.23 (m, 5H), 5.15 (s, 3H), 3.34 (t, *J* = 6.6 Hz, 2H), 2.83 (t, *J* = 6.6 Hz, 2H).

¹³C NMR (75 MHz, CDCl₃) δ 198.2, 172.9, 136.7, 136.0, 133.4, 128.8, 128.7, 128.4, 128.2, 66.7, 33.5, 28.43.

Matching reported literature data.⁵⁸



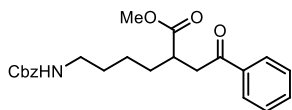
1-phenyl-3-(4-(trifluoromethyl)phenyl)propan-1-one (47b): Prepared according to General Procedure H using *tert*-butyldimethyl((1-phenylvinyl)oxy)silane **42a** (70 mg, 0.3 mmol) and 2,4,6-triphenyl-1-(4-(trifluoromethyl)benzyl)pyridin-1-ium tetrafluoroborate **24e** (111 mg, 0.2 mmol). Time of irradiation: 24 hours at 25 °C. Flash column chromatography (Toluene) to afford product **47b** as a white solid (35 mg, 55% yield).

¹H NMR (300 MHz, CDCl₃) δ 7.97 – 7.90 (m, 2H), 7.59 – 7.50 (m, 3H), 7.48 – 7.44 (m, 2H), 7.41 – 7.35 (m, 2H), 3.33 (t, *J* = 7.5 Hz, 2H), 3.15 (t, *J* = 7.5 Hz, 2H).

¹³C NMR (75 MHz, CDCl₃) δ 198.2, 145.5, 136.8, 136.8, 133.4, 129.1, 128.8, 128.7, 128.1, 125.4 (q, *J* = 3.9 Hz), 124.5 (q, *J* = 270 Hz), 39.9, 29.9.

¹⁹F NMR (376 MHz, CDCl₃) δ –62.49.

Matching reported literature data.⁵⁹



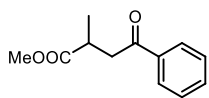
Methyl 6-(((benzyloxy)carbonyl)amino)-2-(2-oxo-2-phenylethyl)hexanoate (47c): Prepared according to General Procedure H using *tert*-butyldimethyl((1-phenylvinyl)oxy)silane **42a** (70 mg, 0.3 mmol) and (±)-1-(6-(((benzyloxy)carbonyl)amino)-1-methoxy-1-oxohexan-2-yl)-2,4,6-triphenylpyridin-1-ium tetrafluoroborate **24f** (135 mg, 0.2 mmol). Flash column chromatography (hexanes/EtOAc 7:3 to 1:1) to afford product **47c** as a yellowish oil (53 mg, 67% yield).

¹H NMR (400 MHz, CDCl₃) δ 7.99 – 7.93 (m, 2H), 7.60 – 7.54 (m, 1H), 7.49 – 7.44 (m, 2H), 7.36 – 7.30 (m, 5H), 5.09 (s, 2H), 4.76 (s, 1H), 3.69 (s, 3H), 3.56 – 3.34 (m, 1H), 3.20 (q, *J* = 6.7 Hz, 2H), 3.15 – 2.99 (m, 2H), 1.77 – 1.50 (m, 5H), 1.39 (m, 1H).

¹³C NMR (101 MHz, CDCl₃) δ 198.2, 176.1, 156.5, 136.8, 136.7, 133.4, 128.8, 128.7, 128.3, 128.2, 66.8, 52.0, 40.9, 40.6, 40.3, 31.9, 29.9, 24.5.

¹³C NMR (101 MHz, CDCl₃) δ 198.2, 176.1, 156.5, 136.8, 136.7, 133.4, 128.8, 128.7, 128.3, 128.2, 66.8, 52.0, 40.9, 40.6, 40.3, 31.9, 29.9, 24.5.

HRMS: calculated for C₂₃H₂₇NNaO₅ (M+Na⁺): 420.1781, found 420.1771 (+2.3 ppm).



Benzyl 2-methyl-4-oxo-4-phenylbutanoate (47d): Prepared according to General Procedure H using *tert*-butyldimethyl((1-phenylvinyl)oxy)silane **42a** (70 mg, 0.3 mmol) and (±)-1-(1-(benzyloxy)-1-oxopropan-2-yl)-2,4,6-triphenylpyridin-1-ium tetrafluoroborate **24g** (111 mg, 0.2 mmol). Time of irradiation: 24 hours at 25 °C. Flash column chromatography (hexanes/EtOAc 98:2 to 90:10) to afford product **47d** as a yellowish oil (39 mg, 69% yield).

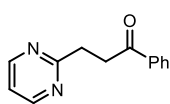
¹H NMR (300 MHz, CDCl₃) δ 8.07 – 7.88 (m, 2H), 7.72 – 7.53 (m, 1H), 7.53 – 7.42 (m, 2H), 7.35 (m, 5H), 5.22 – 5.09 (dd, *J* = 16.5 Hz, 12.4 Hz, 2H), 3.52 (dd, *J* = 17.5 Hz, 7.8 Hz, 1H), 3.22 (m, 1H), 3.06 (dd, *J* = 17.5 Hz, 5.5 Hz, 1H), 1.32 (d, *J* = 7.1 Hz, 3H).

⁵⁸ Dong S.; Wu G.; Yuan X.; Zou C.; Ye J., Visible-light photoredox catalyzed hydroacylation of electron-deficient alkenes: carboxylic anhydride as an acyl radical source. *Org. Chem. Front.* **2017**, *4*, 2230-2234.

⁵⁹ Ding B.; Zhang Z.; Liu Y.; Sugiyama M.; Imamoto T.; Zhang W., Chemoselective Transfer Hydrogenation of α,β-Unsaturated Ketones Catalyzed by Pincer-Pd Complexes Using Alcohol as a Hydrogen Source. *Org. Lett.* **2013**, *15*, 3690-3693.

$^{13}\text{C NMR}$ (75 MHz, CDCl_3) δ 198.1, 175.9, 136.8, 136.2, 133.3, 128.7, 128., 128.2, 128.2, 128.2, 66.5, 42.0, 35.2, 17.4.

Matching reported literature data.⁵⁸

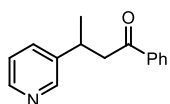


1-phenyl-3-(pyrimidin-2-yl)propan-1-one (47e): Prepared according to General Procedure H at 40 °C using *tert*-butyldimethyl((1-phenylvinyl)oxy)silane **46a** (70 mg, 0.3 mmol) and 2,4,6-triphenyl-1-(pyrimidin-2-ylmethyl)pyridin-1-ium tetrafluoroborate **24h** (98 mg, 0.2 mmol). Flash column chromatography (hexanes/EtOAc 7:3) to afford product **47e** as a yellowish oil (32 mg, 75% yield).

$^1\text{H NMR}$ (300 MHz, CDCl_3) δ 8.66 (d, $J = 4.9$ Hz, 2H), 8.25 – 7.88 (m, 2H), 7.61 – 7.52 (m, 1H), 7.51 – 7.39 (m, 2H), 7.13 (t, $J = 4.9$ Hz, 1H), 3.66 – 3.55 (m, 2H), 3.46 (m, 2H).

$^{13}\text{C NMR}$ (75 MHz, CDCl_3) δ 199.0, 170., 157.1, 137.1, 133.2, 128.7, 128.3, 118.8, 36.2, 33.1.

HRMS: calculated for $\text{C}_{13}\text{H}_{13}\text{N}_2\text{O}$ ($\text{M}+\text{H}^+$): 213.1022, found 213.1020 (+1.0 ppm).

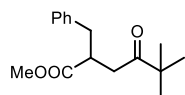


1-phenyl-3-(pyridin-3-yl)butan-1-one (47f): Prepared according to General Procedure H at 60 °C using *tert*-butyldimethyl((1-phenylvinyl)oxy)silane **46a** (70 mg, 0.3 mmol) and (\pm)-2,4,6-triphenyl-1-(1-(pyridin-3-yl)ethyl)pyridin-1-ium tetrafluoroborate **24i** (100 mg, 0.2 mmol). Flash column chromatography (hexanes/EtOAc 8:2) to afford product **47f** as a yellowish oil (20 mg, 44% yield).

$^1\text{H NMR}$ (400 MHz, CDCl_3) δ 8.52 (d, $J = 4.9$, 1H), 8.04 – 7.91 (m, 2H), 7.64 (td, $J = 7.7$ Hz, 1.9 Hz, 1H), 7.58 – 7.49 (m, 1H), 7.48 – 7.37 (m, 2H), 7.30 (d, $J = 7.8$ Hz, 1H), 7.13 (m, 1H), 3.82 – 3.60 (m, 2H), 3.25 (dd, $J = 16.4$ Hz, 5.6 Hz, 1H), 1.40 (d, $J = 6.8$ Hz, 3H).

$^{13}\text{C NMR}$ (101 MHz, CDCl_3) δ 199.3, 164.9, 148.7, 137.3, 133.1, 128.6, 128.3, 123.0, 121.7, 45.0, 37.2, 21.2.

HRMS: calculated for $\text{C}_{15}\text{H}_{16}\text{NO}$ ($\text{M}+\text{H}^+$): 226.1226, found 226.1222 (+1.8 ppm).

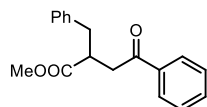


Methyl 2-benzyl-5,5-dimethyl-4-oxohexanoate (47g): Prepared according to General Procedure H with *set-up 2* (75% intensity) and solvent system DMSO/DCE (1:1). 2,6-Lutidine (47 μL , 0.4 mmol, 2.0 equiv.), methyl 2-benzyl-5,5-dimethyl-4-oxohexanoate **46b** (119 mg, 0.5 mmol) and (\pm)-1-(1-methoxy-1-oxo-3-phenylpropan-2-yl)-2,4,6-triphenylpyridin-1-ium tetrafluoroborate **24i** (111 mg, 0.2 mmol). Flash column chromatography (Hexanes/EtOAc from 98:2 to 96:4) to afford product **47g** as a yellow oil (33 mg, 63% yield).

$^1\text{H NMR}$ (400 MHz, CDCl_3) δ 7.31 – 7.26 (m, 2H), 7.24 – 7.19 (m, 1H), 7.17 – 7.10 (m, 2H), 3.63 (s, 3H), 3.21 – 3.09 (m, 1H), 3.01 (dd, $J = 13.6$ Hz, 6.6 Hz, 1H), 2.93 (dd, $J = 18.1$, 8.9 Hz, 1H), 2.73 (dd, $J = 13.6$ Hz, 8.3 Hz, 1H), 2.52 (dd, $J = 18.1$ Hz, 4.6 Hz, 1H), 1.10 (s, 9H).

$^{13}\text{C NMR}$ (101 MHz, CDCl_3) δ 214.2, 175.6, 138.8, 129.1, 128.6, 126.7, 51.9, 44.1, 42.1, 37.93, 37.9, 26.5.

HRMS: calculated for $\text{C}_{18}\text{H}_{21}\text{O}_3$ ($\text{M}+\text{H}^+$): 285.1485, found 285.1475 (+3.5 ppm).



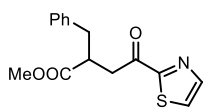
Methyl 2-benzyl-4-oxo-4-phenylbutanoate (47h): Prepared according to General Procedure H using *tert*-butyldimethyl((1-phenylvinyl)oxy)silane **46a** (70 mg, 0.3 mmol) and (\pm)-1-(1-methoxy-1-oxo-3-phenylpropan-2-yl)-2,4,6-triphenylpyridin-1-

ium tetrafluoroborate **24i** (111 mg, 0.2 mmol). Flash column chromatography (hexanes/EtOAc 92:8) to afford product **47h** as a yellowish oil (50 mg, 89% yield).

¹H NMR (400 MHz, CDCl₃) δ 7.93 – 7.87 (m, 2H), 7.59 – 7.50 (m, 1H), 7.43 (dd, *J* = 8.4 Hz, 7.0 Hz, 2H), 7.34 – 7.16 (m, 5H), 3.67 (s, 3H), 3.47 – 3.32 (m, 2H), 3.12 (dd, *J* = 13.6 Hz, 6.0 Hz, 1H), 3.05 – 2.99 (m, 1H), 2.85 (dd, *J* = 13.6, 8.1 Hz, 1H).

¹³C NMR (101 MHz, CDCl₃) δ 198.2, 175.4, 133.4, 129.2, 128.7, 128.7, 128.2, 126.8, 52.1, 42.4, 39.5, 38.0.

HRMS: calculated for C₁₈H₁₈NaO₃ (M+Na⁺): 305.1148, found 305.1142 (+2.0 ppm).

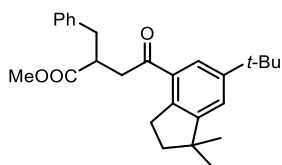


Methyl 2-benzyl-4-oxo-4-(thiazol-2-yl)butanoate (47i): Prepared according to General Procedure H using 2-(1-((tert-butyl)dimethylsilyloxy)vinyl)thiazole **46c** (73 mg, 0.3 mmol) and (±)-1-(1-methoxy-1-oxo-3-phenylpropan-2-yl)-2,4,6-triphenylpyridin-1-ium tetrafluoroborate **24i** (111 mg, 0.2 mmol). Flash column chromatography (Hexanes/Acetone 95:5) to afford product **47i** as a yellowish solid (46 mg, 79% yield).

¹H NMR (300 MHz, CDCl₃) δ 7.98 (d, *J* = 3.0 Hz, 1H), 7.65 (d, *J* = 3.0 Hz, 1H), 7.33 – 7.26 (m, 2H), 7.23 – 7.18 (m, 3H), 3.76 – 3.58 (m, 4H), 3.40 – 3.30 (m, 1H), 3.26 – 3.10 (m, 2H), 2.84 (dd, *J* = 13.6, 8.6 Hz, 1H).

¹³C NMR (75 MHz, CDCl₃) δ 192.0 (C), 174.9 (C), 166.7 (C), 144.9 (CH), 138.5 (C), 129.2 (CH), 128.7 (CH), 126.8 (CH), 126.4 (CH), 52.1 (CH₃), 42.3 (CH), 39.5 (CH₂), 38.0 (CH₂).

HRMS: calculated for C₁₅H₁₅NNaO₃S (M+Na⁺): 312.0665, found 312.0665 (+0.0 ppm).

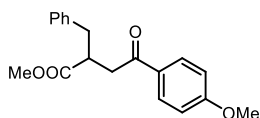


Methyl 2-benzyl-4-(6-(tert-butyl)-1,1-dimethyl-2,3-dihydro-1H-inden-4-yl)-4-oxobutanoate (47j): Prepared according to General Procedure H using tert-butyl((1-(6-(tert-butyl)-1,1-dimethyl-2,3-dihydro-1H-inden-4-yl)vinyl)oxy)dimethylsilane **46d** (108 mg, 0.3 mmol) and (±)-1-(1-methoxy-1-oxo-3-phenylpropan-2-yl)-2,4,6-triphenylpyridin-1-ium tetrafluoroborate **24i** (111 mg, 0.2 mmol). Flash column chromatography (Hexanes/EtOAc 98:2) to afford product **47j** as a yellowish oil (74 mg, 91% yield).

¹H NMR (400 MHz, CDCl₃) δ 7.62 (d, *J* = 1.8 Hz, 1H), 7.33 – 7.26 (m, 3H), 7.24 – 7.17 (m, 3H), 3.66 (s, 3H), 3.47 – 3.22 (m, 2H), 3.14 – 3.07 (m, 3H), 3.05 – 2.97 (m, 1H), 2.84 (dd, *J* = 13.5, 7.9 Hz, 1H), 1.94 – 1.87 (m, 2H), 1.33 (s, 9H), 1.24 (d, *J* = 2.6 Hz, 6H).

¹³C NMR (101 MHz, CDCl₃) δ 200.2, 175.6, 154.5, 150.1, 141.2, 138.9, 133.3, 129.2, 128.6, 126.7, 124.0, 123.5, 52.0, 43.6, 42.6, 41.6, 41.5, 38.1, 34.9, 31.6, 30.88, 28.9.

HRMS: calculated for C₂₇H₃₄NaO₃ (M+Na⁺): 429.2400, found 429.2409 (+2.1 ppm).



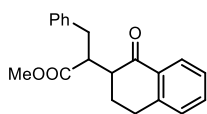
Methyl 2-benzyl-4-(4-methoxyphenyl)-4-oxobutanoate (47k): Prepared according to General Procedure H using tert-butyl((1-(4-methoxyphenyl)vinyl)oxy)dimethylsilane **46e** (80 mg, 0.3 mmol) and (±)-1-(1-methoxy-1-oxo-3-phenylpropan-2-yl)-2,4,6-triphenylpyridin-1-ium tetrafluoroborate **24i** (111 mg, 0.2 mmol). Flash column chromatography (Hexanes/EtOAc 93:7) to afford product **47k** as an off-white solid (52 mg, 83% yield).

¹H NMR (400 MHz, CDCl₃) δ 7.88 (d, *J* = 9.0 Hz, 2H), 7.32 – 7.27 (m, 2H), 7.24 – 7.17 (m, 3H), 6.90 (d, *J* = 9.0 Hz, 2H), 3.86 (s, 3H), 3.66 (s, 3H), 3.44 – 3.26 (m, 2H), 3.10 (dd, *J* = 13.6, 5.9 Hz, 1H), 2.97 (d, *J* = 12.9 Hz, 1H), 2.84 (dd, *J* = 13.6, 7.9 Hz, 1H).

¹³C NMR (101 MHz, CDCl₃) δ 200.2, 175.6, 154.5, 150.1, 141.2, 138.9, 133.3, 129.2, 128.6, 126.7, 124.0, 123.5, 52.0, 43.6, 42.6, 41.6, 41.5, 38.1, 34.9, 31.6, 30.88, 28.9.

¹³C NMR (101 MHz, CDCl₃) δ 196.7, 175.6, 163.7, 138.7, 130.4, 129.9, 129.2, 128.7, 126.8, 113.8, 55.6, 52.0, 42.4, 39.2, 38.0.

HRMS: calculated for C₂₇H₃₄NaO₃ (M+Na⁺): 429.2400, found 429.2409 (−2.1 ppm).

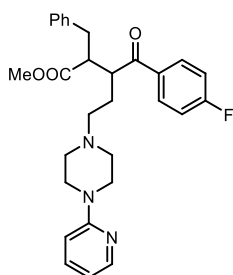


Methyl 2-benzyl-4-(6-(tert-butyl)-1,1-dimethyl-2,3-dihydro-1H-inden-4-yl)-4-oxobutanoate (47l): Prepared according to General Procedure H using tert-butyl((3,4-dihydronaphthalen-1-yl)oxy)dimethylsilane **46f** (104 mg, 0.4 mmol) and (±)-1-(1-methoxy-1-oxo-3-phenylpropan-2-yl)-2,4,6-triphenylpyridin-1-ium tetrafluoroborate **24l** (111 mg, 0.2 mmol). Flash column chromatography (Hexanes/EtOAc from 95:5 to 85:15) to afford product **47l** as an off-green solid (50 mg, 81% yield, 1:1 dr).

¹H NMR (300 MHz, CDCl₃) (1:1 mixture of diastereoisomers) δ 8.02 (ddd, *J* = 9.7, 7.8, 1.5 Hz, 1H), 7.54 – 7.39 (m, 1H), 7.35 – 7.26 (m, 3H), 7.26 – 7.14 (m, 4H), 3.66 – 3.60 (m, 0.4 H), 3.59 (s, 1.1 H), 3.57 (s, 1.8 H), 3.47 – 3.38 (m, 0.6 H), 3.26 – 3.17 (m, 0.5H), 3.05 – 2.75 (m, 4H), 2.66 – 2.58 (m, 0.7H), 2.19 – 2.32 (m, 1H), 1.94 – 1.87 (m, 1H).

¹³C NMR (75 MHz, CDCl₃) (1:1 mixture of diastereoisomers) δ 197.8, 175.3, 174.3, 143.9, 143.7, 139.9, 139.3, 133.7, 133.5, 132.6, 129.2, 129.0, 128.8, 128.8, 128.7, 128.5, 127.7, 127.7, 126.9, 126.8, 126.6, 126.5, 51.80, 50.3, 48.7, 47.3, 46.1, 35.4, 34.7, 29.6, 29.2, 26.1, 25.4.

HRMS: calculated for C₂₀H₂₀NaO₃ (M+Na⁺): 331.1305, found 331.1289 (+4.8 ppm).



Methyl 2-benzyl-3-(4-fluorobenzoyl)-5-(4-(pyridin-2-yl)piperazin-1-yl)pentanoate (47m): Prepared according to General Procedure H using (Z)-1-(4-((tert-butyl)dimethylsilyloxy)-4-(4-fluorophenyl)but-3-en-1-yl)-4-(pyridin-2-yl)piperazine **46g** (133 mg, 0.3 mmol) and (±)-1-(1-methoxy-1-oxo-3-phenylpropan-2-yl)-2,4,6-triphenylpyridin-1-ium tetrafluoroborate **24l** (111 mg, 0.2 mmol), no water is added into the reaction mixture. Flash column chromatography (Hexanes/Acetone from 7:3 to 1:1) to afford product **47m** as an

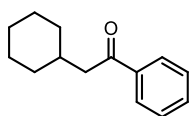
off-white solid (49 mg, 50% yield, 1.2:1 dr).

¹H NMR (500 MHz, CDCl₃) δ 8.14 (m, 1H), 8.05 – 7.97 (m, 2H), 7.47 – 7.39 (m, 1H), 7.25 – 7.14 (m, 4H), 7.13 – 7.04 (m, 5H), 6.62 – 6.51 (m, 2H), 3.95 – 3.82 (m, 1H), 3.49 (s, 1H), 3.44 (s, 2H), 3.28 (t, *J* = 44.1 Hz, 4H), 3.12 – 3.04 (m, 1H), 2.80 – 2.61 (m, 1H), 2.34 (d, *J* = 37.0 Hz, 6H), 2.13 (ddd, *J* = 13.9, 10.4, 6.4 Hz, 1H), 1.99 (s, 1H), 1.70 (s, 1H)

¹³C NMR (126 MHz, CDCl₃) 1:1 mixture of diastereoisomer δ 200.5, 200.1, 174.5, 174.4, 159.5, 148.1, 148.1, 138.8, 138.6, 137.6, 137.6, 135.1, 134.0, 131.2, 131.2, 131.1, 131.0, 129.0, 128.9, 128.6, 128.5, 126.7, 126.7, 115.9, 115.9, 115.8, 115.7, 113.5, 113.4, 107.2, 107.1, 56.1, 55.9, 52.8, 52.6, 51.8, 51.6, 51.4, 49.2, 45.9, 45.6, 44.9, 44.8, 37.2, 34.7.

¹⁹F NMR (376 MHz, CDCl₃) 1:1 mixture of diastereoisomer δ −105.4 (s, 1F), −105.6 (s, 1F).

HRMS: calculated for C₂₉H₃₃FN₃O₃ (M+H⁺): 490.2500, found 490.2500 (0.0 ppm).

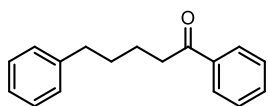


Methyl 2-benzyl-5,5-dimethyl-4-oxohexanoate (47n): Prepared according to General Procedure H with *set-up 1* and no 2,6-Lutidine. tert-butyl(dimethyl)((1-phenylvinyl)oxy)silane **46a** (70 mg, 0.3 mmol) and 1,3-dioxoisindolin-2-yl cyclohexanecarboxylate **23a** (54.5 mg, 0.2 mmol, 1 equiv.). Flash column chromatography (Hexanes/EtOAc from 100:0 to 98:2) to afford product **47n** as a yellow oil (17 mg, 42% yield).

$^1\text{H NMR}$ (400 MHz, CDCl_3) δ 7.98 – 7.92 (m, 2H), 7.58 – 7.51 (m, 1H), 7.49 – 7.42 (m, 2H), 2.82 (d, J = 6.8 Hz, 2H), 2.04 – 1.93 (m, 1H), 1.80 – 1.73 (m, 2H), 1.73 – 1.61 (m, 2H), 1.34 – 1.23 (m, 3H), 1.22 – 1.14 (m, 1H), 1.07 – 0.96 (m, 2H).

$^{13}\text{C NMR}$ (101 MHz, CDCl_3) δ 200.5, 137.6, 133.0, 128.7, 128.3, 46.4, 34.7, 33.6, 26.4, 26.3.

Matching reported literature data.⁶⁰



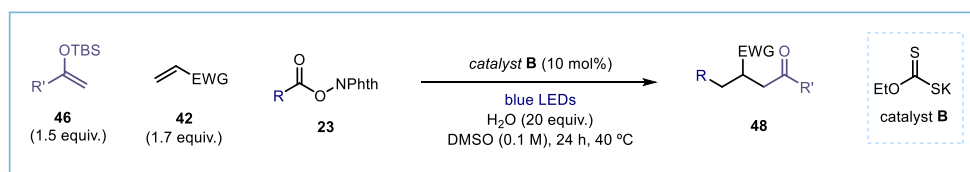
Methyl 2-benzyl-5,5-dimethyl-4-oxohexanoate (47o): Prepared according to General Procedure H with *set-up 1* and no 2,6-Lutidine. *tert*-butyldimethyl((1-phenylvinyl)oxy)silane **46a** (70 mg, 0.3 mmol) and 1,3-dioxoisindolin-2-yl 4-phenylbutanoate **23b** (62 mg, 0.2 mmol, 1 equiv.). Flash column chromatography (Hexanes/EtOAc from 100:0 to 98:2) to afford product **47o** as a yellow oil (18 mg, 38% yield).

$^1\text{H NMR}$ (400 MHz, CDCl_3) δ 7.97 – 7.92 (m, 2H), 7.59 – 7.52 (m, 1H), 7.49 – 7.42 (m, 2H), 7.31 – 7.21 (m, 2H), 7.19 (dt, J = 8.0, 1.8 Hz, 3H), 2.99 (t, J = 7.2 Hz, 2H), 2.67 (t, J = 7.5 Hz, 2H), 1.83 – 1.76 (m, 2H), 1.76 – 1.68 (m, 2H).

$^{13}\text{C NMR}$ (101 MHz, CDCl_3) δ 200.4, 142.4, 137.2, 133.1, 128.7, 128.5, 128.5, 128.2, 125.9, 38.5, 35.9, 31.2, 29.8, 24.1.

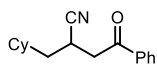
Matching reported literature data.⁶¹

3.6.6.3 General procedure I (three-component reaction)



Reactions performed using *set-up 1* in Figure 3.35. In an oven dried vial, with a Teflon septum screw cap, silyl enol ether **46** (0.3 mmol, 1.5 equiv.) was dissolved in DMSO (2 mL), then phthalimide ester **23** (0.2 mmol, 1.0 equiv.) was added, followed by catalyst **B** (3.2 mg, 0.02 mmol, 0.1 equiv.), electron-poor olefin **42** (0.34 mmol, 1.7 equiv.) and water (4.0 mmol, 20 equiv.). The resulting orange mixture was degassed by bubbling argon for 60 seconds. The vial was then placed in the 3D printed support photoreactor and irradiated under stirring for 24 hours, unless otherwise specified. The crude mixture was diluted with EtOAc and brine was added. The combined organic fractions were dried over anhydrous MgSO_4 and concentrated to dryness. The crude residue was purified by column chromatography on silica gel to afford the corresponding product in the stated yield with >95% purity according to $^1\text{H NMR}$ analysis.

3.6.6.4 Characterization of products with general procedure I



2-(cyclohexylmethyl)-4-oxo-4-phenylbutanenitrile (48a): Prepared according to General Procedure I using *tert*-butyldimethyl((1-phenylvinyl)oxy)silane **46a** (63 mg, 0.24 mmol), 1,3-dioxoisindolin-2-yl cyclohexanecarboxylate **23a** (55 mg, 0.2 mmol), and acrylonitrile **42b** (22 μL , 0.34 mmol). Flash column chromatography (hexanes/EtOAc 94:6) to afford product **48a** as an off-white solid (31 mg, 61% yield).

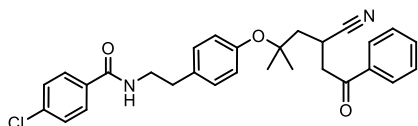
⁶⁰ Kong, W.; Yu, C.; An, H.; Song, Q., Photoredox-Catalyzed Decarboxylative Alkylation of Silyl Enol Ethers To Synthesize Functionalized Aryl Alkyl Ketones. *Org. Lett.* **2018**, *20*, 349-352.

⁶¹ Zheng, Y.-L.; Xie, P.-P.; Daneshfar, O.; Houk, K. N.; Hong, X.; Newman, S. G., Direct Synthesis of Ketones from Methyl Esters by Nickel-Catalyzed Suzuki-Miyaura Coupling. *Angew. Chem. Int. Ed.* **2021**, *60*, 24, 13476-13483.

¹H NMR (300 MHz, CDCl₃) δ 8.04 – 7.86 (m, 2H), 7.72 – 7.59 (m, 1H), 7.52 – 7.45 (m, 2H), 3.52 – 3.30 (m, 2H), 3.30 – 3.13 (m, 1H), 1.89 (d, *J* = 12.9 Hz, 1H), 1.83 – 1.57 (m, 6H), 1.49 – 1.40 (m, 1H), 1.24 – 1.08 (m, 2H), 1.06 – 0.83 (m, 3H).

¹³C NMR (75 MHz, CDCl₃) δ 195.5, 136.1, 134.0, 129.0, 128.2, 122.3, 41.5, 39.9, 35.7, 33.8, 32.2, 26.5, 26.2, 26.0, 24.0.

HRMS: calculated for C₁₇H₂₁NNaO (M+Na⁺): 278.1515, found 278.1511 (+1.4 ppm).



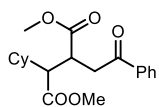
4-chloro-N-(4-((4-cyano-2-methyl-6-oxo-6-phenylhexan-2-yl)oxy)phenethyl)benzamide (48b): Prepared according to General Procedure I using *tert*-butyldimethyl((1-phenylvinyl)oxy)silane **46a** (63 mg, 0.24 mmol), 1,3-

dioxoisindolin-2-yl 2-(4-(2-(4-chlorobenzamido)ethyl)phenoxy)-2-methylpropanoate **23e** (101 mg, 0.2 mmol), and acrylonitrile **42b** (22 μL, 0.34 mmol). Flash column chromatography (hexanes/EtOAc from 7:3 to 1:1) to afford product **48b** as a yellowish fluffy solid (51 mg, 52% yield).

¹H NMR (300 MHz, CDCl₃) δ 8.05 – 7.86 (m, 2H), 7.64 (d, *J* = 8.4 Hz, 3H), 7.57 – 7.46 (m, 2H), 7.42 – 7.38 (m, 2H), 7.14 (d, *J* = 8.4 Hz, 2H), 6.98 (d, *J* = 8.4 Hz, 2H), 6.09 (s, 1H), 3.74 – 3.61 (m, 3H), 3.57 – 3.37 (m, 2H), 2.90 (t, *J* = 6.9 Hz, 2H), 2.23 (dd, *J* = 14.2, 9.2 Hz, 1H), 1.99 (dd, *J* = 14.2, 3.8 Hz, 1H), 1.44 (s, 3H), 1.40 (s, 3H).

¹³C NMR (75 MHz, CDCl₃) δ 195.8, 166.5, 153.4, 136.1, 134.2, 134.0, 133.5, 129.6, 129.0, 128.4, 128.2, 124.3, 79.2, 44.8, 42.3, 35.0, 27.1, 26.2, 21.9.

HRMS: calculated for C₂₉H₂₉ClN₂NaO₃ (M+Na⁺): 511.1759, found 511.1759 (+0.0 ppm).



Dimethyl 2-cyclohexyl-3-(2-oxo-2-phenylethyl)succinate (48c): Prepared according to General Procedure I using *tert*-butyldimethyl((1-phenylvinyl)oxy)silane **46a** (63 mg, 0.24 mmol), 1,3-dioxoisindolin-2-yl cyclohexanecarboxylate **23a** (55 mg, 0.2 mmol), and dimethylfumarate **42c** (43 mg, 0.3 mmol). Flash column chromatography (hexanes/EtOAc 88:12) to afford

the two separable diastereoisomeric products **48c** (major diastereoisomer) and **48c'** (minor diastereoisomer) as off-white solids (d.r. 1:2.5, 50 mg, 72% yield).

Spectroscopic data for 48c:

¹H NMR (300 MHz, CDCl₃) δ 8.05 – 7.86 (m, 2H), 7.63 – 7.52 (m, 1H), 7.52 – 7.45 (m, 2H), 3.69 (s, 3H), 3.67 (s, 3H), 3.67 – 3.59 (m, 1H), 3.46 – 2.94 (m, 2H), 2.71 (dd, *J* = 8.7, 5.6 Hz, 1H), 1.81 – 1.59 (m, 6H), 1.22 – 1.17 (m, 2H), 1.09 – 0.77 (m, 3H).

¹³C NMR (75 MHz, CDCl₃) δ 198.3, 174.7, 173.8, 136.7, 133.4, 128.7, 128.3, 52.6, 52.3, 51.7, 39.8, 37.4, 36.6, 31.1, 30.4, 26.3, 26.3, 26.2.

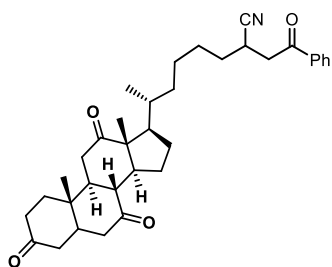
HRMS: calculated for C₂₀H₂₆NaO₅ (M+Na⁺): 369.1677, found 369.1672 (+1.4 ppm).

Spectroscopic data for 48c':

¹H NMR (300 MHz, CDCl₃) δ 8.01 – 7.94 (m, 2H), 7.61 – 7.54 (m, 1H), 7.50 – 7.42 (m, 2H), 3.68 (s, 3H), 3.68 (s, 3H), 3.58 – 3.47 (m, 2H), 3.24 – 3.10 (m, 1H), 2.66 – 2.55 (m, 1H), 1.96 (m, 1H), 1.80 – 1.64 (m, 6H), 1.07 – 0.85 (m, 5H).

¹³C NMR (75 MHz, CDCl₃) δ 197.9, 174.2, 173.9, 136.8, 133.4, 128.8, 128.2, 53.4, 52.2, 51.7, 39.3, 38.1, 37.4, 31.1, 30.9, 26.4, 26.4.

HRMS: calculated for C₂₀H₂₆NaO₅ (M+Na⁺): 369.1677, found 369.1672 (+1.4 ppm).



6-((5S,8R,9S,10S,13R,14S,17R)-10,13-dimethyl-3,7,12-trioxohexadecahydro-1H-cyclopenta[a]phenanthren-17-yl)-2-(2-oxo-2-phenylethyl)heptanenitrile (48d): Prepared according to General

Procedure I using *tert*-butyldimethyl((1-phenylvinyl)oxy)silane **46a** (63 mg, 0.24 mmol), 1,3-dioxoisindolin-2-yl 4-

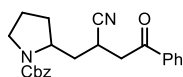
((5S,8R,9S,10S,13R,14S,17R)-10,13-dimethyl-3,7,12-trioxohexadecahydro-1H-cyclopenta[a]phenanthren-17-yl)pentanoate

23d (110 mg, 0.2 mmol), and acrylonitrile **42b** (22 μ L, 0.340 mmol). Flash column chromatography (hexanes/EtOAc 1:1) to afford product **48d** as a white solid (64 mg, 60% yield).

¹H NMR (300 MHz, CDCl₃) δ 8.03 – 7.89 (m, 2H), 7.72 – 7.57 (m, 1H), 7.53 – 7.45 (m, 2H), 3.63 – 3.15 (m, 3H), 2.99 – 2.75 (m, 3H), 2.39 – 1.80 (m, 14H), 1.77 – 1.43 (m, 6H), 1.40 (s, 3H), 1.35 – 1.16 (m, 3H), 1.07 (s, 3H), 0.86 (dd, *J* = 6.4, 2.0 Hz, 3H).

¹³C NMR (75 MHz, CDCl₃) δ 212.0, 209.1, 208.8, 195.3, 135.9, 133.9, 128.9, 128.1, 121.9, 56.9, 51.8, 49.0, 46.9, 45.8, 45.6, 45.0, 42.8, 40.9, 40.8, 38.7, 36.5, 36.0, 36.0, 35.3, 34.8, 32.4, 29.7, 27.9, 26.4, 26.3, 25.2, 24.5, 24.4, 21.9, 19.0, 18.9, 11.9.

HRMS: calculated for C₃₄H₄₃NNaO₄ (M+Na⁺): 552.3081, found 552.3084 (–0.5 ppm).



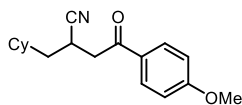
Benzyl 2-(2-cyano-4-oxo-4-phenylbutyl)pyrrolidine-1-carboxylate (48e): Prepared according to General Procedure I using *tert*-butyldimethyl((1-phenylvinyl)oxy)silane

46a (63 mg, 0.240 mmol), 1-benzyl 2-(1,3-dioxoisindolin-2-yl) pyrrolidine-1,2-dicarboxylate **23c** (55 mg, 0.2 mmol), and acrylonitrile **42b** (22 μ L, 0.34 mmol). Flash column chromatography (hexanes/acetone 7:3) to afford product **48e** as a reddish oil (47 mg, 62% yield, 1:1 dr).

¹H NMR (400 MHz, CDCl₃) (1:1 mixture of diastereoisomers) δ 8.01 – 7.79 (m, 2H), 7.68 – 7.59 (m, 1H), 7.50 (t, *J* = 7.6 Hz, 2H), 7.46 – 7.30 (m, 5H), 5.26 – 5.10 (m, 2H), 4.24 – 3.96 (m, 1H), 3.57 – 3.19 (m, 5H), 2.15 – 2.04 (m, 1H), 2.02 – 1.65 (m, 5H).

¹³C NMR (101 MHz, CDCl₃) (1:1 mixture of diastereoisomers) δ 195.3, 194.8, 155.3, 136.8, 136.8, 133.8, 128.8, 128.5, 128.1, 127.8, 123.7, 122.0, 121.1, 66.9, 66.8, 56.2, 55.6, 55.3, 46.4, 41.0, 40.7, 36.9, 36.5, 36.0, 32.5, 30.6, 30.3, 29.7, 24.3, 23.9, 23.4, 23.0.

HRMS: calculated for C₂₃H₂₄N₂NaO₃ (M+Na⁺): 399.1679, found 399.1682 (–0.75 ppm).



2-(cyclohexylmethyl)-4-(4-methoxyphenyl)-4-oxobutanenitrile (48f): Prepared according to General Procedure I using *tert*-butyl((1-(4-methoxyphenyl)vinyl)oxy)dimethylsilane

46e (65 mg, 0.24 mmol), 1,3-dioxoisindolin-2-yl cyclohexanecarboxylate **23a** (55 mg, 0.2 mmol), and acrylonitrile **42b** (22 μ L, 0.34 mmol). Flash column chromatography (hexanes/acetone 88:12) to afford product **48f** as an off-white solid (31 mg, 61% yield).

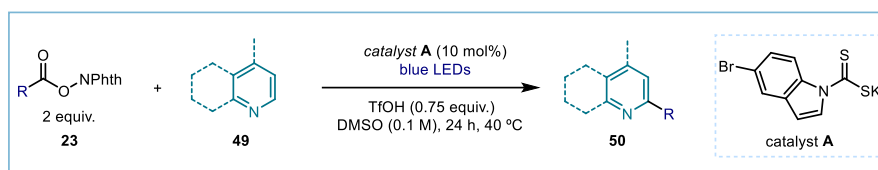
¹H NMR (300 MHz, CDCl₃) δ 7.93 (d, *J* = 8.9 Hz, 2H), 6.95 (d, *J* = 8.9 Hz, 2H), 3.88 (s, 3H), 3.42 – 3.29 (m, 2H), 3.21 – 3.10 (m, 1H), 1.88 (d, *J* = 12.8 Hz, 1H), 1.77 – 1.58 (m, 7H), 1.23 – 1.10 (m, 2H), 1.00 – 0.79 (m, 3H).

¹³C NMR (75 MHz, CDCl₃) δ 193.9, 164.2, 130.5, 129.2, 122.4, 114.1, 55.7, 41.1, 39.9, 35.7, 33.8, 32.2, 26.5, 26.2, 26.0, 24.0.

HRMS: calculated for C₁₈H₂₃NNaO₂ (M+Na⁺): 308.1630, found 308.1621 (+2.9 ppm).

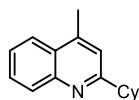
3.6.7 Minisci reaction

3.6.7.1 General procedure J



Reactions performed using *set-up 1*. In an oven dried vial, with a Teflon septum screw cap, heteroarene **49** (0.2 mmol, 1.0 equiv.) and trifluoromethanesulfonic acid (13.3 μ L, 0.15 mmol, 0.75 equiv.) were dissolved in DMSO (2 ml). Then, phthalimide ester **23** (0.4 mmol, 2 equiv.) and catalyst **A** (6.2 mg, 0.02 mmol, 0.1 equiv.) were added. The resulting yellow mixture was degassed with argon sparging for 60 seconds. The vial was placed in the 3D printed photoreactor and irradiated under stirring for 24 hours, unless otherwise specified. The mixture was transferred to an extraction funnel, NaHCO₃ sat. solution was added and the organic layer was extracted with EtOAc. The organic layer was washed with brine twice. The combined organic layers were dried over anhydrous MgSO₄, filtered, and concentrated to dryness. The crude residue was purified by column chromatography to afford the corresponding product in the stated yield with >95% purity according to ¹H NMR analysis.

3.6.7.2 Characterization of products with general procedure J



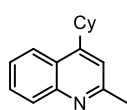
2-Cyclohexyl-4-methylquinoline (50a): Synthesized according to General

Procedure J using 1,3-dioxoisindolin-2-yl cyclohexanecarboxylate **23a** (109 mg, 0.4 mmol, 2 equiv.) and 4-methylquinoline **49a** (26.4 μ L, 0.2 mmol, 1 equiv.). The crude mixture was purified by flash column chromatography on silica gel (10% EtOAc in hexane as eluent) to afford **50a** (39.6 mg, 88% yield) as a yellow oil.

¹H NMR (400 MHz, CDCl₃) δ 8.28 (s, 1H), 7.98 – 7.96 (m, 1H), 7.74 – 7.70 (m, 1H), 7.57 – 7.53 (m, 1H), 7.23 (s, 1H), 3.15 – 3.10 (m, 1H), 2.73 (s, 3H), 2.06 – 2.01 (m, 2H), 1.89 (dt, J = 13.0, 3.3 Hz, 2H), 1.83 – 1.76 (m, 1H), 1.63 (qd, J = 12.3, 3.0 Hz, 2H), 1.49 (qt, J = 12.8, 3.0 Hz, 2H), 1.38 – 1.30 (m, 1H).

¹³C NMR (101 MHz, CDCl₃) δ 166.0, 130.2, 128.1, 127.1, 126.3, 123.8, 120.3, 46.5, 32.9, 26.5, 26.1, 19.3.

Matching reported literature data.⁶²



4-Cyclohexyl-2-methylquinoline (50b): Synthesized according to General Procedure J

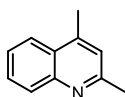
using 1,3-dioxoisindolin-2-yl cyclohexanecarboxylate **23a** (109 mg, 0.4 mmol, 2 equiv.) and 2-methylquinoline **49b** (27.1 μ L, 0.2 mmol, 1.0 equiv.). The crude mixture was purified by flash column chromatography on silica gel (10% EtOAc in hexane as eluent) to afford **50b** (42.3 mg, 94% yield) as a yellow oil.

¹H NMR (400 MHz, CDCl₃) δ 8.05 (t, J = 9.8 Hz, 2H), 7.67 - 7.63 (m, 1H), 7.51 – 7.47 (m, 1H), 7.17 (s, 1H), 3.32 – 3.27 (ddd, J = 11.4, 8.3, 3.4 Hz, 1H), 2.73 (s, 3H), 2.05 – 1.90 (m, 4H), 1.88 - 1.83 (m, 1H), 1.61 – 1.48 (m, 4H), 1.40 – 1.31 (m, 4H).

¹³C NMR (101 MHz, CDCl₃) δ 158.8, 153.8, 147.9, 129.4, 129.1, 125.5, 125.3, 123.0, 118.5, 39.0, 33.7, 27.1, 26.5, 25.5.

Matching reported literature data.⁶²

⁶² McCallum, T.; Barriault, L. "Direct alkylation of heteroarenes with unactivated bromoalkanes using photoredox gold catalysis" *Chem. Sci.* **2016**, *7*, 4754-4758.

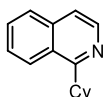


2,4-Dimethylquinoline (50c): Synthesized according to General Procedure J using 1,3-dioxoisindolin-2-yl acetate **23g** (82.1 mg, 0.4 mmol, 2 equiv.) and 2-methylquinoline **49b** (27.1 μ L, 0.2 mmol, 1.0 equiv.) in NMP (2 ml) for 48 hours. The crude mixture was purified by flash column chromatography on silica gel (20% CH_2Cl_2 in MeOH as eluent) to afford **50c** (28.3 mg, 90% yield) as a colorless oil.

$^1\text{H NMR}$ (400 MHz, CDCl_3) δ 8.09 (dt, $J = 8.5, 0.9$ Hz, 1H), 7.89 – 7.85 (m, 1H), 7.72 (ddd, $J = 8.4, 6.9, 1.4$ Hz, 1H), 7.54 (ddd, $J = 8.3, 6.9, 1.3$ Hz, 1H), 6.98 (s, 1H), 2.86 (s, 3H), 2.73 (s, 3H).

$^{13}\text{C NMR}$ (101 MHz, CDCl_3) δ 159.2, 148.6, 129.9, 129.7, 126.4, 124.1, 123.4, 122.1, 29.8, 25.6.

Matching reported literature data.⁶²

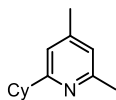


1-Cyclohexylisoquinoline (50d): Synthesized according to General Procedure J using 1,3-dioxoisindolin-2-yl cyclohexanecarboxylate **23a** (109 mg, 0.4 mmol, 2 equiv.) and isoquinoline **49c** (25.8 mg, 0.2 mmol, 1.0 equiv.). The crude mixture was purified by flash column chromatography on silica gel (10% EtOAc in hexane as eluent) to afford **50d** (40.9 mg, 97% yield) as a colorless oil.

$^1\text{H NMR}$ (400 MHz, CDCl_3) δ 8.50 (d, $J = 5.8$ Hz, 1H), 8.25 (d, $J = 8.5$ Hz, 1H), 7.83 (d, $J = 8.3$ Hz, 1H), 7.72 – 7.66 (m, 1H), 7.63 – 7.59 (ddd, $J = 8.3, 6.9, 1.4$ Hz, 1H), 7.53 (d, $J = 5.8$ Hz, 1H), 3.58 (tt, $J = 11.6, 3.2$ Hz, 1H), 2.05 – 1.78 (m, 7H), 1.61 – 1.37 (m, 3H).

$^{13}\text{C NMR}$ (101 MHz, CDCl_3) δ 165.7, 141.1, 136.8, 130.3, 127.8, 127.3, 126.4, 125.1, 119.4, 41.6, 32.7, 27.0, 26.3.

Matching reported literature data.⁶²

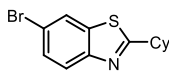


2-Cyclohexyl-4,6-dimethylpyridine (50e): Synthesized according to General Procedure J using 1,3-dioxoisindolin-2-yl acetate **23a** (109 mg, 0.4 mmol, 2 equiv) and 2,4-dimethylpyridine **49d** (23.1 μ L, 0.2 mmol, 1.0 equiv.). The crude mixture was purified by flash column chromatography on silica gel (10% EtOAc in hexane as eluent) to afford **50e** (31.3 mg, 83% yield) as a colorless oil.

$^1\text{H NMR}$ (400 MHz, CDCl_3) δ 6.80 (s, 2H), 2.71 (dd, $J = 8.5, 4.8$ Hz, 1H), 2.50 (s, 3H), 2.29 (s, 3H), 1.95 (dd, $J = 13.4, 3.0$ Hz, 2H), 1.86 – 1.79 (m, 2H), 1.78 – 1.70 (m, 1H), 1.51 – 1.36 (m, 4H), 1.33 – 1.25 (m, 1H).

$^{13}\text{C NMR}$ (101 MHz, CDCl_3) δ 165.8, 157.0, 122.0, 118.6, 44.1, 33.3, 26.7, 26.3, 23.1, 21.2.

Matching reported literature data.⁶²

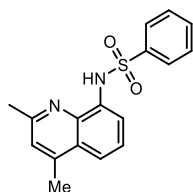


6-Bromo-2-cyclohexylbenzo[d]thiazole (50f): Synthesized according to General Procedure J using 1,3-dioxoisindolin-2-yl cyclohexanecarboxylate **23a** (109 mg, 0.4 mmol, 2 equiv.) and 6-bromo-1,3-benzothiazole **49e** (42.8 mg, 0.2 mmol, 1.0 equiv.). The crude mixture was purified by flash column chromatography on silica gel (10% AcOEt in hexane as eluent) to afford **50f** (49.1 mg, 83% yield) as a white solid.

$^1\text{H NMR}$ (500 MHz, CDCl_3) δ 7.96 (d, $J = 2.0$ Hz, 1H), 7.81 (d, $J = 8.7$ Hz, 1H), 7.53 (dd, $J = 8.7, 2.0$ Hz, 1H), 3.07 (tt, $J = 11.6, 3.6$ Hz, 1H), 2.22 – 2.15 (m, 2H), 1.88 (dp, $J = 10.6, 3.5$ Hz, 2H), 1.76 (dtt, $J = 13.1, 3.4, 1.5$ Hz, 1H), 1.69 – 1.57 (m, 2H), 1.50 – 1.37 (m, 2H), 1.32 (tt, $J = 12.5, 3.5$ Hz, 1H).

$^{13}\text{C NMR}$ (126 MHz, CDCl_3) δ 178.3, 152.1, 136.4, 129.4, 124.2, 123.8, 118.2, 43.5, 33.5, 26.1, 25.9.

Matching reported literature data.⁶³



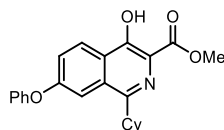
N-(2,4-Dimethylquinolin-8-yl) benzenesulfonamide (50g): Synthesized according to General Procedure J using 1,3-dioxoisindolin-2-yl acetate **23g** (82.1 mg, 0.4 mmol, 2.0 equiv.) and 2-((4-((7-chloro-2-methylquinolin-4-yl) amino) pentyl) (ethyl) amino) ethan-1-ol **49f** (59.7 mg, 0.2 mmol, 1.0 equiv.) in NMP (2 ml, 0.1 M) for 48 hours.

The crude mixture was purified by flash column chromatography on silica gel (20% CH_2Cl_2 in MeOH as eluent) to afford **50g** (37.5 mg, 60% yield) as a white solid.

$^1\text{H NMR}$ (300 MHz, CDCl_3) δ 9.48 (s, 1H), 8.01 – 7.91 (m, 2H), 7.80 (dd, $J = 7.3, 1.5$ Hz, 1H), 7.53 – 7.36 (m, 5H), 6.98 (s, 1H), 2.82 (s, 3H), 2.70 (s, 4H).

$^{13}\text{C NMR}$ (101 MHz, CDCl_3) δ 176.0, 158.0, 139.6, 138.2, 134.0, 133.0, 129.1, 127.4, 126.7, 124.2, 116.7, 115.4, 29.1, 25.3.

HRMS: calculated for $\text{C}_{17}\text{H}_{16}\text{N}_2\text{NaO}_2\text{S}$ ($\text{M}+\text{Na}^+$): 335.3762, found: 335.3768.



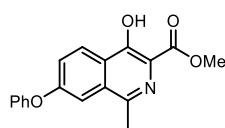
Methyl 1-cyclohexyl-4-hydroxy-7-phenoxyisoquinoline-3-carboxylate (50h): Synthesized according to General Procedure J using 1,3-dioxoisindolin-2-yl cyclohexanecarboxylate **23a** (109 mg, 0.4 mmol, 2.0 equiv.) and Roxadustat analogue **49g** (59.1 mg, 0.2 mmol, 1.0 equiv.). The crude mixture was purified by

flash column chromatography on silica gel (50% EtOAc in hexane as eluent) to afford **50h** (67.1 mg, 89% yield) as a white solid.

$^1\text{H NMR}$ (400 MHz, CDCl_3) δ 8.41 (d, $J = 9.1$ Hz, 1H), 7.62 (d, $J = 2.4$ Hz, 1H), 7.49 – 7.41 (m, 3H), 7.27 – 7.21 (m, 1H), 7.17 – 7.10 (m, 2H), 4.08 (s, 3H), 3.18 (tt, $J = 11.6, 3.3$ Hz, 1H), 1.99 – 1.85 (m, 4H), 1.86 – 1.71 (m, 3H), 1.51 – 1.31 (m, 3H).

$^{13}\text{C NMR}$ (101 MHz, CDCl_3) δ 171.8, 159.0, 156.1, 155.4, 155.4, 131.4, 130.3, 126.2, 124.6, 124.2, 121.9, 119.8, 119.0, 111.4, 53.0, 41.9, 32.2, 26.8, 26.2.

HRMS: calculated for $\text{C}_{23}\text{H}_{24}\text{NO}_4$ ($\text{M}+\text{H}^+$): 378.1700, found: 378.1702.



Methyl 4-hydroxy-1-methyl-7-phenoxyisoquinoline-3-carboxylate (50i): Synthesized according to General Procedure J using 1,3-dioxoisindolin-2-yl acetate **23g** (82.1 mg, 0.4 mmol, 2.0 equiv.) and Roxadustat analogue **49g** (59.1 mg, 0.2 mmol, 1.0 equiv.) in NMP (2 ml) for 48 hours. The crude mixture was

purified by flash column chromatography on silica gel (50% EtOAc in hexane as eluent) to afford **50i** (57.5 mg, 93% yield) as a white solid.

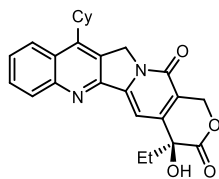
$^1\text{H NMR}$ (300 MHz, CDCl_3) δ 11.83 (s, 1H), 8.44 (d, $J = 9.1$ Hz, 1H), 7.53 – 7.43 (m, 3H), 7.38 (m, 1H), 7.29 (tt, $J = 6.4, 1.2$ Hz, 1H), 7.16 – 7.09 (m, 2H), 4.04 (s, 3H), 2.71 (s, 3H).

$^{13}\text{C NMR}$ (101 MHz, CDCl_3) δ 175.4, 160.1, 156.4, 155.2, 147.5, 130.7, 130.5, 126.7, 125.4, 124.2, 122.4, 120.4, 119.1, 108.6, 53.0, 30.0.

Matching reported literature data.⁶⁴

⁶³ Zidan, M.; Morris, A. O.; McCallum, T.; Barriault, L. "The Alkylation and Reduction of Heteroarenes with Alcohols Using Photoredox Catalyzed Hydrogen Atom Transfer via Chlorine Atom Generation" *Eur. J. Org. Chem.* **2020**, 1453-1458.

⁶⁴ Wei, W.; Wang, L.; Bao, P.; Shao, Y.; Yue, H.; Yang, D.; Yang, X.; Zhao, X.; Wang, H. "Metal-Free $\text{C}(\text{sp}^2)\text{-H/N-H}$ Cross-Dehydrogenative Coupling of Quinoxalinones with Aliphatic Amines under Visible-Light Photoredox Catalysis" *Org. Lett.* **2018**, *20*, 7125-7130.

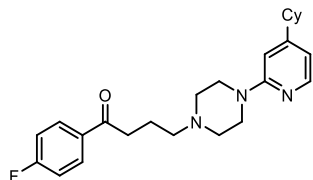


(S)-11-Cyclohexyl-4-ethyl-4-hydroxy-1,12-dihydro-14H-pyrano [3',4':6,7] indolizino [1,2-b] quinoline-3,14(4H)-dione (50j): Synthesized according to General Procedure using J 1,3-dioxoisindolin-2-yl cyclohexanecarboxylate **23a** (109 mg, 0.4 mmol, 2 equiv.) and Camptothecin **49h** (69.7 mg, 0.2 mmol, 1.0 equiv.). The crude mixture was purified by flash column chromatography on silica gel (5% CH₂Cl₂ in MeOH as eluent) to afford **50j** (41,3 mg, 48% yield) as a white solid.

¹H NMR (400 MHz, CDCl₃) δ 8.27 – 8.15 (d, *J* = 8.4 Hz, 2H), δ 7.76 (t, *J* = 7.5 Hz, 1H), 7.66 - 7.61 (m, 2H), 5.74 (d, *J* = 16.3 Hz, 1H), 5.39 (s, 2H), 5.29 (d, *J* = 16.3 Hz, 1H), 3.95 (s, 1H), 3.61 (s, 1H), 2.06 – 1.82 (m, 8H), 1.66 – 1.53 (m, 3H), 1.46 (t, *J* = 12.7 Hz, 1H), 1.03 (t, *J* = 7.4 Hz, 3H).

¹³C NMR (101 MHz, CDCl₃) δ 174.1, 157.7, 150.4, 148.8, 130.9, 130.0, 127.8, 127.1, 118.5, 97.9, 72.9, 66.5, 50.8, 31.9, 31.8, 29.8, 27.1, 26.1, 8.0.

Matching reported literature data.⁶⁵



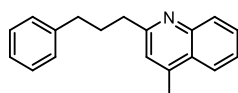
4-(4-(4-Cyclohexylpyridin-2-yl) piperazin-1-yl)-1-(4-fluorophenyl) butan-1-one (50k): Synthesized according to General Procedure J using 1,3-dioxoisindolin-2-yl cyclohexanecarboxylate **23a** (109 mg, 0.4 mmol, 2.0 equiv.) and Azaperone **49i** (65.5 mg, 0.2 mmol, 1.0 equiv.). The crude mixture was purified by flash column chromatography on silica gel (50% EtOAc in hexane as eluent) to afford **50k** (21.3 mg, 26% yield) as a white solid.

¹H NMR (400 MHz, Acetone-*d*₆) δ 8.15 – 8.07 (m, 2H), 7.46 (dd, *J* = 8.4, 7.3 Hz, 1H), 7.30 – 7.24 (m, 2H), 6.63 (d, *J* = 8.4 Hz, 1H), 6.54 (d, *J* = 7.4 Hz, 1H), 3.65 – 3.53 (m, 4H), 3.19 (t, *J* = 6.9 Hz, 2H), 3.00 – 2.90 (m, 5H), 2.52 (tt, *J* = 11.8, 3.4 Hz, 1H), 2.15 – 2.07 (m, 2H), 1.83 – 1.28 (m, 10H).

¹³C NMR (101 MHz, Acetone-*d*₆) δ 198.7, 165.1, 159.5, 138.7, 131.8, 131.7, 116.4, 116.2, 111.1, 105.1, 58.1, 53.5, 47.1, 45.1, 36.4, 33.5, 30.6, 27.3, 26.9.

¹⁹F NMR (376 MHz, Acetone-*d*₆) δ –108.12.

HRMS: calculated for C₂₅H₃₃FN₃O (M+H⁺): 410.2602, found 410.2595 (–1.7 ppm).



4-Methyl-2-(3-phenylpropyl)quinoline (50l): Synthesized according to General Procedure J using 1,3-dioxoisindolin-2-yl 4-phenylbutanoate **23b** (123 mg, 0.4 mmol, 2.0 equiv.) and 4-methylquinoline **49a** (26.4 μL, 0.2 mmol, 1.0 equiv.).

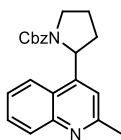
The crude mixture was purified by flash column chromatography on silica gel (10% EtOAc in hexane as eluent) to afford **50l** (46.0 mg, 88% yield) as a white solid.

¹H NMR (400 MHz, CDCl₃) δ 8.11 – 8.03 (m, 1H), 7.95 (dd, *J* = 8.3, 1.4 Hz, 1H), 7.68 (ddd, *J* = 8.4, 6.9, 1.4 Hz, 1H), 7.51 (ddd, *J* = 8.2, 6.9, 1.3 Hz, 1H), 7.33 – 7.26 (m, 2H), 7.26 – 7.15 (m, 3H), 7.13 (d, *J* = 1.1 Hz, 1H), 3.03 – 2.95 (m, 2H), 2.79 – 2.71 (m, 2H), 2.67 (d, *J* = 1.0 Hz, 3H), 2.21 – 2.10 (m, 2H).

¹³C NMR (101 MHz, CDCl₃) δ 162.3, 147.7, 144.6, 142.3, 129.4, 129.3, 128.6, 128.4, 126.9, 125.9, 125.7, 123.7, 122.2, 38.8, 35.9, 31.7, 18.8.

HRMS: calculated for C₁₉H₂₀N (M+H⁺): 262.1586, found 262.1590 (+1.5 ppm).

⁶⁵ Li, G.-X.; Morales-Rivera, C. A.; Wang, Y.; Gao, F.; He, G.; Liu, P.; Chen, G. "Photoredox-mediated Minisci C–H alkylation of N-heteroarenes using boronic acids and hypervalent iodine" *Chem. Sci.* **2016**, *7*, 6407–6412.

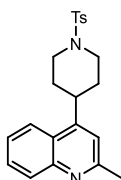


Benzyl 2-(2-methylquinolin-4-yl)pyrrolidine-1-carboxylate (50m): Synthesized according to General Procedure J using 1-benzyl 2-(1,3-dioxoisindolin-2-yl) pyrrolidine-1,2-dicarboxylate **23c** (157 mg, 0.4 mmol, 2 equiv.) and 2-methylquinoline **49b** (27.1 μ L, 0.2 mmol, 1.0 equiv.). The crude mixture was purified by flash column chromatography on silica gel (30% EtOAc in hexane as eluent) to afford **50m** (57.3 mg, 83% yield) as a yellow oil.

¹H NMR (400 MHz, CDCl₃) mixture of rotamers: δ 8.08 (t, $J = 9.5$ Hz, 1H), 7.92 (dd, $J = 8.8, 4.0$ Hz, 1H), 7.67 (dt, $J = 12.4, 7.6$ Hz, 1H), 7.50 (t, $J = 7.5$ Hz, 1H), 7.44 – 7.28 (m, 2H), 7.11 (dt, $J = 14.7, 7.2$ Hz, 2H), 6.98 (d, $J = 3.3$ Hz, 1H), 6.85 (d, $J = 7.4$ Hz, 1H), 5.76 – 5.61 (m, 1H), 5.18 (s, 1H), 5.10 – 4.83 (m, 1H), 3.82 (td, $J = 9.5, 8.2, 3.1$ Hz, 1H), 3.77 – 3.62 (m, 1H), 2.67 (d, $J = 26.7$ Hz, 3H), 2.59 – 2.40 (m, 1H), 2.00 – 1.79 (m, 3H).

¹³C NMR (101 MHz, CDCl₃) mixture of rotamers: δ 158.8, 158.6, 154.9, 149.3, 148.6, 148.0, 136.9, 136.5, 129.5, 129.3, 128.6, 128.3, 128.2, 128.1, 127.8, 127.4, 125.8, 124.1, 124.0, 123.0, 122.8, 117.6, 117.3, 67.2, 66.7, 58.1, 57.5, 47.6, 47.3, 34.2, 33.2, 25.5, 23.7, 23.0.

HRMS: calculated for C₂₂H₂₃N₂O₂ (M+H⁺): 347.1754, found 347.1760 (-1.7 ppm).

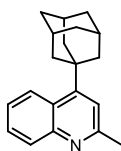


2-Methyl-4-(1-tosylpiperidin-4-yl)quinoline (50n): Synthesized according to General Procedure J using 1,3-dioxoisindolin-2-yl 1-tosylpiperidine-4-carboxylate **23f** (171 mg, 0.4 mmol, 2.0 equiv.) and 2-methylquinoline **49b** (27.1 μ L, 0.2 mmol, 1.0 equiv.) using *set-up 4* at 60 °C. The crude mixture was purified by flash column chromatography on silica gel (30% EtOAc in hexane as eluent) to afford **50n** (56.2 mg, 74% yield) as a white solid.

¹H NMR (400 MHz, CDCl₃) δ 8.04 (dd, $J = 8.5, 1.3$ Hz, 1H), 7.85 (dd, $J = 8.5, 1.4$ Hz, 1H), 7.74 – 7.67 (m, 2H), 7.63 (ddd, $J = 8.3, 6.8, 1.4$ Hz, 1H), 7.43 (ddd, $J = 8.3, 6.8, 1.3$ Hz, 1H), 7.36 (d, $J = 2.0$ Hz, 2H), 7.12 (s, 1H), 4.08 – 3.96 (m, 2H), 3.20 (tt, $J = 11.5, 3.8$ Hz, 1H), 2.71 (s, 3H), 2.47 (m, 5H), 2.07 – 1.85 (m, 4H).

¹³C NMR (101 MHz, CDCl₃) δ 159.0, 150.3, 148.2, 143.8, 133.1, 129.9, 129.8, 129.2, 127.9, 125.8, 124.8, 122.2, 118.6, 47.0, 36.4, 31.8, 25.5, 21.7.

HRMS: calculated for C₂₂H₂₅N₂O₂S (M+H⁺): 381.1627, found 381.1631 (+1.1 ppm).

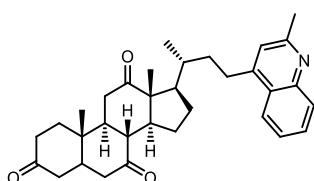


4-((3S)-Adamantan-1-yl)-2-methylquinoline (50o): Synthesized according to General Procedure J using 1,3-dioxoisindolin-2-yl (3*r*,5*r*,7*r*)-adamantane-1-carboxylate **23h** (130 mg, 0.4 mmol, 2 equiv.) and 2-methylquinoline **49b** (27.1 μ L, 0.2 mmol, 1.0 equiv.) using *set-up 4* at 60 °C. The crude mixture was purified by flash column chromatography on silica gel (10% EtOAc in hexane as eluent) to afford **50o** (38.2 mg, 69% yield) as a white solid.

¹H NMR (400 MHz, CDCl₃) δ 8.62 (d, $J = 8.8$ Hz, 1H), 8.35 (s, 1H), 7.69 (ddd, $J = 8.3, 6.8, 1.3$ Hz, 1H), 7.52 (ddd, $J = 8.5, 6.8, 1.5$ Hz, 1H), 7.28 (s, 1H), 2.85 (s, 3H), 2.29 – 2.28 (m, 6H), 2.23 – 2.22 (m, 3H), 1.89 (t, $J = 3.1$ Hz, 6H).

¹³C NMR (101 MHz, CDCl₃) δ 159.5, 130.1, 126.3, 125.4, 125.3, 119.7, 42.3, 39.3, 36.9, 29.1.

HRMS: calculated for C₂₀H₂₄N (M+H⁺): 278.1897, found 278.1903 (+2.2 ppm).



(8*R*,9*S*,10*S*,13*R*,14*S*,17*R*)-10,13-dimethyl-17-((*R*)-4-(2-methylquinolin-4-yl)butan-2-yl)dodecahydro-3*H*-cyclopenta[*a*]phenanthrene-3,7,12(2*H*,4*H*)-trione (50p): Synthesized according to General Procedure J using Dehydrocholic acid phthalimide ester **23d** (219 mg, 0.4 mmol, 2.0 equiv.) and 2-methylquinoline **49b** (27.1

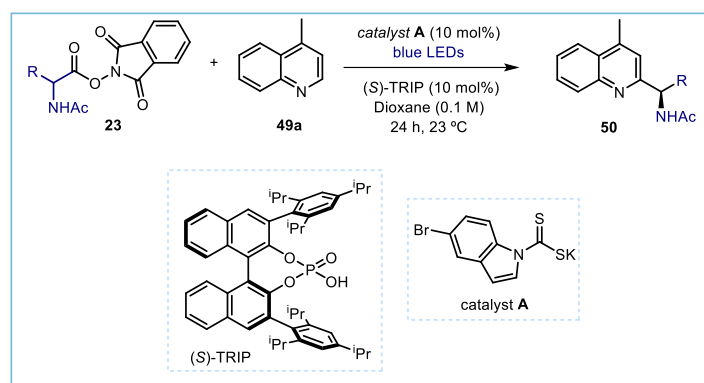
μL , 0.2 mmol, 1.0 equiv.). The crude mixture was purified by flash column chromatography on silica gel (30% EtOAc in hexane as eluent) to afford **50p** (70.0 mg, 61% yield) as a white solid.

$^1\text{H NMR}$ (400 MHz, CDCl_3) δ 8.12 (d, $J = 8.4$ Hz, 1H), 7.96 (dd, $J = 8.5, 1.4$ Hz, 1H), 7.67 (ddd, $J = 8.4, 6.9, 1.4$ Hz, 1H), 7.51 (ddd, $J = 8.2, 6.9, 1.3$ Hz, 1H), 7.14 (s, 1H), 3.15 (ddd, $J = 13.7, 11.7, 5.0$ Hz, 1H), 2.96 – 2.85 (m, 4H), 2.74 (s, 3H), 2.41 – 1.22 (m, 19H), 1.39 (s, 3H), 1.08 (s, 3H), 1.05 (d, $J = 6.6$ Hz, 3H).

$^{13}\text{C NMR}$ (101 MHz, CDCl_3) δ 212.1, 209.1, 208.8, 158.4, 150.6, 146.9, 129.7, 128.6, 126.0, 125.9, 123.4, 121.8, 57.0, 51.9, 49.1, 46.9, 45.7, 45.6, 45.1, 42.9, 38.7, 36.6, 36.5, 36.3, 36.1, 35.4, 29.5, 27.9, 25.2, 24.8, 22.0, 19.2, 12.0.

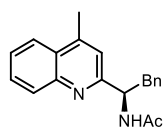
HRMS: calculated for $\text{C}_{33}\text{H}_{42}\text{NO}_3$ ($\text{M}+\text{H}^+$): 500.3157, found: 500.3159 (+0.4 ppm).

3.6.7.3 General procedure K (enantioselective variant)



Reactions performed using *set-up 4*. In an oven dried vial, with a Teflon septum screw cap, 4-methylquinoline (26.4 μL , 0.2 mmol, 1.0 equiv.) and chiral phosphoric acid (*S*)-TRIP (7.5 mg, 0.01 mmol, 5 mol%) were dissolved in dioxane (2 ml). Then, phthalimide ester **23** (0.4 mmol, 2 equiv.) and catalyst **A** (6.2 mg, 0.02 mmol, 0.1 equiv.) were added. The resulting yellow mixture was degassed with argon sparging for 60 seconds. The vial was placed in the one-position photoreactor with temperature control and irradiated under stirring for 24 hours, unless otherwise specified. The solvent was evaporated, and the residue purified by column chromatography to afford the corresponding product in the stated yield with >95% purity according to $^1\text{H NMR}$ analysis.

3.6.7.4 Characterization of products with general procedure K (enantioselective variant)

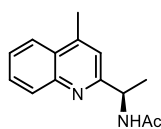


(*R*)-*N*-(1-(4-methylquinolin-2-yl)-2-phenylethyl) acetamide (50q**):** Synthesized according to General Procedure K using 1,3-dioxoisindolin-2-yl acetylphenylalaninate **23i** (140 mg, 0.4 mmol) and 4-methylquinoline **49a** (26.4 μL , 0.2 mmol). The crude mixture was purified by flash column chromatography on silica gel (40% EtOAc in hexane as eluent) to afford **50q** (60.0 mg, 97% yield) as a white solid.

$^1\text{H NMR}$ (400 MHz, CDCl_3) δ 8.05 (dt, $J = 8.5, 0.9$ Hz, 1H), 7.96 (ddd, $J = 8.3, 1.5, 0.6$ Hz, 1H), 7.70 (ddd, $J = 8.4, 6.9, 1.5$ Hz, 1H), 7.59 – 7.51 (m, 1H), 7.27 (s, 1H), 7.18 – 7.13 (m, 3H), 6.99 – 6.92 (m, 2H), 6.82 (d, $J = 1.2$ Hz, 1H), 5.39 (td, $J = 7.7, 5.4$ Hz, 1H), 3.35 (dd, $J = 13.3, 5.4$ Hz, 1H), 3.17 (dd, $J = 13.3, 7.9$ Hz, 1H), 2.59 (d, $J = 0.9$ Hz, 3H), 2.07 (s, 3H).

$^{13}\text{C NMR}$ (101 MHz, CDCl_3) δ 169.6, 158.9, 147.1, 144.9, 137.3, 129.8, 129.5, 129.4, 128.2, 127.6, 126.6, 126.3, 124.00, 121.7, 55.6, 42.3, 23.7, 18.9.

Matching reported literature data.³²



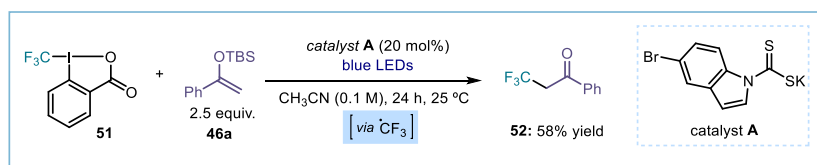
(R)-N-(1-(4-methylquinolin-2-yl) ethyl) acetamide (50r): Synthesized according to General Procedure K using 1,3-dioxoisindolin-2-yl acetylalaninate **23j** (110 mg, 0.4 mmol) and 4-methylquinoline **49a** (26.4 μ L, 0.2 mmol). The crude mixture was purified by flash column chromatography on silica gel (40% AcOEt in hexane as eluent) to afford **50r** (38.3 mg, 84% yield) as a white solid.

$^1\text{H NMR}$ (400 MHz, CDCl_3) δ 8.08 (dt, $J = 8.1, 1.0$ Hz, 1H), 7.98 (ddd, $J = 8.3, 1.5, 0.7$ Hz, 1H), 7.71 (ddd, $J = 8.4, 6.9, 1.4$ Hz, 1H), 7.56 (ddd, $J = 8.3, 6.9, 1.3$ Hz, 1H), 7.51 (s, 1H), 7.17 (d, $J = 1.1$ Hz, 1H), 5.21 (p, $J = 6.8$ Hz, 1H), 2.70 (d, $J = 1.0$ Hz, 3H), 2.11 (s, 3H), 1.54 (d, $J = 6.8$ Hz, 3H).

$^{13}\text{C NMR}$ (101 MHz, CDCl_3) δ 169.6, 160.7, 146.9, 145.8, 129.6, 129.3, 127.6, 126.4, 123.9, 120.5, 50.1, 23.74, 22.8, 19.0.

Matching reported literature data.³²

3.6.8 Trifluoromethylation



Reactions performed using *set-up 3* in Figure 3.37. In an oven dried vial with a Teflon septum screw cap, silyl enol ether **42a** (117 mg, 0.5 mmol, 2.5 equiv.) was dissolved in MeCN (2 mL), then the Togni reagent **47** (105 mg (60% Wt) 0.2 mmol, 1.0 equiv.), catalyst **A** (6.2 mg, 0.02 mmol, 0.1 equiv.). The resulting orange mixture was degassed bubbling argon for 60 seconds. The vial was then placed in the irradiation setup, maintained at a temperature of 25 °C (25–26 °C measured in the central well), and the reaction, unless otherwise stated, was stirred for 24 hours under continuous irradiation from a blue LED strip. The crude mixture was diluted with AcOEt and brine was added. The combined organic fractions were dried over anhydrous MgSO_4 , filtered, and concentrated to dryness. The crude mixture was purified by flash column chromatography on silica gel (Hexane/AcOEt) to afford **48** (22 mg, 58% yield) as a yellow oil.

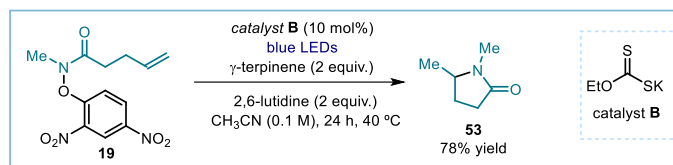
$^1\text{H NMR}$ (300 MHz, CDCl_3) δ 8.01 – 7.91 (m, 2H), 7.69 – 7.61 (m, 1H), 7.60 – 7.46 (m, 3H), 3.82 (q, $J = 10.0$ Hz, 2H).

$^{19}\text{F NMR}$ (376 MHz, CDCl_3) δ –62.11.

$^{13}\text{C NMR}$ (126 MHz, CDCl_3) δ 135.7, 134.2, 128.9, 128.4, 124.7, 42.2.

Matching reported literature data.⁶⁶

3.6.9 Amidyl radical



Reactions performed using *set-up 1* in Figure 3.35 In an oven dried vial, with a Teflon septum screw cap, **19** (29 mg, 0.1 mmol, 1 equiv.) and catalyst **B** (1.6 mg, 0.01 mmol, 0.1 equiv.) were dissolved in CH_3CN (1 mL), then 2,6-lutidine (23 μ L, 0.2 mmol, 2.0 equiv.) was added, followed by γ -terpinene (32 μ L, 0.2 mmol, 2 equiv.). The resulting orange mixture was degassed with argon sparging for 60 seconds. The vial was then placed in the 3D printed support photoreactor and irradiated under stirring for 16 hours. The crude

⁶⁶ Jacquet J.; Cheaib K.; Ren Y.; Vezin H.; Orio M.; Blanchard S.; Fensterbank L.; Desage El Murr M. "Circumventing Intrinsic Metal Reactivity: Radical Generation with Redox-Active Ligands" *Chem. Eur. J.* **2017**, *23*, 15030–15034.

mixture was concentrated to dryness. Trichloroethylene was added as internal standard (9 μL , 0.1 mmol, 1.0 equiv) and NMR yield was determined by ^1H NMR in CDCl_3 matching reported literature data.²⁶

3.6.10 Large scale reactions

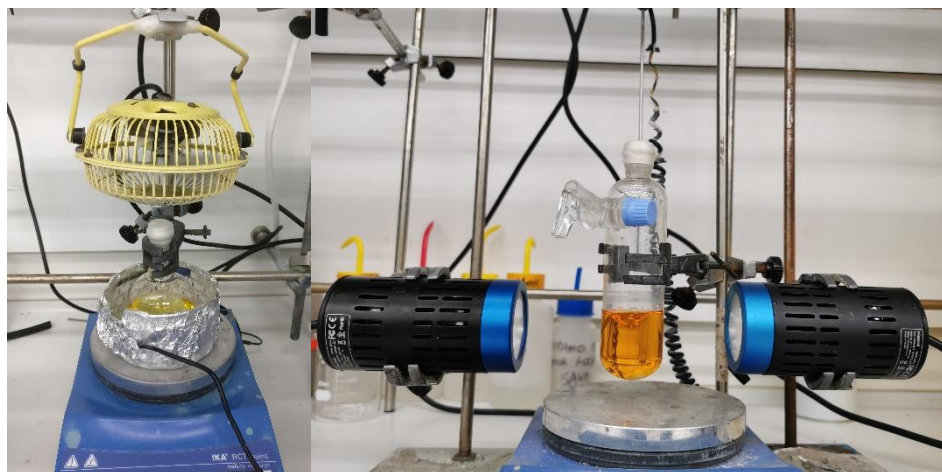
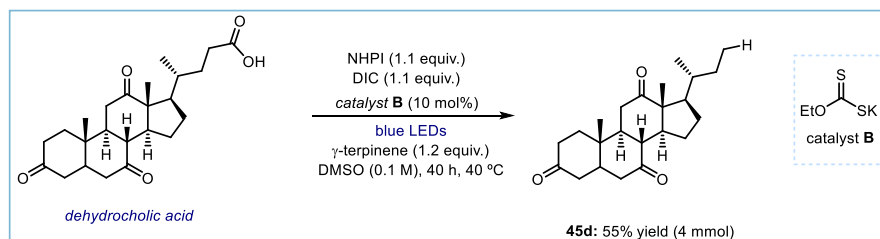


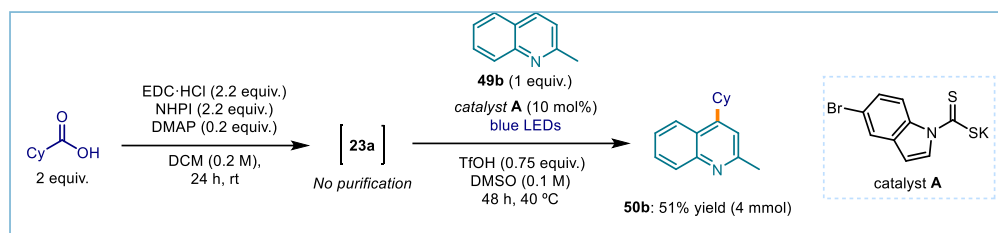
Figure 3.41. Scale-up set-ups. Barton decarboxylation (left). Minisci reaction (right).

3.6.10.1 Barton decarboxylation



Using set-up in Figure 3.40 (left). In a 100 mL round bottom flask with a Teflon cap, dehydrocholic acid (1,62 g, 4 mmol, 1 equiv.), *N*-hydroxyphthalimide (NHPI, 716 mg, 4.4 mmol, 1.1 equiv.), and xanthogenate catalyst **A** (64 mg, 0.4 mmol, 0.1 equiv.) were dissolved in DMSO (40 mL), and *N,N'*-diisopropylcarbodiimide (DIC, 760 μL , 4.4 mmol, 1.1 equiv.) was added via syringe. Then, γ -terpinene (760 μL , 4.8 mmol, 1.2 equiv.) was added. The resulting orange mixture was degassed with nitrogen sparging for 5 min. The round bottom flask was then irradiated for 40 hours with a 1-meter 14W blue LED strip and cooled with a fan to keep the temperature between 30 and 35 $^\circ\text{C}$ (Figure 3.41, left). The mixture was transferred to an extraction funnel, NaOH 1M solution was added and the organic layer was extracted with CH_2Cl_2 . The organic layer was dried over anhydrous MgSO_4 , filtered, and concentrated to dryness. The crude residue was purified by chromatography on silica gel (10% AcOEt in hexanes) to afford 800 mg of product **45d** (2.2 mmol, 55% yield) as an off white solid. NMR analysis was consistent with product synthesized in the small scale process.

3.6.10.2 Minisci reaction



Using set-up in Figure 3.41 (right panel). In a 100 mL round bottom flask, cyclohexanecarboxylic acid (1.03 g, 8 mmol, 2 equiv.), EDC·HCl (1.69 g, 8.8 mmol, 2.2 equiv.), DMAP (97.7 mg, 0.8 mmol, 0.2 equiv.), and *N*-hydroxyphthalimide (1.44 g, 8.8 mmol, 2.2 equiv.) were dissolved in CH₂Cl₂ (20 mL). The reaction was stirred at ambient temperature for 24 hours. The mixture was transferred to an extraction funnel, NaHCO₃ sat. solution was added and the organic layer was extracted with CH₂Cl₂. The organic phase was concentrated to dryness under vacuum to obtain the crude phthalimide ester, which was used without further purification in the next step.

In a 100 mL Schlenk flask with a Teflon septum, the crude phthalimide ester was dissolved in DMSO (40 mL). Then, 2-methylquinoline (540 μL, 4.00 mmol, 1.0 equiv.), trifluoromethanesulfonic acid (265 μL, 3.00 mmol, 0.75 equiv.) and catalyst A (124 mg, 0.40 mmol, 0.1 equiv.) were added. The resulting orange mixture was degassed with nitrogen sparging for 5 minutes. The Schlenk flask was irradiated with stirring for 48 hours using two 50 W Kessil blue LED lamp (one PR160L-456 and one PR160L-427, 100% intensity, 4-5 cm away) (Figure 3.4, right panel). The mixture was transferred to an extraction funnel, NaHCO₃ sat. solution was added and the organic layer was extracted with CH₂Cl₂. The organic layer was dried over anhydrous MgSO₄, filtered, and concentrated to dryness. The crude residue was purified by chromatography on silica gel (10% AcOEt in hexanes) to afford 459 mg of product **50b** (2.04 mmol, 51% yield) as a yellowish oil. NMR analysis was consistent with product synthesized in the small scale process.

3.6.11 Unsuccessful substrates

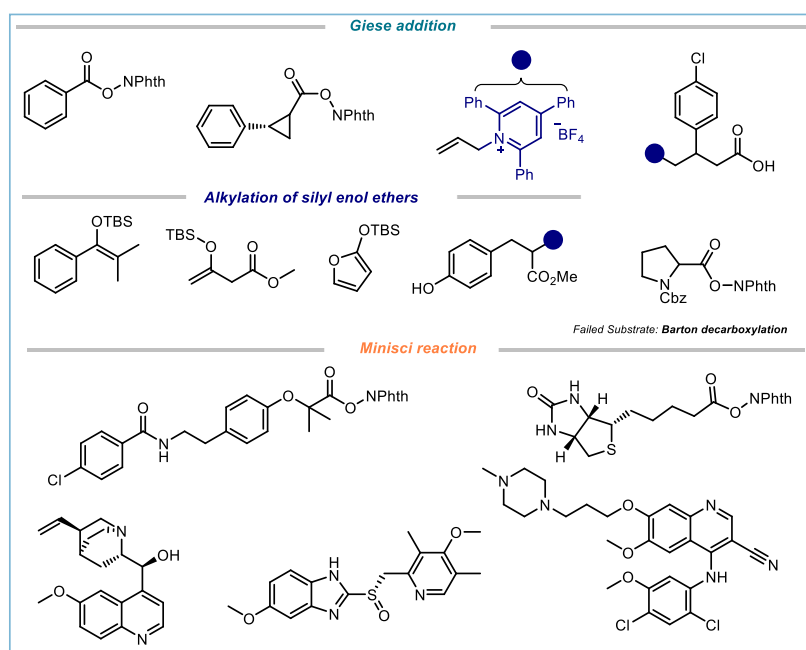


Figure 3.42. Unsuccessful substrates that offered poor yields (ranging from 0 to <20%).

3.7 Mechanistic studies

3.7.1 Control experiments

3.7.1.1 Experiments with green light

For the reactions performed under green light irradiation, an EvoluChem™ P303-30-1 LEDs (18 W, $\lambda_{\text{max}} = 520$ nm) was used. The reaction temperature was measured to be between 25 °C and 30 °C using the setup depicted in Figure 3.43).

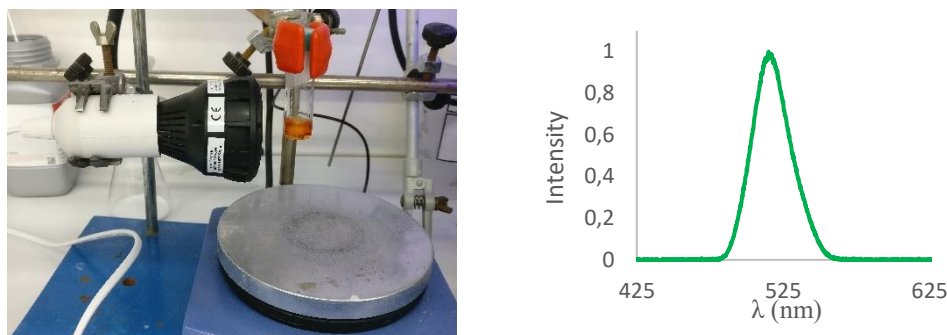


Figure 3.43. Reaction set-up for green light irradiation (*left*). Emission spectrum of the 520 nm EvoluChem™ P303-30-1 LEDs used in this reactor (*right*).

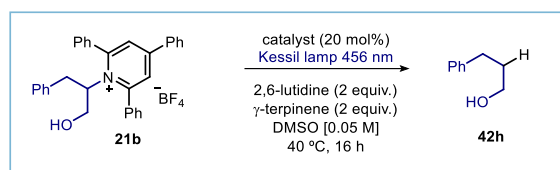
3.7.1.2 Optimization studies

Table 3.4 Barton decarboxylation.

entry	catalyst	deviation	yield (%) ^a
1	B	none	80 (77) ^b
2	B	isolated RAE	80
3	A	none	traces
4	B	under air	0
5	B	no light	0
6	none	none	0

Reactions performed using *set-up 1* in Figure 3.36.

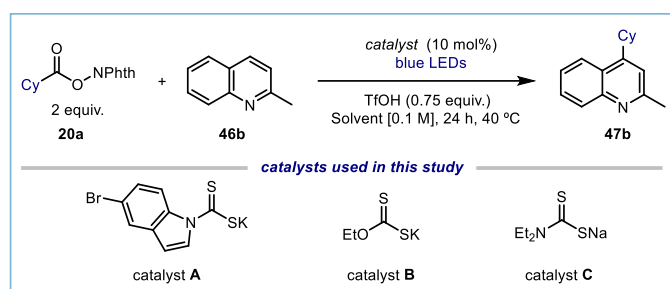
Table 3.5 Deamination with pyridinium salts as radical precursors.



entry	catalyst	deviation	yield (%) ^a
1	A	none	95 (78) ^b
2	A	under air	0
3	A	no light	0
4	none	none	0

Reactions performed using *set-up 2* in Figure 3.37.

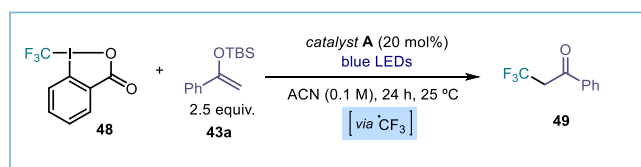
Table 3.6. Minisci reaction.



entry	catalyst	Solvents	deviation	yield (%) ^a
1	A	DMSO	TFA	82
2	B	DMSO	TFA	0
3	C	DMSO	TFA	0
6	A	DMSO	none	97(95) ^b
8	A	DMSO	Green light	8
9	A	DMSO	No acid	0
10	A	DMSO	No light	0
11	A	DMSO	under air	0
12	none	DMSO	none	0

Reactions performed using *set-up 2* in Figure 3.38.

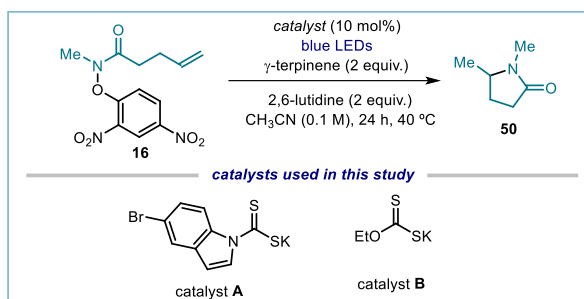
Table 3.3. Trifluoromethylation of silyl enol ethers.



entry	catalyst	Base	deviation	yield (%) ^a
1	A	-	Acetone	21
2	A	-	none	63(58%) ^b
3	A	2,6-lutidine (1 equiv.)	none	62
4	B	-	none	22
5	C	-	none	27
6	-	-	No catalyst	0

Reactions performed using *set-up 3* in Figure 3.39.

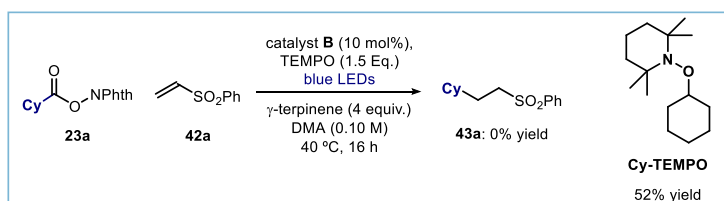
Tbale 3.8 Amidyl radical cyclization



entry	catalyst	deviation	yield (%) ^a
1	A	None	86
2	B	None	78
3	A	No base	60
4	B	No base	50
5	A	Under air	0
6	A	No light	0
7	none	None	0

Reactions performed using *set-up 1* in Figure 3.40.

3.7.1.3 TEMPO trapping experiment



Reactions performed using *set-up 1*. In an oven dried vial with a Teflon septum screw cap, potassium ethyl xanthogenate **B** (1.6 mg, 0.01 mmol, 0.1 equiv.), phthalimide ester **23a** (0.1 mmol, 27.3 mg, 1 equiv.), 2,2,6,6-tetramethylpiperidine 1-oxyl (TEMPO, 0.15 mmol, 23.5 mg, 1.5 equiv.) and **42a** (0.15 mmol, 25.2 mg, 1.5 equiv.) were dissolved in DMA (1 mL). Then, γ -terpinene (64 μ L, 0.4 mmol, 4 equiv.) was added. The resulting orange mixture was degassed by argon sparging for 60 seconds. The vial was then placed in the 3D printed support photoreactor and irradiated under stirring for 16 hours. The mixture was transferred to an extraction funnel, brine was added and the organic layer was extracted with EtOAc. The organic layer was dried over anhydrous $MgSO_4$, filtered, and concentrated to dryness. The crude residue was then purified by column chromatography (2% EtOAc in hexanes) to afford the corresponding **Cy-TEMPO** adduct in 52% yield. No product corresponding with giese addition was detected in the crude NMR or during the purification.

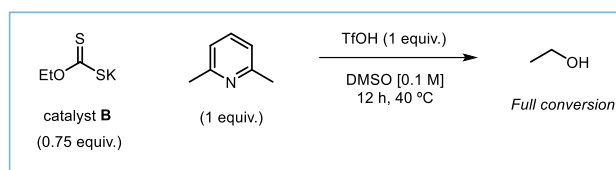
¹H NMR (500 MHz, $CDCl_3$) δ 3.68 – 3.64 (m, 1H), 2.07 (brs, 2H), 1.76 (brs, 2H), 1.57 – 1.54 (m, 2H), 1.48 – 1.45 (m, 4H), 1.31 – 1.06 (m, 19H).

¹³C NMR (126 MHz, $CDCl_3$) δ 81.7, 59.6, 40.3, 32.9, 26.0, 25.1, 17.3.

Characterization data matching data reported in the literature.⁶⁷

⁶⁷ Tobisu M.; Koh K.; Furukawa T.; Chatani N. "Modular Synthesis of Phenanthridine Derivatives by Oxidative Cyclization of 2-Isocyanobiphenyls with Organoboron Reagents" *Angew. Chem., Int. Ed.* **2012**, *51*, 11363-11366.

- **Catalyst B:**



In an oven dried vial with a Teflon septum screw cap, 2,6-lutidine (0.1 mmol, 12 μ L) was added followed by triflic acid (0.1 mmol, 8.9 μ L). The resulting pyridinium salt was then dissolved in 1 mL of d^6 -DMSO, followed by the addition of catalyst **B** (12 mg, 0.075 mmol). The mixture was left stirring overnight and the crude mixture is analyzed by ^1H NMR. Catalyst **B** showed complete degradation to ethanol (Figure 3.45).

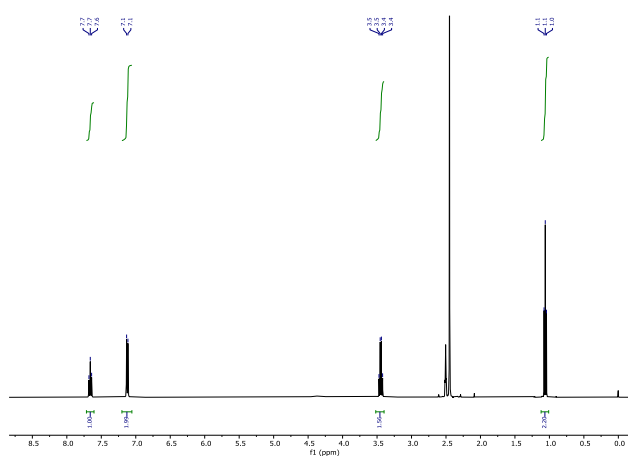


Figure 3.45. ^1H NMR analysis to evaluate catalyst **B** stability.

3.7.3 UV-Vis spectroscopy

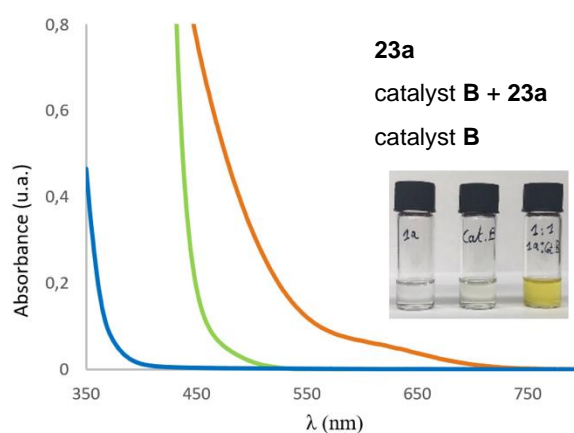


Figure 3.46. Optical absorption spectra, recorded in DMA in 1 mm path quartz cuvettes using a Shimadzu 2401PC UV-vis spectrophotometer, and visual appearance of the separate reaction components and of the colored EDA complex between catalyst **B** and 23a. $[\mathbf{23a}] = 0.10$ M, $[\text{catalyst } \mathbf{B}] = 0.01$ M.

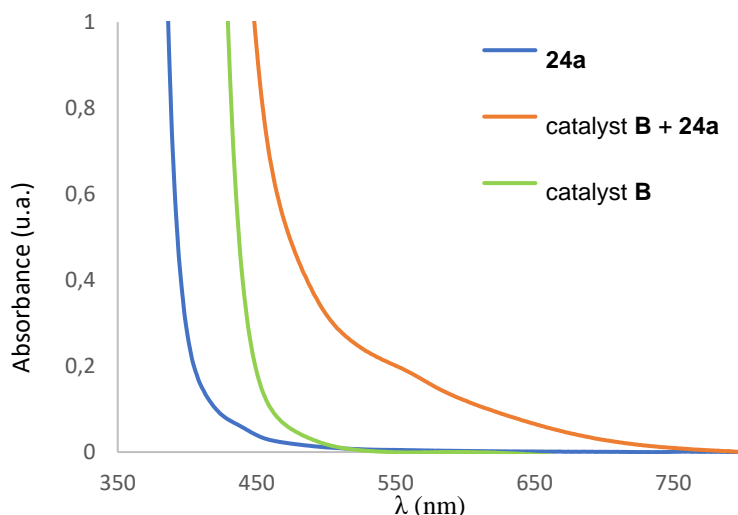


Figure 3.467. Optical absorption spectra, recorded in DMA in 1 mm path quartz cuvettes using a Shimadzu 2401PC UV-vis spectrophotometer of the separate reaction components and of the colored EDA complex between catalyst B and **24a**. [**24a**] = 0.10 M, [catalyst B] = 0.01 M.

3.7.4 Transient absorption spectroscopy (TAS)

Studies with microsecond transient absorption spectroscopy (TAS) were performed using an excitation source of NdYAG (neodymium-doped yttrium aluminium garnet) Opolette laser with an optical parametric oscillator (OPO) system that allows variable wavelength excitation from 400 -1800 nm, pulse width of 6 ns, up to 2 mJ of energy from OPO output with fiber optic coupled, and high energy output from direct NdYAG harmonics 355 (20 mJ, 5 ns) and 532 (45mJ, 6 ns). The system is completed with 150 W tungsten lamp as probe; 2 monochromators Minuteman MM151; Si amplified photodetector module for VIS; DSPDAU high speed data rate recorder and interface software from RAMDSP. Laser intensity for the chosen wavelength was 355 nm – 1.30 mJ.

We selected a logarithmic time scale suitable for clearly showing the decay of the transient species in the samples. The characteristics of the detected transient species match literature data.³⁵

In a typical transient absorption spectroscopy experiment, solutions in DMA of a mixture of **23a** and catalyst **B** was prepared under an argon atmosphere and transferred into a screw-top 3.0 mL quartz cuvette for measurement. Upon irradiation with the appropriated wavelength, the decay of absorption at 620 nm of the transient xanthyl radical **Ib** was recorded. Irradiation at 420 nm and 460 nm of the sample also provided signal absorbing at 620 nm, but in a much lower intensity and higher noise.

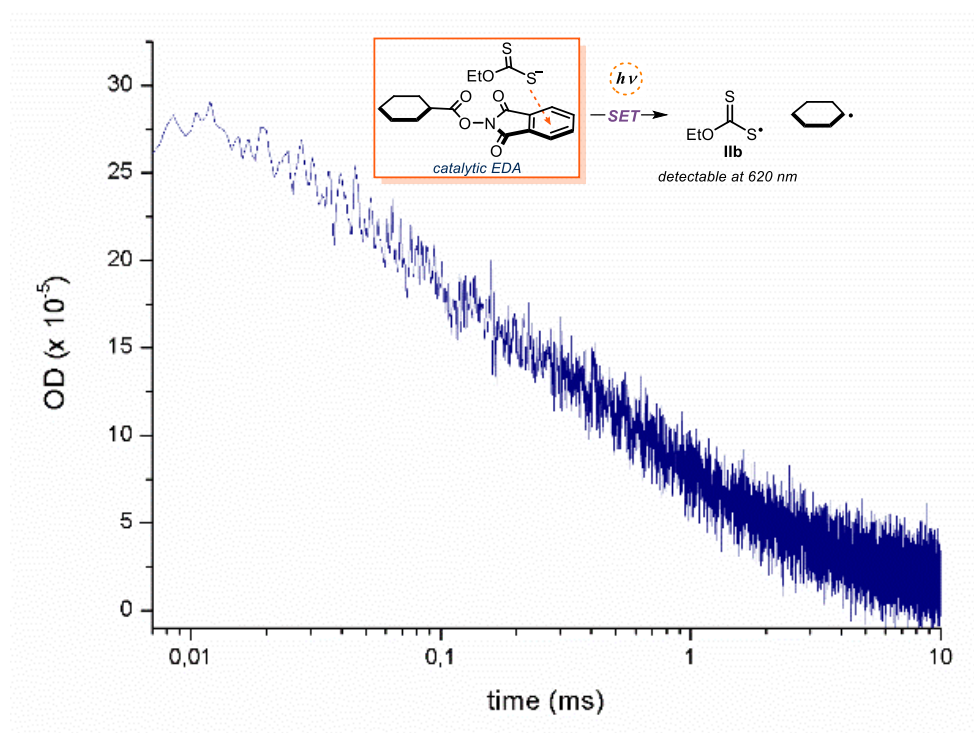


Figure 3.48. Absorption at 620 nm of the transient xanthyl radical **IIb** (blue line) generated upon 355 nm laser excitation of a 1:1 mixture of **23a** and catalyst **B** 30 mM in DMA. Note logarithmic scale for time. ΔOD : optical density variation.

3.7.5 Cyclic voltammetry measurements

For all cyclic voltammetry (CV) measurements, a glassy carbon disk electrode (diameter 3 mm) was used as the working electrode. A silver wire coated with AgCl immersed in a 3.5 M aqueous solution of KCl and separated from the analyte by a fritted glass disk was employed as the reference electrode. A Pt wire counter-electrode completed the electrochemical setup. The scan rate used in each CV experiment is indicated case by case.

Potentials are quoted with the following notation: E_p^C refers to the cathodic peak potential, E_p^A refers to the anodic peak potential, while the E^{red} value describes the electrochemical properties of the referred compound.

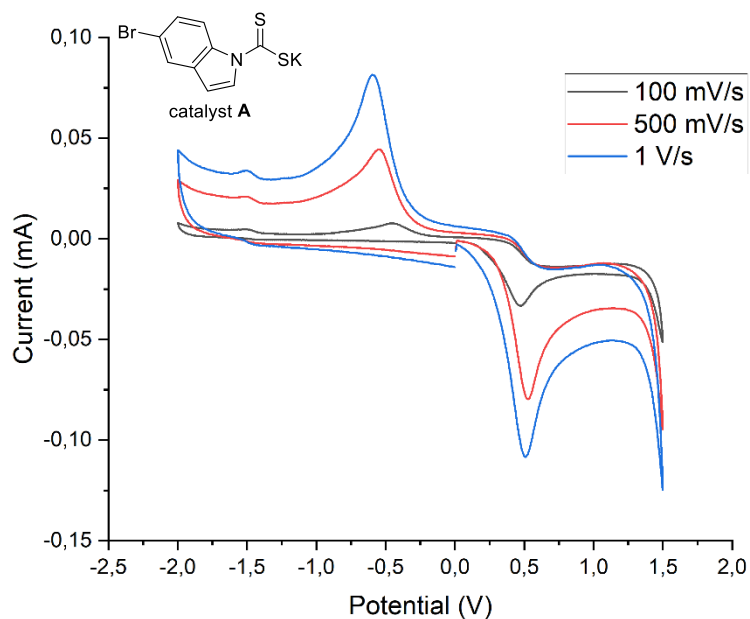


Figure 3.49. Cyclic voltammogram for catalyst A [0.02 M] in [0.1 M] TBAPF₆ in CH₃CN. Measurement started by oxidation from 0 to +1.5 V, followed by reduction from +1.5 V to -2.0 V, and finishing at 0 V. Glassy carbon electrode working electrode, Ag/AgCl (KCl 3.5 M) reference electrode, Pt wire auxiliary electrode. Two irreversible peaks observed increasing with sweep rate.

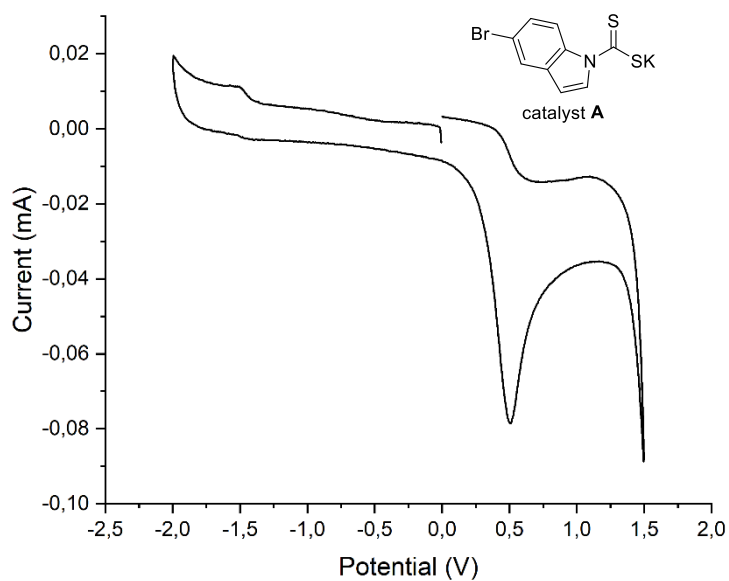


Figure 3.50. Cyclic voltammogram for catalyst A [0.02M] in [0.1 M] TBAPF₆ in CH₃CN. Measurement started by reduction from 0 to -2.0 V, followed by oxidation from -2.0 V to +1.5 V, and finishing at 0 V. Glassy carbon electrode working electrode, Ag/AgCl (KCl 3.5 M) reference electrode, Pt wire auxiliary electrode. Only one irreversible peak observed. Sweep rate: 500 mV/s.

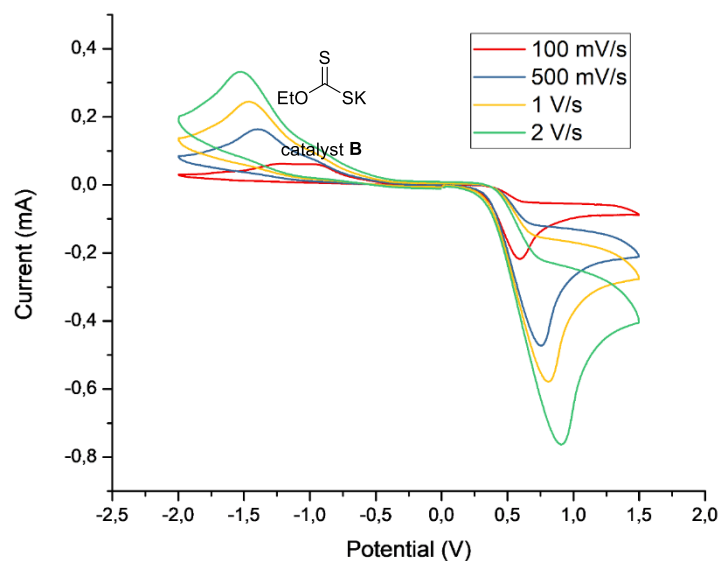


Figure 3.51. Cyclic voltammogram for catalyst B [0.02 M] in [0.1 M] TBAPF₆ in CH₃CN. Measurement started by oxidation from 0 to +1.5 V, followed by reduction from +1.5 V to -2.0 V, and finishing at 0 V. Glassy carbon electrode working electrode, Ag/AgCl (KCl 3.5 M) reference electrode, Pt wire auxiliary electrode. Two irreversible peaks observed increasing with sweep rate.

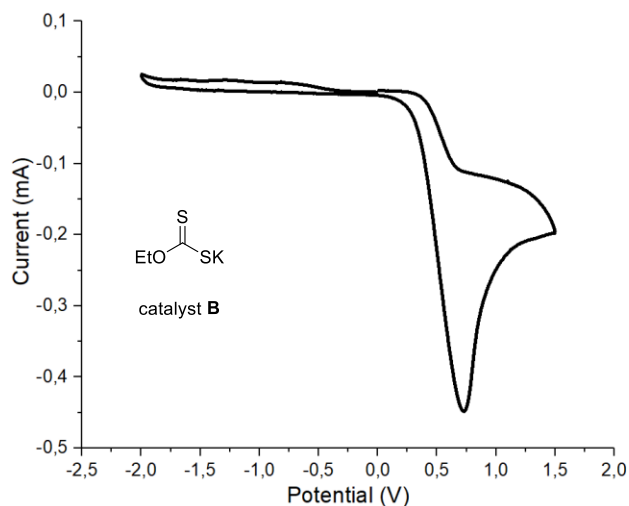


Figure 3.52. Cyclic voltammogram for catalyst B [0.02M] in [0.1 M] TBAPF₆ in CH₃CN. Measurement started by reduction from 0 to -2.0 V, followed by oxidation from -2.0 V to +1.5 V, and finishing at 0 V. Glassy carbon electrode working electrode, Ag/AgCl (KCl 3.5 M) reference electrode, Pt wire auxiliary electrode. Only one irreversible peak observed. Sweep rate: 500 mV/s.

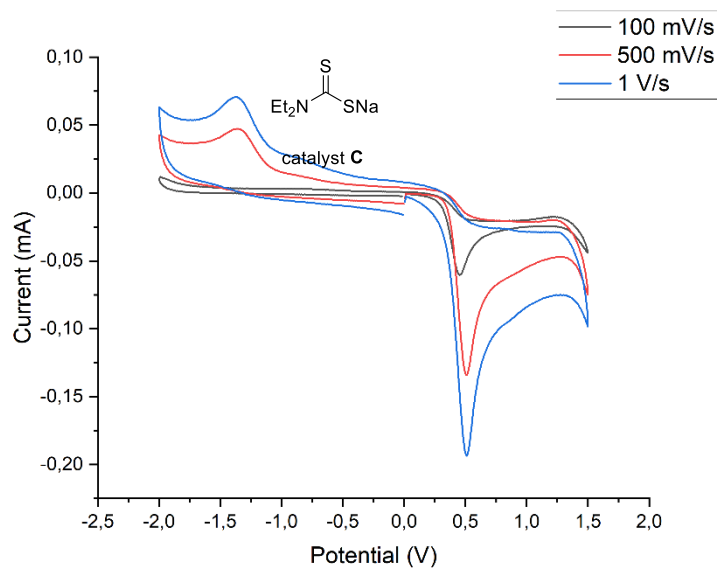


Figure 3.53. Cyclic voltammogram for catalyst C [0.02 M] in [0.1 M] TBAPF₆ in CH₃CN. Measurement started by oxidation from 0 to +1.5 V, followed by reduction from +1.5 V to -2.0 V, and finishing at 0 V. Glassy carbon electrode working electrode, Ag/AgCl (KCl 3.5 M) reference electrode, Pt wire auxiliary electrode. Two irreversible peaks observed increasing with sweep rate.

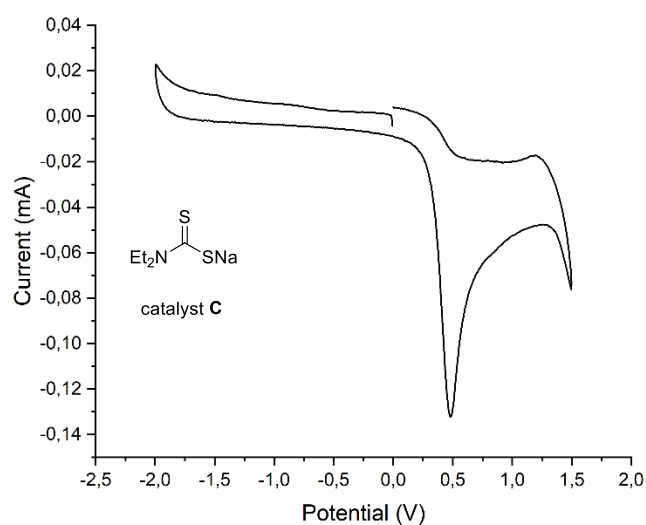


Figure 3.54. Cyclic voltammogram for catalyst C [0.02M] in [0.1 M] TBAPF₆ in CH₃CN. Measurement started by reduction from 0 to -2.0 V, followed by oxidation from -2.0 V to +1.5 V, and finishing at 0 V. Glassy carbon electrode working electrode, Ag/AgCl (KCl 3.5 M) reference electrode, Pt wire auxiliary electrode. Only one irreversible peak observed. Sweep rate: 500 mV/s.

3.7.6 Quantum yield determination

3.7.6.1 Giese addition

A ferrioxalate actinometer solution was prepared by following the Hammond variation of the Hatchard and Parker procedure outlined in the Handbook of Photochemistry.⁶⁸ The ferrioxalate actinometer solution measures the decomposition of ferric ions to ferrous ions, which are complexed by 1,10-phenanthroline and monitored by UV/Vis absorbance at 510 nm. The moles of iron-phenanthroline complex formed are related to moles of photons absorbed. The following solutions were prepared and stored in a dark laboratory (red light):

1. Potassium ferrioxalate solution: 294.8 mg of potassium ferrioxalate (commercially available from Alfa Aesar) and 139 μL of sulfuric acid (96%) were added to a 50 mL volumetric flask, and filled to the mark with water (HPLC grade).
2. Phenanthroline solution: 0.2% by weight of 1,10-phenanthroline in water (100 mg in 50 mL volumetric flask).
3. Buffer solution: 2.47 g of NaOAc and 0.5 mL of sulfuric acid (96%) were added to a 50 mL volumetric flask and filled to the mark with water (HPLC grade).

The actinometry measurements were done as follows:

1. 1 mL of the actinometer solution was added to a Schlenk tube (diameter = 12 mm). The Schlenk tube was placed in one of the positions of the 3D printed reactor. The solution was irradiated at 460 nm. This procedure was repeated 4 times, quenching the solutions after different time intervals: 1 s, 2 s, 4 s, and 8 s.
2. Then 1 mL of the model reaction following general procedure A with **23a** (0.10 mmol) and **42a** as substrates was placed in a Schlenk tube, degassed via argon bubbling, placed in the irradiation set up and irradiated for 15 minutes. This procedure was performed a total of four times with different irradiation times (30 min, 45 min, 60 min).
3. After irradiation, the actinometer solutions were removed and placed in a 10 mL volumetric flask containing 0.5 mL of 1,10-phenanthroline solution and 2 mL of buffer solution. These flasks were filled to the mark with water (HPLC grade).
4. The UV-Vis spectra of the complexed actinometer samples were recorded for each time interval. The absorbance of the complexed actinometer solution was monitored at 510 nm.

The moles of Fe^{2+} formed for each sample is determined using Beers' Law (Eq. 1):

$$\text{Mols of Fe(II)} = V_1 \times V_3 \times \Delta A(510 \text{ nm}) / 10^3 \times V_2 \times l \times \epsilon(510 \text{ nm}) \quad (\text{Eq. 1})$$

where V_1 is the irradiated volume (1 mL), V_2 is the aliquot of the irradiated solution taken for the determination of the ferrous ions (1 mL), V_3 is the final volume after complexation with phenanthroline (10 mL), l is the optical path-length of the irradiation cell (1 cm), $\Delta A(510 \text{ nm})$ is the optical difference in absorbance between the irradiated solution and the one stored in the dark, $\epsilon(510 \text{ nm})$ is the extinction coefficient the complex $\text{Fe}(\text{phen})_3^{2+}$ at 510 nm (11100 L mol⁻¹ cm⁻¹). The moles of Fe^{2+} formed (x) are plotted as a function of time (t). The slope of this line was correlated to the moles of incident photons by unit of time ($q_0^{n,p}$) by the use of the following Equation 2:

$$\Phi(\lambda) = dx/dt \cdot q_0^{n,p} / [1 - 10^{-A(\lambda)}] \quad (\text{Eq. 2})$$

where dx/dt is the rate of change of a measurable quantity (spectral or any other property), the quantum yield (Φ) for Fe^{2+} at 458 nm is 1.1,⁶⁹ $[1 - 10^{-A(\lambda)}]$ is the ratio of absorbed photons by the solution, and $A(\lambda)$ is the absorbance of the actinometer at the wavelength used to carry out the experiments (460 nm). The absorbance at 460 nm $A(460)$ was measured using a Shimadzu 2401PC UV-Vis spectrophotometer in a 10 mm path quartz cuvette, obtaining an absorbance of 0.183. $q_0^{n,p}$, which is the photon flux, was determined to be 5.3×10^{-7} .

⁶⁸ Murov, S. L. Ed. *Handbook of Photochemistry* (Marcel Dekker, New York, 1973).

⁶⁹ Holubov C. A.; Langford C. H. "Wavelength and temperature dependence in the photolysis of the chemical actinometer, potassium trisoxalatoferrate(III), at longer wavelengths" *Inorg. Chim. Acta.* **1981**, 53, 59-60.

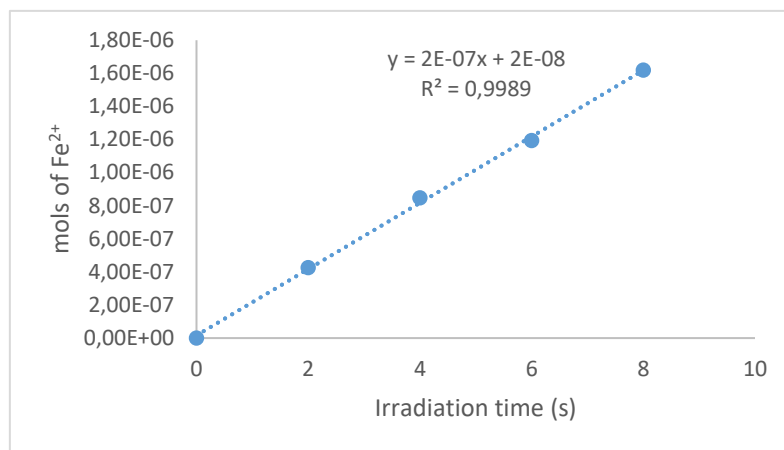


Figure 3.55. Plot of mols of Fe²⁺ formed vs irradiation time. Slope of the line correlates to the moles of incident photons by unit of time.

The moles of product **43a** formed for the model reaction were determined by GC measurement (FID detector) using 1,3,5-trimethoxybenzene as internal standard. The moles of product per unit of time are related to the number of photons absorbed.

The photons absorbed are correlated to the number of incident photons by the use of Equation 1. According to this, if we plot the moles of product (y) versus the moles of incident photons (q₀ n,p-dt), the slope is equal to: $\Phi \cdot (1 - 10^{-A(460 \text{ nm})})$, where Φ is the quantum yield to be determined and A(460 nm) is the absorption of the reaction under study. A(460 nm) was measured using a Shimadzu 2401PC UV-Vis spectrophotometer in 10 mm path quartz. An absorbance of 0.049 was determined for the model reaction mixture (1:4 dilution). The quantum yield (Φ)_{cat.} of the photochemical transformation was measured to be 0.01.

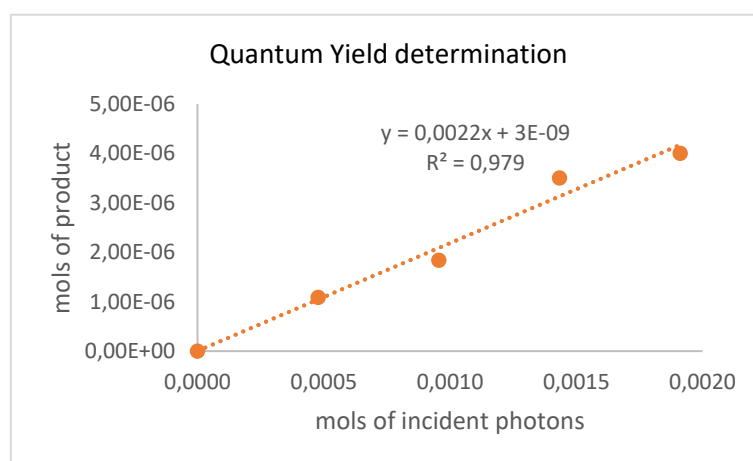


Figure 3.56. Plot of mols of incident photons vs mols of product formed. Slope of the line correlates to quantum yield of the photochemical transformation.

3.7.6.2 Barton decarboxylation

A ferrioxalate actinometer solution was prepared by following the Hammond variation of the Hatchard and Parker procedure outlined in the Handbook of Photochemistry.⁶⁸ The ferrioxalate actinometer solution measures the decomposition of ferric ions to ferrous ions, which are complexed by 1,10-phenanthroline and monitored by UV/Vis absorbance at 510 nm. The moles of iron-phenanthroline complex formed are related to moles of photons absorbed. The following solutions were prepared and stored in a dark laboratory (red light):

1. Potassium ferrioxalate solution: 294.8 mg of potassium ferrioxalate (commercially available from Alfa Aesar) and 139 μ L of sulfuric acid (96%) were added to a 50 mL volumetric flask and filled to the mark with water (HPLC grade).
2. Phenanthroline solution: 0.2% by weight of 1,10-phenanthroline in water (100 mg in 50 mL volumetric flask).
3. Buffer solution: 2.47 g of NaOAc and 0.5 mL of sulfuric acid (96%) were added to a 50 mL volumetric flask and filled to the mark with water (HPLC grade).

The actinometry measurements were done as follows:

1. 1 mL of the actinometer solution was added to a Schlenk tube (diameter = 12 mm). The Schlenk tube was placed in one of the positions of the 3D printed reactor. The solution was irradiated at 460 nm. This procedure was repeated 4 times, quenching the solutions after different time intervals: 1 s, 2 s, 4 s, and 8 s.
2. Then 1 mL of the model reaction following general procedure F starting from isolated **23f** (0.10 mmol) as substrate was placed in a Schlenk tube, degassed via argon bubbling, placed in the irradiation set up and irradiated for 15 minutes. This procedure was performed a total of four times with different irradiation times (30 min, 60 min, 120 min).
3. After irradiation, the actinometer solutions were removed and placed in a 10 mL volumetric flask containing 0.5 mL of 1,10-phenanthroline solution and 2 mL of buffer solution. These flasks were filled to the mark with water (HPLC grade).
4. The UV-Vis spectra of the complexed actinometer samples were recorded for each time interval. The absorbance of the complexed actinometer solution was monitored at 510 nm.

The moles of Fe²⁺ formed for each sample is determined using Beers' Law (Eq. 1):

$$\text{Mols of Fe(II)} = V_1 \times V_3 \times \Delta A(510 \text{ nm}) / 10^3 \times V_2 \times l \times \epsilon(510 \text{ nm}) \quad (\text{Eq. 1})$$

where V_1 is the irradiated volume (1 mL), V_2 is the aliquot of the irradiated solution taken for the determination of the ferrous ions (1 mL), V_3 is the final volume after complexation with phenanthroline (10 mL), l is the optical path-length of the irradiation cell (1 cm), $\Delta A(510 \text{ nm})$ is the optical difference in absorbance between the irradiated solution and the one stored in the dark, $\epsilon(510 \text{ nm})$ is the extinction coefficient the complex Fe(phen)₃²⁺ at 510 nm (11100 L mol⁻¹ cm¹). The moles of Fe²⁺ formed (x) are plotted as a function of time (t). The slope of this line was correlated to the moles of incident photons by unit of time ($q_{n,p}^0$) by the use of the following Equation 2:

$$\Phi(\lambda) = dx/dt \cdot q_{n,p}^0 / [1 - 10^{-A(\lambda)}] \quad (\text{Eq. 2})$$

where dx/dt is the rate of change of a measurable quantity (spectral or any other property), the quantum yield (Φ) for Fe²⁺ at 458 nm is 1.1,⁶⁹ $[1 - 10^{-A(\lambda)}]$ is the ratio of absorbed photons by the solution, and $A(\lambda)$ is the absorbance of the actinometer at the wavelength used to carry out the experiments (460 nm). The absorbance at 460 nm $A(460)$ was measured using a Shimadzu 2401PC UV-Vis spectrophotometer in a 10 mm path quartz cuvette, obtaining an absorbance of 0.183. $q_{n,p}^0$, which is the photon flux, was determined to be 5.2×10^{-7} .

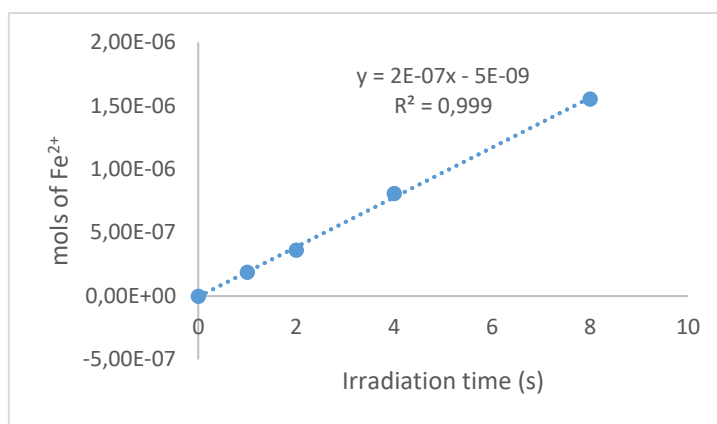


Figure 3.57. Plot of mols of Fe²⁺ formed vs irradiation time. Slope of the line correlates to the moles of incident photons by unit of time.

The moles of product **45b** formed for the model reaction were determined by GC measurement (FID detector) using 1,3,5-trimethoxybenzene as internal standard. The moles of product per unit of time are related to the number of photons absorbed.

The photons absorbed are correlated to the number of incident photons by the use of Equation 1. According to this, if we plot the moles of product (y) versus the moles of incident photons ($q_0 n, p \cdot dt$), the slope is equal to: $\Phi \cdot (1 - 10^{-A(460 \text{ nm})})$, where Φ is the quantum yield to be determined and $A(460 \text{ nm})$ is the absorption of the reaction under study. $A(460 \text{ nm})$ was measured using a Shimadzu 2401PC UV-Vis spectrophotometer in 10 mm path quartz. An absorbance of 0.052 was determined for the model reaction mixture. The quantum yield (Φ)_{cat.} of the photochemical transformation was measured to be 0.01.

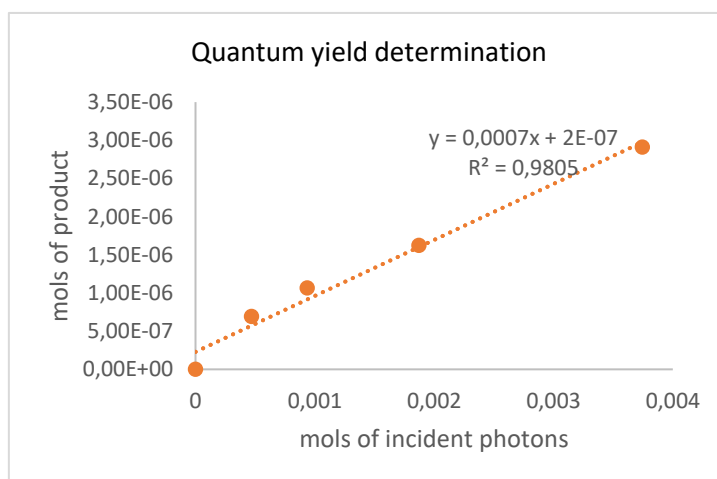


Figure 3.58. Plot of mols of incident photons vs mols of product formed. Slope of the line correlates to quantum yield of the photochemical transformation.

3.7.6.3 Alkylation enol ethers

A ferrioxalate actinometer solution was prepared by following the Hammond variation of the Hatchard and Parker procedure outlined in the Handbook of Photochemistry.⁶⁸ The ferrioxalate actinometer solution measures the decomposition of ferric ions to ferrous ions, which are complexed by 1,10-phenanthroline and monitored by UV/Vis absorbance at 510 nm. The moles of iron-phenanthroline complex formed are related to moles of photons absorbed. The following solutions were prepared and stored in a dark laboratory (red light):

1. Potassium ferrioxalate solution: 294.8 mg of potassium ferrioxalate (commercially available from Alfa Aesar) and 139 μL of sulfuric acid (96%) were added to a 50 mL volumetric flask and filled to the mark with water (HPLC grade).
2. Phenanthroline solution: 0.2% by weight of 1,10-phenanthroline in water (100 mg in 50 mL volumetric flask).
3. Buffer solution: 2.47 g of NaOAc and 0.5 mL of sulfuric acid (96%) were added to a 50 mL volumetric flask, and filled to the mark with water (HPLC grade).

The actinometry measurements were done as follows:

1. 1 mL of the actinometer solution was added to a Schlenk tube (diameter = 12 mm). The Schlenk tube was placed in a single HP LED 1.5 cm away from the light source (irradiance 10 mW/cm²).¹² The solution was irradiated at 460 nm. This procedure was repeated 4 times, quenching the solutions after different time intervals: 5 s, 10 s, 20 s, and 40 s.
2. Then 1 mL of the model reaction following general procedure H with **42a** (0.10 mmol) and **24I** as substrates was placed in a Schlenk tube, degassed via argon bubbling, placed in the irradiation set up and irradiated for 15 minutes. This procedure was performed a total of four times with different irradiation times (30 min, 50 min, 70 min).
3. After irradiation, the actinometer solutions were removed and placed in a 10 mL volumetric flask containing 0.5 mL of 1,10-phenanthroline solution and 2 mL of buffer solution. These flasks were filled to the mark with water (HPLC grade).
4. The UV-Vis spectra of the complexed actinometer samples were recorded for each time interval. The absorbance of the complexed actinometer solution was monitored at 510 nm.

The moles of Fe²⁺ formed for each sample is determined using Beers' Law (Eq. 1):

$$\text{Mols of Fe(II)} = V_1 \times V_3 \times \Delta A(510 \text{ nm}) / 10^3 \times V_2 \times l \times \epsilon(510 \text{ nm}) \quad (\text{Eq. 1})$$

where V_1 is the irradiated volume (1 mL), V_2 is the aliquot of the irradiated solution taken for the determination of the ferrous ions (1 mL), V_3 is the final volume after complexation with phenanthroline (10 mL), l is the optical path-length of the irradiation cell (1 cm), $\Delta A(510 \text{ nm})$ is the optical difference in absorbance between the irradiated solution and the one stored in the dark, $\epsilon(510 \text{ nm})$ is the extinction coefficient the complex Fe(phen)₃²⁺ at 510 nm (11100 L mol⁻¹ cm¹). The moles of Fe²⁺ formed (x) are plotted as a function of time (t). The slope of this line was correlated to the moles of incident photons by unit of time (q_0 n.p) by the use of the following Equation 2:

$$\Phi(\lambda) = dx/dt \cdot q_{n,p} \cdot 0 [1 - 10^{-A(\lambda)}] \quad (\text{Eq. 2})$$

where dx/dt is the rate of change of a measurable quantity (spectral or any other property), the quantum yield (Φ) for Fe²⁺ at 458 nm is 1.1,⁶⁹ $[1 - 10^{-A(\lambda)}]$ is the ratio of absorbed photons by the solution, and $A(\lambda)$ is the absorbance of the actinometer at the wavelength used to carry out the experiments (460 nm). The absorbance at 460 nm $A(460)$ was measured using a Shimadzu 2401PC UV-Vis spectrophotometer in a 10 mm path quartz cuvette, obtaining an absorbance of 0.148. q_0 n.p, which is the photon flux, was determined to be 1.18×10^{-7} .

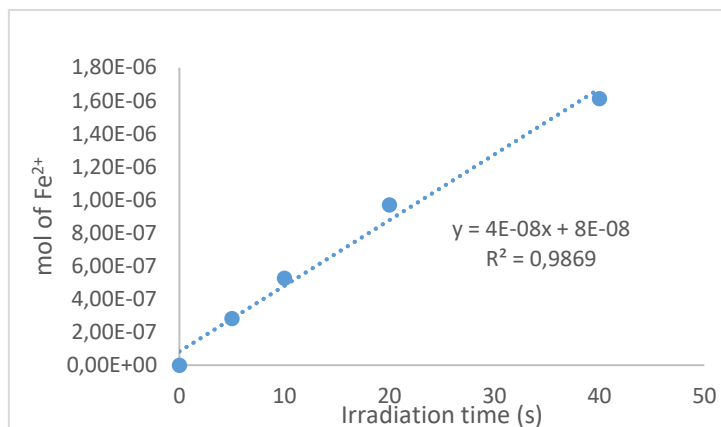


Figure 3.59. Plot of mols of Fe²⁺ formed vs irradiation time. Slope of the line correlates to the moles of incident photons by unit of time.

The moles of product **47h** formed for the model reaction were determined by GC measurement (FID detector) using 1,3,5-trimethoxybenzene as internal standard. The moles of product per unit of time are related to the number of photons absorbed.

The photons absorbed are correlated to the number of incident photons by the use of Equation 1. According to this, if we plot the moles of product (y) versus the moles of incident photons (q₀ n_p·dt), the slope is equal to: $\Phi \cdot (1 - 10^{-A(460 \text{ nm})})$, where Φ is the quantum yield to be determined and A(460 nm) is the absorption of the reaction under study. A(460 nm) was measured using a Shimadzu 2401PC UV-Vis spectrophotometer in 10 mm path quartz. An absorbance of 0.018 was determined for the model reaction mixture (1:100 dilution). The quantum yield (Φ)_{cat.} of the photochemical transformation was measured to be 0.02.

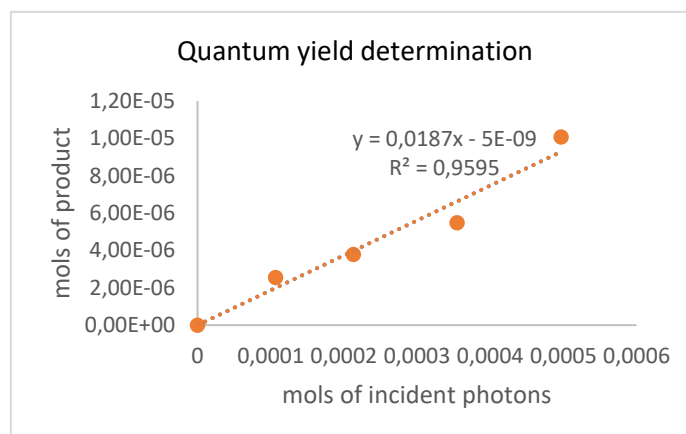


Figure 3.60. Plot of mols of incident photons vs mols of product formed. Slope of the line correlates to quantum yield of the photochemical transformation.

3.7.6.4 Minisci reaction

A ferrioxalate actinometer solution was prepared by following the Hammond variation of the Hatchard and Parker procedure outlined in the Handbook of Photochemistry.⁶⁸ The ferrioxalate actinometer solution measures the decomposition of ferric ions to ferrous ions, which are complexed by 1,10-phenanthroline and monitored by UV/Vis absorbance at 510 nm. The moles of iron-phenanthroline complex formed are related to moles of photons absorbed. The following solutions were prepared and stored in a dark laboratory (red light):

1. Potassium ferrioxalate solution: 294.8 mg of potassium ferrioxalate (commercially available from Alfa Aesar) and 139 μ L of sulfuric acid (96%) were added to a 50 mL volumetric flask, and filled to the mark with water (HPLC grade).
2. Phenanthroline solution: 0.2% by weight of 1,10-phenanthroline in water (100 mg in 50 mL volumetric flask).
3. Buffer solution: 2.47 g of NaOAc and 0.5 mL of sulfuric acid (96%) were added to a 50 mL volumetric flask, and filled to the mark with water (HPLC grade).

The actinometry measurements were done as follows:

1. 1 mL of the actinometer solution was added to a Schlenk tube (diameter = 12 mm). The Schlenk tube was placed in one of the position of the 3D printed reactor. The solution was irradiated at 460 nm. This procedure was repeated 4 times, quenching the solutions after different time intervals: 1 s, 2 s, 4 s, and 8 s.
2. Then 1 mL of the model reaction following general procedure J with **23a** (0.10 mmol) and 2-methylquinoline **49b** as substrates was placed in a Schlenk tube, degassed via argon bubbling, placed in the irradiation set up and irradiated for 60 minutes. This procedure was performed a total of four times with different irradiation times (90 min, 120 min, 150 min).
3. After irradiation, the actinometer solutions were removed and placed in a 10 mL volumetric flask containing 0.5 mL of 1,10-phenanthroline solution and 2 mL of buffer solution. These flasks were filled to the mark with water (HPLC grade).
4. The UV-Vis spectra of the complexed actinometer samples were recorded for each time interval. The absorbance of the complexed actinometer solution was monitored at 510 nm.

The moles of Fe²⁺ formed for each sample is determined using Beers' Law (Eq. 1):

$$\text{Mols of Fe(II)} = V_1 \times V_3 \times \Delta A(510 \text{ nm}) / 10^3 \times V_2 \times l \times \epsilon(510 \text{ nm}) \quad (\text{Eq. 1})$$

where V_1 is the irradiated volume (1 mL), V_2 is the aliquot of the irradiated solution taken for the determination of the ferrous ions (1 mL), V_3 is the final volume after complexation with phenanthroline (10 mL), l is the optical path-length of the irradiation cell (1 cm), $\Delta A(510 \text{ nm})$ is the optical difference in absorbance between the irradiated solution and the one stored in the dark, $\epsilon(510 \text{ nm})$ is the extinction coefficient the complex Fe(phen)₃²⁺ at 510 nm (11100 L mol⁻¹ cm¹). The moles of Fe²⁺ formed (x) are plotted as a function of time (t). The slope of this line was correlated to the moles of incident photons by unit of time ($q_{n,p}^0$) by the use of the following Equation 2:

$$\Phi(\lambda) = dx/dt \cdot q_{n,p}^0 [1 - 10^{-A(\lambda)}] \quad (\text{Eq. 2})$$

where dx/dt is the rate of change of a measurable quantity (spectral or any other property), the quantum yield (Φ) for Fe²⁺ at 458 nm is 1.1,⁶⁹ $[1 - 10^{-A(\lambda)}]$ is the ratio of absorbed photons by the solution, and $A(\lambda)$ is the absorbance of the actinometer at the wavelength used to carry out the experiments (460 nm). The absorbance at 460 nm $A(460)$ was measured using a Shimadzu 2401PC UV-Vis spectrophotometer in a 10 mm path quartz cuvette, obtaining an absorbance of 0.183. $q_{n,p}^0$, which is the photon flux, was determined to be 4.68×10^{-7} .

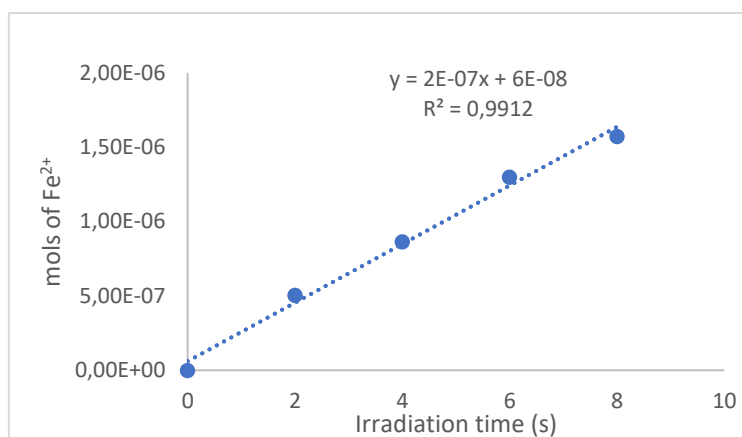


Figure 3.61. Plot of mols of Fe²⁺ formed vs irradiation time. Slope of the line correlates to the moles of incident photons by unit of time.

The moles of product **50b** formed for the model reaction were determined by GC measurement (FID detector) using 1,3,5-trimethoxybenzene as internal standard. The moles of product per unit of time are related to the number of photons absorbed.

The photons absorbed are correlated to the number of incident photons by the use of Equation 1. According to this, if we plot the moles of product (y) versus the moles of incident photons ($q_0 n, p-dt$), the slope is equal to: $\Phi \cdot (1 - 10^{-A(460 \text{ nm})})$, where Φ is the quantum yield to be determined and $A(460 \text{ nm})$ is the absorption of the reaction under study. $A(460 \text{ nm})$ was measured using a Shimadzu 2401PC UV-Vis spectrophotometer in 10 mm path quartz. An absorbance of 0.174 was determined for the model reaction mixture (1:10 dilution). The quantum yield (Φ)_{cat.} of the photochemical transformation was measured to be 0.0003.

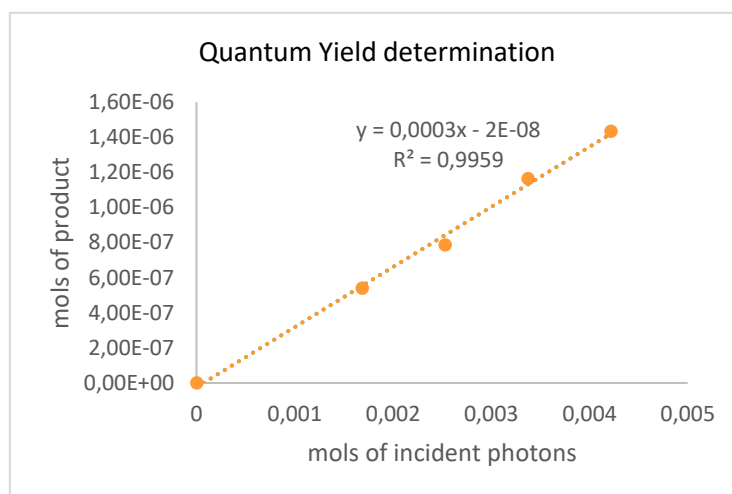


Figure 3.62 Plot of mols of incident photons vs mols of product formed. Slope of the line correlates to quantum yield of the photochemical transformation.

Chapter IV

General Conclusions

In my doctoral studies, I have exploited dithiocarbamate and xanthate anions as organocatalysts for the generation of radicals under photochemical conditions. Interestingly, this new class of catalysts could use distinct and complementary mechanisms to activate different substrates towards radical formation.

Chapter II described a new photochemical approach for the radical α -alkylation of ketones using silyl enol ethers as stable nucleophiles, which synthetically complemented traditional two-electron strategies and enriched the radical-based approaches developed so far. The highly *nucleophilicity* of our dithiocarbamate catalyst was leveraged towards a unique activation mode, namely an *S_N2-based pathway*, by which radicals were formed from simple alkyl (pseudo)-halides. The method's mild reaction conditions and functional group tolerance allowed us to install, at the ketones' α -position, moieties not compatible with classical anionic processes. In addition, the redox neutral conditions of this process made it tolerant of a cinchona-based amine catalyst, which was used to develop an effective protocol for the asymmetric alkylation of cyclic ketones.

In Chapter III, I studied and exploited the high *electron-donicity* of dithiocarbamates and xanthogenates as catalytic donors for the development of a catalytic electron donor-acceptor (EDA) platform to activate electron-poor radical precursors. Light irradiation of the catalytically generated EDA complex delivered radicals without the need for harsh reaction conditions and toxic reagents. Furthermore, the ability to fine tune the properties of the catalysts' scaffold allowed us to design mechanistically different processes, including net-reductive and redox-neutral reactions. Finally, the catalytic nature of the system has been proven by mechanistic investigations, confirming the power of the organocatalysts to be turned over and to iteratively drive each catalytic cycle.

In conclusion, dithiocarbamate and xanthate anions have been shown to be a versatile class of organocatalysts useful to activate a variety of radical precursors and generate open-shell intermediates under photo-irradiation with low-energy photons. The developed catalytic strategies can enrich the tools available in synthetic organic chemistry.

UNIVERSITAT ROVIRA I VIRGILI
DITHIOCARBAMATES: NEW ORGANIC CATALYSTS FOR THE PHOTOCHEMICAL GENERATION OF RADICALS
Davide Spinnato

UNIVERSITAT ROVIRA I VIRGILI
DITHIOCARBAMATES: NEW ORGANIC CATALYSTS FOR THE PHOTOCHEMICAL GENERATION OF RADICALS
Davide Spinnato

